

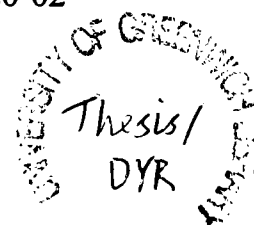
**QUANTIFICATION AND MITIGATION OF  
SEGREGATION IN THE HANDLING OF  
ALUMINA IN ALUMINIUM PRODUCTION  
- PHD THESIS FOR ARE DYRØY -**

Tel-Tek Report no. 4104020-02

University of Greenwich

© Are Dyrøy  
Tel-Tek Dept. POSTEC  
Kjoelnes Ring, N-3918 Porsgrunn, Norway  
Tel-Tek report no. 4104020-02

December 2006



## DECLARATION

I certify that this work has not been accepted in substance for any degree, and is not currently being submitted for any degree other than that PhD being studied at the University of Greenwich. I also declare that this work is the result of my own investigations except where otherwise identified by references and that I have not plagiarised another's work.

Place/ Date

Place/ Date

Place/ Date

First Tutor

Second Tutor

PhD Candidate

## SYNOPSIS

This thesis addresses the development, evaluation and modelling of an anti-segregation system ("AS-System") for use in larger silos handling alumina in the aluminium smelting industry.

This work is unlike much of what has gone before because it is much more grounded in the technical and economic consequences of segregation for a particular manufacturing process. Segregation of particulates, i.e. separation of components due to differences in properties such as size, density etc., has an extensive literature going back as far as 1915, but this focuses mainly on the segregation process itself and largely ignores the context and the consequences. The consequence of segregation is loss of homogeneity; the impact that has on any given process, is generally not addressed very deeply. Surveying the literature on segregation, and studying the total processes of aluminium production, creates a basis for understanding the importance of segregation for aluminium production, as well as the importance of powder technology in general for this industry.

A method for quantification of segregation in this production process, based on sampling, has been established. This was intended to give the fundamental information necessary for measuring the extent of the problem and the degree of improvement achieved. By placing sampling points along the logistic chain for the alumina, and by sampling these points for a long enough period, information about the influence of the various handling steps on the bulk solids can be identified. Segregation by particle size is the main type of influence, although the work has shown that attrition is another. Standardised statistical expressions have been used for analysing the bottlenecks of the logistic loops, and study of the results has led to a useful way of expressing the level of segregation, the change of segregation level in a handling step (silo filling and discharge), and improvements in this change.

The degree of segregation when handling alumina has proven to be quite considerable in terms of effects on the production process. The effects on the efficiency of the aluminium smelting process, and the environment, have both been evaluated. Variations in the alumina due to segregation have been found to correlate with both dust concentration in the smelter pot room, and anode effects (an unwanted upset in the smelting process). An economical evaluation of an investment in anti segregation systems has been made. This evaluation has shown significant economic consequences, clearly justifying both the investigations of segregation, and the implementation of anti segregation measures.

To remedy the effects of air current segregation in the aluminium industry, a complete Anti Segregation System (AS-System) based around Anti Segregation Tubes (AST) utilising a special inlet

configuration has been developed. In a number of full size installations, this solution has proved itself capable of handling the variations and transients of process conditions which occur in the industry, with a large operational capacity range, due to the special inlet configuration.

The effect of the full scale installed anti segregation systems have been measured, and compared to other systems. The AS-System clearly demonstrated a homogenising effect no matter how low the ingoing variations in particle size were. Other commercial systems which have been evaluated have turned out to be no more than Segregation Effect Damping Systems, since they only seem to reduce the segregation effect after it has happened, instead of trying to eliminate the problem by directly attacking the segregation mechanism itself which is what the AS-System does.

A new scaled down test rig for the AS-System was developed, consisting of three ASTs fed from a central distributor. To test the potential effect of the AS-System, to determine its efficiency in countering segregation, tests with repeated filling and emptying of a scale silo were carried out. The results clearly showed that the AS-System very much reduced segregation, compared to conventional filling, even in a small-scale silo.

Improved models have been developed for the function of the AST and these have been verified against measurements from the new test rig. The early version of the test rig for the AST used only one centre-mounted tube, with one pressure measurement in the top of the tube. The first models were based on the assumption of the pressure being linear, and assumed full dispersion of the falling material inside the tube; and calibrated from the single pressure measurement inside at the top of the tube. Although this simple model calculated very conservative values of the negative pressure, the model was used for the initial development and design of the AST, and later the AS-System (Anti Segregation System). A second model was derived, where the material velocity was calculated based on free fall. This model was also based on the idea of full dispersion, but was in better agreement with measured values during further tests, which showed a considerable deviation from the original assumption of a linear pressure distribution once intermediate pressure measurements were available.

When using the multi-phase-flow-simulation-program-code FLUENT to simulate the pressure distribution of the AST, the results were quite disappointing, however the FLUENT program was able to identify an initial positive pressure generated by the flow from the inlet box to the tube. Implementing this initial pressure into the simple non-linear model above, both the trend and values correspond quite well with the measured values.

A single particle drag model was tried, but dismissed after calculating the maximum possible capacity for known tubes and finding the predictions to be unrealistically low. A new approach was introduced, modelling the fall of the powder in a continuous layer along the inner wall of the tube on one side, creating skin drag along the surface between the falling solid powder and the air. The length of the tube and the width of the chosen AST profile define this surface. This approach assumes that the powder falls like a layer along the tube wall. Previous theory for pressure drop in pneumatic conveying inspired this approach, but it had not previously been used for gravity flow in vertical tubes, and as a result the novel Solid Surface Body Drag Model (SSBDM) was developed. This analytical model gives very good correspondence with the measured data for the pressure distribution inside the AST, yet is extremely simple to use. When comparing the model with measured data, the SSBDM was able to predict the pressure distribution within the error boundaries of the test measurements.

A method for design of the AST was derived from the SSBDM, using a dimensionless parameter function determined for the pressure drop model. The models giving the design indicate that the capacity is more than proportional to the cross sectional area of a chosen tube profile, which is in agreement with observations. The model suggests that the capacity is proportional to the cross sectional area in the power of 1.25. This model allowed the study of the effect of tube shape, which revealed that a square profile for the AST does not seem to be the optimum design; rather, a rectangular profile should be chosen for maximum capacity. The model suggests that the capacity is proportional to the width of the side of the tube along which the powder layer is falling, but proportional to the perpendicular side in a rectangular profile in the power of 1.5.

The model gives an equation for pressure drop which can also be utilised to place the first valve on the tube. It also shows that for high capacities, and large silos, a system consisting of several ASTs should be chosen (AS-System). Predictions from the model have been tested against the measured capacities of full scale installed systems and give good agreement.

Overall, the AS-System has been shown to be cost-effective in reducing segregation; results measured from the full scale installations show a homogenising factor (reduction in variation of the material being handled) of 1-1.5. As a result of these verifications and the simplicity of the model presented in this thesis, the plant engineer can confidently design a system which will function correctly and make a positive, predictable improvement in the homogeneity of the alumina in his plant.

## ACKNOWLEDGEMENTS

Since this work started many persons, institutions, and industrial companies have been involved. Due to the historical economical situation in Tel-Tek dept. POSTEC, the work has been carried out whenever time was available, i.e. it has been a part time job, resulting in a long time span of work. A time span, which has given me many grieves and joys, fortunately most of the latter.

Great thanks are extended to my two tutors Prof. Gisle Enstad (Tel-Tek dept POSTEC) and Prof. Michael Bradley (Greenwich University, Wolfson Centre), for their help and encouragement with my long overdue thesis. Also thanks to Ali Ghaderi for being a mathematical wizard. Furthermore, thanks are due to Caroline Chapman at Wolfson, for making the “red tape” of the University of Greenwich possible to handle.

Throughout the years, I have been fortunate to act as tutor for students visiting dept POSTEC, all of them, which have contributed very much to my work. Especially Michael Stillwell and Martin Hubrich, without their effort my results would have harder to accomplish.

Great thanks also due to my own administration in Tel-Tek, for their help and fruitful companionship throughout the years. They have made my commercial workload that at times has been too heavy, much easier to carry. Then thanks to all of my past and present colleagues in dept. POSTEC, which have been essential in both this specific work and in the commercial work. Without these colleagues, most of my work would have been impossible to carry out.

The commercial work, although at times tough, has not only been hard, but also a very educational fun, especially thanks to my “*brother in arms*” throughout the years, Morten Karlsen in Hydro Aluminium (HAL) Research Centre. All the days on the road, cold, hot, and dusty hours spent in the factories have been quite an experience. People might call us for “Pompel & Pilt”, but we have been able to do much fun. In addition others from HAL, has contributed to my work, and thank you very much all of you. Specially Carl Behrens for your very much appreciated input and help with the understanding of the alumina re-

finery world.

As mentioned, the work has taken me around the globe, literary several times, meaning being away from home. During such travels, both my birth family and married family have been most supportive. Nevertheless, nothing of this can match the patience and support from my own dear wife Lilly. Without your support, backing and at time nagging, the work would have been much harder to carry out.

At last, I will address two very important persons lost during this journey. My, for many years leader late Prof. Sunil de Silva, whose signature and influence, can clearly be seen from the best parts of this thesis. His help, during stressful times, was imperative. Then my longest friend and confidant, Gunnstein Mjåseth, his chronic disease ended his life in late 2001, this was a great loss for me. Looking at the hardships, he had to endure during that time, a feeling of shamefulness raises. However, he always replied when this was mentioned; *“any persons problem is a genuine problem, otherwise it would not be a problem for this person”*. His situation really put the need for research on the agenda, even the research that has no direct payback should be carried out.

Therefore, this work will be dedicated to the memory of

Sunil de Silva

&

Gunnstein Mjåseth

Porsgrunn December 22<sup>th</sup> 2006

Are Dyrøy

## CONTENTS

1. INTRODUCTION	11
1.1 What is Segregation?	11
1.2 The Importance of Segregation	11
1.3 Aims for this work	12
2. LITERATURE SURVEY	14
2.1 Mechanisms of segregation	14
2.2 Mechanisms and Processes of Segregation	17
2.2.1 Trajectory Segregation	18
2.2.2 Air Current Segregation	18
2.2.3 Rolling Segregation	19
2.2.4 Sieving	20
2.2.5 Impact Segregation	20
2.2.6 Push-away /Embedding	21
2.2.7 Angle of Repose Effects	21
2.2.8 Displacement Segregation	22
2.2.9 Percolation	22
2.2.10 Fluidization Segregation	23
2.2.11 Concentration driven displacement (Diffusion)	24
2.2.12 Agglomeration	24
2.3 Air Current Segregation	25
2.3.1 Air Current Segregation in General	25
2.3.2 Air Current Segregation in the Filling and Discharge from Silos	27
2.4 Segregation and aluminium production	28
2.4.1 Handling of alumina in aluminium production	29
2.4.2 Production of Alumina	30
2.4.3 Aluminium Production	32
2.5 Summary and Commentary of Literature Survey	36



---

3. SURVEY OF SEGREGATION IN AN ALUMINIUM PLANT	38
3.1 Philosophy behind full factory campaigns	38
3.2 Sampling of whole factories	39
3.2.1 Designing sampling of an aluminium plant	40
3.2.2 How is the sampling done	42
3.2.3 Method of analysing the sample results from sampling campaigns	43
3.2.4 A constructed example of a campaign	45
3.3 Segregation and Consequences in the aluminium industry	51
3.3.1 Bulk solids changes found during campaigns	52
3.3.2 Process influences found during campaigns	62
3.3.3 Environmental effects found during campaigns	65
3.3.4 Effect of anti segregation measures	66
3.3.5 Economical calculation of full Anti segregation system implementation	72
3.4 Summary and Commentary for Survey of Segregation in an Aluminium Plant	77
4. DEVELOPMENT OF AN ANTI-SEGREGATION TUBE (AST)	79
4.1 The AST Concept	79
4.1.1 The Inlet of the Anti Segregation Tube	81
4.1.2 The Valves	83
4.1.3 The Tube	85
4.2 Basic development model	85
4.3 Initial Development tests	87
4.4 New test rig	95
4.5 Experimental test setup of the AS-System with three AST's, equipment and procedures	96
4.5.1 Operational Procedure	100
4.6 Pressure measurement tests for AS-System	102
4.7 Lab-scale tests of the effect from anti segregation tubes	108
4.8 Summary and Commentary of AST development	111
5. MODELLING OF THE AST	113

5.1	Initial simple linear model	113
5.2	FLUENT simulations	115
5.3	Initial simple non linear model	118
5.4	Single Particle Drag Model (SPDM)	122
5.5	Solids Surface Body Drag Model (SSBDM)	126
5.6	Summary and Commentary of modelling the AST	138
6.	DESIGNING THE ANTI SEGREGATION TUBE	140
6.1	Designing the size of the tube for capacity	140
6.2	Placing the first valve at the top of the AST	144
6.2.1	Choice of configuration and placement	145
6.3	Summary and commentary of designing the AST	145
7.	CONCLUSIONS	147
8.	SUGGESTED FURTHER WORK	150
9.	REFERENCES	151
	APPENDIX A NOMECLATURE AND ABBREVIATIONS	157
	APPENDIX B LIST OF FIGURES AND TABLES	162
	APPENDIX C CALIBRATION CERTIFICATES AND RE CALIBRATIONS OF PRESSURE TRANSDUCERS	168
	APPENDIX D PCT PATENT OF THE AS-SYSTEM	181
	APPENDIX E INSTALLATIONS OF THE AS-SYSTEM	183
	APPENDIX F TEST SET UP FOR AS-SYSTEM	188

## 1. INTRODUCTION

This project is a continuation of the work on segregation carried out by Mosby [Mosby, 1996] at Tel-Tek's Department of Powder Science and Technology (POSTEC). Mosby identified and systematised the various segregation mechanisms described in the literature, and investigated the relation between process parameters and the segregation mechanisms in laboratory scale testers. This work will mainly focus on the handling of alumina in the aluminium industry, and air current segregation. However, the definitions and general descriptions of all the segregation mechanisms will be given, and their occurrence in handling or processing particulate materials discussed in 2.1.

### 1.1 What is Segregation?

One definition of segregation is “separation due to different properties”. Most commonly, known is the separation of human races carried out by various regimes throughout history. Keeping to the general definition, one may say that segregation occurs often. People with the same interests, the same social status, and so forth tend to stick together, because this group finds it pleasant to enjoy the company of people with similar identities and interests. When moving to the area of powder and bulk solids handling, the definition of segregation would be “segregation of particles due to differences in mobility”. Differences in mobility may be caused by particle properties such as size, size distributions, shape, density, coefficients of restitution etc, or by the process conditions and the type of equipment used. The most common particle properties causing segregation are the particle size, and size distributions.

### 1.2 The Importance of Segregation

Segregation is one topic that influences almost every aspect of powder technology. First, consider the difficulty of obtaining a representative sample of powder from a storage unit or a process. Segregation is one of the most frequent disturbances resulting in not representative samples. The fundamentals of different designs of handling, conveying, and processing systems for bulk solids are designed based on samples and, since sampling is

affected by segregation, so will the design of equipment. When classifying bulk solids using sieves and air-classifiers, one uses the very causes of segregation in order to separate into the different classes of particles. A particle of a specific size will pass through a sieve, or will have a certain ability to be carried in air streams, giving the wanted separation.

Almost all processes in industry involve bulk solids and powders. Some move millions of tonnes every year, and some handle a few grams of components with a value way beyond that of gold. Irrespective of the quantity handled, if the process in any way depends on more or less constant composition, segregation will influence the outcome. Also considering the fact that competition in the process industry continuously forces companies to try to improve yield and reduce environmental impact (both local and global) the margins are forced to minima, and despite all the sophistication of the regulation systems implemented, these systems need a set point or a definition of the variables in the system. This is not an easy task when one of the major inputs is a powder or a bulk solid, and in order to be able to give such set points and definitions of variables, one needs to consider conveying and storage of bulk solids and powders as a part of the total process. The traditional way of handling bulk materials in industry has been conveying from A to B, and storage in sacks, buckets, containers, or silos. Lately, the greater knowledge of the effects of segregation and other phenomena has slowly changed attitudes when designing a new factory. In addition, an increased demand for low emissions of dust to the atmosphere has forced industry to increase focus on the handling of bulk materials.

### **1.3 Aims for this work**

The work in this thesis is aimed to, as given in the title, to quantify and counter the segregation in the aluminium industry. For quantification of the segregation, one needs to sample factories, and from the sample results define points of actions in terms of eliminating or reducing the effect of segregation. Further, once the points of needed actions in the logistic loop of alumina are defined, a proper and sufficient counter action must be found. This may both be implementation of proper equipment and/or alteration of procedures.

The work also will emphasise on development of methods and equipment for identifying

and counter segregation. The development of equipment will not only be focused on making a system, mechanical sane and functional design for implementation, but also seeking to model the system to such an extent that the basics for understanding and basis for design can be established and optimised. The development of methods will mainly be to find a pragmatic approach to sampling of full or partial factories (campaigns), and the ways to analyse and interpret the results from such campaigns in terms of segregation, degradation, and process influences.

Process influences are perhaps one of the most important points, because in order to get funding to work with both sampling and segregation, the only justification in industry will be the economical and environmental importance, although even the economical effects would enough to invoke the investigations.

## **2. LITERATURE SURVEY**

This work will concentrate on preventing segregation primarily during the filling of silos. It is this author's belief that in order to defeat an "enemy" one needs to know as much about him/ her as possible. With this in mind, a detailed review of the literature describing the phenomena encountered in segregation has been carried out.

### **2.1 Mechanisms of segregation**

Segregation is a phenomenon that has long been recognised as the cause of several problems in materials handling situations. However, many more problems are due to this phenomenon than industry appears to recognize. The case often seems to be that industry does not know that segregation causes the problem with the varying particle properties. Some of the earliest investigations were related to the handling of coal [Wettich, 1915, Garve, 1925, Taggart, 1927, Sherman and Kaiser, 1937, Mitchell, 1938, Peacock, 1938, Brown, 1939, Stock, 1944]. In 1925, Garve found what later has been accepted to be the traditional segregation pattern, that small particles were found in the centre of a silo or heap when being filled, and larger particles were found at the walls of the silo or at the edge of the heap. After these pioneers, there seems to be a gap in time before investigators such as Williams [1963, 1973, 1976] and Bridgewater [Bridgewater and Ingram, 1971, Scott and Bridgewater, 1975, 1976, Stephens and Bridgewater, 1978, Cooke and Bridgewater, 1978, Drahn and Bridgewater, 1983, Foo and Bridgewater, 1983] and their co-workers provided information on a number of mechanisms that may act during heap formation, based on systematic research. Significant contributions have also been made by Johanson [1978, 1987, 1988, and 1991], Bagster [1983, 1985, and 1996], and Standish [1985]. Attempts at modelling the segregation process have also been undertaken, notably by Shinohara [1968/69, 1968, 1970, 1972, 1979, 1984, 1985, 1987, 1990, 1992, 1993], Savage [1984, 1988], Popplewell et al [1989], Alonso et al [1991], Arteaga and Tuzün [1991], Dolgunin and Okolov [1995] and Meakin and Jullien [1992]. However, these models seem not to be able to give a complete explanation of segregation, and one may wonder if the shortest way forward is through analytical modelling, or if maybe statistical models would be a good intermediate solution.

At Tel-Tek's Department of Powder Science and Technology (POSTEC), the problems of segregation have been an area of major interest for a number of years. The approach taken has been of a more practical nature. It has been directed to first identifying the mechanisms, and then minimising the effects, the mechanisms of segregation that are most likely to dominate in any given situation. Initially this was not an easy task since the mechanisms that were important were not identified, and one were unable to prove that downstream problems were caused by segregation rather than by some other cause [De Silva and Enstad, 1990]. The work done at POSTEC has therefore been directed at solving industrial problems via identifying the nature and causes of the mechanisms involved, and in this respect Mosby [1996] made a valuable contribution both in systemizing and identifying most of the mechanisms that could be involved. Also in distinguishing between segregation mechanisms and segregation processes or situations, like filling particles into a heap, where several segregation mechanisms become active, Mosby [1996] made a valuable contribution.

Mosby [1996] identified ten different mechanisms of segregation. These are:

- Rolling
- Sieving
- Push-away
- Angle of Repose
- Percolation
- Displacement
- Trajectory
- Air Current
- Fluidization
- Impact

De Silva [1997] added two more:

- Concentration driven displacement (Diffusion)
- Agglomeration

In a more recent work on segregation testers, Salter [1997] also identified a mechanism, which he called 'embedding'. This, however, could probably be the same as that which Mosby called "push-away effects".

Various terms are used to describe these mechanisms, also there are different opinions as to what ought to be called 'mechanisms', and what ought to be called 'processes'. However, at POSTEC it has been decided to stick to the following definitions:

A segregation **mechanism** is a localised event, which leads to the separation of one type of component or size class from another.

A segregating **process** is a situation in which one or more of the mechanisms can become active, for example in the formation of a heap, the filling or discharging of a silo, or the transport of materials on belts or in containers, and their subsequent discharge.

In short, we define the mechanisms as the building blocks of a segregating process.

Others like Bates [1997] have another view of these definitions, he defines what here are defined as mechanisms as processes and vice versa. However, this authors view is that the differences of opinion are restricted to definitions of terms and that the practical consequences are non-existing.

When handling powders or bulk solids, the segregation mechanisms likely to dominate are defined by the powder itself and the actual methods used in handling and processing them. Examples of the latter are airflows set up during the filling of silos, local shear caused by movements or vibrations, rapid or slow filling of heaps, mass- or funnel flow in the discharge of silos, or the introduction of material into processes or systems, which preferentially accelerate or retard the different components in a mixture. Short descriptions of the mechanisms and alternative terms are given later. Systemising the mechanisms defined by Mosby [1996] and de Silva [1997] their place of occurrence are shown in Figure 2-1, naming the mechanisms occurring in the free falling region, together with mechanisms occurring in the heap or silo, which are all mechanisms included in the heap segregation process. The mechanisms below the dotted line are mechanisms occurring as a response to external mechanical vibrations and movements, as well as internal spontaneous rearrangements. The mechanism of agglomeration will change the bulk solids properties with regard to the other mechanisms.



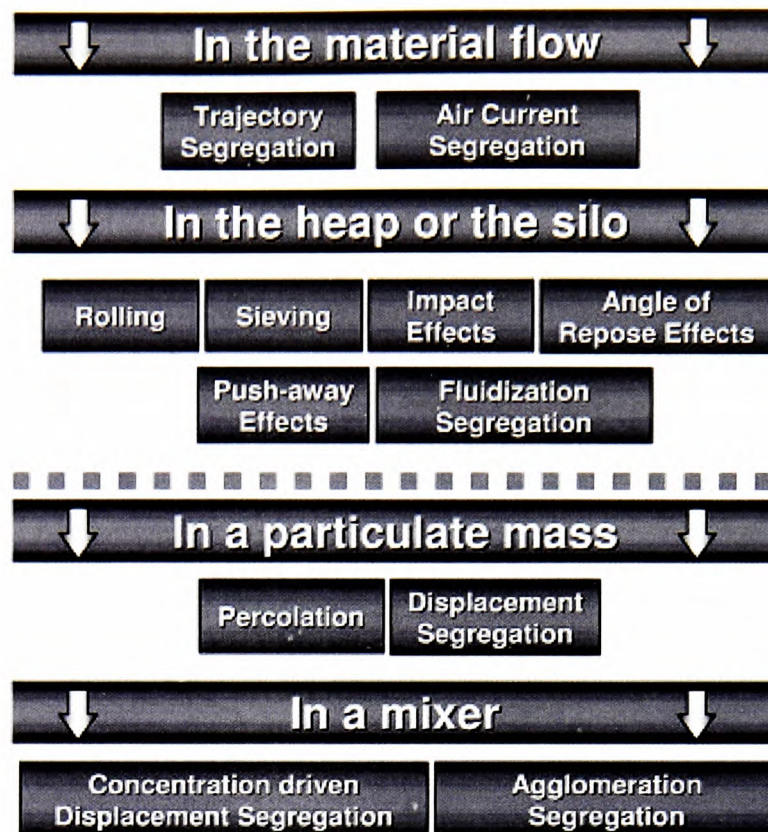


Figure 2-1 Mechanisms of segregation and where they occur, e.g. during filling of a silo, on a transport belt, or in a mixer.

The mechanism of main interest in this work is air current segregation. This is because the property of alumina, and the configuration of the handling process (pneumatic conveying and filling of silos), makes air current segregation the dominant mechanism. Caruthers [1987], de Silva et.al [1991], and own work Dyrøy [1998] suggests this. One might say that fluidisation mechanism should be considered, and it has been, but observations supported the air current mechanism.

## 2.2 Mechanisms and Processes of Segregation

The well-known heap segregation is a segregation process where several mechanisms may be responsible for the segregation that takes place, like trajectory segregation, rolling segregation, sieving, impact segregation, push away effects, and angle of repose effects. Several other mechanisms and segregation processes may cause segregation of particle solids.

### 2.2.1 Trajectory Segregation

Trajectory segregation is caused by the fact that air drag reduces the speed of smaller particles, in free flight, faster than larger (or heavier) ones, which possess a higher level of inertia at the point of discharge. This mechanism could therefore possibly be better called “inertia segregation”. The mechanism is shown in Figure 2-2.

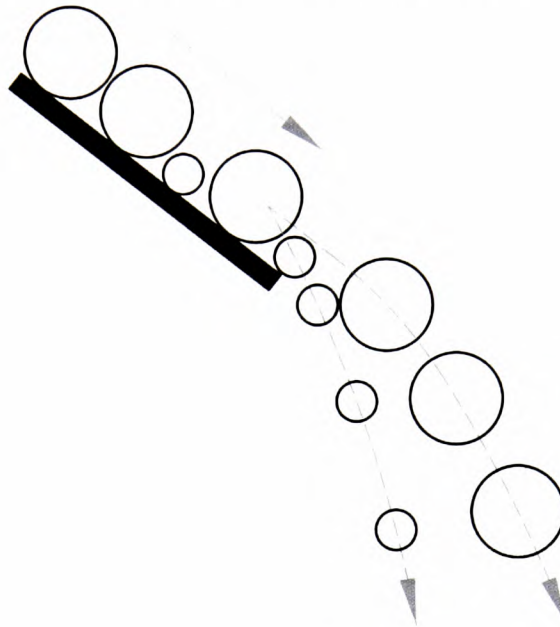


Figure 2-2. Trajectory (or inertia) segregation.

### 2.2.2 Air Current Segregation

This mechanism is caused by a handling regime, for example during the filling of a silo, when a circulating air current is set up from the centre to the walls, which carries fine particles (here air-borne super fines, i.e.  $\sim 50 \mu\text{m}$ ) away from the centre, and deposits them at the walls. This will be commented on at greater length later, since it is this mechanism that will be the main topic of this thesis. The phenomenon is illustrated in Figure 2-3.

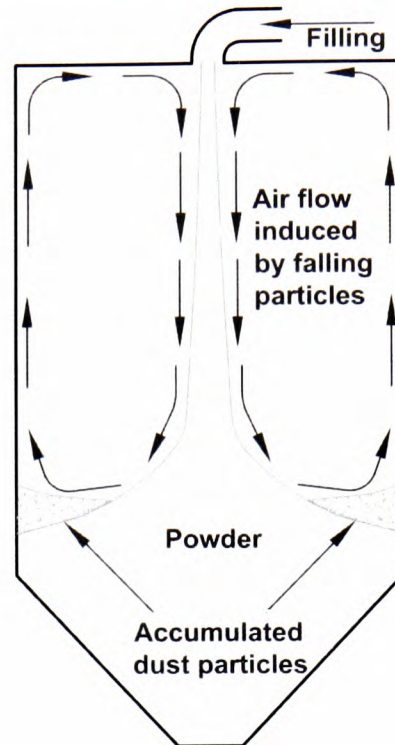


Figure 2-3. Air-current segregation.

### 2.2.3 Rolling Segregation

This is a mechanism by which large or rounded particles roll further down the surface of a heap during its formation than smaller or more angular particles. The principle is illustrated in Figure 2-4.

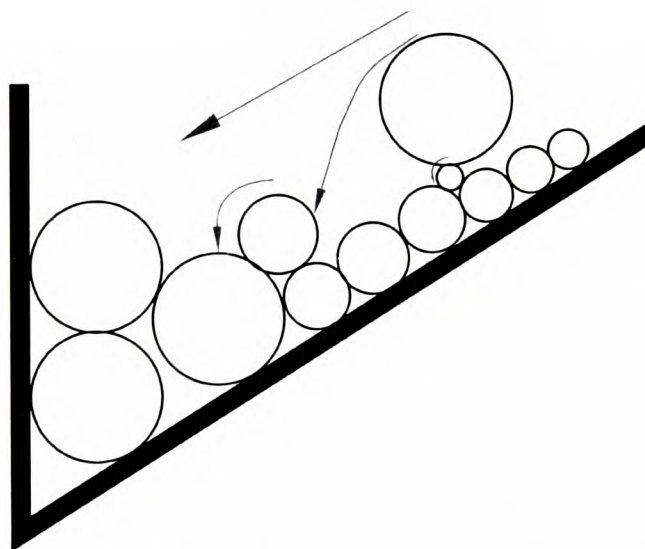


Figure 2-4. Rolling of coarse particle on surface made by finer particles.

## 2.2.4 Sieving

Sieving is a segregation mechanism by which smaller particles flow downward through a rolling or sliding layer of large particles. This mechanism is often referred to as percolation, which, arguably, can be defined as a mechanism in its own right (see Section 2.2.9). The sieving mechanism is shown in Figure 2-5.

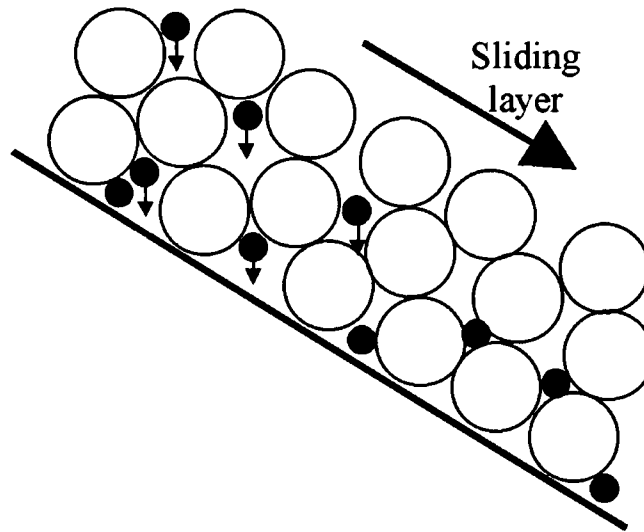


Figure 2-5. Sifting of finer particles between coarser particles when layers slide down a heap surface.

## 2.2.5 Impact Segregation

This segregation mechanism occurs when particles with higher coefficients of restitution bounce off a heap surface, and are found further away from the centre than those with lower coefficients. It could also be called "bouncing". It is also encountered when filling heaps via chutes with bends [Engrav et al, 1991]. The bouncing mechanism when filling a heap is shown in Figure 2-6.

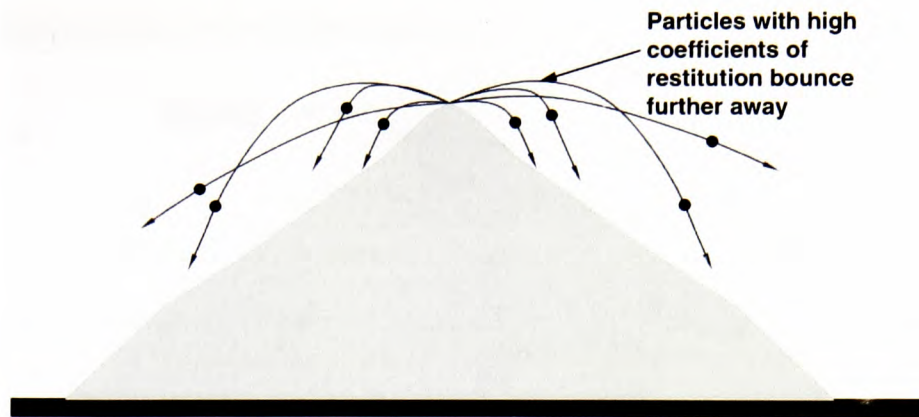


Figure 2-6. Impact effects when filling a heap.

### 2.2.6 Push-away /Embedding

This is an inertia-based mechanism, which causes larger or denser particles to penetrate a layer on the surface of a heap at its apex, and become locked there. It is shown in Figure 2-7.

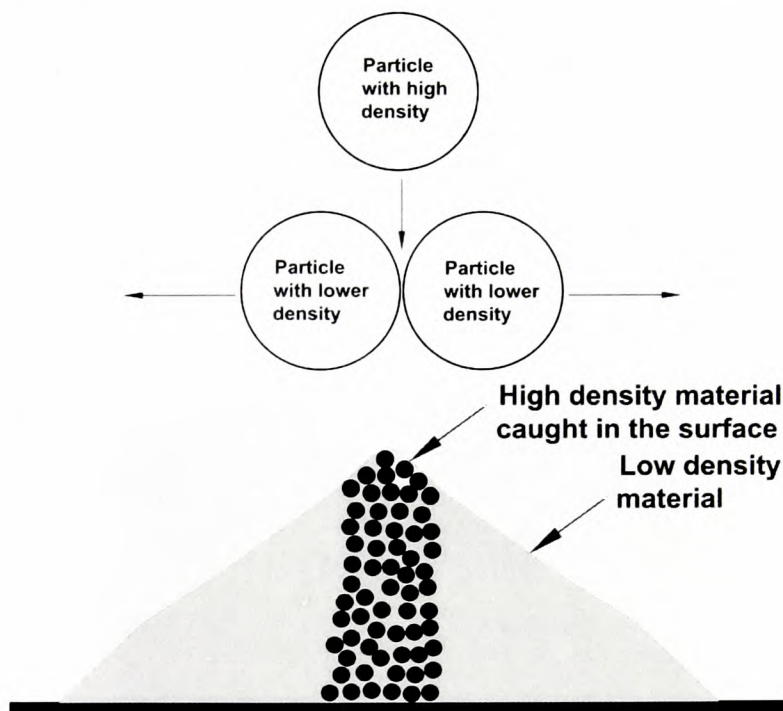


Figure 2-7. Push-away or embedding effect.

### 2.2.7 Angle of Repose Effects

This mechanism is caused by different angles of repose of different components filled sequentially onto a heap, whereby the component with a lower angle of repose flows over

that with a higher angle, towards the edges of a heap, as shown in Figure 2-8.

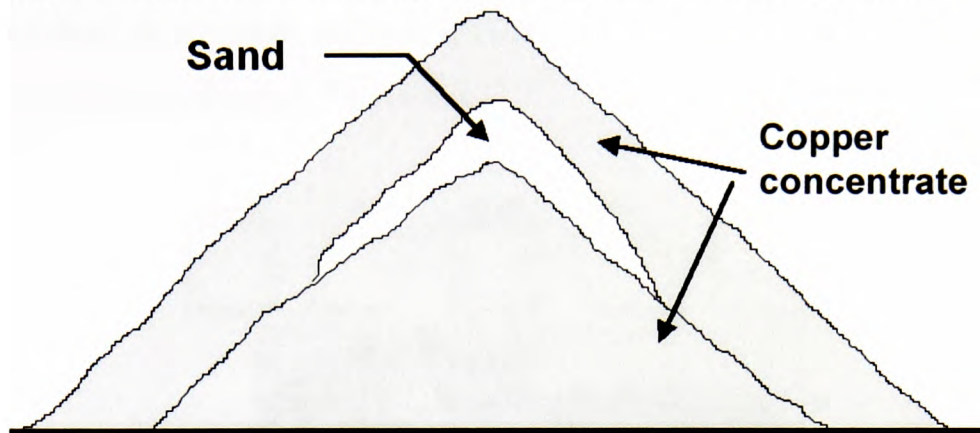


Figure 2-8. Angle of repose effects (here illustrated by sand and copper concentrate).

### 2.2.8 Displacement Segregation

This mechanism, originally identified by Williams [1973], by which larger particles raise to the surface of a mixture of large and small particles in stages, as a result of vertical vibrations. The vibrations, which have to have vertical amplitudes, move a large particle upwards. Small particles flow into the space vacated, and prevents its return. The mechanism has been called “floating migration” by Salter [1997], and is shown in Figure 2-9.

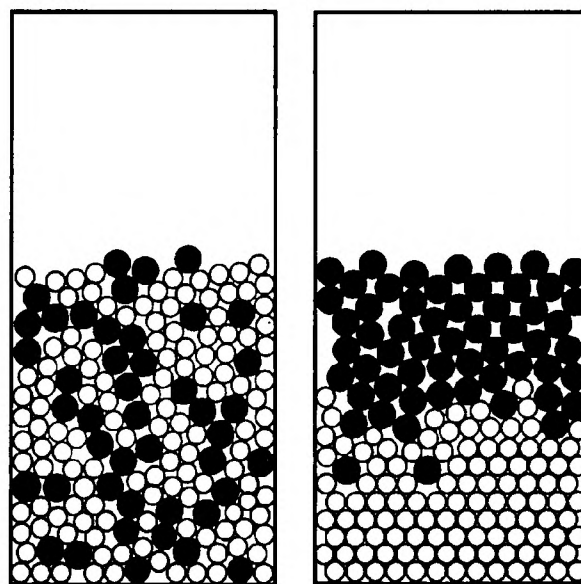


Figure 2-9. Displacement segregation in a vertical vibrating regime.

### 2.2.9 Percolation

Percolation is a mechanism that causes smaller particles to fall through gaps between larger particles because of localised shear. Although similar to sieving, this mechanism does

not require the larger particles to be in a flowing layer. The mechanism can be activated by vibrations or local shear planes, and may also enhance the displacement upwards of larger particles. Its effects are shown in Figure 2-10.

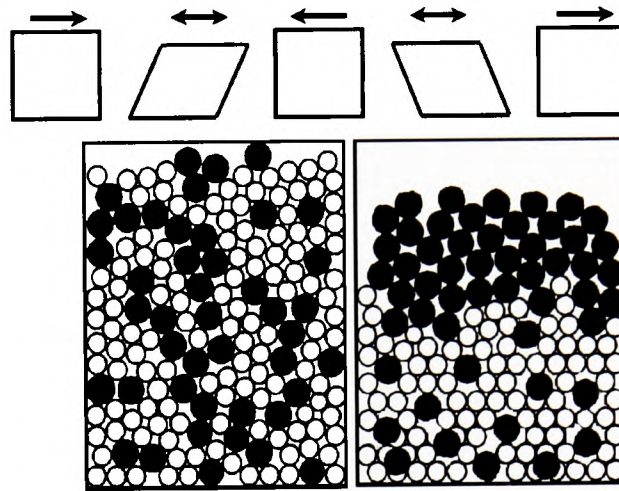


Figure 2-10. Percolation in a horizontal shear regime.

### 2.2.10 Fluidization Segregation

Fluidisation segregation is a mechanism, that keeps a fluidisable component of lighter or finer particles on the surface of the contents during, for example, the filling of a container or a silo, as shown in Figure 2-11.

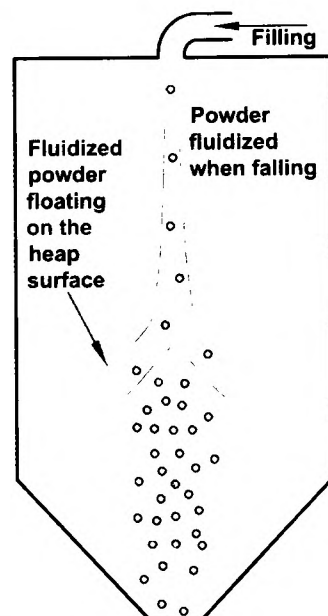


Figure 2-11. Fluidization segregation when filling a silo.

### 2.2.11 Concentration driven displacement (Diffusion)

A mechanism encountered in rotating systems (e.g. drum mixers) where the mobility of fine particles is much higher than that of large particles, leading them to concentrate in zones. The fine particles can pass through the coarse ones, but not vice versa. The forming of the fine core is shown in the end view of the drum in Figure 2-12, and the forming of bands is shown in Figure 2-12 side view.

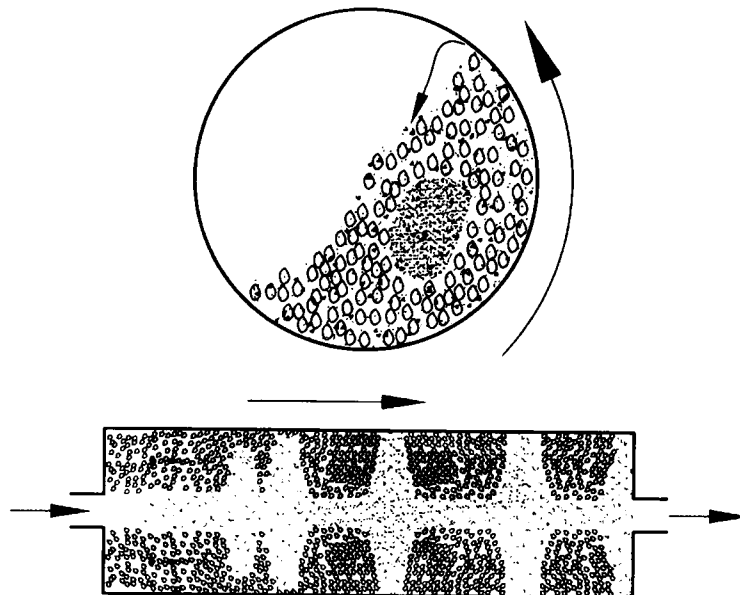


Figure 2-12. Concentration driven displacement (Diffusion)

### 2.2.12 Agglomeration

A mechanism which causes very fine particles to form larger aggregates with greater mobility, again mainly encountered in mixing, as illustrated in Figure 2-13, and in filling of heaps, causing agglomerated fines to be concentrated at the edge of the heap.



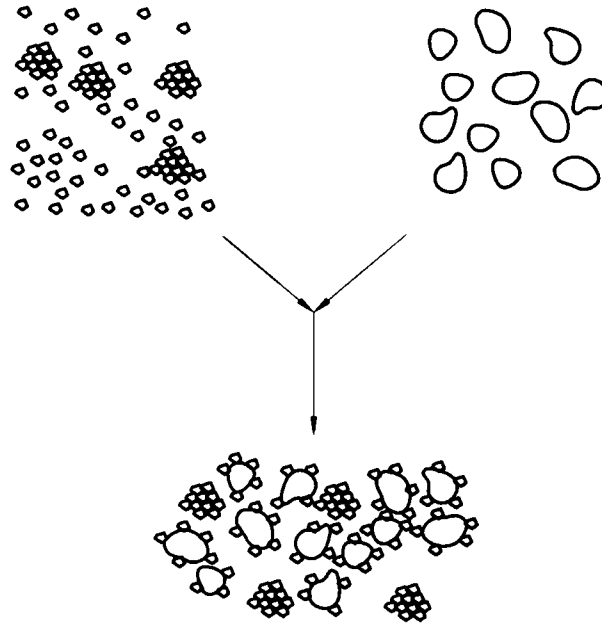


Figure 2-13. Agglomeration of fines creating coarser particles, with different mobility.

## 2.3 Air Current Segregation

Since the work carried out by Tel-Tek dept POSTEC for the aluminium industry, has shown that air current segregation is the most dominating mechanism, a more thorough elaboration of this mechanism is included.

### 2.3.1 Air Current Segregation in General

Air current segregation is covered in detail by only a few authors. One of the few attempts to describe this concept was by Carson et al [1986]. They suggest that finer particles will remain suspended in an air stream for a longer time than coarser ones. Therefore, the air currents created when filling vessels may have the ability to carry small particles away from the filling point before being deposited. In addition, they state that it affects materials with sizable fractions under 50  $\mu\text{m}$  in diameter, while being very important if there is an appreciable quantity of fines with a diameter less than 10  $\mu\text{m}$ .

Mosby [1996] adds to this by asserting that larger particles could well be affected in a similar manner. In particular, if the particles were flaky, air currents could transport them

easily. An example can be taken from everyday life, which would seem to support this suggestion. When leaves fall from trees, the wind often blows them a considerable distance before they come to rest, whereas apples and other fruits will stay where they landed under the tree. While the wind velocity outside may be somewhat greater than the air currents in a silo, the size of leaves are also far greater than the 50  $\mu\text{m}$  reported by Carson et al.

Mosby also reports that a study by Medema [1991] into segregation in alumina storage vessels found that air current segregation caused a considerable separation of the alumina. It was further noted that in addition to the air current segregation transporting finer particles to the periphery of the vessel, another mechanism (fluidisation segregation) caused further concentration of the fines in a layer on the surface of the solids.

While the term air current segregation is specific in identifying air, as the medium that segregates the particles, Bates [1997] prefers a general approach recognising fluid drag as a force that may lead to segregation. Bates also takes a broader approach to the properties that may affect the materials' likelihood to segregate in this manner, listing particle size, shape, density, and surface morphology.

The fluid drag force is then linked to three different processes that cause segregation, i.e. elutriation, transverse and counter current gas flow. The separation of particles when filling a storage vessel is likely to be a combination of these three processes. Initially, elutriation of the particles may cause their separation from the bulk of the powder, followed by further segregation by transverse air currents, as the powder settles out due to the diminishing lateral air velocity. Finally, as the air currents travel up the side of the vessel, some counter current segregation may occur as some particles settle out, while the air stream carries others away.

Johanson [1978, 1987 & 1988] regarded segregation caused by fluid drag forces to be particularly important during the horizontal discharge of solids, e.g. from a belt conveyor. When discharged with a horizontal velocity, small particles will be affected more by the air resistance than larger particles. In this manner, the horizontal velocity component of

the smaller particles will be reduced faster than that of the larger particles. This in turn leads to the larger particles travelling a greater distance from the feed point than their smaller counterparts.

While this effect is caused by those same forces that are responsible for air current segregation in storage vessels, it will lead to a different result. Johanson does give one qualification on the ability of fluid drag to cause the segregation of particles saying, “a stream of material drags a stream of air along with it, preventing the full drag force from being felt by each individual particle”. This idea can be taken further by saying that only particles at the edge of the stream feel the drag forces while those in the centre of a particle stream are unlikely to feel any drag forces. From this it may be assumed that if the particles are tightly packed together in the stream, such as that encountered during the gravity discharge of a silo, they will be less affected than those in a diffuse cloud such as that created from the discharge of a dilute phase pneumatic conveying system.

### 2.3.2 Air Current Segregation in the Filling and Discharge from Silos

Air current segregation occurs when filling tall silos with material having a wide size distribution and a significant dust content (particles below 50  $\mu\text{m}$ ). Alumina used in the manufacture of aluminium is such a material. Air currents are induced by material streams falling through the middle of a silo, and turn outwards on meeting the surface of the material heap already in the silo. Air currents are also generated from transport air when using pneumatic conveying. As the airflow moves towards larger radii it loses velocity and finer and finer particles are deposited near the walls of the silo, with nearly all the dust present being deposited as the airflow turns upwards at the walls. When the policy of keeping constant level over longer periods of time is practiced in a funnel flow silo, fines are accumulated near the walls and introduced to downstream processes, when the level is allowed below a certain height, as shown in Figure 2-14. This silo is operated in core/ funnel flow, and therefore the material by the wall is stagnant. The alumina consists in principal of two crystalline phases, alpha and betha. These have different particle density (betha 2,8 and alpha 3,9), and this could suggest that impact segregation could occur, however, the surface area of these small particles are dominating compared to the specific weight, also the

smaller particles (alpha) is the heaviest of the two, and based on the density a beta particle 1,4 times larger than the alpha would behave similar.

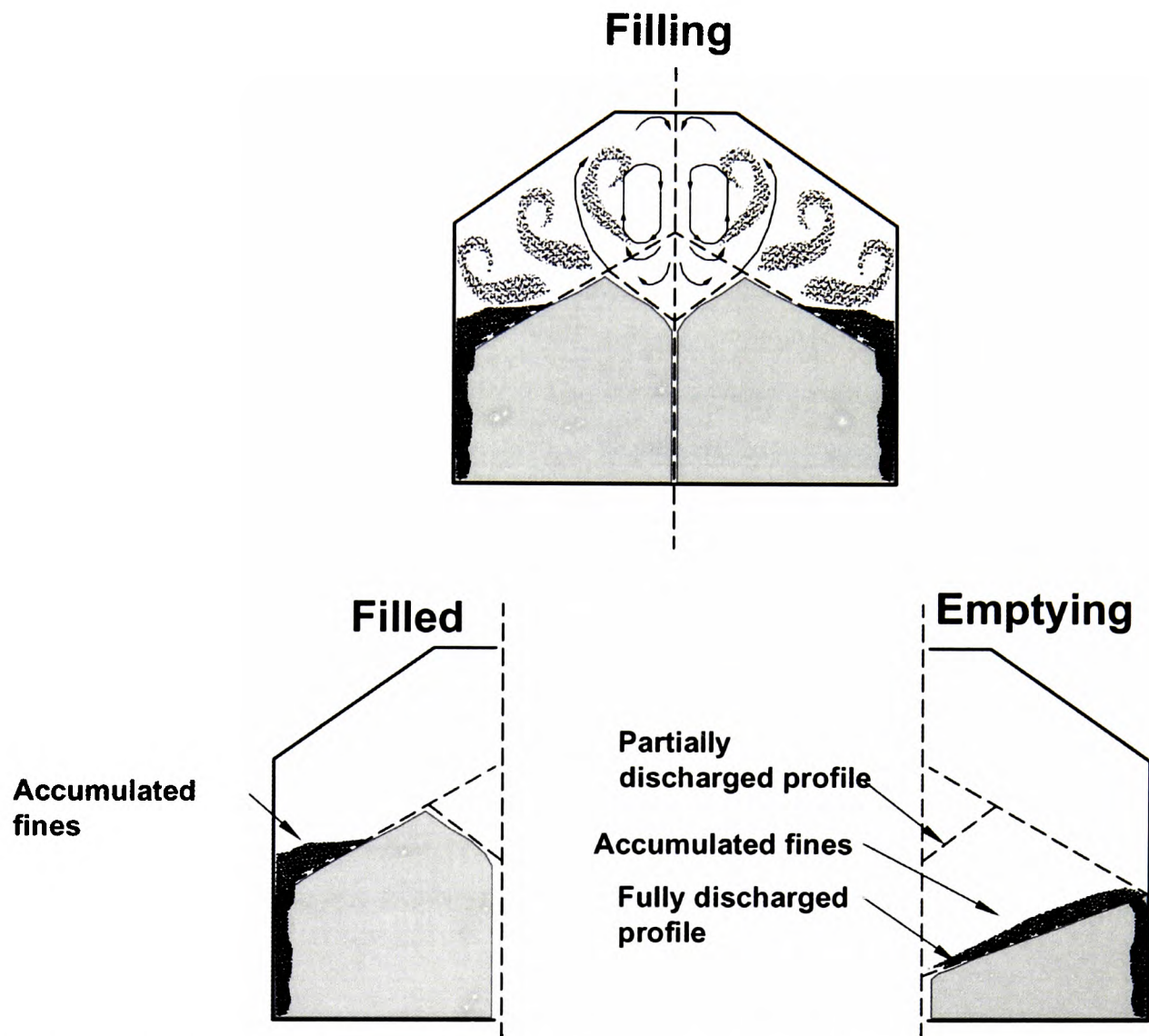


Figure 2-14. Air current segregation when filling a silo causes accumulation of fines when keeping a constant level, which is introduced to the process when the silo is discharged more than normally [Carruthers, 1987].

## 2.4 Segregation and aluminium production

Tests have shown that the mechanism of air current segregation dominates in the handling of alumina and in the total aluminium production, i.e. from bauxite through alumina to aluminium. In order to understand the potential influence of segregation one first needs to know the overall process for aluminium production.

### 2.4.1 Handling of alumina in aluminium production

On a worldwide basis the production of alumina is somewhere between 40-50 million tonnes per year. The price of alumina when bought on long-term contracts between the refinery and the aluminium producer varies between 11-13% of the aluminium price at the London Metal Exchange. Beside this market, there is also a spot market, in which the prices vary from 200 to 400 USD. Given these quantities and prices, and knowing that the same alumina is handled several times: at the refineries, between refineries and aluminium producers, and within aluminium plants, the total quantity of alumina handled becomes very large. Taking into account that alumina is a free flowing material, which will segregate readily, and that segregation is likely at every transfer point, the potential for quality variations at the point of use, i.e. at the entry to the electrolysis cells, is significant.

In order to understand the importance of the phenomenon of segregation when producing aluminium, however, one needs to understand the total process from the manufacture of alumina from bauxite, through the various operations involving the alumina right through to the conversion of the alumina to aluminium. All the operations on the refinery site as well as on the primary metal site need to be considered.



Figure 2-15. Bauxite, alumina and aluminium.

## 2.4.2 Production of Alumina

The description of the process can be found in (<http://www.qal.com.au>). Alumina is today mostly produced using the Bayer Process, which has been found to be an economical method of producing aluminium oxide. The process was discovered by the Austrian chemist Karl Bayer and patented in 1887. The process dissolves the aluminium component of bauxite ore in sodium hydroxide (caustic soda). Further one removes the impurities from the solution and precipitates aluminium tri-hydrate (aluminium hydroxide, hydrate,  $\text{Al}_2\text{O}_3 \cdot 3\text{H}_2\text{O}$  or  $\text{Al}(\text{OH})_3$ ), which is then calcined to aluminium oxide.

### 2.4.2.1 *Bauxite and Bauxite Mining*

Alumina recoverable by the Bayer process is found in bauxite as gibbsite (tri-hydrate), boemite (monohydrate) and diaspor (also a monohydrate). Bauxite is the residue of weathering process of other rock formations. These weathering processes take place in tropical wet climates over millions of years. The bauxite contains a number of other weathering products such as metal oxides (iron, titanium, etc.), silicates, clays, and quartz.

Bauxites are normally found in pockets (Jamaica) or blankets (South America, Australia) and are mined in open pit mines after removal of the overburden. In some areas such as Southern Europe, the bauxite has been subject to secondary geological transformations. These bauxites lie deeper and require under ground mining.

In open pit mining, it is common practice to restore the area after the bauxite has been mined out. The overburden is returned with the top soil on top and the area reclaimed.

### 2.4.2.2 *Digestion of Bauxite*

Bauxite is ground in mills to allow better solid liquid contact during digestion. Recycled caustic soda solution is added to produce pumpable slurry, and lime is introduced for phosphate control and mud conditioning.

The silica component of the bauxite is chemically attacked by caustic soda, causing alumina, and soda losses by combining to form solid desilication products. To desilicate the slurry prior to digestion, it is heated and held at atmospheric pressure in pre-treatment tanks, reducing the build-up of scale in tanks and pipes. Most desilication products pass out with the mud waste as sodium-aluminium-silicate-compounds.

The monohydrate slurry is pumped through agitated, vertical digesters. Mixed with steam and caustic solution, alumina in the bauxite forms a concentrated sodium aluminate solution leaving undissolved impurities, principally inert iron and titanium oxides, and silica compounds.

#### 2.4.2.3 *Clarification of the Liquor Stream*

Most red mud waste solids are settled from the liquor stream in settling tanks. The mud is washed with fresh water to recover the soda and alumina content in the mud before being pumped to large disposal dams. Slaked lime is added to dilute caustic liquor in the washing process to remove carbonate ( $\text{Na}_2\text{CO}_3$ ) which forms by reaction with compounds in bauxite and also will emit carbon dioxide to the atmosphere, which reduces the effectiveness of the liquor in dissolving alumina. The overflow liquor from the settlers is filtered.

#### 2.4.2.4 *Precipitation of Aluminium Hydrate*

Dissolved alumina is recovered from the liquor by precipitation of hydrate crystals ( $\text{Al}_2\text{O}_3 \cdot 3\text{H}_2\text{O}$ ). The cooled pregnant liquor flows to precipitation tanks, which are seeded with crystalline aluminium tri-hydrate. The entry temperature and the temperature gradient across the row, seed rate, and caustic concentration are control variables used to achieve the required particle size distribution in the product. As correct particle size is important to smelter operations, sizing is carefully controlled.

The finished mix of crystal sizes is settled from the liquor stream and separated into different size ranges in multi stage "gravity" classification tanks. In plants that are more mod-

ern, hydro cyclones are used for classification. The primary classifiers collect the coarse fraction, which becomes the product hydrate. The intermediate and fine crystals from the secondary and tertiary classifiers are washed and returned to the precipitation tanks as seed.

After precipitation, the liquor (spent liquor) is heated, and the excess water picked up in the cycle is evaporated and used as steam for heating. The liquor is then returned to digestion for another cycle through the process. Makeup of lost soda is done as an early stage in digestion.

#### 2.4.2.5 *Calcination of Alumina*

The coarse hydrate slurry ( $\text{Al}_2\text{O}_3 \cdot 3\text{H}_2\text{O}$ ) from the primary thickeners is pumped to hydrate storage tanks and is filtered and washed on horizontal-table vacuum filters to remove process liquor. The resulting filter cake from the vacuum filters is fed to calcining units. These units are circulating fluidised bed calciners, fluid flash calciners, or rotary kilns. The feed material is calcined to remove both free moisture and chemically combined water. The finished alumina is cooled and discharged on to conveyors, which convey it to storage such as silos or A-frames where it is stored before shipment. The typical capacity of a refinery is between 0,6 to 4 mill. tonnes per year. The shipments may vary from 10 kton to 40 kton (Panamax ~ 60 kt Australia to US or other intercontinental routes), however, the size of ships delivering to the aluminium plants tend to increase towards the maximum 60 kton. The size of the shipments defines the size of the main storage both at the refinery and at the receiving aluminium plants. This main storage has the form of either a silo/ silo battery or an A-frame storage. Neither is exempt from the effects of segregation.

### 2.4.3 Aluminium Production

#### 2.4.3.1 *Storage and Conveying of Alumina at Aluminium Plants*

Main storage units used for alumina at the aluminium factories are silos and A-frames, with capacities equivalent to one or several shipments of alumina (10-60.000 tonnes).



These silos are filled whenever the shipments arrive, and are drained at a rate of approximately twice the tonnage capacity of produced aluminium.

For conveying the alumina from the site of reception (in Norway generally a quay) to the plant, and for transport internally in the plant, trucks, conveyer belts, pneumatic conveyors, air slides and other types of conveyors are used. When conveying large quantities usually belt conveyors are used, but transport internally within the plant involves nearly the use of as many systems as there are plants! Downstream from the main storage facilities there are fume treatment facilities, fed from a buffer silo of primary alumina, and one silo after these for storage of the secondary alumina, as it is called after it has been used in dry scrubbing. From this buffer silo, the secondary alumina is conveyed to the pot-rooms.

#### 2.4.3.1.1 Distribution of Alumina to the Electrolysis Cells (Pots)

This is done in several ways. Some plants use front loaders, which are driven from cell to cell, and the alumina is filled into small feed silos on the cells. Others use overhead cranes. Pneumatic conveying systems are used by some, but maintenance with these has been found to be high due to the erosive nature of alumina. The latest system that this author is acquainted with uses a tank wagon, which fills specially designed feed silos pneumatically. During a long-standing cooperation between Tel-Tek and the Technology Centre at the Hydro Aluminium Aardal Plant, a system based on air-slides has been developed, which has been shown to work very satisfactorily. This system runs at low velocities, and involves a minimum of manual intervention.

#### 2.4.3.1.2 Feeding Alumina to Electrolysis Cells

Traditionally alumina is fed to the cell by volumetric dosing. Various systems are again used. The main parameters that one wishes to determine are the optimal frequency of the doses and their optimal sizes, with regard to solution time, temperature, and power consumption in the cell. Investigations so far point towards clear advantages of using frequent small doses. Example, pots are feed with 200 g pro dose, and the frequency given by the

consumption of alumina, which depends on the amperage for the electrolysis pot, and the number of feeding points.

#### *2.4.3.2 The Electrolysis Process*

Aluminium is obtained from alumina by electrolytic reduction - the removal of oxygen atoms from aluminium oxide in a process of electrolysis. The calcined alumina is reduced to aluminium metal in electrolytic cells, or "pots", connected in series to a direct current power source. The cells are rectangular steel pots lined with refractory bricks and carbon blocks acting as the cathode.

The pot contains a molten electrolyte, called "bath" in which alumina is dissolved. The electrolyte is a mixture of cryolite ( $\text{Na}_3\text{AlF}_6$ ), a molten salt, and certain additives to give it appropriate density, conductivity, and viscosity. The principal additive is aluminium fluoride ( $\text{AlF}_3$ ) which must be replaced from time to time due to losses through evaporation and a chemical reaction converting it into more cryolite. The emitted fluorides are collected, treated, and recycled to the pots, in the form of secondary alumina.

Suspended in the electrolyte are a number of anodes (positive electrodes) which act as electrical conductors for the high intensity direct current.

Electric current passing from the anode through the electrolyte to the pot wall, which acts as the cathode, reduces the alumina molecules into aluminium and oxygen at a temperature of approximately  $950^\circ\text{C}$ . This process is called electrolysis. The oxygen is released at the carbon anode, where it combines with the carbon to form carbon monoxide and carbon dioxide ( $\text{CO}$  and  $\text{CO}_2$ ). The aluminium, being heavier than the bath, settles to the bottom of the pot. Considerable electrical energy, between 13 and 17 kWh per kilogram of aluminium, is consumed in the process.

#### 2.4.3.3 *Fume treatment using alumina (dry scrubbers)*

Each pot is tightly closed to achieve greater energy efficiency, and ventilated to capture the pollutants emitted, which are then treated to reduce environmental pollution to a minimum. There is, however, a concern regarding particulate emissions. These occur when the alumina is being introduced into the pots, during which a hole is made in the crust of the bath, and the alumina allowed trickling in through the hole. If there are too many fines in the feed material, these are either sucked out by the ventilation system, or come out into the working environment whenever the pots are opened.

At regular intervals, the molten aluminium is sucked from the bottom of the pot into large ladles and transferred to holding furnaces for casting.

#### 2.4.3.4 *What effects the aluminium production*

The production of aluminium through electrolysis is a complex process. Several variables affect production. These can be the lining material and operational behaviour, the composition of the anodes, and of course the operational method. When operating a potline, a phenomenon called Anode Effects (AE), occurs from time to time. Grjotheim and Welsh [Grjotheim and Welsh 1998], describes it as a sudden increase in the cell voltage, from normal operating conditions. The increase in voltage defined as an AE vary depending on the cell technology. The increase can be from a few volts up to 50 volts, this increase leads to production of carbon-tetra-fluoride-gas, and minor amounts of other fluorides. These gases have an overall CO<sub>2</sub> equivalent of approximately 8 000 to 10 000, hence this phenomenon is not wanted in a high frequency. All increase in voltage during an AE is transferred into heat, affecting the thickness of the side ledges, and the overall heat balance in the pot. The AE decreases the Current Efficiency, hence the effect consumption of producing the aluminium. AE are depending on the concentration of alumina in the molten cryolythic bath, and the concentration of the alumina is again depending on the nature of the alumina, i.e. the particle size distribution. Knowing this and that alumina is the main raw material for the aluminium production variations, of the alumina would be of importance. Fines (sub 45 µm) are considered to have lower dissolving rates, and thereby the

process stability would be influenced by large and rapid variations in the alumina fed to the electrolysis cells. In addition, the concentration of  $\text{AlF}_3$  in the cell influences the heat in the cell, and therefore the recirculation of  $\text{AlF}_3$  is desired to be as constant as possible. Overall, any variable or incident affecting the heat balance in the pots, have a deterring influence of the efficiency in which one produces aluminium.

In addition, dust emissions to working atmosphere during operations at the pot are influenced. Furthermore, the frequency of operations needed to be carried out at one specific pot, increases by the deviations created by variations in the alumina feed to the pot. This leads to exposure to heat, hazardous gases, and dust for the operators.

When considering the above, and all the aspects in which variation in bulk solids may influence the overall efficiency of aluminium production, it does not seem far fetched when experts in the community suggests that up to 1 % of the current efficiency is lost because of segregation, depending on the value of the initial current efficiency.

## **2.5 Summary and Commentary of Literature Survey**

The segregation phenomena have been discussed in many publications, dating back to as early as 1915, and even perhaps earlier. One should therefore believe that the problem should have been well debated and solutions developed. However, this is not the case. In the academic world of powder technology, discussions of details like definitions of what is a mechanism or a process are taking place. In this work mechanisms are defined as the small building blocks creating the total picture of segregation in given processes or situations. Overall there has been singled out 12 mechanisms from the literature during this work, and the processes and situations in which they occur have been described. Although the literature on segregation is quite extensive, it seems that the description of segregation itself has been in focus and not the impact that segregation has in a given situations/ processes, although one should expect that this would have been of great interest. The intent of this literature survey of segregation is to seek to understand segregation, in terms of finding means to identify and counter it. The literature also shows that when handling alumina, the mechanism called air current segregation is the dominant one, although it is the firm

belief of this author that all the identified mechanisms occur all the time, just with varying degrees depending on the circumstances. The air current mechanism can and will accumulate fines at the silo walls, if the material surface there is not renewed quite frequently.

The production of aluminium starts at the alumina refinery. The quality of alumina is determined even when the first shuffle is put into the ground digging out bauxite. The chemical composition of the resources determines the downstream potential quality of the alumina. In addition, the refining process itself has a long development, but it seems that it is just in the later (from say the 1970-ies) years that the quality of the finished alumina has come into focus. The calcining and dissolution processes have been thoroughly investigated in order to optimise the quality and yield, but even more so the digestion step. The calcination process today more and more moves away from the traditional rotary kilns into so-called fluid-flash method, utilising high temperature fluidisation techniques. The typical refineries now are growing in size, and it is anticipated that a refinery could become up to 7 million tonnes of annual production. Whithout a proper understanding of topics like segregation, handling of such amounts can cause many problems.

Getting into the electrolysis process quickly reveals an in many ways uncharted very complex process, although it is an old process concept. Not, in any way, under estimating the efforts made by people in the industry, but clearly suggested effects by segregation on the process have been ignored for years. The reason for this neglecton may be that the effects of segregation have drowned in the noise from other more dominant electrolysis issues. However, the literature suggests that variations in any way of the raw material composition will affect the heat balance, i.e. the energy consumption of production, and the occurrence of anode effects, hence the current efficiency. With that as an inspiration, the challenges ahead in time will be many, when forcing downwards the margins in electrolysis design and production of aluminium.

### **3. SURVEY OF SEGREGATION IN AN ALUMINIUM PLANT**

When discussing the segregation and anti measures that can be undertaken one often forget the most important tool in anti segregation work. Of course the Anti Segregation System and Anti segregation Tube are by this author considered quite important, but no system can act blindly, therefore it this author's strong belief that the most important anti segregation measure one can have is characterisation. If the information about the factory in terms of variations, and where the variations occur, is not accurate, implementation of anti segregation measures are easily wasted. It is strange that at new sites one invest in all kinds of process control, lab equipment etc, but when installing the bulk handling system no sampling points are even considered, not even a flange creating an easy access. To get a thorough control over a factory, a standardised sampling procedure and points should be established as a part of the installed equipment. All the campaigns carried out as a basis for this work, have, been a compromise of accessibility, extent of work and of course costs, as can be seen later. The costs would have been much smaller if sampling points were embedded in the design of the factory, instead of implemented when needed for campaigns or other troubleshooting.

#### **3.1 Philosophy behind full factory campaigns**

The study of the interaction between the aluminium reduction process and powder technology, represented largely by segregation is inspired by the fact that the handling of alumina is an essential element in the production of aluminium. The alumina is stored at a main storage site, conveyed to buffer silos, passed through the fume treatment plant, stored in buffer silos for secondary alumina, distributed to the pots and eventually fed to the electrolysis process. Regarding this path, one may see that logistics, process, and environment are interacting all the way. The logistics have impacts on both the process and the environment. Logistic has an environmental impact trough the dust emissions when conveying and handling alumina. Further the logistic needs to supply a constant feed of alumina to the process in order to make it stable. A stable process requires less operator intervention, hence less exposure for operators to heat, dust, and gases. As a result, the total emissions of gases and dust to the atmosphere are reduced. The alumina plays an active role in the

regaining of fluoride from the process gases (fume treatment -dry scrubber), and also here the stability of the raw material input is a key feature, in ensuring good cleaning efficiency (philosophy illustrated in Figure 3-1).

Environmental demands from governments and the public therefore enforces the need for a controlled interaction between the process and raw material handling.

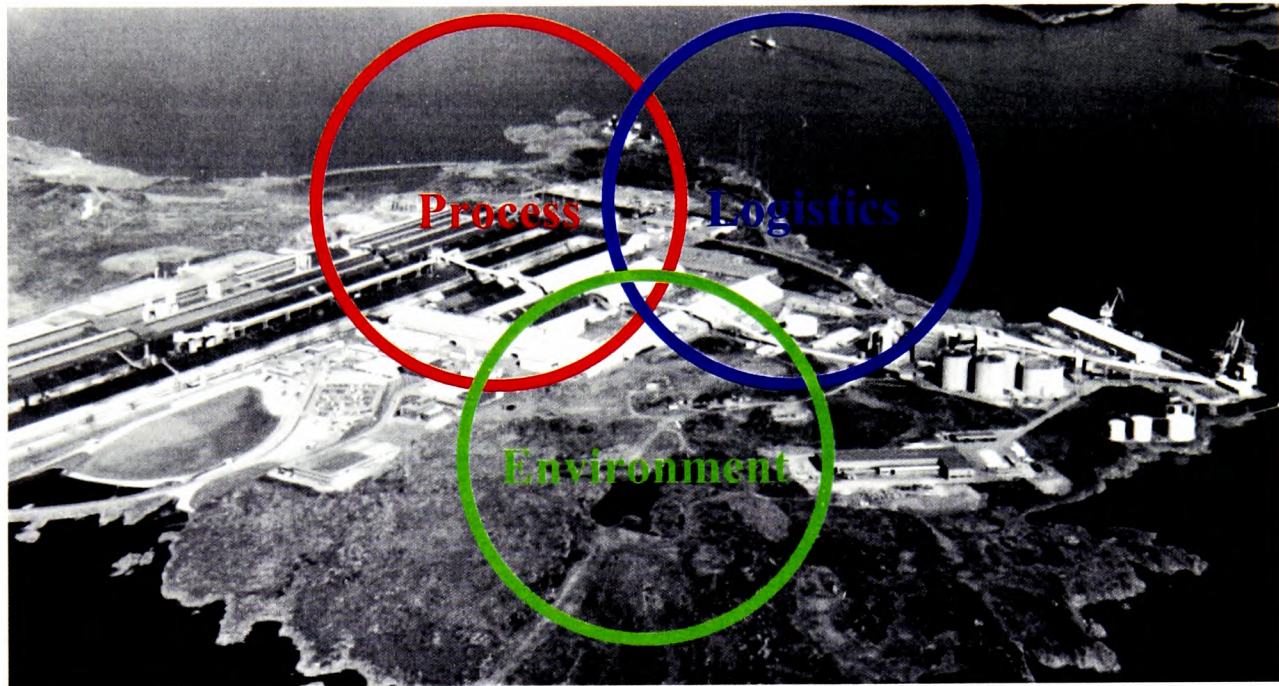


Figure 3-1. Philosophies behind the anti segregation work in industry.

### 3.2 Sampling of whole factories

As other industries, the aluminium industry have built their sampling on standards, for sampling they utilise ISO 2927 [ISO 2927, 1973] and for analysis they use ISO2926 [ISO 2926], and for preparation and storage of samples ISO 802 [ISO 802]. The standards for sampling are quite similar for both coke and fertilizers [ISO Technical Report 7553, ISO 3963], in calculating the minimum size of sample, namely based on the mean diameter of the particle in the sampled bulk. The standards goes on to describe the method of retrieving the sample from belt conveyers, by either stopping the belt or utilising a mechanical sampling, taking a whole section of the belt. The methods described in the standards are coherent with the basic principle described by Gy [Gy 1998]. However, Gy clearly ques-

tions the practicality of stopping belts for sampling, based on the fact that the energy needed to restart full belts of some length. This can only be seconded by this author. Another fact that also needs to be put on the agenda is the point of effect of stops to the belt conveyer during unloading ships, which would be the typical case in the aluminium industry. The costs for a sampling will increase dramatically if it dictates the time needed for unloading a ship, due to de-murage costs for the ship. Gy also quite clearly states his opinion of what usually are referred to as “grab samples”. This should by his opinion be avoided, and he supports this with statistical theory. This will not be disputed here, but the standards and Gy have all one thing in common, they are aimed to get a representative sample of the bulk, whereas the usual need in the process, industry is to see relative changes in the bulk. By aiming for the correct sampling principle of taking a sample of the whole stream, cutting one section of a linear one-dimensional conveyer, a consequent repetition of the sampling and picture of the changes through a material loop can be quantified. The size of the sample must of course be big enough, so that one can reduce that part of errors. The minimum needed for the sampling campaigns in the aluminium industry has been to be able to characterise the relative changes of the bulk after being stored, conveyed or treated in any way.

### 3.2.1 Designing sampling of an aluminium plant

Below in Figure 3-2, a simplified layout of a single lined aluminium smelter is shown. In Figure 3-2 sample points A through H are given. These points represent the typical approach used for campaigns. Characteristic for the sampling points are placement before and after a major handling operation. Sample point A, is taken during a shipment of a larger amount of alumina for the main storage. This filling of a main storage typically is carried out during a shorter period of time, and to a rate varying between 100 and 800 t/h, therefore the sampling frequency is set to match at least one sample for each increment representing the tonnage equal to the daily consumption of alumina for the electrolysis process. If possible, a larger frequency is preferred, but this is adjusted to fit the rest of a large campaign, both in cost and resources.



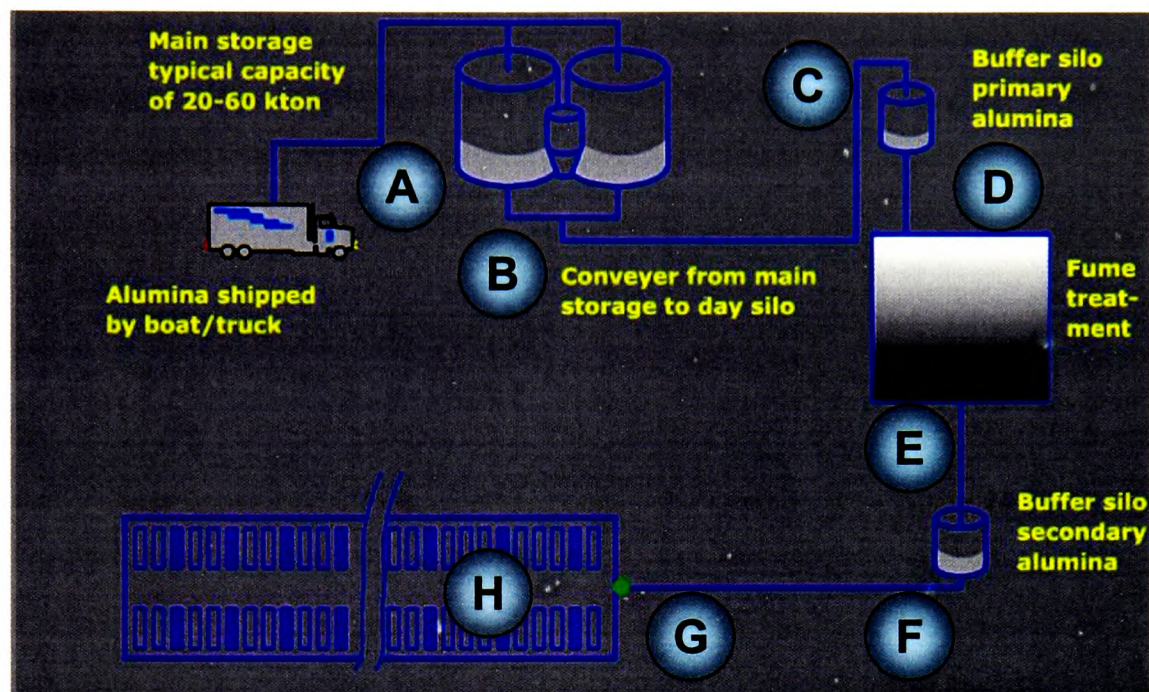


Figure 3-2. Simplified layout of aluminium plant.

The samples in such points are preferably taken from air slides, where the sampling of the full stream is easiest, but also samples from belt conveyers are taken as what best would be characterised as stroke samples, simulating the action from any mechanical sampler. Later sampling of such ship unloading will be shown in more detail.

The points further down the stream from B to H are collected once or twice a day, depending on how many parallel electrolysis lines are covered or in existence, meaning that point C could possibly be sub divided in CA, CB, CC until Cn, where n is the number of fume treatment plants at the smelter. This will consequently result in a large number of samples, especially when considering the fact that the samples taken at the electrolysis cells/ pots will be from at least 11 pots in each line.

The duration of the sampling is determined by the process cycles, specially the cycles of alumina shipment, but just as important the anode change cycle of the cells/pots. Usually this takes 28 days, but this varies from smelter to smelter. In addition, the shipments of alumina have a cycle, and are usually once a month. In order to cover the different routines the typical campaign has been set to 40 days, to be able to identify cycles, and not bias the sampling at the end or beginning of any cycles. Looking at Figure 3-2, and imagining the

parallels, knowing the number of cells sampled, duration of sampling and the frequency (once a day), one can quickly calculate that these campaigns become considerable. The campaigns will vary between 1 000 to 3 000 samples of alumina, each sample of 1 kg, resulting in a total of alumina in samples up to 3 tonnes.

### 3.2.2 How is the sampling done

The sampling in itself is carried out, aiming for the good practice described both by ISO standards and by Gy, namely by collecting a cross section of the complete material stream. For air slides, this has two outcomes. One, if the air slide is shut down, and a complete section of the powder in the air slide is removed similar to the isolation of a section on a belt. The length of such a section depends on the degree of filling in the air slide, but the sample size usually becomes approximately 1 kg. Two, if the air slide is running, the sample collector used is formed in such a way that the whole stream is cut during the time it takes to fill the collector. Samples from the electrolysis pots are collected by collecting a full dose from the dosing system on the pot. Overall, by collecting samples in the size range of 1 kg, and considering the largest particle being 200  $\mu\text{m}$ , the disturbance has been found to be, if not eliminated so at least much damped. When collecting from a belt conveyor, the sampling becomes slightly less according to the standards. For belt conveyers with low capacity one is able to collect the full stream by stroke the collector across the belt, but for belts with high capacity this becomes difficult, and therefore such samples are collected in transition points, or in the nearest air slide available in the logistic string.

When sampling in a continuously running process, one must remember that, all sampling demands accessibility to the process, to be able to collect the sample undisturbed. If there are operations on the cells/pots or in the process in general in conflict with the sampling when the sampler arrives, the process routines always have priority. Therefore, constant time intervals between samples become impossible to achieve. Therefore, one has rather tried to take it completely in the other direction, namely varying the time for sampling in any given point as much as possible.

### 3.2.3 Method of analysing the sample results from sampling campaigns

When the samples are collected and brought back to the lab for particle size analysis, the analyses of the “happenings” are carried out using ordinary statistics. Equation 3-1 through Equation 3-3 are basic statistical equations, whereas Equation 3-4 is a definition much used in the powder and bulk solids handling, de Silva [1997].

$$\bar{X} = \frac{1}{n} \cdot \sum_{i=1}^n X_i \quad \text{Equation 3-1}$$

$$S = \sqrt{\frac{\sum_{i=1}^n (X_i - \bar{X})^2}{n-1}} \quad \text{Equation 3-2}$$

$$C_{\text{var}} = \frac{S}{\bar{X}} = \frac{\sqrt{\frac{\sum_{i=1}^n (X_i - \bar{X})^2}{n-1}}}{\frac{1}{n} \cdot \sum_{i=1}^n X_i} \quad \text{Equation 3-3}$$

$$H_{\text{fact}}^{\frac{i}{j}} = \frac{C_{\text{var } i}}{C_{\text{var } j}} = \frac{\frac{S_i}{\bar{X}_i}}{\frac{S_j}{\bar{X}_j}} = \frac{S_i \cdot \bar{X}_j}{\bar{X}_i \cdot S_j} \quad \text{Equation 3-4}$$

Where:

- $\bar{X}$                       The average value of a series of n samples
- $S$                         The standard deviation, based on n-1, for a series of samples
- $C_{\text{var}}$                  The coefficient of variation for a sample series
- $H_{\text{fact}}^{\frac{i}{j}}$                 The homogenisation factor between the series i and j

The Homogenising factor ( $H_{\text{fact}}$ ) is often used commercially as the standard deviation of the material in divided by the standard deviation of the material going out. This will only give a correct picture when the average value of both series are identical, and maybe in an ideal world this is always true, but in most cases it is not. Therefore, here the definition given above has been chosen, where the variations are related to its average value. The term; Homogenising factor, might be of discussion, when considering the statements of

Gy [1998], claiming homogeneity is defined as the unachievable state, and all states between full segregation and homogeneity are called Heterogeneity. However, since the factor is meant to describe a step in the direction of homogeneity, the name homogenising factor is quite describing. Ideal homogeneity is achieved when the homogenising factor goes to infinity, and for this to be achieved the outgoing standard deviation  $S_j$ , would have to be zero. This state is, by experience not something likely to occur in an aluminium plant handling alumina, at least not for many years to come.

The homogenising factors are interpreted as follows:

- $H_{\text{fact}} < 1$ , indicates segregation. If  $H_{\text{fact}} = 0,5$  the standard coefficient of variation has doubled
- $H_{\text{fact}} = 1$ , indicates no segregation and no homogenisation. This is the target value for the later described anti segregation system.
- $H_{\text{fact}} > 1$ , indicates homogenisation, meaning that the variation in the material has been reduced.

From the definition of homogenisation factor, it is clear that the smaller the ingoing deviations/ variations are, the more difficult it becomes to keep the homogenising factor above one.

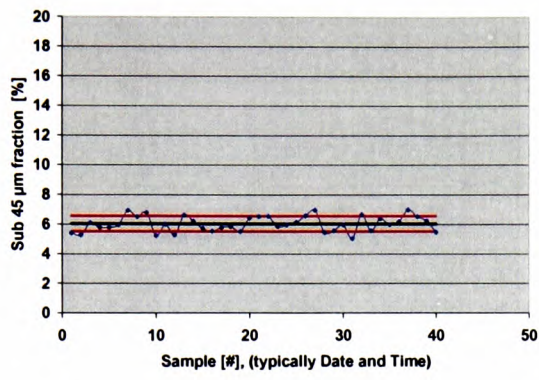
The particle size distributions are measured for all the samples, which are collected, but in order to simplify the further treatment only one specific fraction is considered for the further analysis. The fraction that is chosen is fraction less than  $45\mu\text{m}$  (also in earlier times sub  $42\mu\text{m}$  due to equipment settings). There are mainly two reasons for choosing this fraction. First because the fraction is below  $50\mu\text{m}$ , and as can be seen in section 2.3.1 this is the fraction most likely to be exposed to air current segregation. Furthermore, the fraction below  $45\mu\text{m}$  represents a size that is not at the lower end of the laser equipment used for analysis and is of such a size that the number is not too much affected by the weaknesses of the equipment for the smallest size fractions. Second, the size sub  $45\mu\text{m}$  is in consensus with the international standard for the alumina trading where the 325-mesh sieve is used for certification [ISO 2926].

### 3.2.4 A constructed example of a campaign

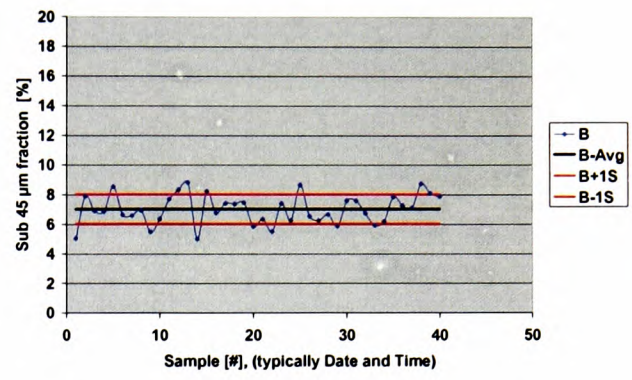
Below in Figure 3-3, data has been generated to fit the general sampling campaign described through Figure 3-2. The generated data have been shaped in the term that it matches what typically has been found during campaigns. The example is meant to demonstrate the method used for analysis of factories, to explain the basics, before showing measured results.

In Figure 3-3 all the “measured” data are shown. Please observe that the scales of each plot, and for later plots showing the variations in the sub 45  $\mu\text{m}$  fraction, are set to the same value. This might seem like a minor detail, and obvious for most people considered as “common sense”. However, to quote late Prof de Silva, “*common sense is not so common*”, and he was quite right. When browsing through data on sites, the scales are jumping up and down, seemingly only controlled by the auto scale function in Excel or other spreadsheet programmes. By keeping the desired principle as described above, the Figure 3-3 gives a clear picture of the development of the material throughout the process, and condensed into one plot, Figure 3-4, the “signature” of each point can be seen.

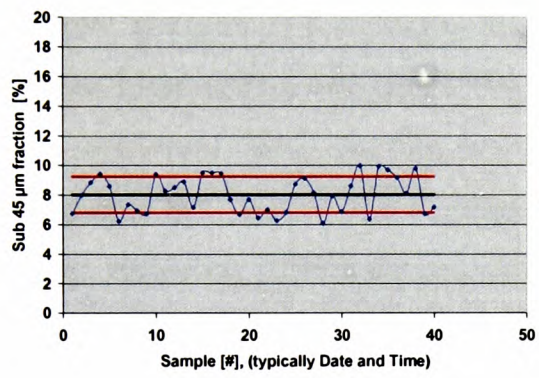
(On the following figures, horizontal axis, ‘Samples’ could be either the number of samples taken (one, two etc.) or it could be the date and/or time of when the samples were taken)



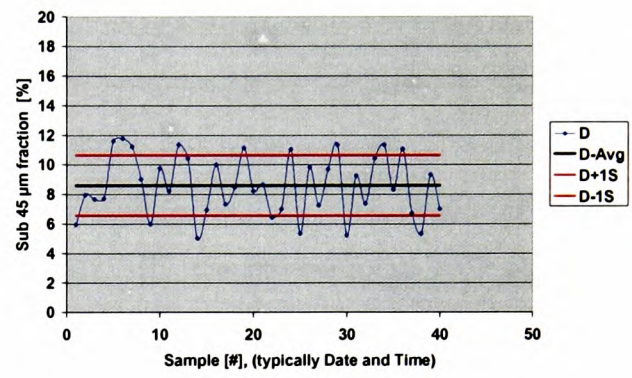
A



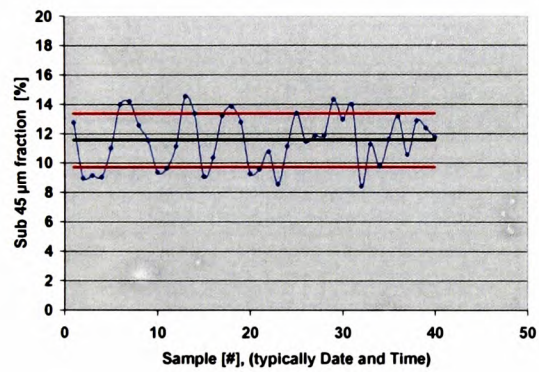
B



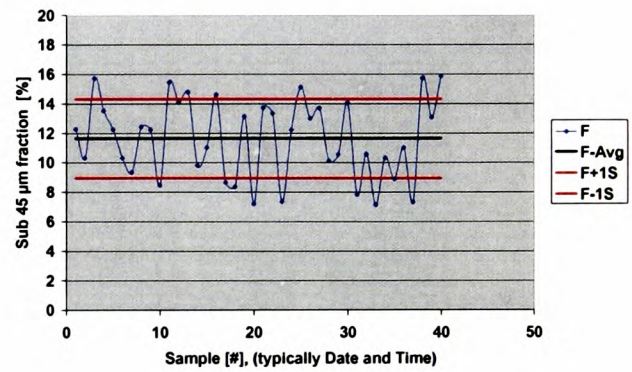
C



D



E



F

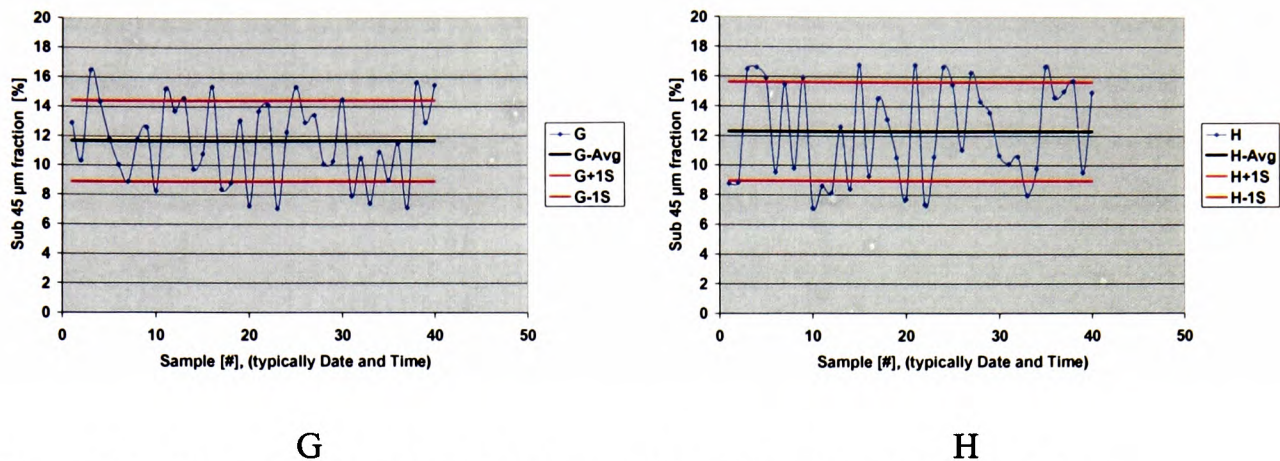


Figure 3-3. Generated data for different sampling points given in Figure 3-2.

The plot in Figure 3-4, is similar to the ones used in the campaigns, but instead of Lower Process Limit (LPL), and Upper Process Limit (UPL), as would be the case for Statistical Process Control (SPC), the plus and minus one standard deviation is given. The reason for bringing in SPC was to find a “language” in which to communicate with people in the industry. However, in SPC the calculation of UPL and LPL are proportional with the standard deviation by a factor determined by the SPC algorithm, hence in a general purpose the standard deviation gives in this case quite the same desired information.

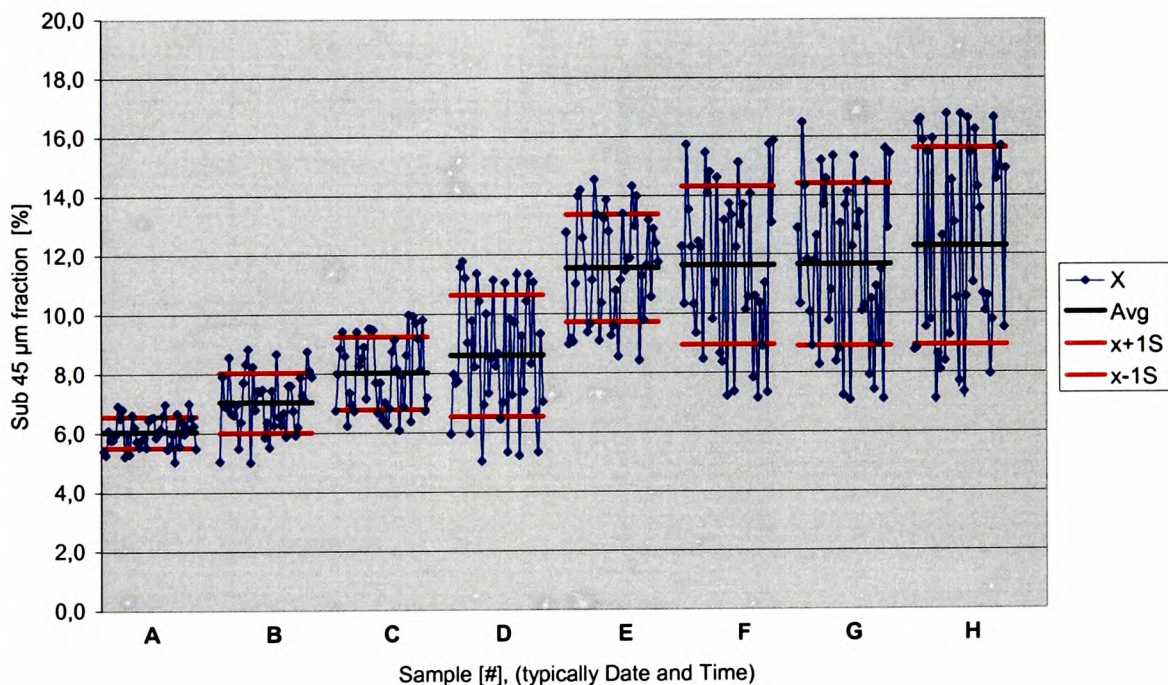


Figure 3-4. Samples given in Figure 3-3 combined in one plot. Plus and minus one standard deviation for each sampling point are indicated by the red lines.

The information that is sought is the development of the bulk, in terms of averages and variations. The averages plotted in Figure 3-5 indicate the changes that might occur due to the handling processes. For example, if the transport between B and C are pneumatic conveying, the increase in averages can indicate crushing of the material, however, the difference between the averages are here not high enough to state this for a fact. Consulting back to Figure 3-4, one could clearly see that the confidence in such a statement would be very low, given the standard deviations.

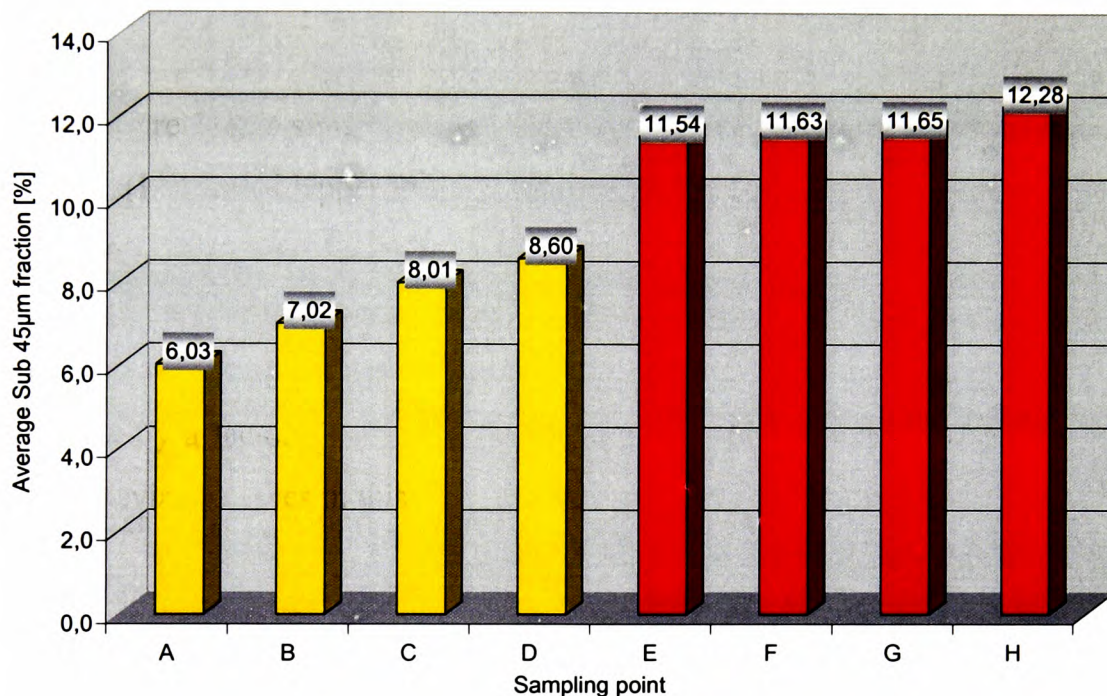


Figure 3-5. Averages for the samples shown in Figure 3-3.

In Figure 3-5, the columns are coloured differently, and distinguishes the primary alumina from the secondary alumina, e.g. the difference between the alumina before and after the FTP (Fume Treatment Plant). The difference between D and E is quite clear. Nevertheless, to state that this is from crushing in the FTP would be to jump to conclusion, and it is here that the knowledge of the material flows in an aluminium plant must be utilised. The only way to say anything certain about this increase are to set up a mass balance of the material flows in and out of the FTP, as will be shown later. Recirculation of fines from the pots to the FTP is a more likely explanation.



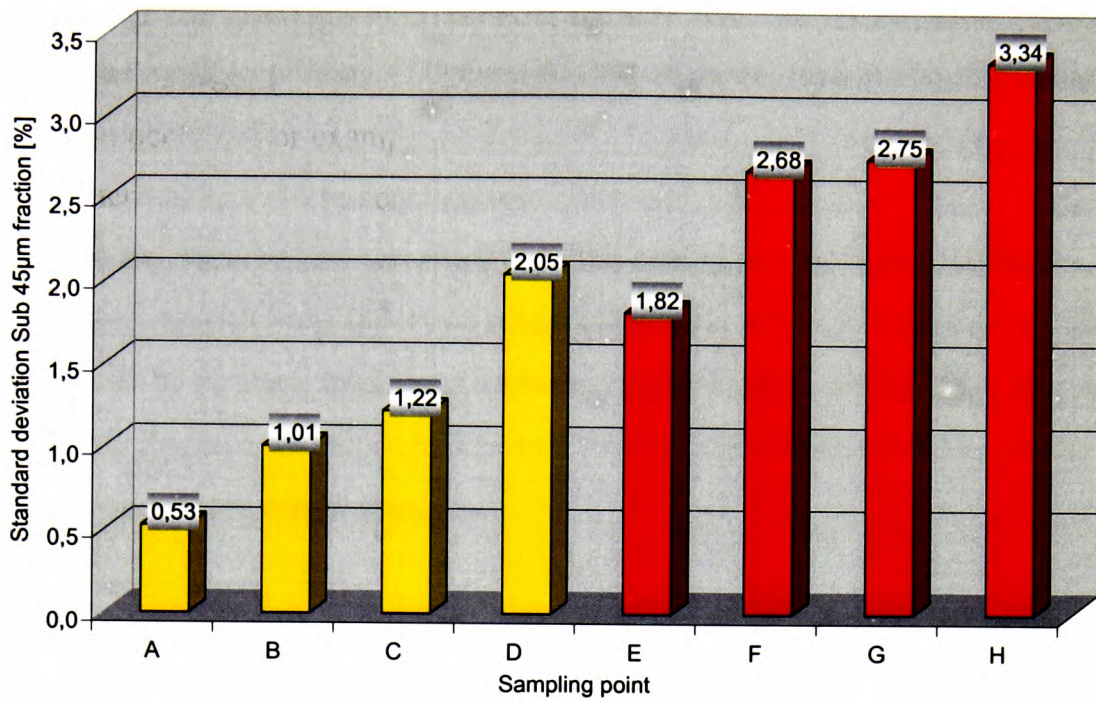


Figure 3-6. Standard deviations of the data given in Figure 3-3.

Figure 3-6 shows the development of the standard deviations through the logistic loop.

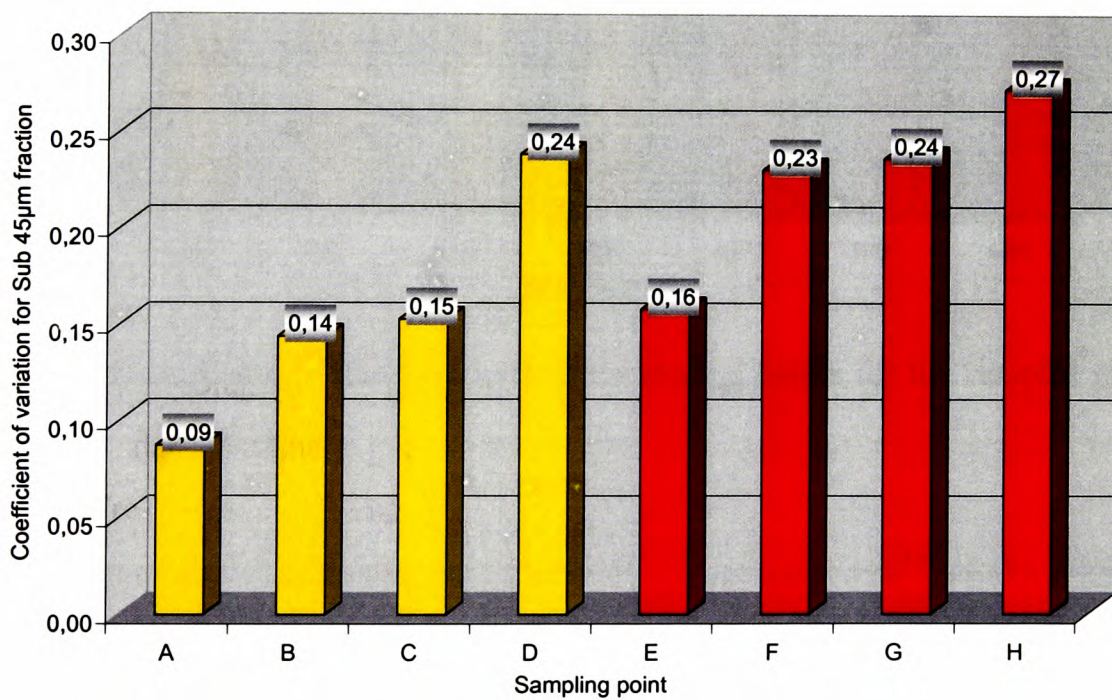


Figure 3-7. Coefficient of variation for the data given in Figure 3-3.

Moreover, as an indication, one now already can get an idea of the segregation or homog-

enisation through the loop. However, to be on the safe side, one should leave these conclusions until after looking at Figure 3-7, because one might be deceived by the changing averages.

To confirm segregation or not one should use the homogenising factors in Figure 3-8. As can be seen this “factory” would be in a miserable state in terms of segregation. Except for the step from D to E, from primary to secondary alumina through the FTP, all stages are segregating the material. In addition, the main reason of the homogenisation in the FTP is the large increase of the sub 45  $\mu\text{m}$  fraction.

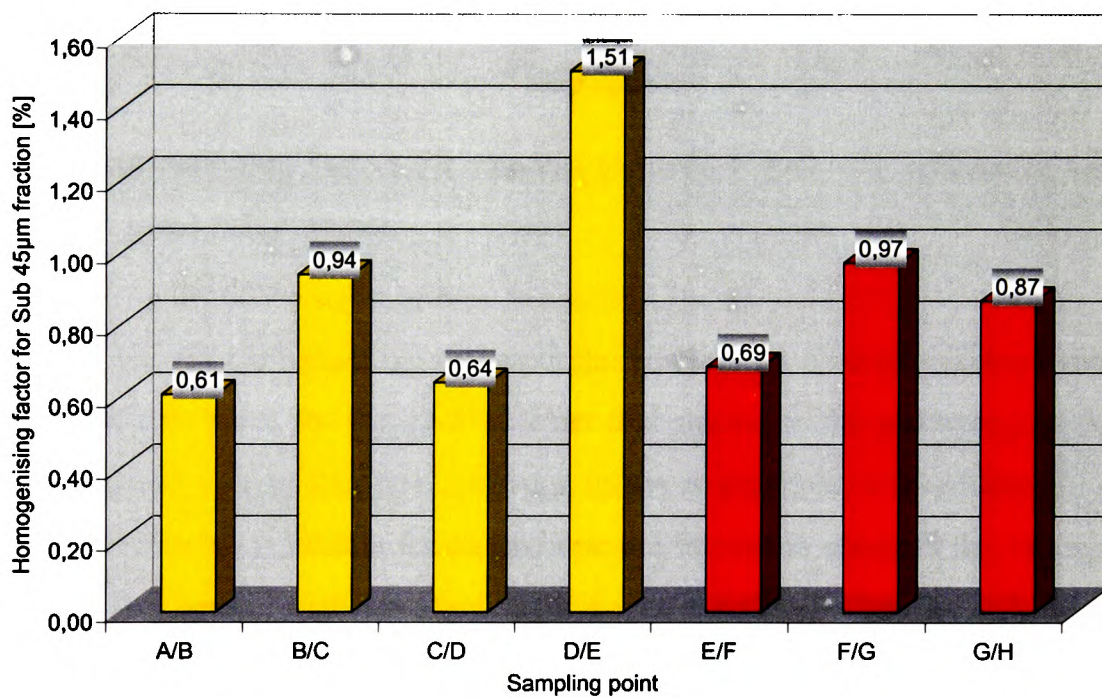


Figure 3-8. Homogenising factors between the sampling points for the samples given in Figure 3-3.

Another point is that although the segregation/ homogenisation easily can be detected by these methods, one should remember that air slides, other bulk handling systems and electrolysis cells are not running on relative changes of fines content, but rather on the fraction itself. Hence, a reduced coefficient of variation due to increased fine content might result in problems in the process.

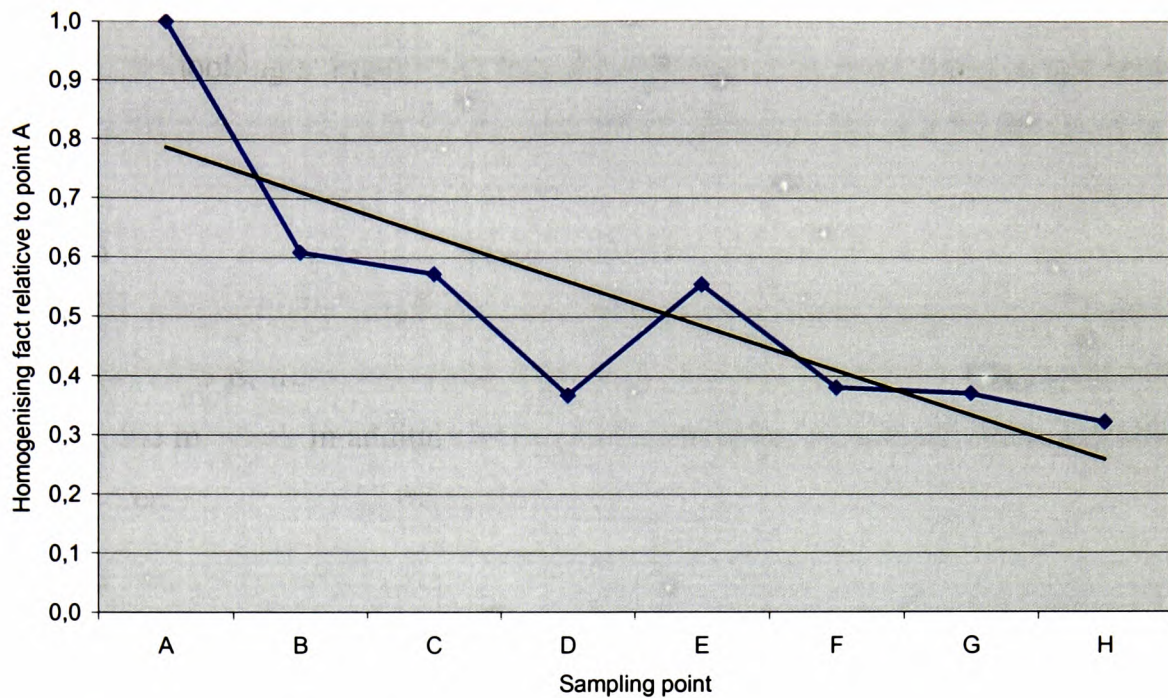


Figure 3-9. Homogenising factors for samples given in Figure 3-3, relative to sampling point A (the input).

At the end, to see what is happening to the purchased alumina, a homogenising factor relative to the point A is set up, Figure 3-9. What this shows, is the worsening of the purchased heterogeneity of the alumina. Although this is an example, it is unfortunately quite representative for what is usually found, and one might start to question the use and need for shipment certificates, with specified particle size fractions, when so little is done to maintain the quality inside the plants.

### 3.3 Segregation and Consequences in the aluminium industry

This section highlights the investigations of full factories in the period 1998 to 2003 [Dyrøy 1998-2003] in terms of measured and quantified segregation and crushing, and the process ramifications these investigations led to. The sampling campaigns only address the alumina logistics. This does by no means indicate that the other bulk solids handled by the alumina industry are without segregation during handling, on the contrary. Coal, crushed electrolytic bath, fluoride, and dross, to mention a few, and every intermediate mixes of the mentioned materials, are all exposed to segregation. All of these materials are basically

free flowing, and with the width of their particle size distributions, they are all strongly segregating materials. By mentioning this, the intention is to show that a single focus on alumina handling is not enough for the aluminium industry, but will be the focus in this thesis.

Although the data from the campaigns have been analysed using tools such as Multi Variate Analysis techniques, the converted form to the industry has after trying this once been changed to the given in the simple form of two variables, to aim the focus towards the findings.

### 3.3.1 Bulk solids changes found during campaigns

It is a known fact that silo operators try to counteract the pulses of fines at the end of the emptying process by simply keeping the silo nearly full, and not emptying the silo completely. This will only postpone the problem, because what goes in has to come out eventually. A full-scale investigation of the variation of the sub 42  $\mu\text{m}$  fraction in an alumina transporting system was carried out in 1998 [Dyrøy 1998]. Some results are shown in Figure 3-10, where significant variations in the fines content are found to be closely related to the variations of the level in the day silo.

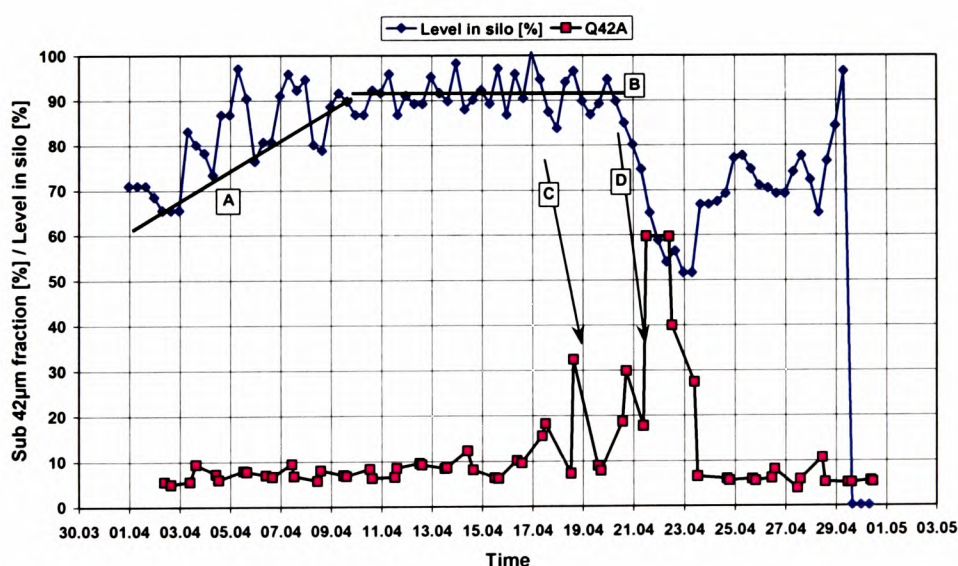


Figure 3-10 Variation of fines content of alumina discharged from a silo, and the filling level in the silo.

In case A, where there is an overall increase of the level in the silo, the content of fines is low in the discharging alumina. In such a situation, there will be accumulation of fines in the silo, and hence there is a low content of fines in the alumina leaving the silo with small variations. This is caused by the fact that air current segregation accumulates the fines at the walls, where it is continuously being covered by fresh alumina. In this silo, only alumina from the centre of the silo will be discharged (Figure 2-14). Thus, the fines near the walls continue to accumulate in the period between A and B (Figure 3-10). The clearest proof of accumulation of fines is at point D. Here the silo has been held at a level between 85 and 95 % (B), and suddenly the level is reduced to 50 %. This causes the fines content to increase from the usual 9-10 % to almost 60 %. If all this were to go further down the line to equipment designed for nearly free-flowing alumina, the functionality of such equipment would be dangerously compromised.

When the level in the silo falls below the “usual” before the silo is re-filled, the accumulated fines will create a pulse of high fines content in the discharged alumina. This causes the effect seen in Figure 3-10, where the fines content further down the process line increases in the case of C and D, where the levels in the silo are low, causing transport problems which will be explained below.

One of the much referred works within the fluidisation area is the powder classifications of Geldart [1973]. Geldart classified the powders by the results from a fluidised column, the velocity needed for fluidisation, the specific pressures drop, and expansion of the powder and the flow patterns during the test. Geldart [1973] ends up with four classes of powder:

- A-powders: Aerate able powders, characterised by the fact that when fluidised just above the minimum fluidising velocity, the expansion is homogeneously distributed in the fluidised bed.
- B-powders: Bubbly, generally coarser than A-powders, and as indicated in the name, generates bubbles when fluidised. The expansion when fluidised is not homogeneously distributed, but is defined by the volume of the bubbles.
- C-powders: The C stands for cohesive powders. C powders are finer than both A and B powders. Characterised with the fact that cracks emerges when

passing the minimum fluidising velocity, resulting in a considerable less pressure drop than the bed height would suggest.

**D-powders:** D-powders are the last class from Geldart, and are the coarsest of the four classes. When fluidised above minimum fluidising velocity, spouting is typical.

The classes from Geldart [1973] are very coarse, and based only on his work with a catalytic material. However, when plotting the classes in a plot of density and particle size, a plot such as given in Figure 3-11 is generated. This plot can reveal potential effects of segregation in terms of fluidisability, although a rough indication it has proven itself useful.

Much of the transport of alumina in the industry into the secondary oxide silos is based on pneumatic conveying and, lately, increasingly based on air-slides. This is because the alumina is easily fluidised in its “normal” condition. If the state values of the fines rich material at point D in Figure 3-11 is placed into Geldart’s diagram used to classify powders with regard to their fluidisation behaviour, Figure 3-11, one can see that the characteristics of the powder moves from being an A powder (A = aerateable), point (1) in Figure 3-11, to become a C powder (C = cohesive), point (2) in Figure 3-11. Air-slides for transport of alumina are mounted at a certain angle (usually 1°) and are run at a certain fluidising air velocity, based on the fluidisability of the material being transported. If the material changes in nature from an A powder to a C powder, the velocity required may, and the angle required will, increase. Since the requirement for an increased angle is not satisfied, a plug will form in the air-slide. If the amount of powder of type C that enters the system is large, the plug will become so long that it will get stuck, and the system will stop transporting. The potential risk was identified during a sampling campaign in April’98, and in August, the same year the chocking of the transport system actually occurred. After this, systematic vacuum cleaning of the conveying systems was established to counter this from occurring again.

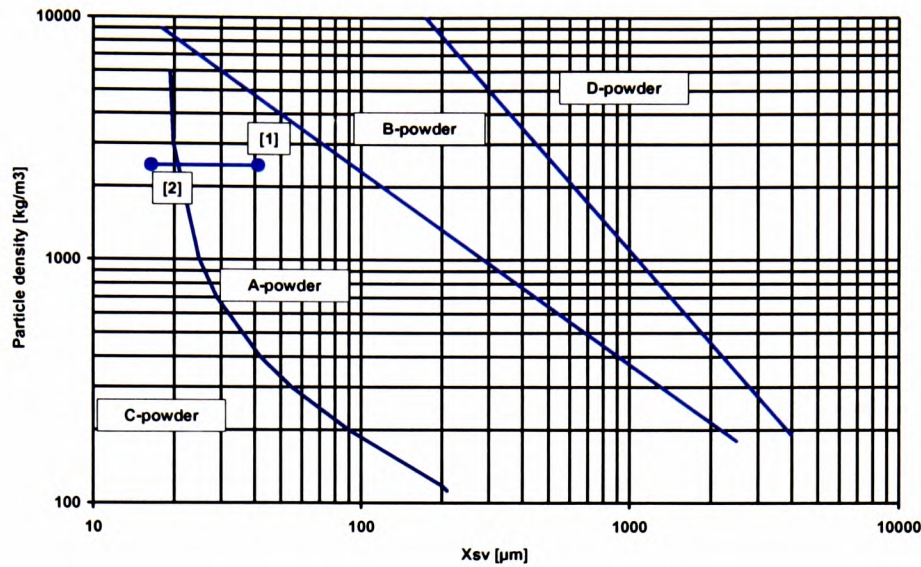


Figure 3-11. Diagram for classifying powders according to their fluidisation behaviour, from Geldart.

One might state that materials classified as C material by Geldart easily is conveyed in air slides, and this is true. However, air slides designed for alumina has an inclination of 0.5-3° down angle, and 2 cm/s fluidisation velocity. To test the effect of fines content changes, tests measuring the changes in capacity for an air slide were carried out [Dyrøy & Berdal 1999]. The test rig is shown in Figure 3-12.

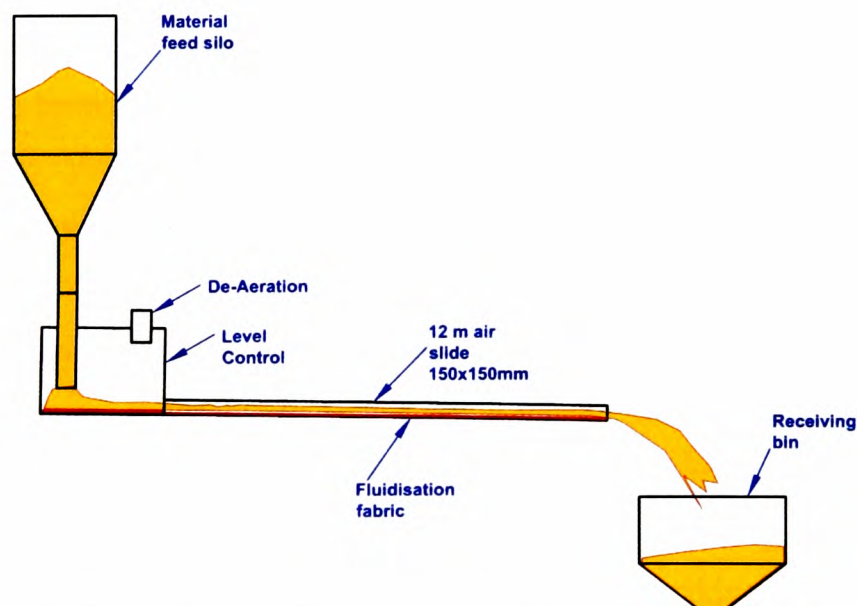


Figure 3-12. Test set up for air slide capacity for different fines fractions.

The overall results from the tests carried out with the rig shown in Figure 3-12, when the

finer content changes the alumina from A-powder to C-powder, the capacity of the air slide is reduced, and in severe cases there is full stop, as can be seen from a test done on a specific air slide for pot distribution in Figure 3-13. As can be seen the angle is essential, and the air velocity of minor importance in this case.

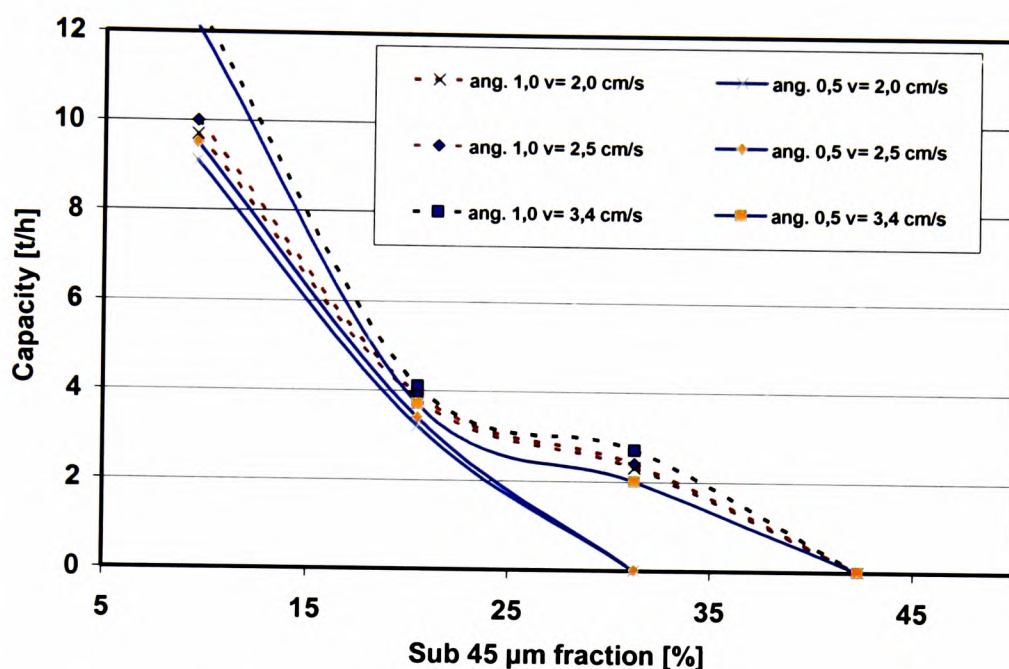


Figure 3-13. Air slide capacity for alumina when fines content increases.

When filling silos or A-frame storage systems with alumina, air current segregation will occur, which has been proven. Traditionally one keeps the level constant or one does not empty the storage system completely, due to requirements for emergency reserves. The price to be paid is accumulation of fines in dead storage areas.

This fine material will from time to time be introduced to the downstream process. One may wonder what kind of security of supply one achieves when looking at the content of fines found in some regions of the A-frame, shown in Figure 3-15. Spot samples were taken inside an A-frame about to be replaced by two new silos having an anti-segregation system. The amount of residual alumina in the A-frame when taking the samples was approximately 6500 tonnes. This would be enough alumina to supply the factory in question for 6 days. The pattern of sample points is illustrated with circles in Figure 3-15. The samples were taken by removing the top layer of material (approximately 150 mm) and then



the samples were collected by a sampling scoop. The heaps in the storage can be seen in Figure 3-14.

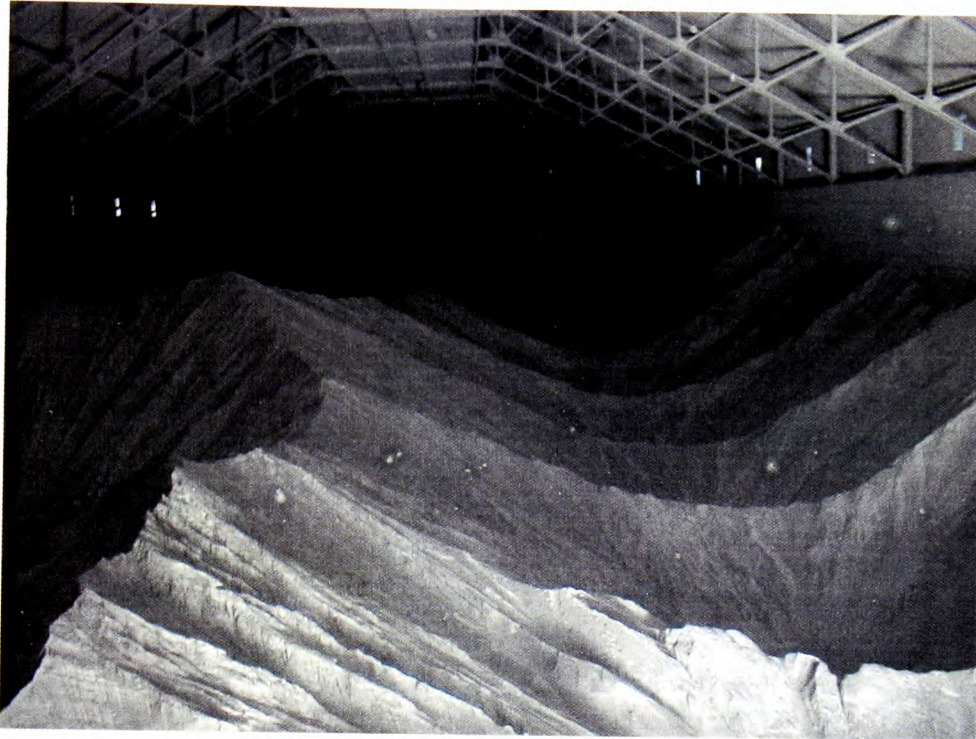


Figure 3-14. A-frame storage sampled.

The results indicate a tremendous accumulated content of fines in the expected zones when considering the airflow patterns induced by the free falling alumina and the configuration of the filling points (marked by squares in Figure 3-15). Values up to 97 wt% below 42  $\mu\text{m}$  were measured in the southeast corner of the storage facility. Due to the high values of the fines content one found it necessary to mix it into the main stream, at a rate of no more than 10 %, in order to keep the impact on the downstream logistics and processes to a minimum. One may then argue that this super fine alumina should not have been introduced to the process at all, but considering that the alumina spot price varies between 200-400 \$/ton and that long term prices are 11-13% of the LME aluminium price, the draining of the A-frame was a very profitable action.

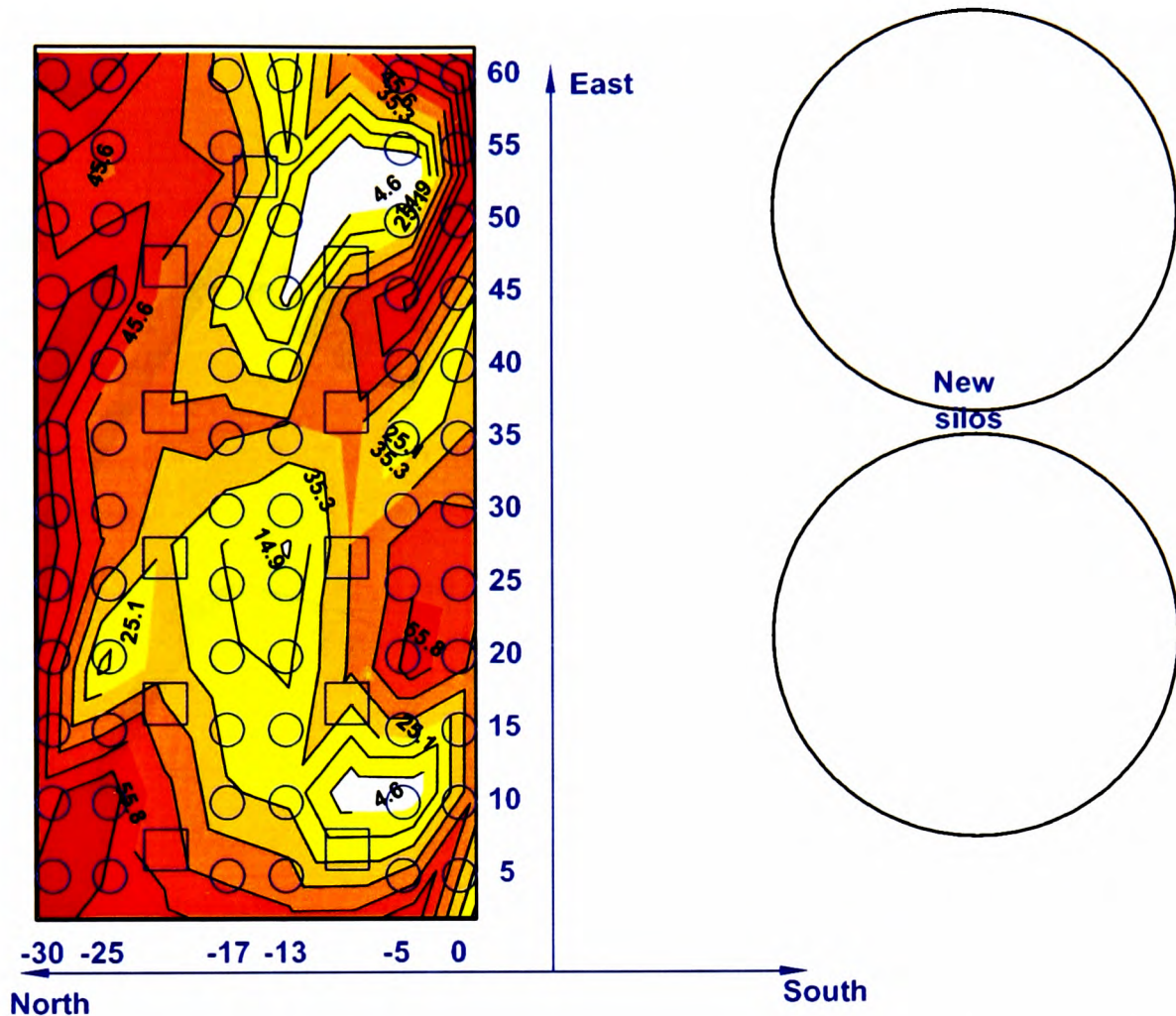


Figure 3-15. A-frame sampling results, showing the sub 42  $\mu\text{m}$  fractions in different areas in the A-frame.

In a joint project between Tel-Tek's Department of POSTEC and Norwegian aluminium producers, a new concept called the Anti Segregation Tube (AST) was developed to counter this particular type of segregation.

As mentioned earlier, the campaigns also try to identify the degradation, i.e. crushing, of the alumina, and the clearest example of this was found in a campaign in 1999 and investigated further the following year [Dyrøy 1999, 2000].

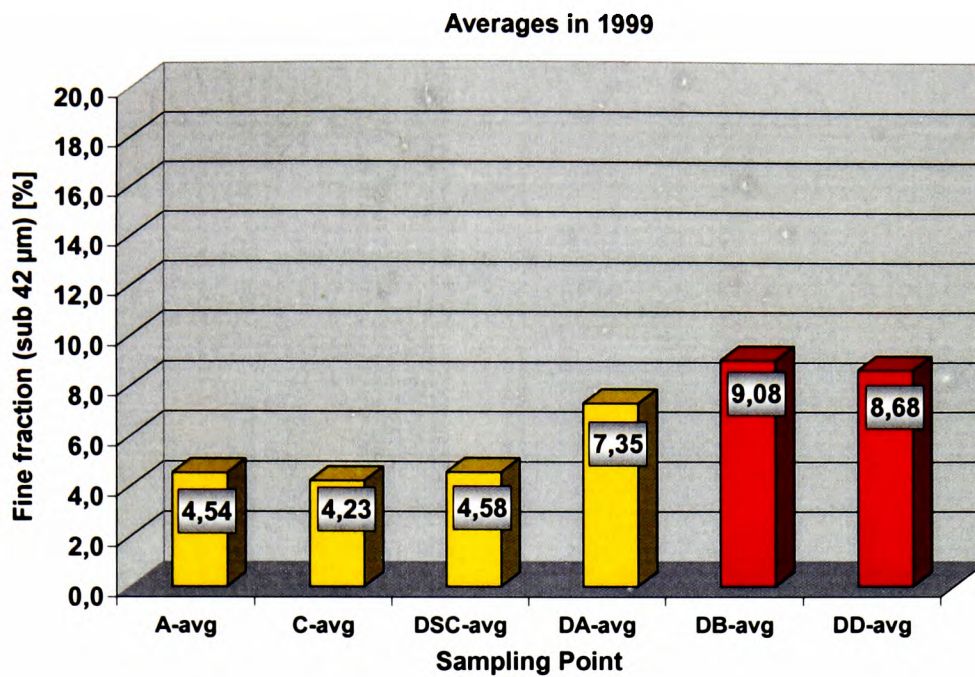


Figure 3-16. Averages of sub 42 µm fraction for a given logistic loop in campaign in 1999, Dyrøy [1999]

As can be seen from Figure 3-16, the change of fines increases dramatically between the point DSC and DA, these points of sampling are specific for the mentioned campaigns, but in same principle as for the described campaigns in general. The process unit in between these points is Möller Turboflow pneumatic conveying, delivered by Möller Materials Handling GmbH, Germany, a type with inner tube for by pass air for plug avoidance. These increases in the fines content led this author, after leaving the topic for a while, to believe that the point DA was after the FTP, where an increase of fines would be natural. However, after re-consulting the sampling plan, it was clear that the samples from DA were in fact primary alumina after what could only be described as a “traumatic” transport. The length of the transport was a bit over 700 meters, and when investigating the matter closer, it was found that some of the sections with inner piping were ruined, and therefore in order to meet the capacity need, as often happens, the pressure and air settings were boosted. After the tubes had been replaced and original settings were reset, the outcome was measured the following year as given in Figure 3-17.

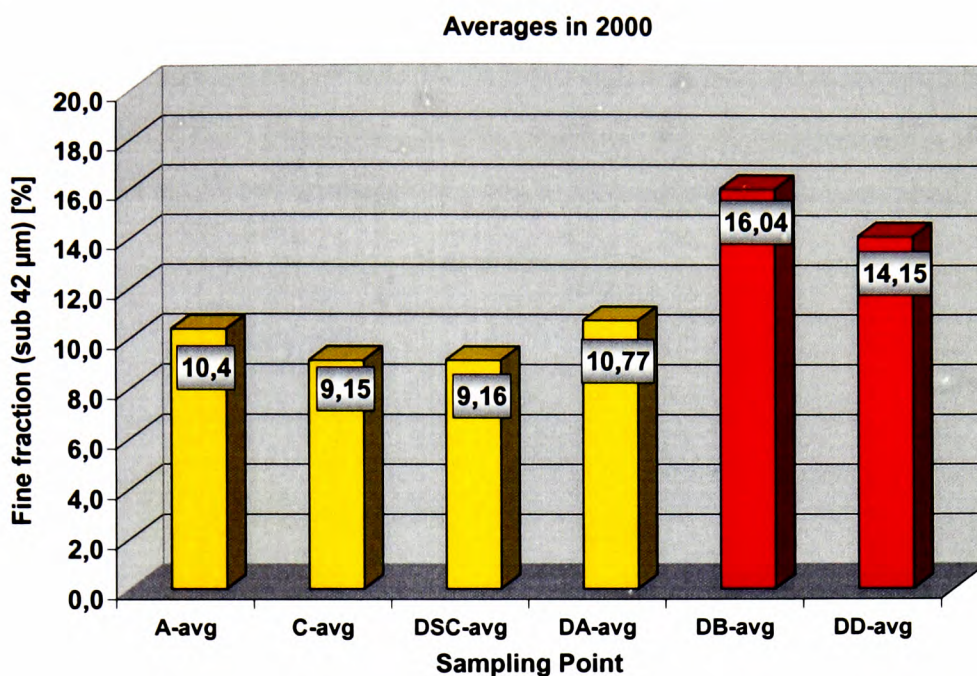


Figure 3-17. Averages of sub 42 µm fraction for a given logistic loop in campaign in 2000, same loop as given in Figure 3-16, Dyrøy [2000].

To compare the situation before and after the adjustment, each sampling campaign has been put relative to the input point A and the results come out as shown in Figure 3-18.

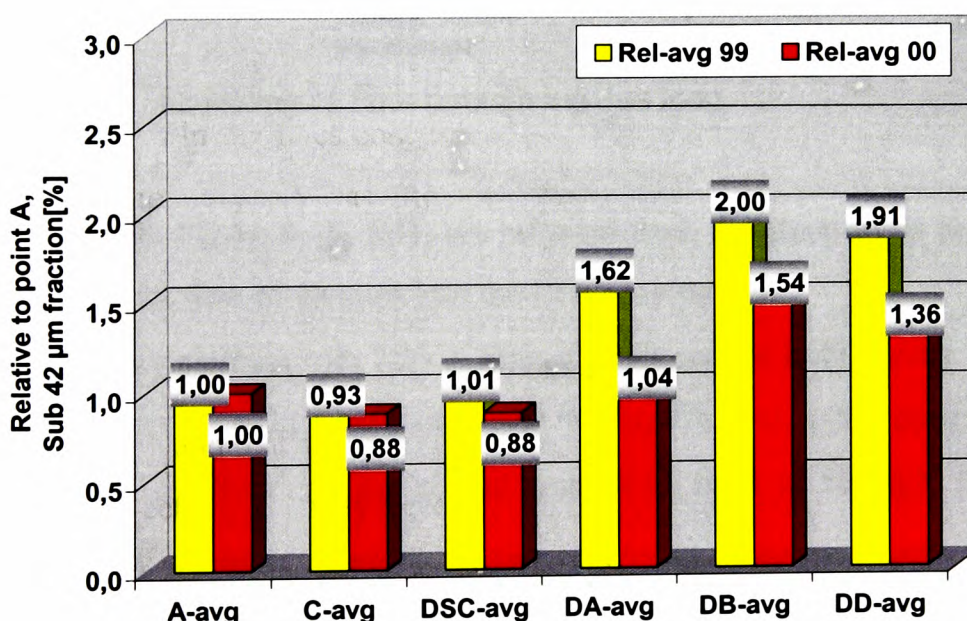


Figure 3-18. Averages relative to the fines content of material put into the process at point A for the logistic loop before and after adjustments (1999 and 2000) Dyrøy [1999,2000].

Going back to Figure 3-16, one can see that the increase from DA to DB through the FTP (from 7,35 % to 9,08 %), is of 1,73 %. When seen in earlier days this has been interpreted as crushing in the FTP. However, before drawing any conclusions one needs to see the mass balance for this FTP. In Figure 3-19, the material flows are indicated.

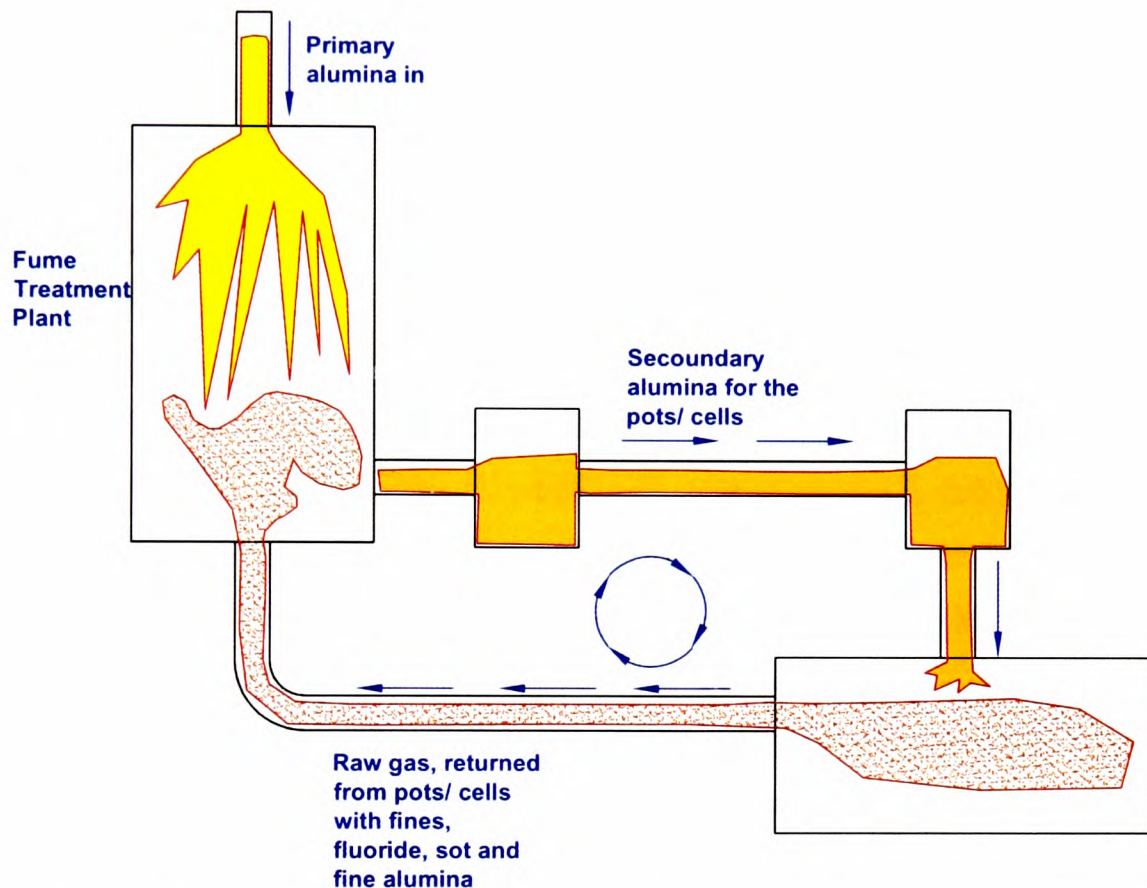


Figure 3-19. Recycling of fines through raw gas loop.

As indicated in Figure 3-19, fines are recycled from the electrolysis pots by the raw gas, and the material flow of alumina into the FTP consists of:

- Primary alumina with 7,35 % fines, for this section is 48,4 t/day
- Gas suction from same section 142 500 Nm<sup>3</sup>/h, with a dust concentration measured to 393 mg/Nm<sup>3</sup>, giving a total amount of fines to 56 kg/h, therefore 1 344 kg fines/day

Calculating the numbers to see the expected concentration of fines, assuming that all of the recycled material is below 42µm, the calculations become as can be seen in Equation 3-5 below.

$$\frac{48,4}{49,74} \cdot 7,35[\%] + \frac{1,344}{49,74} \cdot 100[\%] = 9,85[\%] \quad \text{Equation 3-5}$$

The calculations show an expected sub 42  $\mu\text{m}$  fraction of 9,85%, while the measurement shows 9,08 %, indicating agglomeration instead of crushing in the FTP.

### 3.3.2 Process influences found during campaigns

As discussed in section 2.4.3.4, the concentration of fluoride and alumina influences the heat balance in the cell. In terms of fluoride, if remembering the recycling of fines through the gas from the pots, the secondary alumina will have a fines fraction enriched on fluoride. Considering this the segregation will then not only influence the particle size of the alumina, but also the chemical balance in the cell. Also suggested is that the composition of the alumina fed to the cell influences the heat balance. The concentration of alumina in the pot sets the conditions in which the AE (anode effects) occur, and the AE's really adjusts the heat balance in the cell. From the earlier addressed sampling campaigns, the content of fines in samples from the pots is checked against the occurrence of AE. Since AE is an integer, and concentration of fines is a real number, some processing must be done to the number. By using Equation 3-6 (standard centering method from statistic literature), the variations in the values can be compared. When doing so the plot shown in Figure 3-20 is obtained.

$$Y_i = \frac{X_i - \bar{X}}{S} \quad \text{Equation 3-6}$$

where

- $Y_i$  normalized and centred value
- $X_i$  measured value
- $\bar{X}$  average value of all samples (1 to n)
- $S$  standard deviation of the sample series

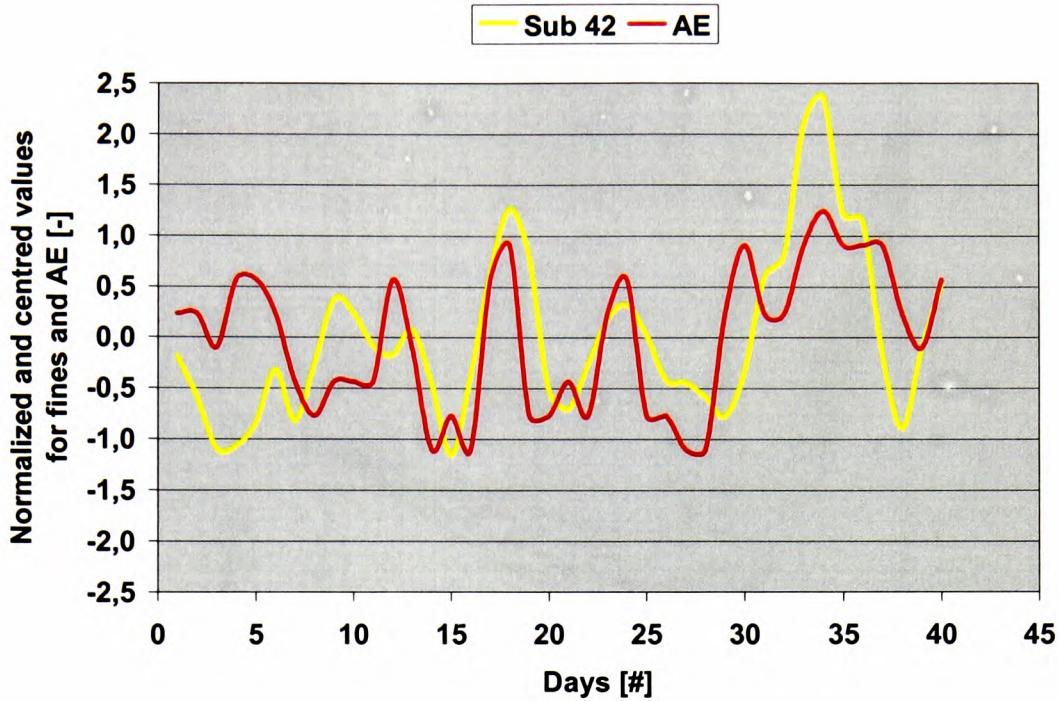


Figure 3-20. Centred and normalized sub 42  $\mu\text{m}$  content and number of anode effects (AE) per day.

The values in Figure 3-20 are moving averages over two days, because of the response time of alumina fed to the cells and the frequency of collecting the alumina samples. As can be seen from the plot, there are more than a random co-variation. Moreover, the same co-variation is found in the other campaigns as well. The level of fines in itself does not necessarily result in an AE, but rather the rate of change. Looking at the curves in Figure 3-21 below, and remembering that the AE is defined as a sudden change in cell voltage, the change in alumina concentration does not have to be large before achieving an AE. The control systems of pots are based on periodically “starving” the pot down in alumina concentration, and then “over feed” it, to be able to measure the change in cell voltage, in order to stay as long as possible in the sweet spot, demanding the least amount of energy (voltage) for aluminium production.

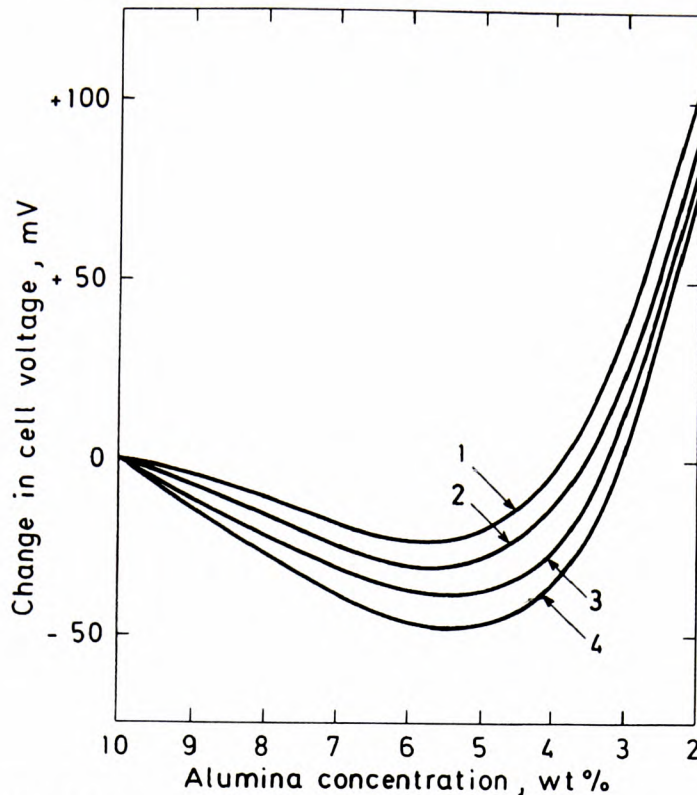


Fig. 6.9. Variation in cell voltage with alumina concentration;  
 curve 1:  $CD = 0.6 \text{ A} \cdot \text{cm}^{-2}$ ,  $ACD = 4 \text{ cm}$ ;  
 curve 2:  $CD = 0.8 \text{ A} \cdot \text{cm}^{-2}$ ,  $ACD = 4 \text{ cm}$ ;  
 curve 3:  $CD = 1.0 \text{ A} \cdot \text{cm}^{-2}$ ,  $ACD = 4 \text{ cm}$ ;  
 curve 4:  $CD = 0.8 \text{ A} \cdot \text{cm}^{-2}$ ,  $ACD = 5 \text{ cm}$ .

Figure 3-21. Cell voltage versus alumina concentration [Grjotheim & Welsh 1998]

In Figure 3-21, the typical situation in the aluminium industry today is to move around in the area to the right of the minimum point. If a pot suddenly gets a large lump of fines, the amount of undissolved alumina in the pot increases, called sludging. This occurs since the amount of so-called alpha-alumina (over calcined) is higher in the fine fraction. The alpha alumina has little crystallised water, hence little reaction when hitting the molten bath, also it needs 10-15% more energy to dissolve. This causes in some cases the feeding system to perceive it as high concentration of alumina, and the feeding goes into the starving mode. However, sludged alumina cannot be calculated as alumina concentration, therefore the fines deceives the control system to work against its own purpose. Furthermore, the recovered Fluoride is found mostly in the fine fraction and the fluoride balance in the pot really influences the heat balance.

The AE's generated from variations in fines content, i.e. segregation, do not only affect the direct yield of the pot, but also as mentioned earlier increases production of hazardous



gases, which will during a counter action of an anode effect in need of manual compensation harm the operators and later the environment. The carbon fluoride gases produced during an AE are only man made, and have a damaging effect on nature, both globally and locally, and it is therefore desirable to keep the emissions as low as possible.

### 3.3.3 Environmental effects found during campaigns

Besides the environmental ramifications mentioned in the previous section, the variations in particle size distribution as shown earlier, changes the handling system's efficiency and function. The dustiness is also affected, as was found during campaigns, below in Figure 3-22. The data has here been normalised and centred as the data for the AE's in section 3.3.2.

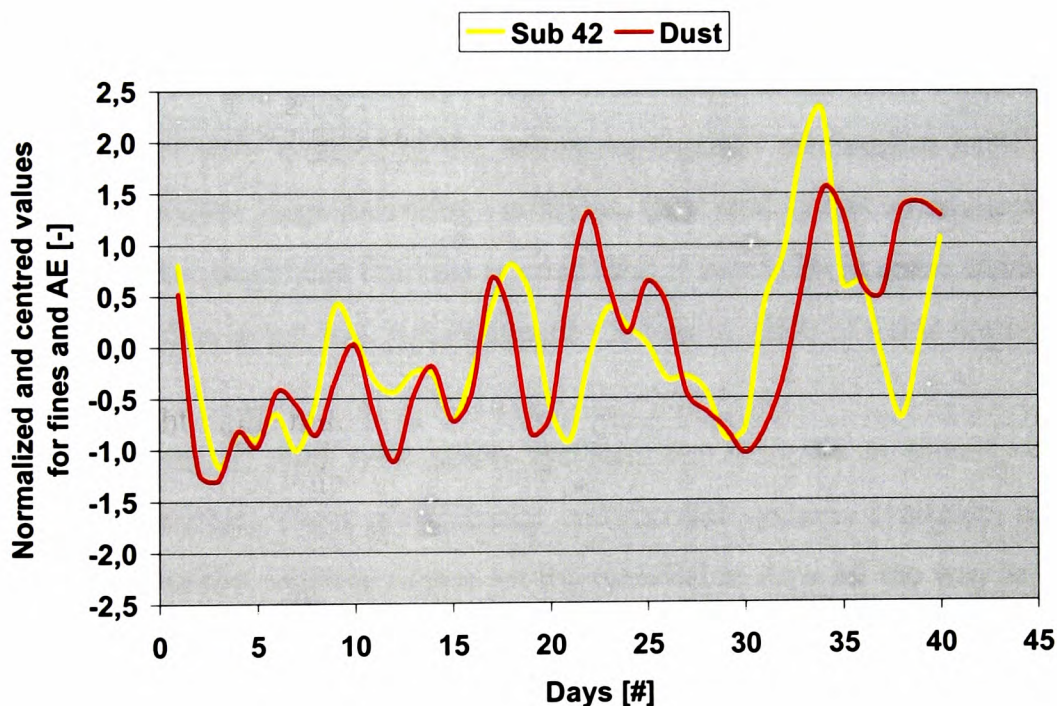


Figure 3-22. Centred and normalized data for sub 42  $\mu\text{m}$  content and dust concentration in pot room.

The environmental impacts from dusting are, as can be seen from Figure 3-22, clearly influenced by the variation of fines content in the alumina. In addition, this shows that varying fines content will affect the working environment for the operators, and the sub 45  $\mu\text{m}$  fraction also contains the respiratory considered dangerous fraction less than 10  $\mu\text{m}$ .

### 3.3.4 Effect of anti segregation measures

One of the primary reasons for launching the sampling campaigns was to pin point the place to implement anti segregation measures, and of course to verify them after implementation. Before presenting such results, some definitions need to be established.

- i.) Segregation effect damping equipment
- ii.) Anti segregation equipment

The first concept, i) Segregation damping equipment, only does what the name describes. Typical examples of this is splitting the filling stream into several filling points, discharge from different levels in the silo, and selling it off as anti segregation systems. However, as the results will show, these systems although quite suitable for given circumstances, are in the case of air current segregation, only damping the effect. The systems are operating more in the term of homogenising systems, but not quite at the same scale, because the systems are not directly countering the acting segregation mechanism itself. Moreover, although able to reduce large incoming variations, they tend to fail when incoming variations are small. One might say that this is good, and it would be in some cases. However, opinion of this author is that loss in homogeneity is loss in value of a raw material.

The second system, ii) Anti segregation systems, are designed to directly counter the mechanism in progress. There are different commercial systems available, common for them is that they utilise tubes or chutes for the material to flow all the way to the surface silo content. The system available for this author to test has been the system developed for Hydro aluminium by Tel-Tek dept POSTEC, called the AS-System. The others are known, but measured results from these systems have never been made accessible for this author.

### 3.3.4.1 Segregation damping equipment

In this section, results from two different segregation damping system are to be shown. The first is a system for silo filling, and is in full operation in a smelter. The second was never installed as a segregation damping device, but as a distribution system for pot lines. However, the results show that the system is able to reduce segregation, simply by the way it is operated.

#### 3.3.4.1.1 Silo filling

The system, of which the efficiency is measured in this section, is a system splitting the filling of a silo into six parts. The six split fillings are then fed to a silo on the half radii of the silos. Four silos of this type have been measured, as a part of a campaign [Dyrøy 2003], and the results are shown below in Figure 3-23.

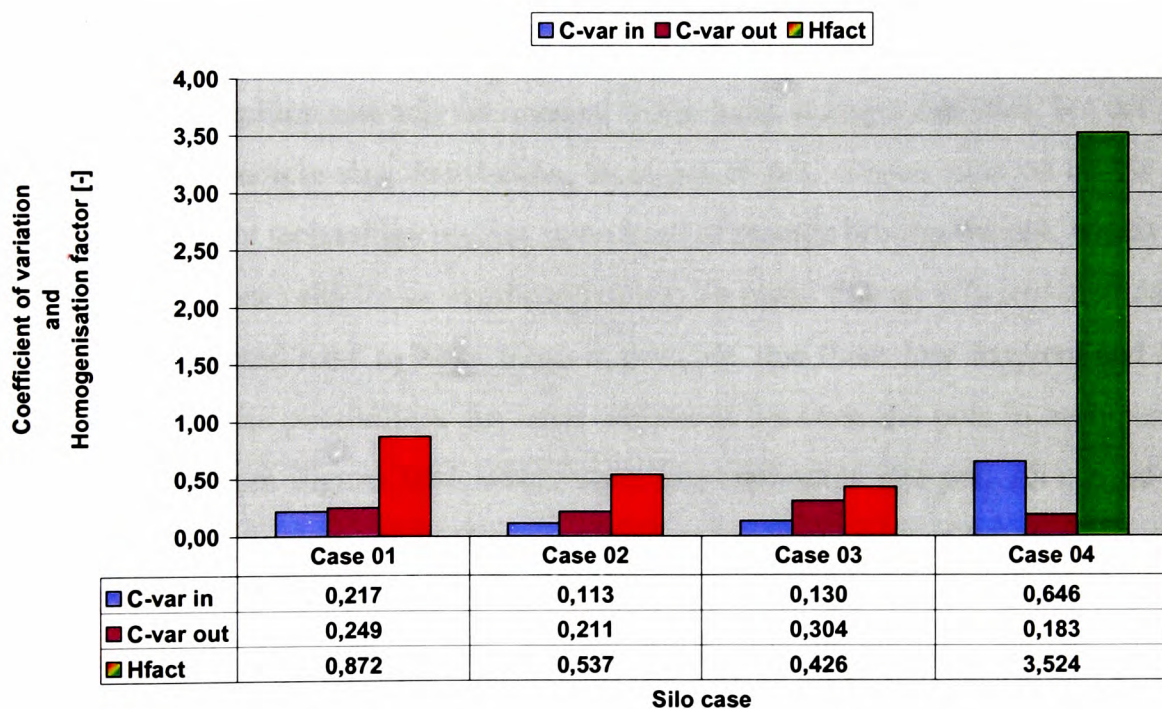


Figure 3-23. Segregation effect damping system, measured effect in four cases.

In Figure 3-23, it can be seen that when the incoming variation is high (Case 04 marked green) the outgoing are reduced in comparison with the incoming. What also can be seen is that when the incoming variation is low, the outgoing is increased. The colours are

changed from red to green whenever the homogenising factor is equal or larger than 1.

Red = homogenising factor  $<1$  ie. segregation

Green = homogenising factor  $>1$  ie. homogenisation

Table 3-1. Averages and standard deviations for the cases in Figure 3-23.

	Case 01	Case 02	Case 03	Case 04
Average in	5,794	8,227	6,136	12,382
Stdev in	1,258	0,932	0,796	7,994
Average out	7,847	9,721	8,180	11,199
Stdev out	1,953	2,050	2,490	2,052

Now the incoming variations in the case 02 and 03 are very low, so low that one might say that the standard deviations, that can be seen in Table 3-1, are within the internal segregation of a sample, however, as will be shown later this can be pushed even further down.

#### 3.3.4.1.2 Distribution to pots

The long term segregation can only be handled in the main storages facilities, but the short term variations in particle size distribution, from pot to pot, can be reduced by the way they are fed. Most pot technology utilises some kind of storage bins on the pot, which used to be refilled by either vehicles or overhead cranes. To make this an efficient method, the size of one refill would have to be as large as possible, and these low frequent and large re-fillings enhance the possibilities for large variations between the pots in each section. This can be seen from Figure 3-24, where each line represents one pot. As can be seen from the figure, these pots are not to be considered as “one” in terms of fed alumina.

If one should want to keep the conditions for each individual pot as constant as possible for the whole sections, one need a high frequency small-filling system. This will chop the potential incoming variations because of segregation into small pieces, and all the pots will each get one small portion of approximately the same material. There are several versions of such automated systems, however, some systems delivered have reduced their sending frequency, in order to be able to reach around the full potline, and this can then become just as bad as overhead cranes, or worse.

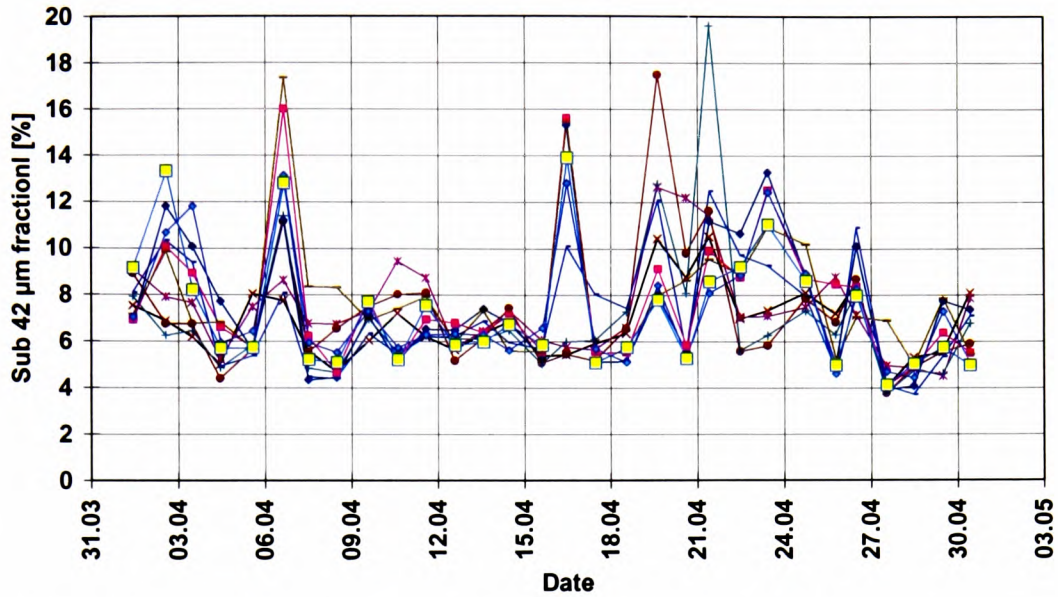


Figure 3-24. Sub 42 µm fraction for different cells, distribution by overhead crane, i.e. large amount at low frequency.

Below in Figure 3-25, the results are given from a section fed by a system sending once each hour to each pot. The silo feeding these pots is the same silo feeding the pots in Figure 3-24, and in fact is the same silo that gave the results given in Figure 3-10.

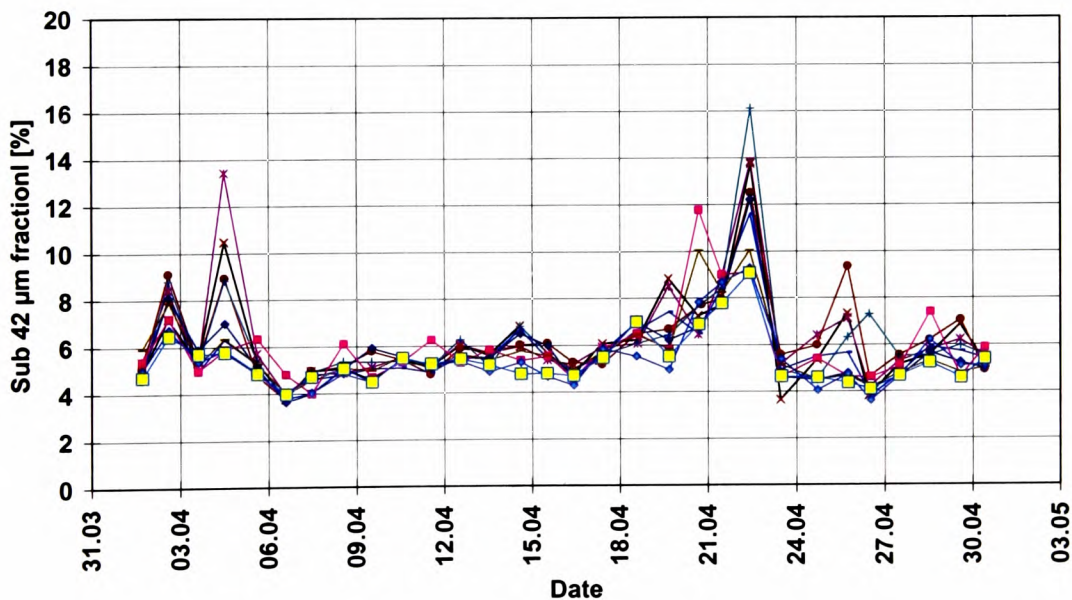


Figure 3-25. Sub 42 µm fraction for different cells, distribution by Aerated Distribution System (ADS©), i.e. small amount at a high frequency.

As said, there are several automated systems for distribution. Some utilise air-slide technology and some pneumatic conveying. When conveying secondary alumina, one runs the risk of scaling, a growth of an amorphous layer of material on surfaces exposed to dust, like the inside of pneumatic pipelines. When knowing that probably one of the main keys for formation of scaling is pressure drop (based on plant observations), this author thinks it is a paradox that a conveying system based on a pressure drop as its main principle of transport, i.e. pneumatic transport is chosen.

### 3.3.4.2 Anti Segregation System (AS-System)

To demonstrate the effect of the developed anti segregation system (see description in chapter 4), all large silos, i.e. larger than 2 000 tonnes equipped with this system, have been measured through different campaigns [Dyrøy et al. 1999 through 2003]. The situations before and after implementation are shown in Figure 3-26.

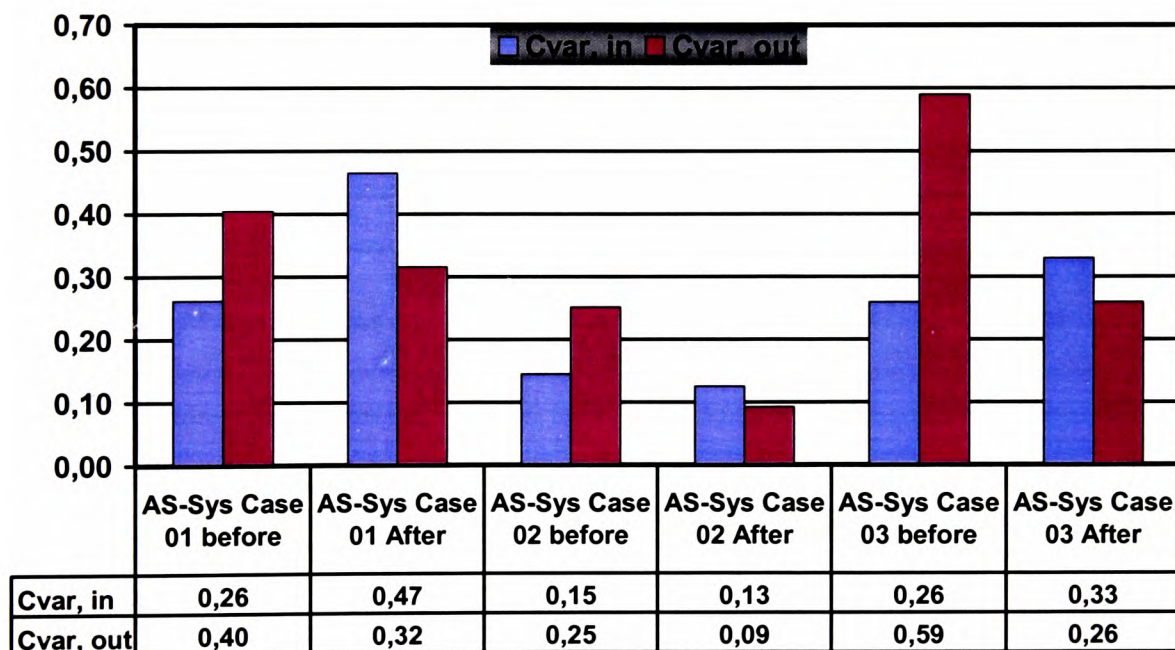


Figure 3-26. Coefficient of variation for storage before and after implementation of AS-System.

The argument that it is easy to get a homogenising factor above one if the ingoing varia-

tions are big is still true, but by closer inspection of the AS-System Case 02 in Figure 3-26, one can see that the AS-System manages to reduce variations, even when they are initially quite small. For the particulate case shown in Figure 3-26, the standard deviation for Case 02 was ingoing 0,8 and outgoing below 0,5, which quite demonstrated what was stated earlier, that the AS-System attacks the mechanism directly and therefore will keep or reduce the variations. Comparing the results shown in Figure 3-23, where the segregation damping system only gives homogenisation in the case of very high variations in the ingoing material, with the results of the AS-System shown in Figure 3-26, where there is homogenisation even in Case 02 with very low variations in the ingoing material, it is fair to say that an anti segregation system for sure gives a far better result than a segregation effect damping one.

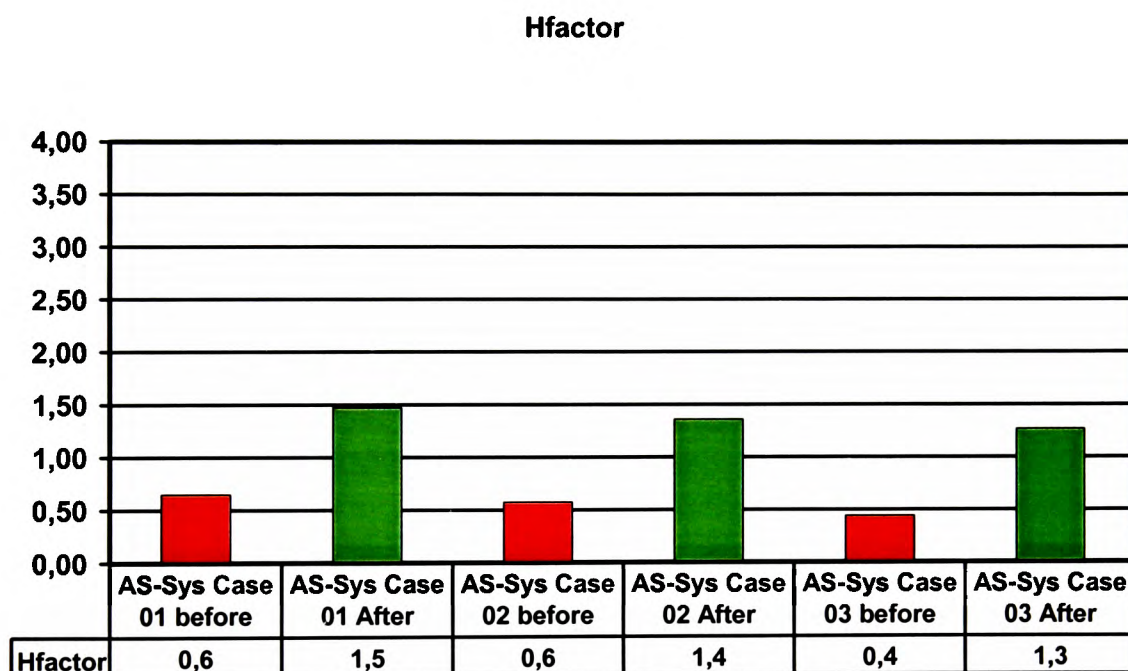


Figure 3-27. Homogenising factor for 3 cases before and after implementation of AS-System

As can be seen from Figure 3-27, all the AS-System implementations have a homogenising effect, and the improvement from the state before the implementation is an average of 170%. Knowing this, it can be stated that not only can segregation be avoided, there is even a potential of reducing fluctuations by the raw material logistics in an aluminium process, and this is actually not very difficult.

### 3.3.5 Economical calculation of full Anti segregation system implementation

Before investing in an anti-segregation system, its economical viability has to be investigated. Usually the payback time of such an installation would provide sufficient information for the decision makers, and an attempt of indicating what pay back time can be expected for an anti segregation system is therefore included here.

The effects of segregation suggested in 3.3 are made quite plausible, if not proved. Some of the extra effects on the logistic loop, like less plugging and other flow problems, as well as better stability in the FTP's are quite hard to quantify in terms of economical value. The environmental impacts are also difficult to count in terms of money, but are never the less important. However, the suggested impact on the heat balance, hence the influences on current efficiency may be estimated. Based on this estimate it is possible to calculate the actual pay back time, and the net present value for a full anti segregation installation for a given aluminium factory. In order to do such calculations one needs to calculate it as an example of a full factory. Furthermore, as for any economical evaluation of this type one need to make some assumptions of prices etc. The prices that will be used here will be based on the experience of the author from building such systems in actual factories, hence direct references cannot be given due to the sensitivity of these numbers.

#### 3.3.5.1 *Economical estimate of a 600 kton smelter*

When building a smelter of this size, the layout is decided based on several variables. Some of the variables/ parameters will be:

- Cell design
  - Current
  - Suction rate of the cells
  - Current Efficiency (CE)
- Pot room design
  - Double or single hall
- Fume Treatment Plant (FTP) layout
  - Size
  - Arrangement



To design the plant one needs to establish how many pots one needs to produce approximately 600 ktonnes of aluminium, below is a rough empirical formula for calculating the production of one pot/ cell, given the current and current efficiency, rule of thumb equation used in aluminium industry.

$$Annual\ Prod = 8,052 \left[ \frac{kgAl}{day \cdot kA} \right] \cdot I [kA] \cdot \frac{CE[\%]}{100} \cdot \frac{365}{1\,000} \left[ \frac{day}{\frac{kg}{t}} \right] \quad \text{Equation 3-7}$$

Where

I                      Current used in electrolysis cell [kA]

CE                     Current Efficiency [%]

Setting the current I to 300 kA (current for example commercially known AP30 cells from Pechiney sold world wide), and a current efficiency (CE) of 93-95 %, one pot ends up producing ~ 820 - 840 tonnes of aluminium annually. In order to meet the goal of 600 kt one then needs 716 - 732 pots, rounded to an easy number to be divided into a symmetrical layout for gas ducts. If each of the pots needs a suction rate of 6 600 Nm<sup>3</sup>/h, a total FTP capacity of ~ 4,8 MNm<sup>3</sup>/h will be required knowing that FTPs of 1, 2 MNm<sup>3</sup>/h are available, although the size is close to the upper limit, the number of FTPs needed for the smelter would be 4.

In simplified terms the system requires two silos, one for primary alumina, and one for secondary alumina (alumina that has been used for adsorption of fluoride). Therefore, the 600 kt smelter needs 4 x 2 silos with AS-Systems for the FTPs. These silos are typically in the size range of 2 - 5 kt each, and by experience, an AS-System installation such a silo size would amount to about 2 MNOK/ silo, giving the total need for anti segregation investment for the FTPs to 16 MNOK.

Any smelter would need a main storage, which should be able to sustain the smelter with alumina for one month, with some extra. As indicated earlier, one needs approximately 2 kg Al<sub>2</sub>O<sub>3</sub> to produce 1 kg Al. The annual consumption of alumina to is therefore 1,2 Mt.

This results in a monthly consumption of ~100 kt/month. The main storage needs to match this and also preserve the demands for a safety storage. This author would in this case therefore recommend a storage of 160 kt, divided in say 4 silos of 40 kt each, estimated to a total cost of 30 MNOK for the installation of the AS-System in all 4 silos.

Total investment in anti segregation for the aluminium smelter, given in the text above would then amount to 46 MNOK. For the following calculation the interest rate will be set to 10%, \$US exchange rate 6,5 NOK/\$US, self cost for production of extra produced aluminium due to current increase 800 \$US/t, and a long term London Metal Exchange pricing for aluminium of 1 700 \$US/t. The latter might be seen as an optimistic value, however, the self-cost is conservative.

To calculate the pay back time, and the net present value, the following equations can be used [Sydsæter et.al 1998]:

$$A_t = \frac{R_1}{(1+r)^1} + \frac{R_2}{(1+r)^2} + \dots + \frac{R_t}{(1+r)^t} = \sum_{i=1}^t \frac{R_i}{(1+r)^i} \quad \text{Equation 3-8}$$

$$T = \frac{\ln\left(\frac{R}{R-r \cdot A}\right)}{\ln(1+r)} \quad \text{Equation 3-9}$$

Where:

- $A_t$  Net present value after t periods
- $A$  Total investment [NOK, \$US or £]
- $t$  Period number [#]
- $T$  Definite number of periods, i.e. number of periods needed for pay back (f.ex. number of years)
- $r$  Interest rate [-]
- $R$  The periodic return, if constant [NOK, £ or US\$]
- $R_i$  Periodic return for the period i [NOK, £ or US\$]

Using Equation 3-8 to calculate the NPV ( $A_t$ ) for different CE between 0 and 1%, the results are given in Table 3-2 and Figure 3-28

Table 3-2. NPV calculation for different CE increases.

Exchange Rate [NOK/\$US]		6,5								
LME Al price [\$US/t]		1 700								
Self cost [\$US/t]		800								
Smelter size [t/year]		600 000								
CE Increase	0,20 %	0,30 %	0,40 %	0,50 %	0,60 %	0,70 %	0,80 %	0,90 %	1,00 %	
Increased Profit [NOK]	7 020 000	10 530 000	14 040 000	17 550 000	21 060 000	24 570 000	28 080 000	31 590 000	35 100 000	
Investment	-46 000 000	-46 000 000	-46 000 000	-46 000 000	-46 000 000	-46 000 000	-46 000 000	-46 000 000	-46 000 000	
Interest rate	10 %	10 %	10 %	10 %	10 %	10 %	10 %	10 %	10 %	
Year	0,20%	0,30%	0,40%	0,50%	0,60%	0,70%	0,80%	0,90%	1,00%	
0	-46 000 000	-46 000 000	-46 000 000	-46 000 000	-46 000 000	-46 000 000	-46 000 000	-46 000 000	-46 000 000	
1	-39 618 182	-36 427 273	-33 236 364	-30 045 455	-26 854 545	-23 663 636	-20 472 727	-17 281 818	-14 090 909	
2	-33 816 529	-27 724 793	-21 633 058	-15 541 322	-9 449 587	-3 357 851	2 733 884	8 825 620	14 917 355	
3	-28 542 299	-19 813 449	-11 084 598	-2 355 748	6 373 103	15 101 953	23 830 804	32 559 654	41 288 505	
4	-23 747 545	-12 621 317	-1 495 089	9 631 139	20 757 366	31 883 594	43 009 822	54 136 049	65 262 277	
5	-19 388 677	-6 083 015	7 222 646	20 528 308	33 833 969	47 139 631	60 445 292	73 750 954	87 056 616	
6	-15 426 070	-139 105	15 147 860	30 434 825	45 721 790	61 008 755	76 295 720	91 582 685	106 869 651	
7	-11 823 700	5 264 450	22 352 600	39 440 750	56 528 900	73 617 050	90 705 200	107 793 350	124 881 501	
8	-8 548 818	10 176 773	28 902 364	47 627 955	66 353 546	85 079 137	103 804 728	122 530 319	141 255 910	
9	-5 571 653	14 642 521	34 856 694	55 070 868	75 285 042	95 499 215	115 713 389	135 927 562	156 141 736	
10	-2 865 139	18 702 292	40 269 722	61 837 153	83 404 583	104 972 014	126 539 444	148 106 875	169 674 305	
11	-404 672	22 392 992	45 190 657	67 988 321	90 785 985	113 583 649	136 381 313	159 178 977	181 976 641	
12	1 832 117	25 748 175	49 664 233	73 580 291	97 496 350	121 412 408	145 328 466	169 244 525	193 160 583	
13	3 865 561	28 798 341	53 731 121	78 663 901	103 596 682	128 529 462	153 462 242	178 395 022	203 327 803	
14	5 714 146	31 571 219	57 428 292	83 285 365	109 142 438	134 999 511	160 856 584	186 713 657	212 570 730	
15	7 394 678	34 092 017	60 789 356	87 486 695	114 184 034	140 881 373	167 578 713	194 276 052	220 973 391	
16	8 922 435	36 383 652	63 844 869	91 306 087	118 767 304	146 228 521	173 689 739	201 150 956	228 612 173	
17	10 311 304	38 466 956	66 622 608	94 778 261	122 933 913	151 089 565	179 245 217	207 400 869	235 556 521	
18	11 573 913	40 360 869	69 147 826	97 934 782	126 721 739	155 508 695	184 295 652	213 082 608	241 869 565	
19	12 721 739	42 082 609	71 443 478	100 804 348	130 165 217	159 526 087	188 886 956	218 247 826	247 608 695	
20	13 765 217	43 647 826	73 530 435	103 413 043	133 295 652	163 178 261	193 060 869	222 943 478	252 826 087	
21	14 713 834	45 070 751	75 427 668	105 784 585	136 141 502	166 498 419	196 855 336	227 212 253	257 569 170	
22	15 576 213	46 364 319	77 152 425	107 940 532	138 728 638	169 516 744	200 304 851	231 092 957	261 881 063	
23	16 360 193	47 540 290	78 720 387	109 900 483	141 080 580	172 260 677	203 440 773	234 620 870	265 800 967	
24	17 072 903	48 609 355	80 145 806	111 682 258	143 218 709	174 755 161	206 291 612	237 828 064	269 364 515	
25	17 720 821	49 581 231	81 441 642	113 302 052	145 162 463	177 022 873	208 883 284	240 743 694	272 604 105	

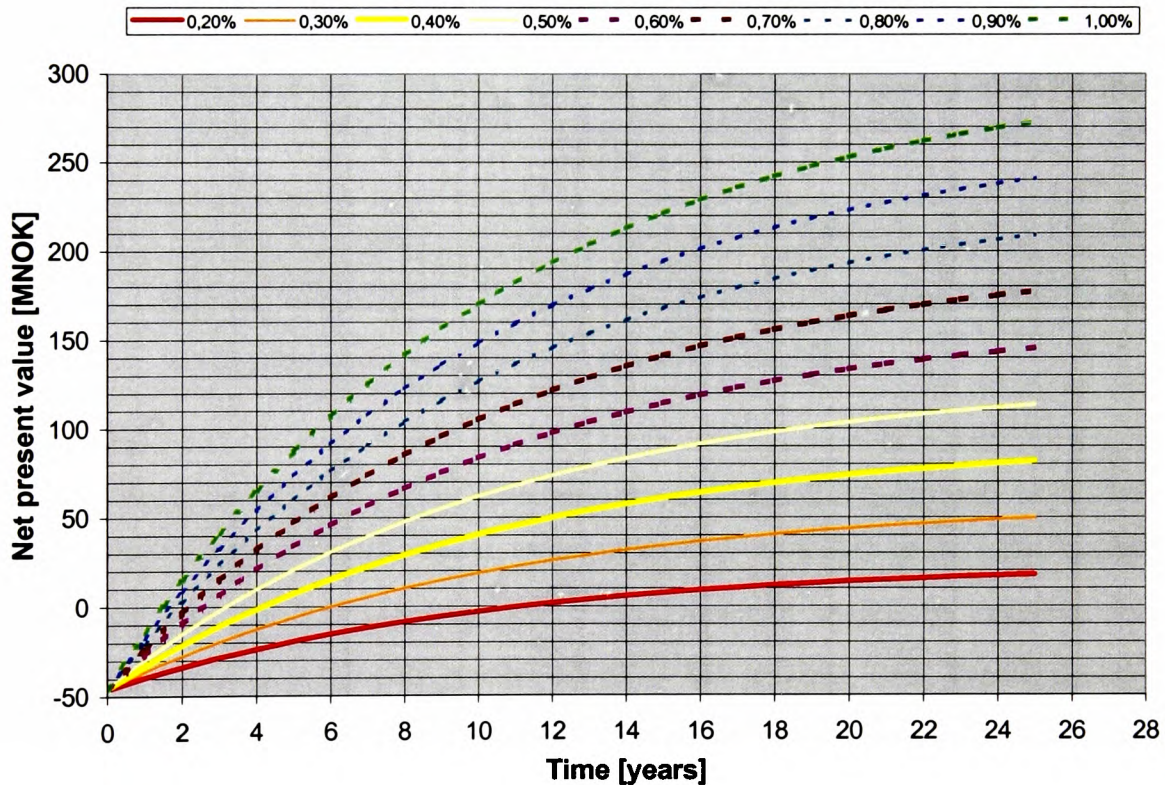


Figure 3-28 Net Present Values (NPV) for different gained Current Efficiency (CE) with 10% interest rate, 46 MNOK invest, 800\$US self cost, LME 1700\$US and exchange rate 6,5 NOK/ \$US.

From Table 3-2 and Figure 3-28 one can see that it is only a CE increase below 0,30 % that gives what could be considered a doubtful “pay back”. All the others, i.e. 0,30-1% give reasonable returns. Furthermore, dismissing CE increases above 0,50% as over-optimistic, one can see that the remaining 0,30-0,50 % give break even after 6 years. This can more clearly be seen from Figure 3-29, generated by using Equation 3-9.

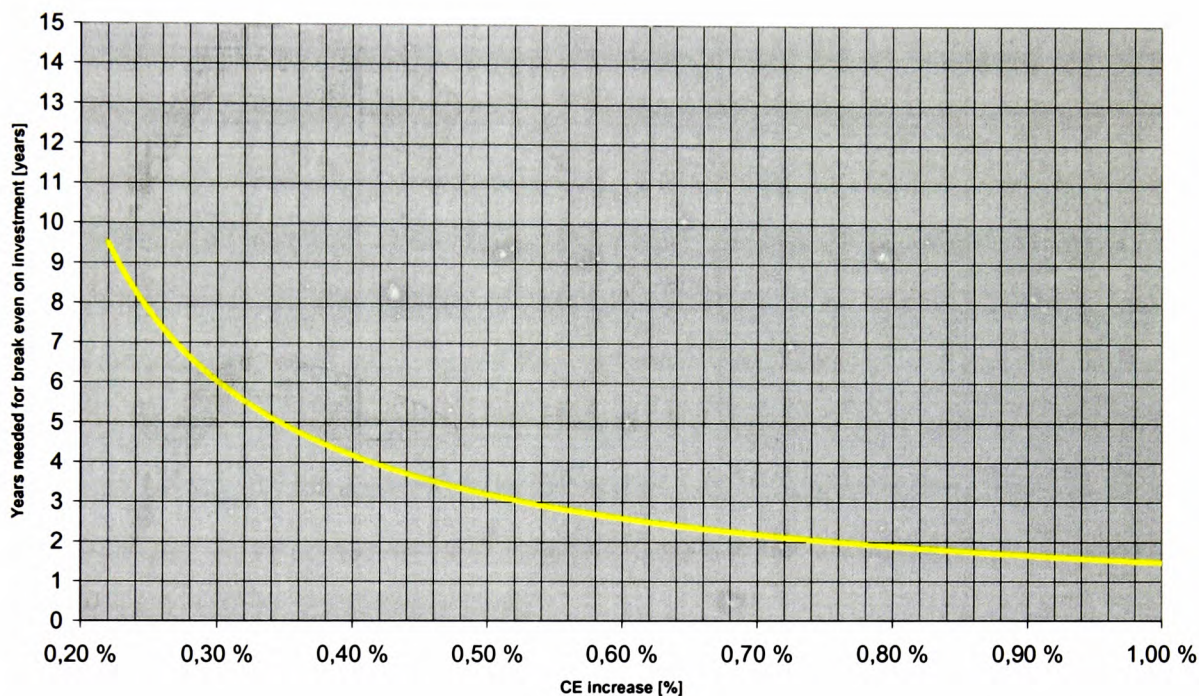


Figure 3-29. Periods for break even on investment, for different gaining Current Efficiency (CE) with 10% interest, 46 MNOK investment, 1200\$US self cost, LME 1800\$US and exchange rate 6,5 NOK/ \$US.

From the above the potential direct process response of anti segregation work should be quite clear and justified. Furthermore, this calculation does not include the reduction of self-cost that installation of anti segregation measures will invoke, by ensuring transport, and less deviations to be handled by the whole of the process, both logistical and by the electrolysis side. By implementing the AS-System, a more accurate specification can be given for other alumina handling systems, hence reducing the price by buying equipment with less wide operational range, or the range can be kept and the needed maintenance frequency can be reduced. In addition to the increased yield, the reduction of AEs and dust emissions reduces the environmental impacts considerably.

### **3.4 Summary and Commentary for Survey of Segregation in an Aluminium Plant**

The quantification of segregation is the most important “Anti Segregation Measure”. Without the information about the situation in the process stream, and information making one capable to decide what and where to fight segregation, one can simply not do anything about the segregation. With some pragmatic choices, a full factory sampling campaign is possible. Although this sometimes means to deviate from what is considered good practice in literature and standards, the process of implementing sampling as a natural part of a process is of high value. By placing sampling points along the logistic loop for one or several materials, and sampling these points for a long enough period, information on the influence of the units on the quality of the bulk solids can be identified. Such influence might be segregation and crushing of the material. Standardised statistically expressions can then be used for analysing the bottlenecks of the logistic loops, and from this information, any anti segregation, and crushing measures can be implemented. Such factory sampling campaigns are essential tools to map and increase the understanding of the influence of the raw materials on the process itself.

The degree of segregation when handling alumina has proven itself to be quite considerable, not only in terms powder technology but also in direct process influence. The powder technology bit clearly shows that the transportability and flowability of alumina can be very altered by the handling processes in a logistic loop. These old logistic loops are historically designed for transport between A and B in terms of capacity, and also storage volume. The transport is usually designed without any consideration of crushing or suitability for the material in hand, and storages are often dimensioned for gross volume, not considering what is available volume.

Beside the problems identified in the actual handling of alumina, direct process and environmental influences have also been found. The influence has been identified in terms of correspondence between variations due to segregation and dust concentration in the smelter pot room, and also between variations by segregation and anode effects. Furthermore, it has been found plausible that segregation can influence the current efficiency of electrolysis cells, especially cells run close to optimum performance. Without including

the costs from unidentifiable actions needed to compensate for bad or no flow of alumina, or dry scrubbing efficiency, or environmental influences, an economical evaluation of an investment in anti segregation system has been made. This evaluation clearly justifies both the investigations in segregation, and the implementation of anti segregation measures.

Installed anti segregation systems have been tested, together with other systems. The AS-System clearly demonstrated a homogenising effect no matter how low the ingoing variations were. The other systems can only be considered as Segregation Effect Damping Systems, since they only seek to remedy the effects of the segregation instead of directly attacking the segregation mechanism itself. For silo filling, splitting into several heaps is a known method of choice, but these systems were found only to homogenise the alumina when the ingoing variations were large. Furthermore, systems with high frequent dosing of small increments created much better process situations than systems distributing with low frequency and large doses.

## 4. DEVELOPMENT OF AN ANTI-SEGREGATION TUBE (AST)

### 4.1 The AST Concept

The concept of an AST for counteracting air current segregation of alumina when filling silos was suggested by de Silva, based on a similar concept marketed by Trelleborg AB, as mentioned by Dyrøy and Enstad [1997]. The concept was developed in lab-scale experiments described by Enstad et al. [1992], and later tested in a full-scale installation at the Årdal Smelter in Norway [Karlsen et al, 1999]. Since first introduced, the AST valves and inlet configurations have been modified several times.

The functional principle of the AST described by Dyrøy and Enstad [1997] is to prevent the air current segregation by preventing induction of the airflow. This can be accomplished by preventing the powder from contact with air in the silo. The tube removes the contact between the air on the outside of the tube and the falling particles on the inside, and thereby restricts the airflow to the inside of the tube. To get the powder out into the silo, the tube must have valves that open sequentially at different levels in the silo. These valves are made by holes in the tube covered by flaps closing them from the outside. When powder drops down inside the tube, it drags air from the top of the tube, creating an under pressure. This under pressure closes the non-active valves. The basic function of the AST is shown in Figure 4-1.

The powder mixture falls down inside the tube (Figure 4-1), and the valve nearest to the powder surface opens and allows the powder to flow out into the silo. As the level in the silo increases, the next valve opens and so on, until the top valve opens. The under pressure diagram in Figure 4.1 indicates the under pressure along the AST, where the pressure is zero near the active valve, and has its maximum at the top of the tube. This principle does not work unless there is an inlet and a valve configuration that prevents air from entering the tube together with the powder. The key to getting the AST to work is to make the powder entrance as well as the valves as *airtight* as possible.

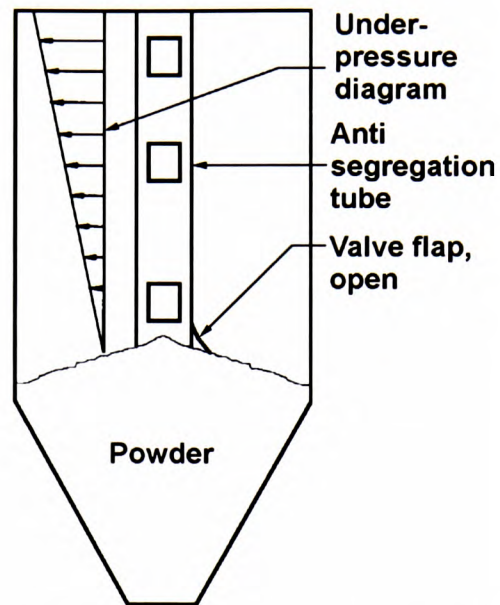


Figure 4-1. AST with valves. The diagram shows the under pressure in the tube due to falling powder.

The present total system of the AST in a silo is shown in Figure 4-2. The powder (alumina) is filled into a box on the top (inlet seal of the AST) of the silo, and moves from this into the tube with valves on the sides.

The AST system can be divided into 3 main parts:

Inlet configuration of the AST

The valves of the AST

The tube itself



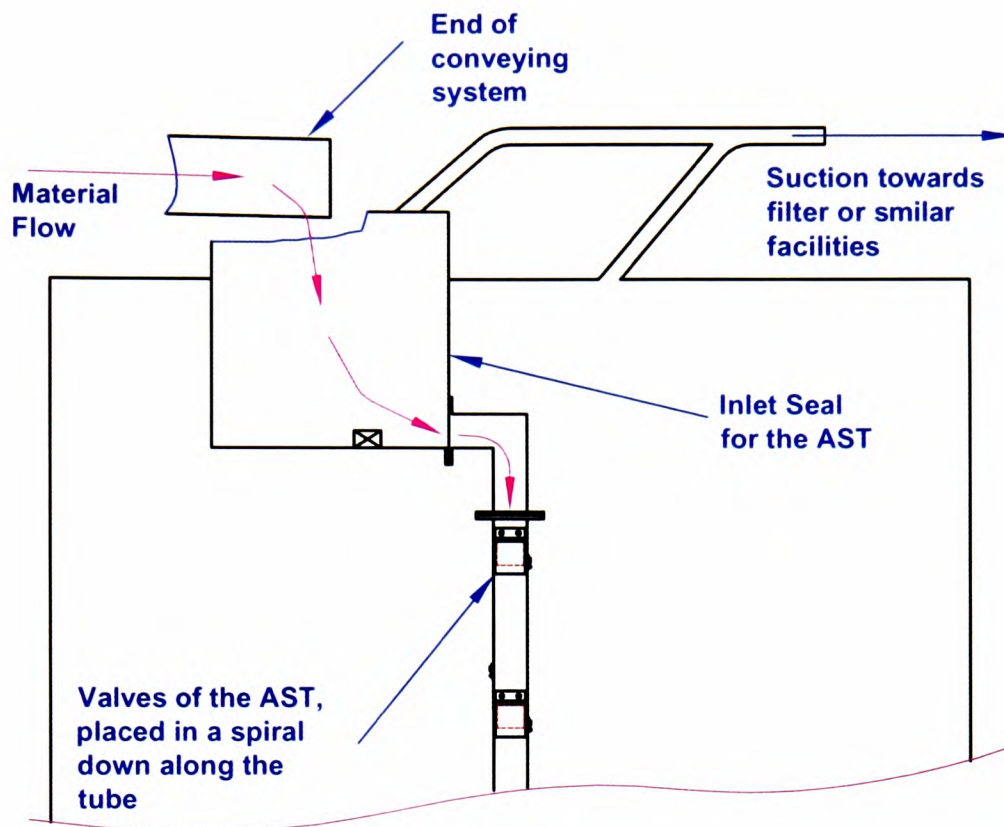


Figure 4-2. Total system of the AST, inlet box and tube with mounted valves.

#### 4.1.1 The Inlet of the Anti Segregation Tube

The first type of seal used to make the inlet of the tube airtight is shown in Figure 4-3.

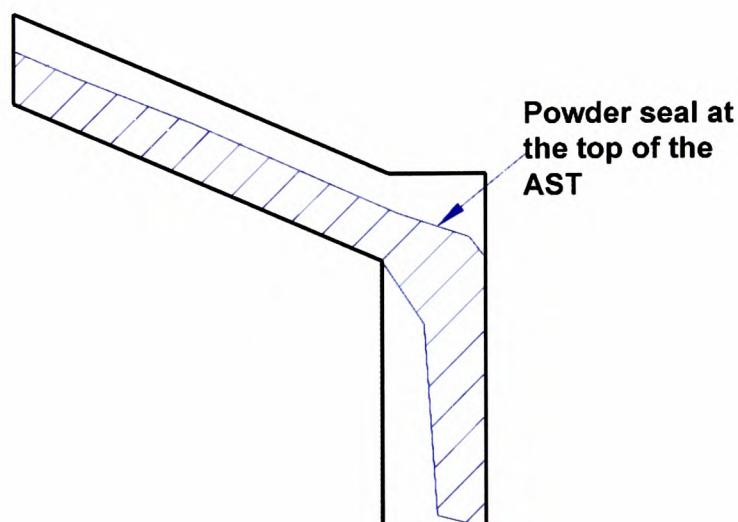
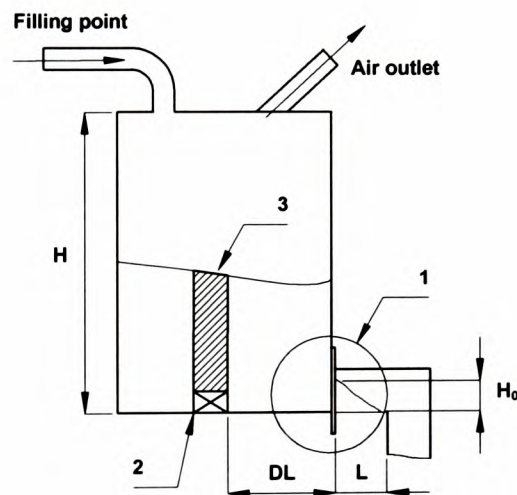


Figure 4-3. Inlet slide to the AST, using a powder bed as sealing mechanism.

The powder slides down the chute and creates a powder bed that flows across the tube, forming a dynamic seal. The negative pressure in the tube and the thickness of the sealing powder bed across the inlet increase when the feed rate increases. Therefore, it functions as a self-regulating system. However, this configuration did not work for tubes above a certain height, which was too small for practical purposes. The author tested many different configurations of this type of seal, but none of the designs could handle the variations specified by the industry for a tube that was about 3m high.

After many further ideas had been tested out, including the suggestion of a buffer silo with level controls, the principle shown in Figure 4-4 was developed. This inlet seal works as a sealing silo with a self-regulating level control, utilising fluidization. The horizontal tube outside the outlet prevents the powder from flowing out of the seal, before the contents of the seal are partly fluidised and the filling level is above a certain minimum height.



- |                |  |
|----------------|--|
| 1              | Outlet opening of the seal                             |
| 2              | Fluidizing element                                     |
| 3              | The fluidized powder zone                              |
| L              | Length of the horizontal part of the 90° tube bend     |
| DL             | Distance between the outlet and the fluidizing element |
| H              | Total height of the inlet seal                         |
| H <sub>0</sub> | Height of the outlet opening                           |

Figure 4-4. Inlet seal designed by Dyrøy and Knutsen at POSTEC, [Dyrøy, and Enstad, 1997].

As fluidization proceeds, or as the hydrostatic pressure increases due to an increasing level in the seal, more and more material is discharged, thus preventing the seal from overflowing. The challenge lies in ensuring that the amount of air entering the AST is kept to a minimum. The size of the outlet opening of the inlet seal 1, in Figure 4-4, is adjusted to the capacity range that the inlet seal should handle. It also determines the horizontal tube length  $L$ , since  $L$  is a function of the angle of repose of the powder and the height of the outlet opening. The fluidising element marked 2 activates the fluidized powder zone 3, with a fluidising velocity equal to the minimum fluidising velocity or more, and can be looked upon as the controlling element of the inlet seal. Dimension  $DL$  is a variable that is adjusted to the capacity, and its function is to prevent the powder from containing too much air as it flows through the outlet. Height  $H$  is a design variable that depends on capacity, on  $DL$ , and on the outlet opening marked 1 of the inlet seal. This must be custom designed.

#### 4.1.2 The Valves

The first AST made and installed in the aluminium industry used rubber flaps in a configuration similar to the one shown in Figure 4-5, no. 2. The rubber selected did not withstand the temperature and the chemical components it was exposed to. The rubber became brittle in a relatively short time, and the flaps fell off and caused problems in the downstream process. When using spring steel laminated with special rubber (Viton), the valves seemed to be much tougher. The steel handles the mechanical forces, such as the suction forces on each flap, and the rubber makes the connection between the flaps and the tube airtight. In Figure 4-5, one can see the development of the valve configuration during the last 2 years of development before the current solution.

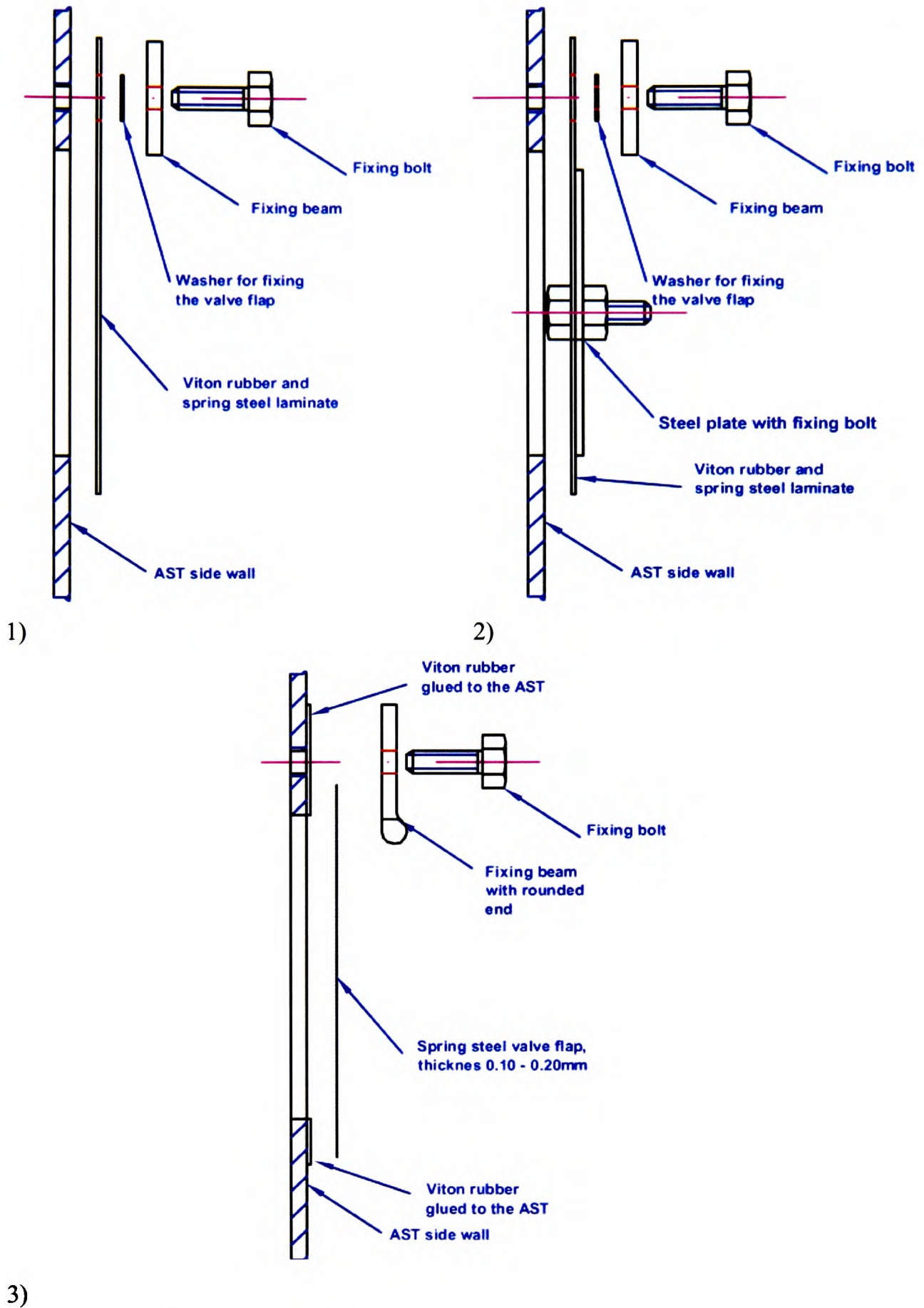


Figure 4-5. Different valve configurations.

Configuration design no. 1 in Figure 4-5 had to be changed because of closing problems, because the two materials laminated together had mechanical properties that were too stiff. Configuration no. 2 in Figure 4-5 was installed in pilot silo Hydro AAPP, and the tests shown later are based on this configuration of the valves. However, the complexity of the valve configuration no. 2, and the weakness of using a sharp edge towards the flap, provided the basis for configuration no. 3 in Figure 4-5.

### 4.1.3 The Tube

The tube itself is a standard steel square profile. Holes for the valves are made down along the tube. The holes in the tube are squared and are placed so that the lower edge of one hole on one side is placed at the same level as the upper edge of the next hole on the adjustment side. Following the holes down the tube, the path describes a spiral. Later development has shown that in larger silos the forces acting on a centre mounted tube, will demand such sizes that it has been found better to use several tubes mounted around the walls, and fed by an air-slide based distribution system on the top of the silo.

## 4.2 Basic development model

As has been indicated before, a way of mathematically estimating the pressure difference  $\Delta P$  developed between the top surface of the alumina in the inlet lock and the air inside the anti segregation tube has been suggested as shown by the following equation (variables explained in Figure 4-6):

$$\Delta P = P_1 - P_2 = \rho_1 \cdot g \cdot h_1 + \frac{\dot{m}_2 \cdot g \cdot h_2}{v_2 \cdot A_2} \quad \text{Equation 4-1}$$

This is based on the basic equation for hydrostatic pressure:

$$P = \rho \cdot g \cdot h \quad \text{Equation 4-2}$$

The density in the inlet box is set to the bulk density of aerated alumina, whereas the density inside the tube is expressed by dividing the mass flow with the product of velocity

multiplied by the horizontal internal cross sectional area of the tube as shown below:

$$\rho_2 = \frac{\dot{m}_2}{v_2 \cdot A_2} \quad \text{Equation 4-3}$$

This equation by nature assumes a complete, instant dispersion of the alumina inside the anti segregation tube, after entering the vertical part of the tube with a velocity  $v_2$  which remains constant during the entire fall inside the tube (as indicated in Figure 4-6).

The pressure difference given by this equation is considered the driving force bringing alumina from the inlet lock into the tube. When analysing the equation, one can see that the system would be self-regulated, as a larger throughput will give a higher driving force.

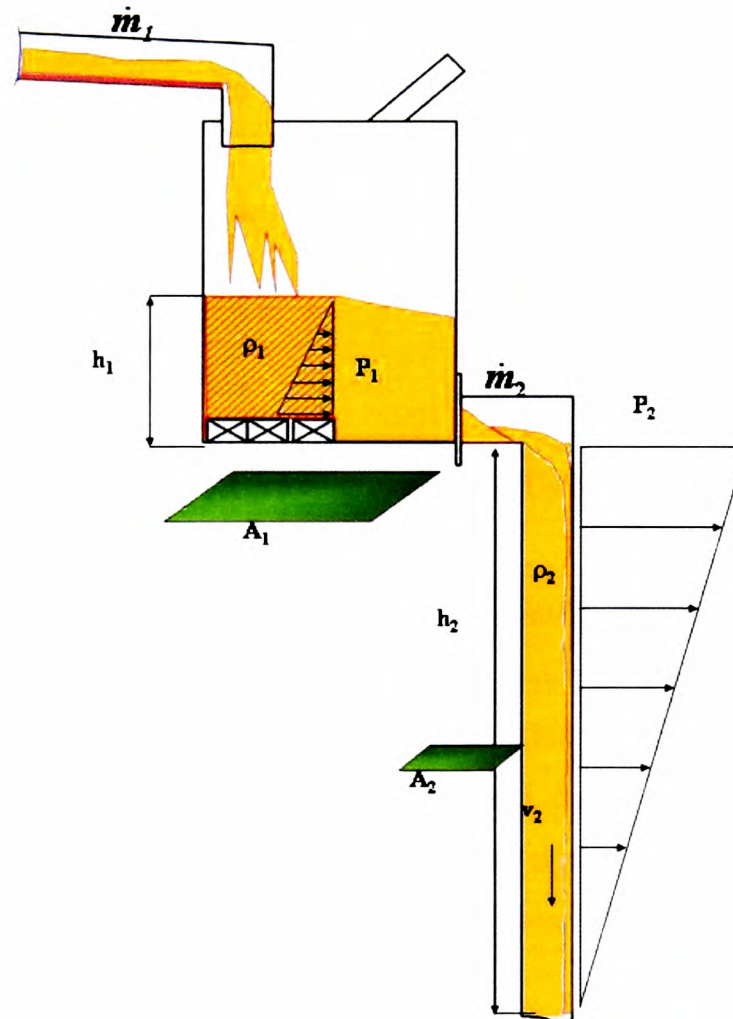


Figure 4-6. AST parameters and variables.

### 4.3 Initial Development tests

During the initial development of the anti segregation tube many configurations were used, Hubrich [1998], was given test set up as shown in Figure 4-7 for his Student Arbeit assignment, carried out at dept. POSTEC. The tube here, was of a centre mounted type (will be addressed later), and the total height was 3,4 meters height and a quadratic profile type 100x100 t=4 mm.

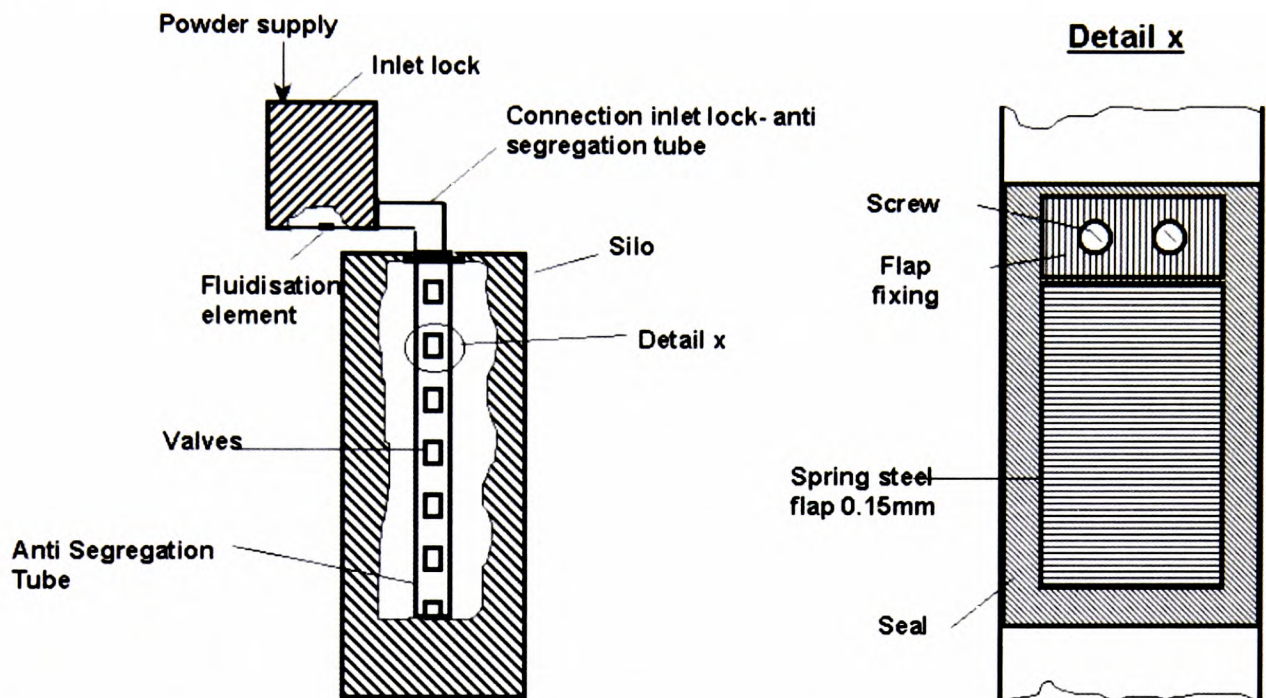


Figure 4-7. Test set-up during initial development, from Hubrich [1998].

The aim for these tests was first to find a valve configuration (Figure 4-5), that not only opened on desired time, but also was airtight and had endurance. The Initial tests utilised only one pressure measurement in the top of the tube. This was based on the assumption that the pressure was linear with the height of the tube, as given from equations represented under section 4.2. However, in posterior even the simplest estimates of the velocity inside the tube indicate that the pressure should not be linear.

In Figure 4-8 through Figure 4-11, the filling height of the inlet box and the negative pressure in the tube are shown for different capacities, as it progresses with time. What one could especially notice is Figure 4-8, is that the pressure and filling height are moving in cycles. What is happening in this situation is that the feeding capacity of the system is so

low that the transport through the tube starts and stops. The starts and stops occur because of the higher capacity of the tube, resulting in decrease of the level in the inlet box, hence punctuation of the seal when the box is nearly emptied and thus loss of the under pressure of the tube. The transport starts again when the level in the inlet box is sufficient to give a hydrostatic pressure in the inlet box that can push the alumina into the tube.

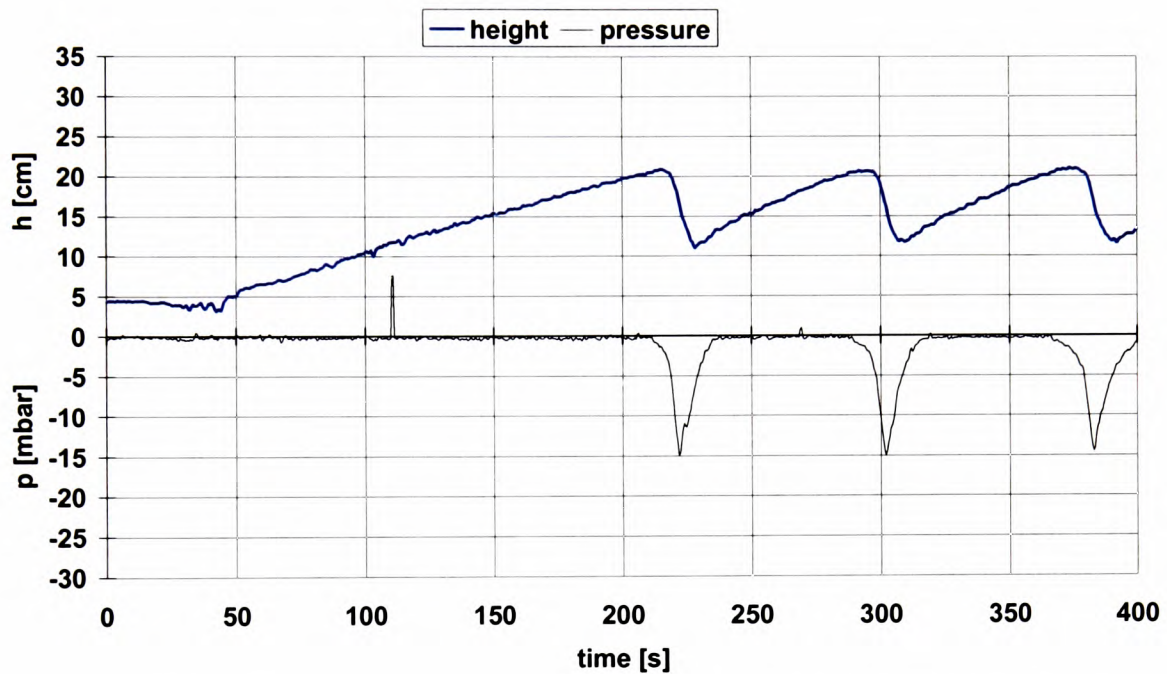


Figure 4-8. Development tests, 1 t/h, filling height and negative pressure in tube.



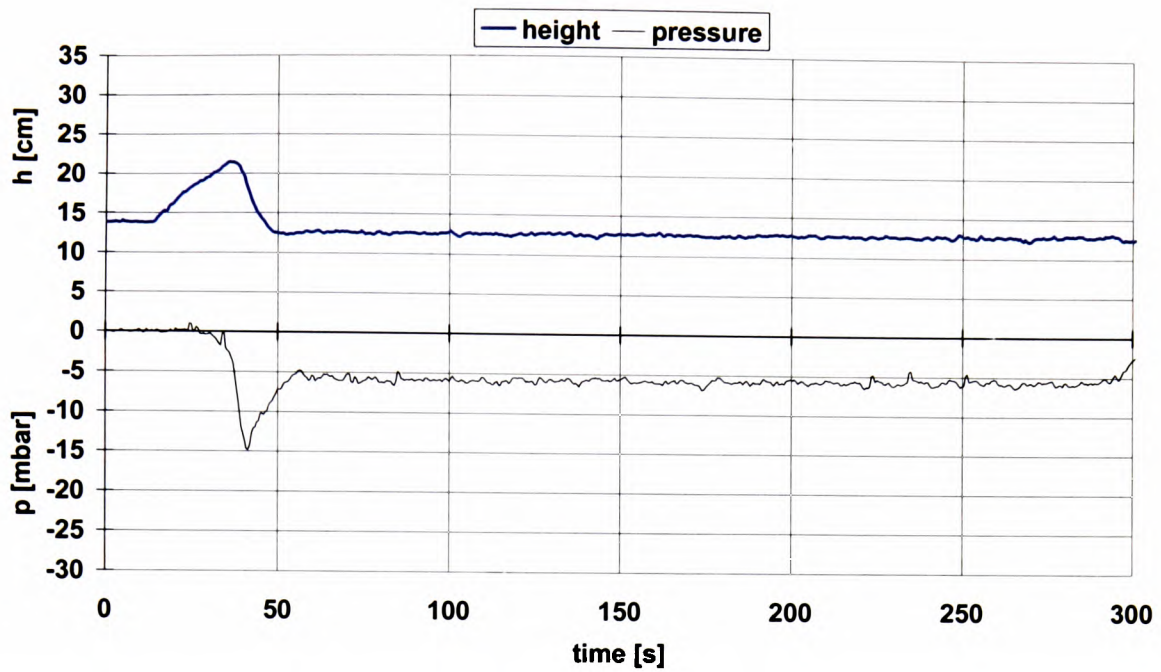


Figure 4-9. Development tests, 3 t/h, filling height, and negative pressure in tube.

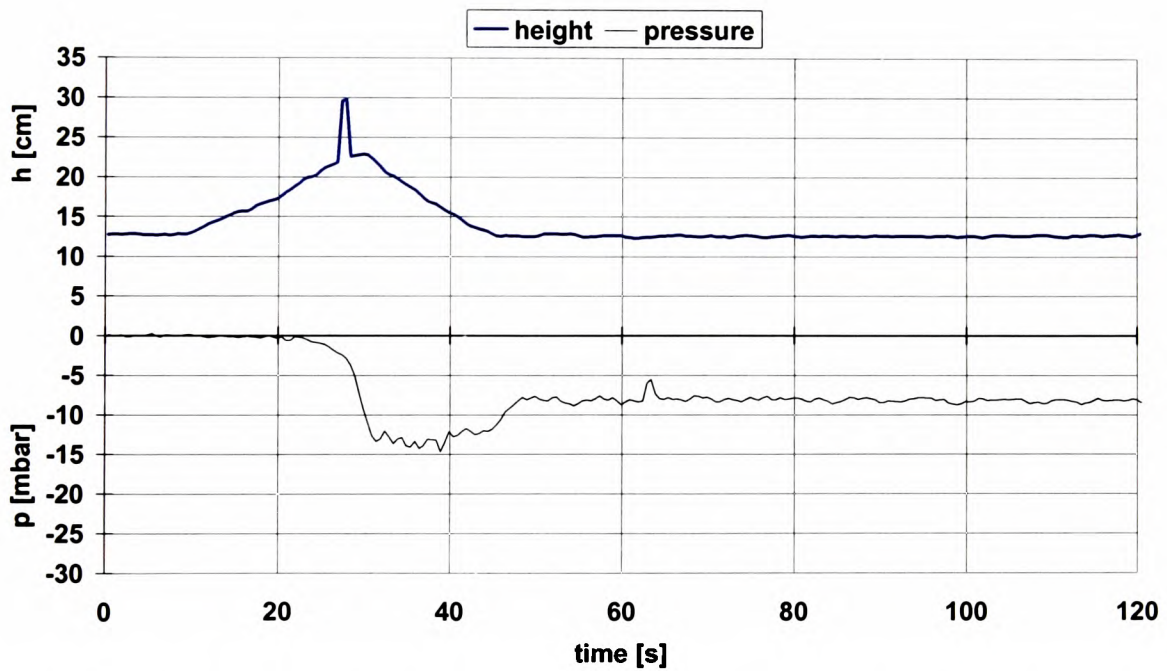


Figure 4-10. Development tests, 5 t/h, filling height, and negative pressure in tube.

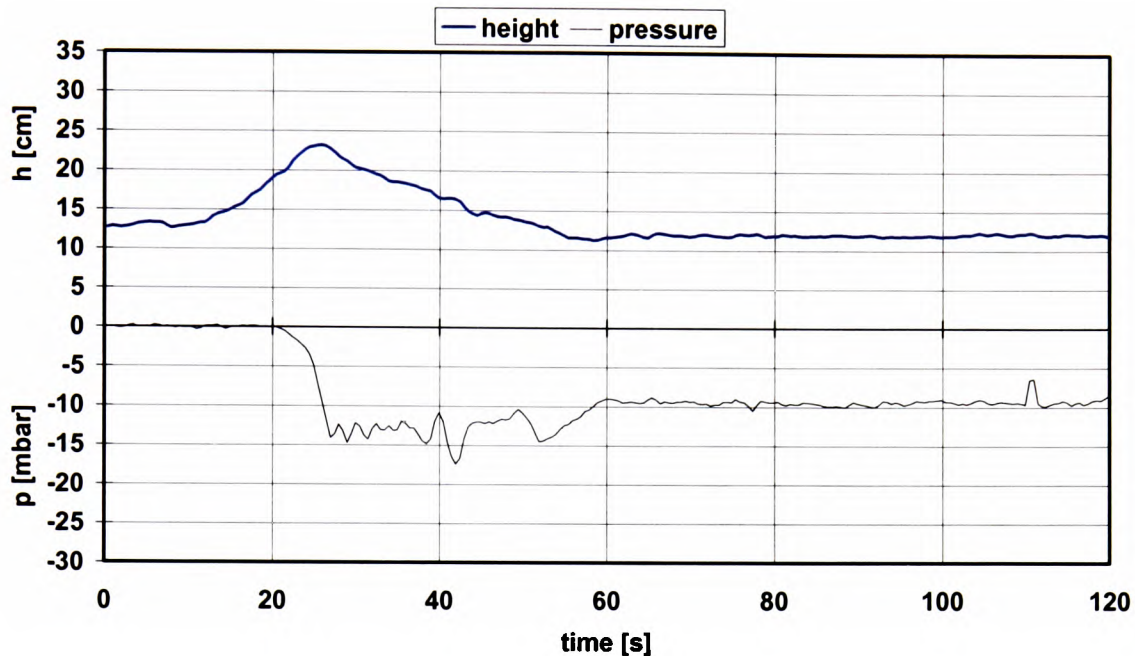


Figure 4-11. Development tests, 7 t/h, filling height, and negative pressure in tube.

For the tests with capacities higher than 1 t/h, the fluctuations pointed out above, do not occur. The reason is not that the max capacity of the tube is being reached, as later data will demonstrate, but rather that by this capacity the outlet from the inlet-box is covered at all times. Therefore, the negative pressure in the tube plus the hydrostatic pressure from the level in the inlet-box is able to maintain continuous transport. The results of the tests summarised in the plots above, indicate that the inlet box is a self regulating system, and that the driving force of the system is the total pressure drop from the top of the alumina in the inlet box to after the 90° elbow. Furthermore, the fact that the tube is changing into a start-stop mode in the lower capacity region, indicates that the system has no lower operational limit, it simply changes the transport mode.

On all the tests, one can see and will see in later sections, that the initial negative pressure at the top of the tube has a peak, before stabilising. The reason for this will be more explained in the modelling of the tube in section 5.

After establishing that the anti segregation tube with its inlet, does not have a lower limit for a given tube size, the logical question then becomes, what is the upper limit? A test set up, seeking to find this limit is shown in Figure 4-12, Hubrich [1998].

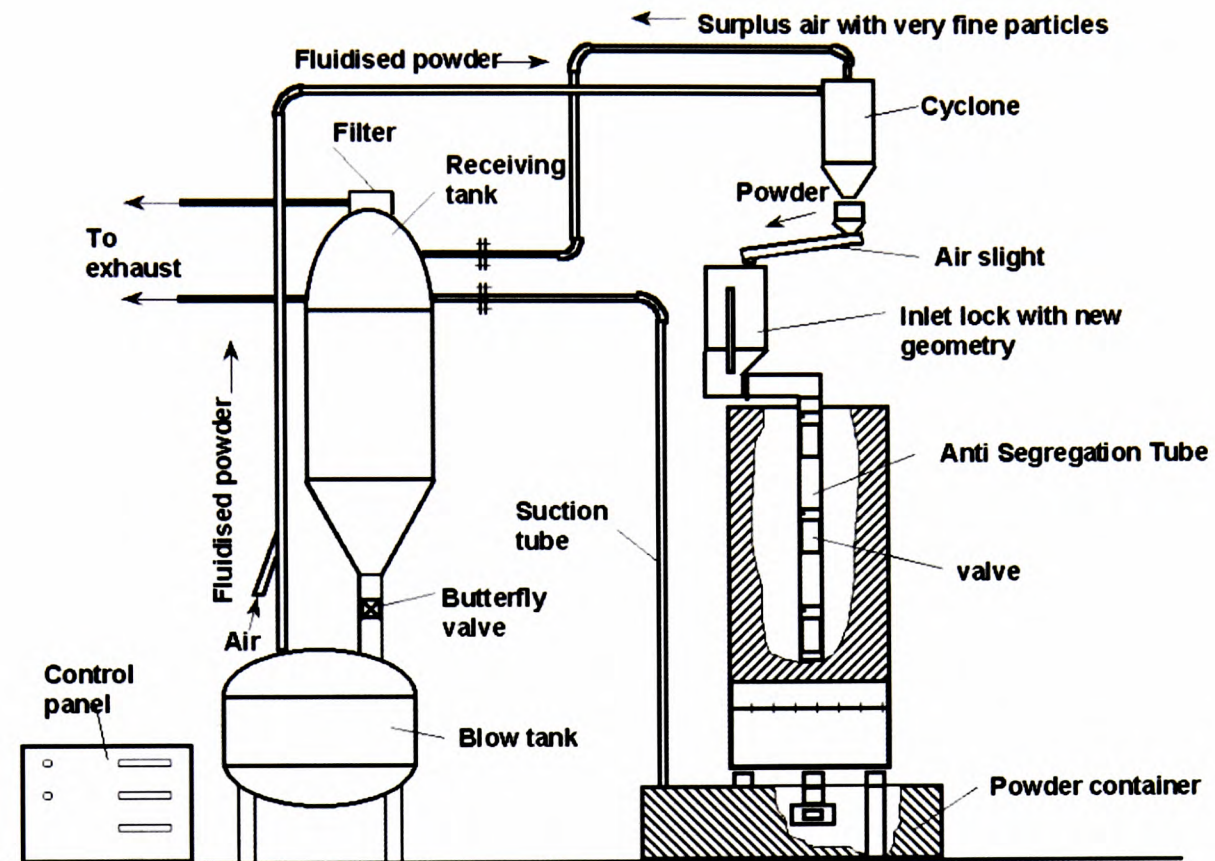


Figure 4-12. High Capacity tests during initial development, from Hubrich [1998].

After running with the test setup, utilising a Hethon screw feeder, with limited capacity, something with a higher capacity had to be set up, in order to reach the upper limit of the capacity of the tube. In Figure 4-12, a schematic test-setup is shown. The rig is the same as before except for the feeding unit, which is a pneumatic transport system. To remove the transport air a cyclone, connected to a blower and a filter is implemented, and from the cyclone an air slide is feeding the inlet box of the anti segregation tube. After each filling, the silo with the AST is emptied, and a suction system using the same blower, fills the alumina powder into the receiving tank, which feed the pressure vessel below. To have control of the capacity during the actual filling test, a calibration of the transport capacity as a function of the initial pressure in the pressure vessel are set up and is shown in Figure 4-13 below.

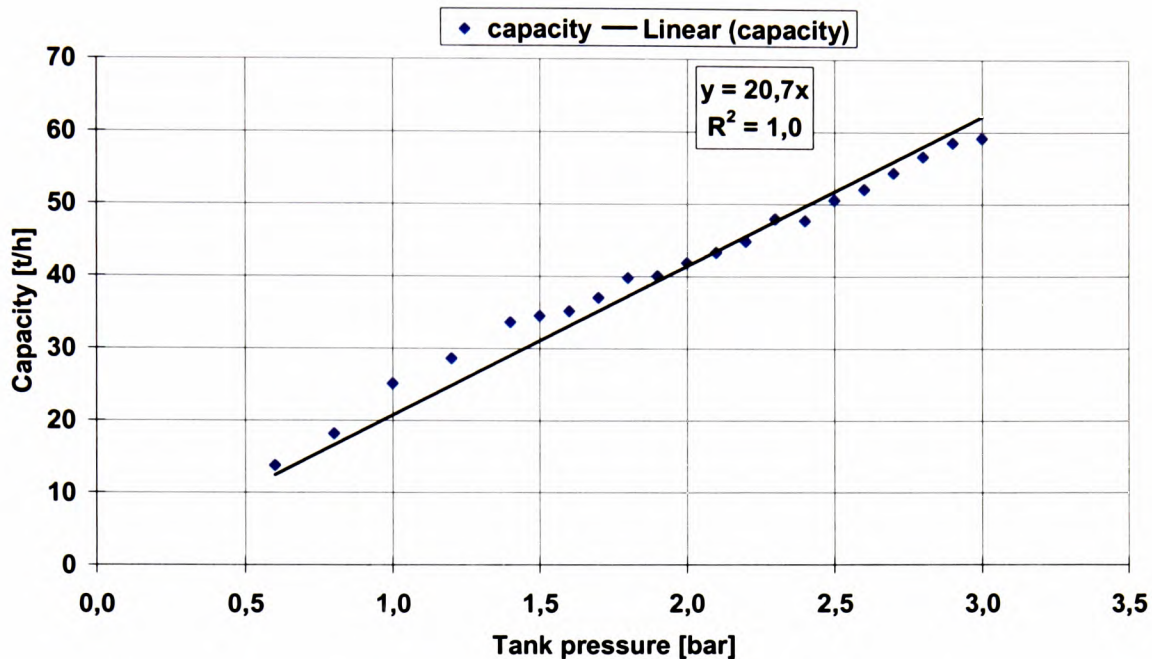


Figure 4-13. Calibration of capacity as a function of the initial pressure for pneumatic conveying of alumina.

To calibrate the feed as shown in Figure 4-13, is of course not a recommended way of determining capacity of a pneumatic conveying system, however, for this purpose the calibration turned out to be a suitable tool. The actual capacity achieved had to be calculated after each run.

Tests spanning from 10 t/h towards 50 t/h, in real capacity were carried out for the 100x100 t=4 mm profile, and this tube seemed to have a limit of 50 t/h. Figure 4-14 shows an example of such a high capacity test, here 30 t/h. From the plot, one can see that the negative pressure decreases with time and at the same time the filling height of the inlet increases. These phenomena are caused by the increasing filling level in the silo, as the fall height the negative pressure in the AST decreases, and to maintain the same capacity, the level in the inlet box increases making the hydrostatic pressure in the inlet box increase to maintain the driving force of the system, which is the total pressure difference. From these tests, a rough estimate of the capacity for a given tube is based. The designing factor became  $500 \text{ kg}/(\text{cm}^2\text{h})$ , where the square is calculated from the open cross sectional area inside the tube (i.e. profile width minus two times the wall thickness).

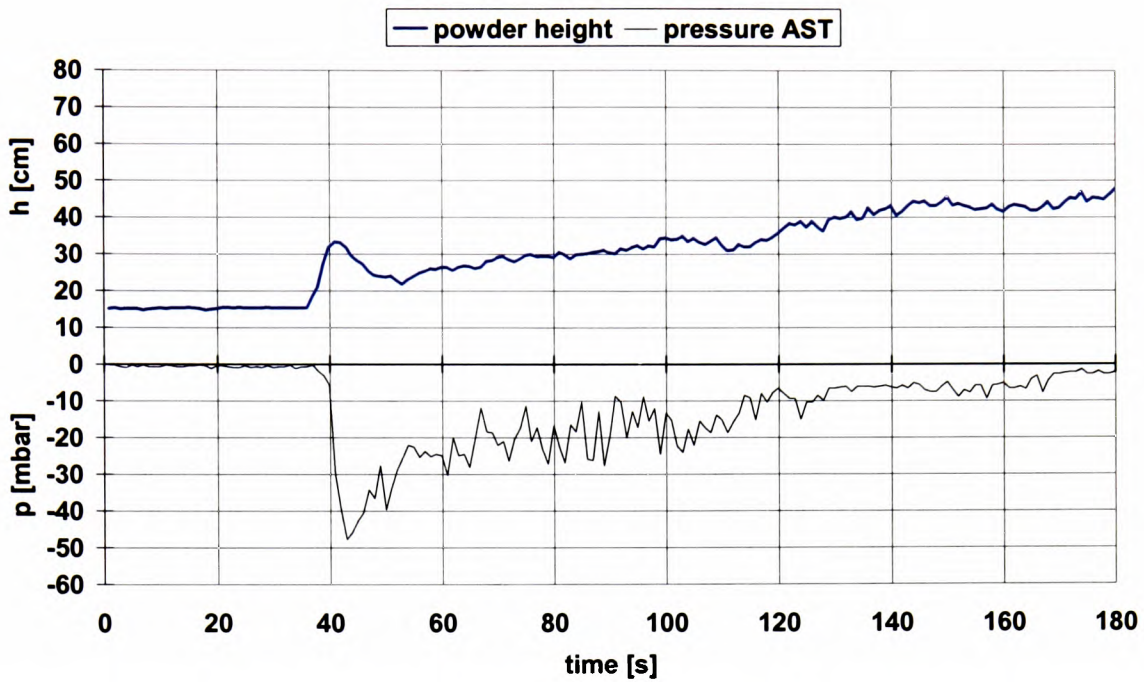


Figure 4-14. High capacity test example, here 30 t/h.

An example of the constant driving force, i.e. pressure drop through the ninety-degree bend from the inlet box to the AST, is shown in the 5 t/h test in Figure 4-15. The total driving force for one capacity, i.e. one velocity is at least in this region seemingly stable.

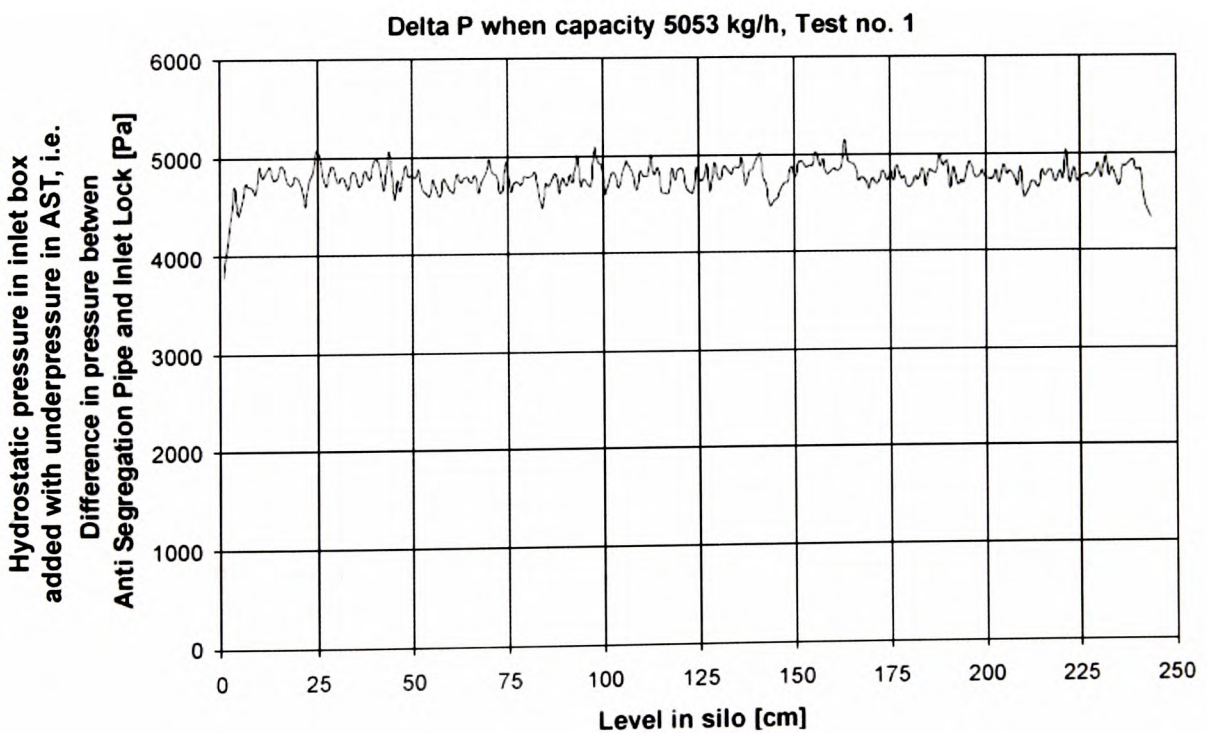


Figure 4-15. Driving force plot for a 5 t/h test.

Looking for something similar for the high capacity tests, the driving force for a given capacity here also seems constant. Calculating the driving force in principal from the measurements shown in Figure 4-16, one gets the results shown in Figure 4-17.

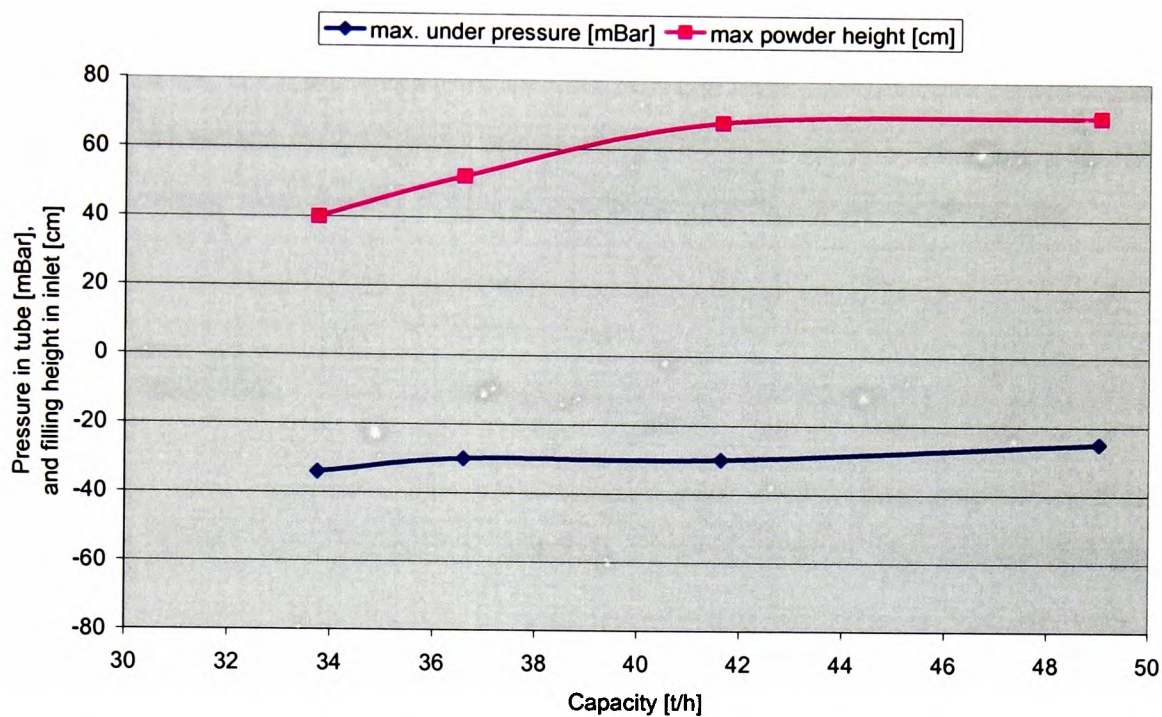


Figure 4-16. High capacity tests, max negative pressure, and filling height of inlet box.

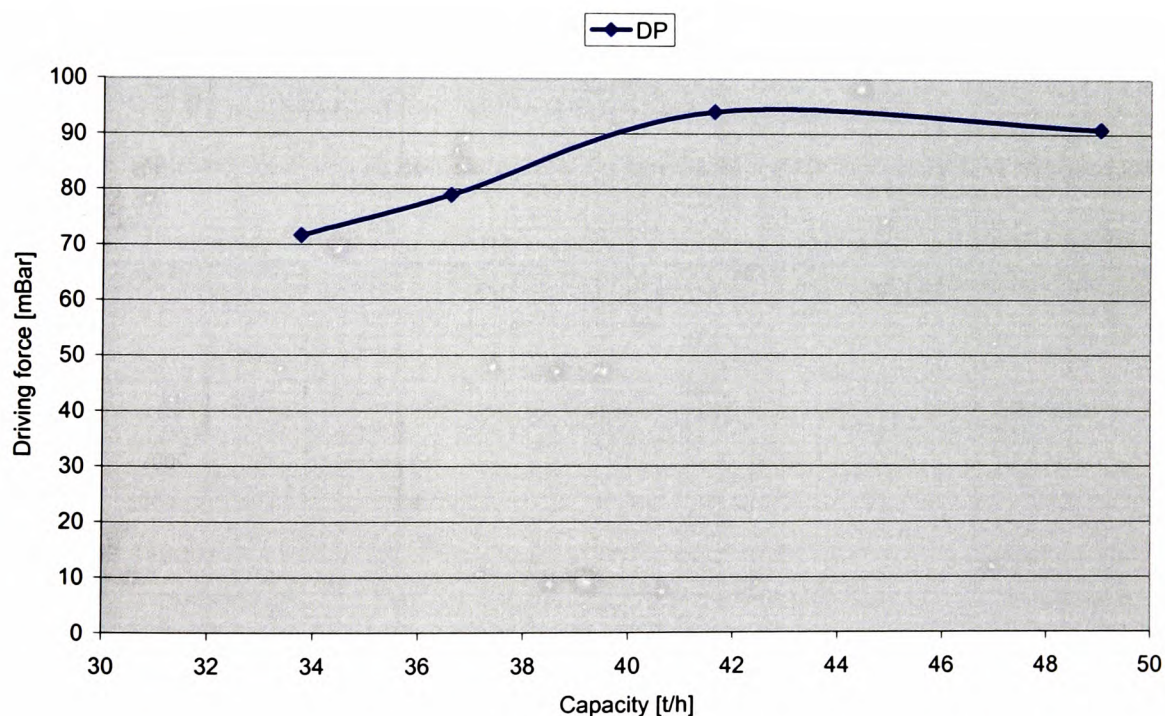


Figure 4-17. Calculated driving force based on the measurements shown in Figure 4-16.

The results in Figure 4-17 are calculated by the use of Equation 4-1 and Equation 4-2. As can be seen the driving force bends off and shows a slight decrease above approximately 45 t/h. This can probably be explained by the residence time in the inlet box. When the capacity is increased, the time spent in the inlet box is reduced, since the size of the inlet box is constant. Hence, the de-aeration time for the alumina is shortened, and therefore the bulk density of the alumina decreases and the sealing effect of the inlet box are reduced. The capacity where the driving force bends off and starts to drop with increasing capacity is close to the upper limit for the AST configuration used for these experiments.

#### **4.4 New test rig**

After the initial development of the anti segregation tube, some pilot implementations became actual. During the engineering of these implementations, the mechanical strength needed for a centrally mounted tube in large silos forced the tubes to become very large. The forces during potential avalanches and side forces from the flowing alumina demanded quite rigid tubes. Therefore, the idea of placing the tubes at the wall of the silo came up. For this idea, one needed a central distributor, with transport to the tubes at the wall. Furthermore, after working with the AST for quite some time, this author suspected that the pressure inside the tube could not be linear. Hence, the idea of pressure measurements along the length of the tube became a reality.

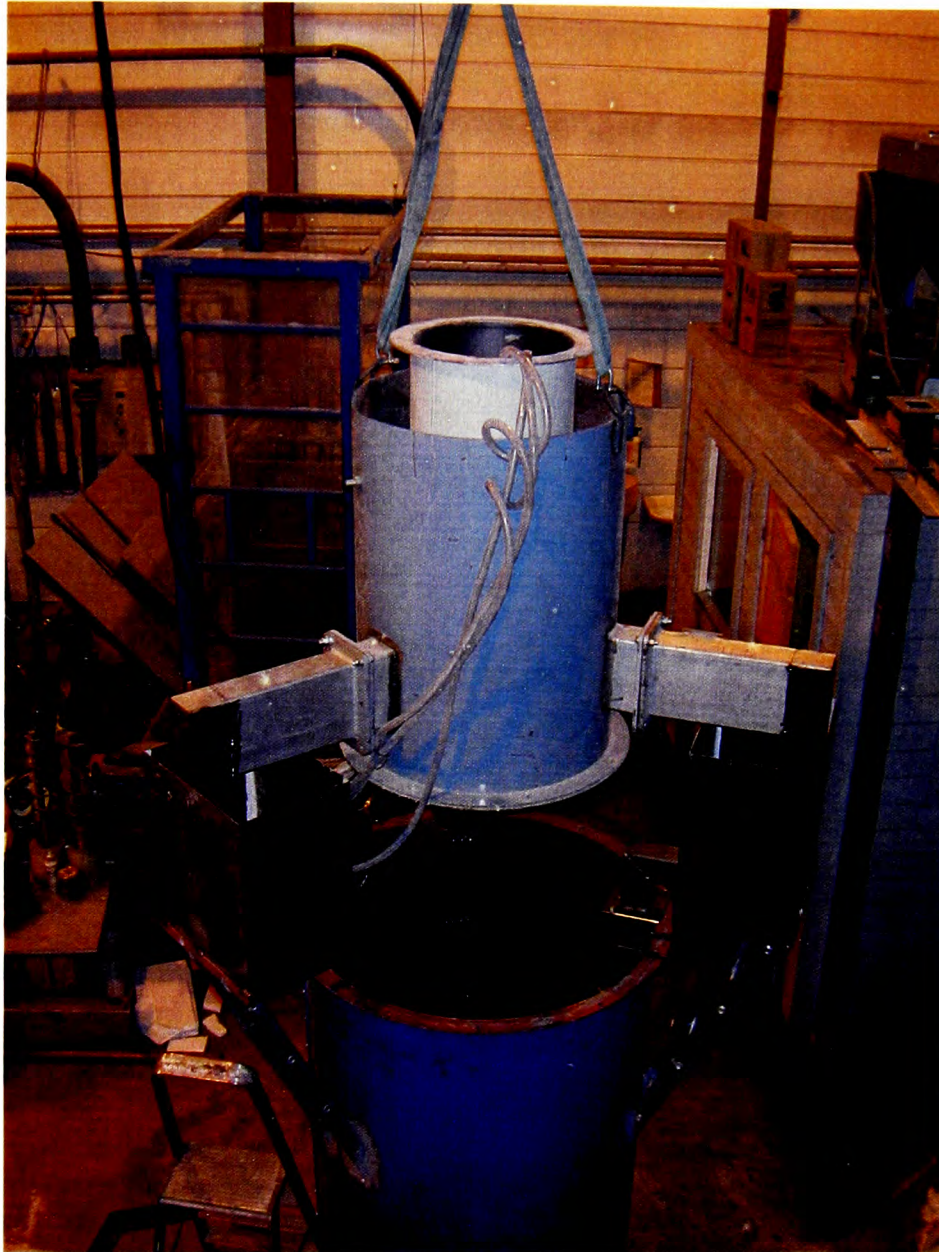


Figure 4-18. Anti segregation system developed and test rig.

Figure 4-18 shows the total Anti Segregation System (AS-System©), development and test rig. The rig is intended for two types of tests. First, to test the effect of the anti segregation system, as described in section 4.7, second for the research of the pressure distribution, and flow inside the tube itself. In the latter test, only one tube will be utilised.

#### 4.5 Experimental test setup of the AS-System with three AST's, equipment and procedures

As mentioned above, the experimental AS-System silo contained three AST units, but



only a single unit was used for the measurement of pressure.

Figure 4-19 shows the complete equipment set-up, with the data recording system positioned in the foreground. A schematic drawing of the designed test set up is given in Appendix F.



Figure 4-19. The assembled test equipment.

Seven pressure transducers were purchased from Endress & Hauser, capable of measuring positive and negative pressures between 0 and 50 mbar with an electronic output of 4 to 20 mA. They were labelled P1 to P7 starting from the top of the tube-section to the bottom. Each transducer was calibrated by the manufacturer to within 0.07% of the actual current (mA) output value; the calibration certificates are located in Appendix C. Four of the transducers (P1, P3, P5, and P7) were re-calibrated by POSTEC to verify their accuracy, and all were found to be acceptable.

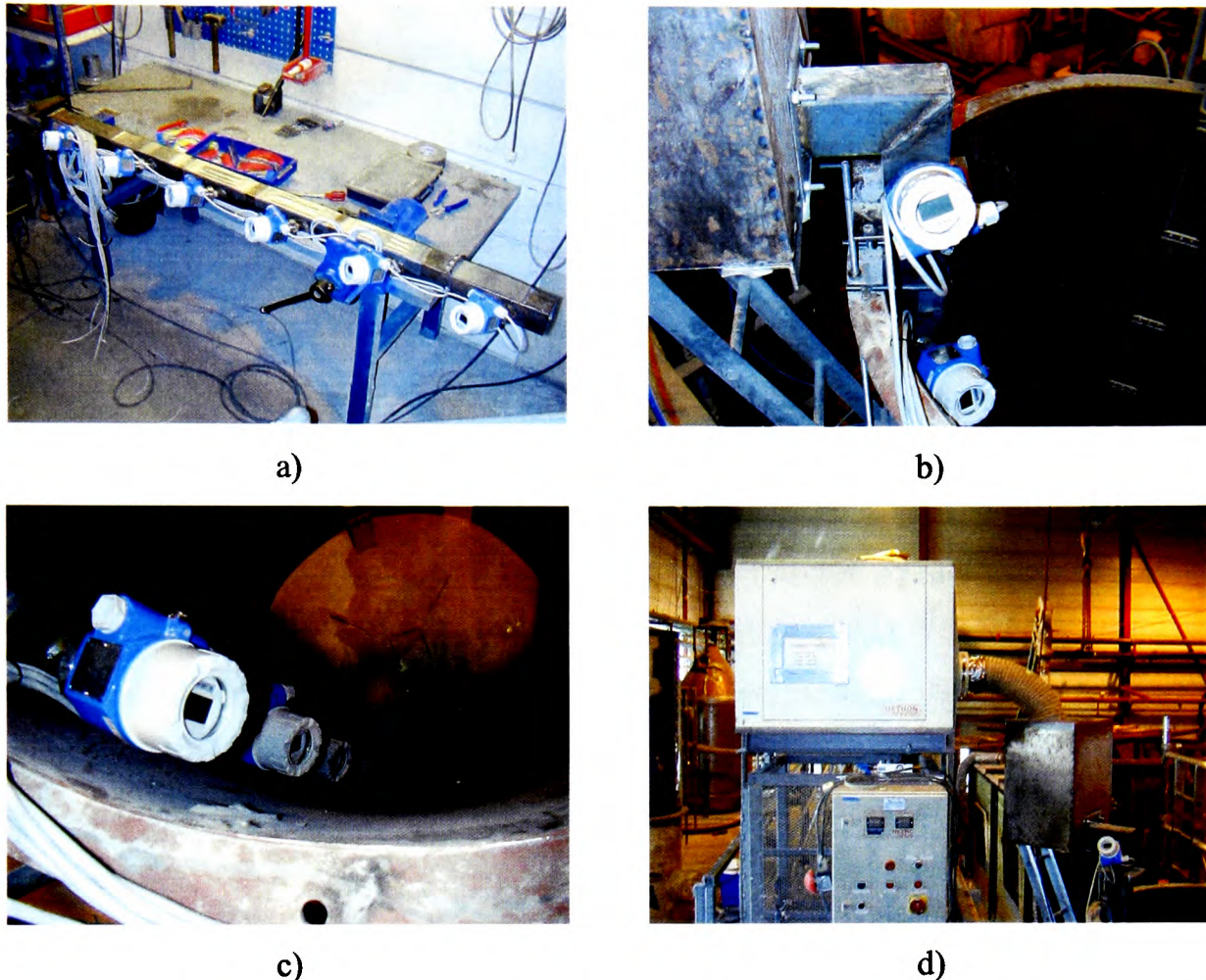


Figure 4-20. (a) Transducers P2 to P7 located on the tube cross-section (b) P1 located above the flange (c) Tube-section installed into the silo (d) Hethon screw-feeder located above the AST box-section.

The first transducer P1 was located at a point equidistant between the right-angle bend and the flange of the tube-section (Appendix F). The final transducer P7 was positioned on an equal level with the bottom of the last valve, and the remaining five transducers were positioned at equal distance between these two points. The electrical wiring was then installed in order to connect the transducers to the data recorder. The four upper valve flaps were removed, the holes were sealed using tape, and the lowest valve was left to function as normally, see Figure 4-20a). The tube-section was then positioned inside the silo and attached to the box section, see Figure 4-20 b), and Figure 4-20 c).

A Hethon screw-feeder was used to supply a constant flow of powder from the 600 kg charging tank to the box-section of the AST. The screw-feeder speed settings were calibrated for alumina prior to installation. This involved filling the screw feeder storage hop-

per with alumina, adjusting the flow rate counter on the feeder, and turning the machine on. The powder was dispensed for a measured amount of time and collected in a plastic bowl, which was subsequently weighed using a weigh scale. The mass flow rate was calculated in tonnes/hour for that particular counter setting on the feeder. The calibration results are shown in the form of a chart in Appendix C. The equation of the line of best fit, which was forced through the origin, allows any desired mass flow rate to be selected within the operating limits of the feeder.

A clear Perspex lid was prepared for the top of the box-section, which contained two holes of diameters 14 cm and 11 cm for the powder inflow (from the screw-feeder) and outflow (vent to atmosphere) respectively. A short piece of flexible tubing, with a constant internal diameter of 14 cm, was used to connect the screw-feeder outlet to the box-section inflow. All connections between the lid, box-section, tube and screw feeder outlet were sealed using tape. During the equipment testing, a metal deflector plate had to be fitted to the inside box-section to ensure that the inflow hit the fluidised bed region and was not drawn directly into the tube-section. This plate was not included in the computational geometry, and is required solely for the purposes of the practical testing.

The compressed air line supplies the AST box-section fluidisation pad and the air slide used to discharge the silo. The air pressure to each device can be altered using local regulators.

The tube under-pressure values were recorded using a PXI data recorder running a Lab VIEW computer programme. The 24-Bit PXI data recorder is capable of measuring signals between +10V to -10V on eight separate input channels, and can provide high-resolution data plots. The eight channels included the seven pressure transducers and an optional measuring device if required. The data recorder was connected to an external electronic filter that could remove the electrical spikes produced from any undesirable high-energy signals.

The PXI can record data over a predefined frequency range of 1 kHz to 100 kHz. However, the pressure transducers have a response time of 600 mille-seconds, and a frequency

of 1.67Hz. Therefore, the Lab-VIEW programme was written to record at a frequency of 10kHz, and plot the averaged values of 5000 points every half a second. This procedure helps to minimise the effect of any peaks produced by the transducers due to their high response time. During the experiments, a chart could be viewed that compares the magnitude of the measured pressure values for each of the transducers, and a secondary chart displayed the real-time pressure data for a history of 1000 data points, which equates 500s of real time operation. The linear equation of the pressure/voltage calibration chart for transducer P1 in Appendix C was used in the Lab VIEW programme to convert mV electrical readings from the transducers into mbar pressure values. After testing, the recorded data was incorporated into an Excel spreadsheet for further analysis.

#### 4.5.1 Operational Procedure

The purpose of the experiments was to investigate the pressure profile inside the tube-section of the AST at different powder feed rates, and to record any observations that will assist in the assessment of the modelling of the tube. The alumina feed rates are indicated in Table 2, and each feed rate test was performed five times for a four minute period using the following procedures:

##### 4.5.1.1 Start Up Procedure

At the start of each test, the data recording equipment was switched on and the correct LabVIEW file was loaded. The charging bin was filled with alumina and then raised to the desired position above the Hethon screw-feeder, using the overhead crane. Having switched on the vacuum system, the butterfly valve at the bottom of the charging tank was manually opened to allow a gravity flow of alumina directly into the screw-feeder hopper below. The dust cloud produced from this operation was removed using the vacuum system. Note that during testing, the remaining alumina inside the charge tank could naturally drop into the screw-feeder hopper, until the charge tank was empty. At feed rates of 5 tonnes/hour and higher, the 600 kg charge tank could only hold enough powder for a single test run. After each test run, the powder held in the collection tank was emptied back into the charge tank using a forklift truck.

The main compressor was switched on to supply air to the distribution point of the equipment. The supply to the air slide was fully opened in order to ensure complete removal of alumina from the silo. The AST box-section fluidisation air was regulated using a pressure gauge. However, only a small amount of fluidising air was required, and for typical industrial applications, a superficial air velocity of 3 cm/s is used. Therefore, the valve was opened until a visual inspection of the initial powder bed in the box-section showed air bubbles penetrating the surface of the material. This was enough to ensure the powder flows into the tube once the feeding begins. The actual pressure reading could not be recorded due to inappropriate scaling of the display.

The anti-dust sheeting was sealed properly, the two vacuum hoses were located correctly, and the vacuum system was switched on. The desired screw-feeder setting was selected using the linear equation from the calibration chart shown in Appendix F. The values used are shown in Table 4-1.

Table 4-1. Screw-feeder speed settings for alumina (Hethon 500).

<b>Feed Rate (tonnes/hour)</b>	1	3	5	7	10
<b>Screw Feeder Setting</b>	70	211	352	493	704

Once the computer programme had been set to record, the screw-feeder was switched on and ran for a period of 4 minutes. The screw-feeder was then switched off, the recording programme was switched off, and the under-pressure data was saved as a 'txt' file. This procedure was repeated five times for each alumina feed rate. The charge tank was reloaded for the next test, if required using the same alumina, which was accumulated in the collecting tank at the exit of the air slide discharging the test silo.

#### 4.5.1.2 Shut Down Procedure

At the completion of each test series, the screw-feeder was switched off, the air supplies to the fluidiser and the air slide were turned off using the valves at the local distribution panels, and the main compressor was shut down. The charging tank was stored in a safe loca-

tion on the ground, and the overhead crane was located out of the way and switched off at the main power supply.

#### 4.6 Pressure measurement tests for AS-System

Figure 4-21 through Figure 4-24, show examples of the log-results during a test. Each capacity has been tested several times, and Figure 4-25 through Figure 4-30 shows the averages of the parallel tests for each capacity for each pressure measurement.

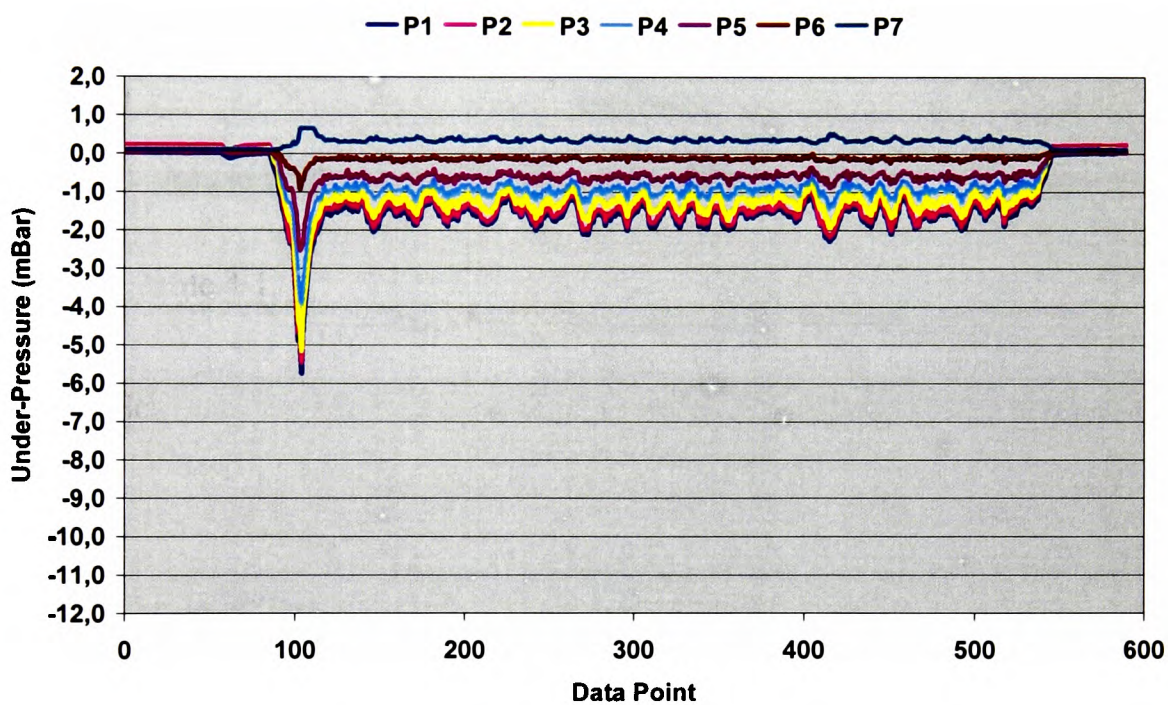


Figure 4-21. Example of pressure values measured for 1 t/h.

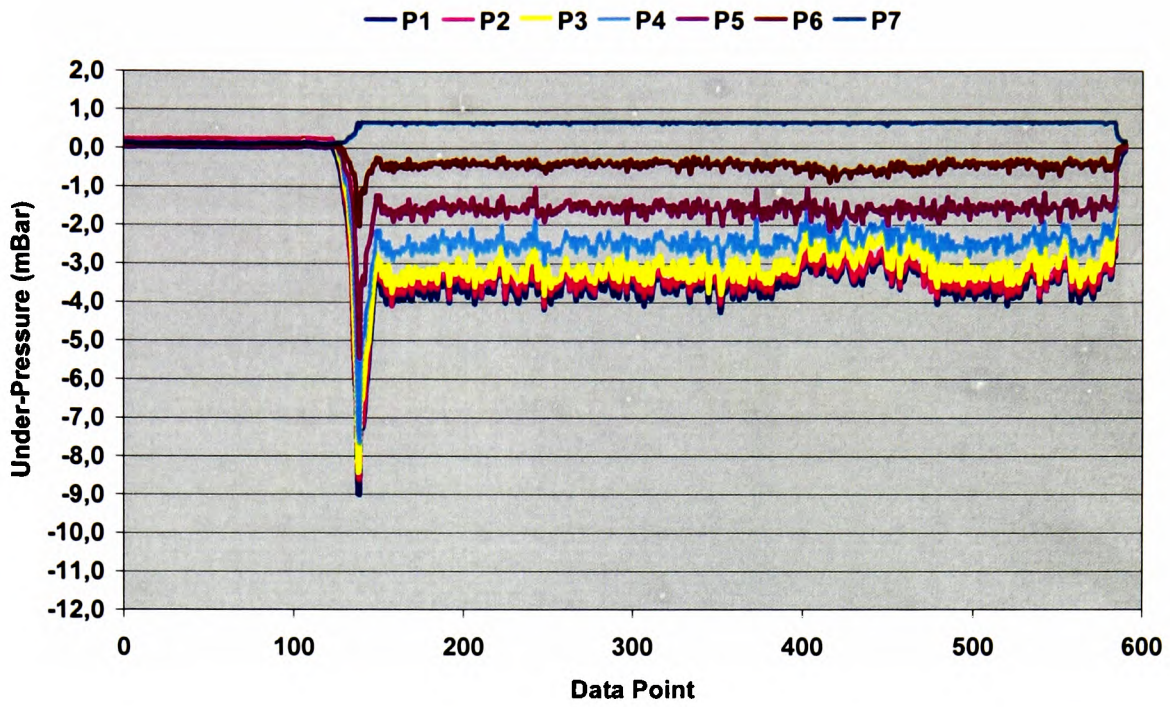


Figure 4-22. Example of pressure values measured for 3 t/h.

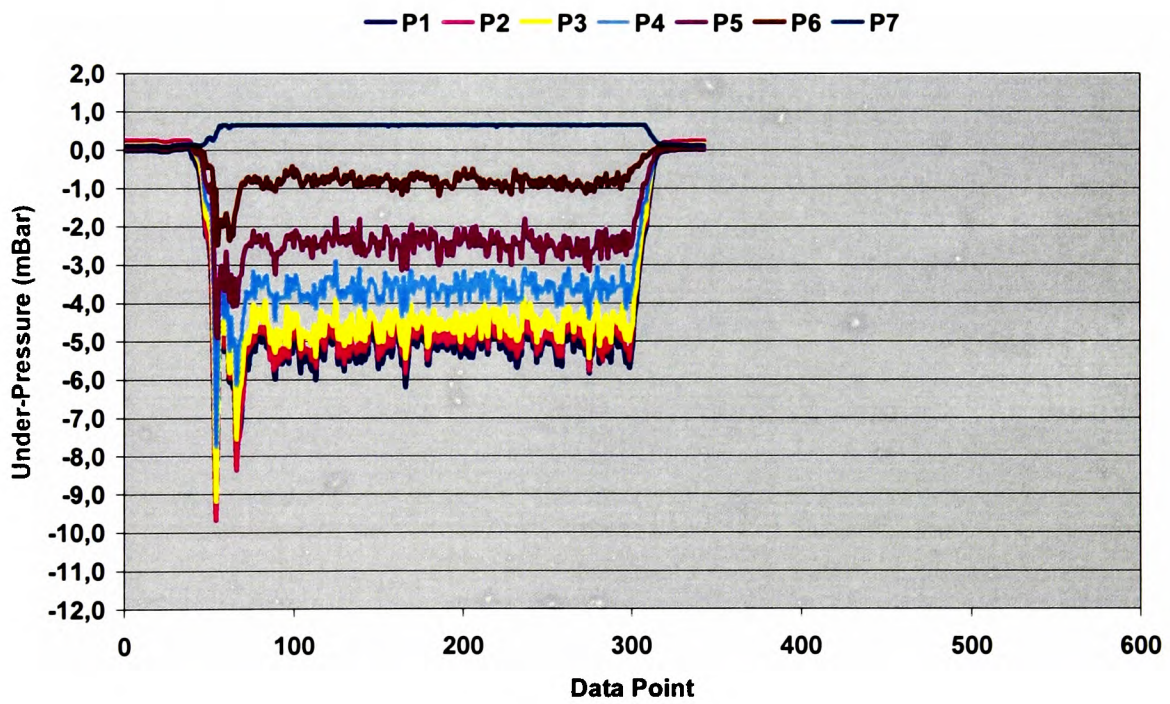


Figure 4-23. Example of pressure values measured for 5 t/h.

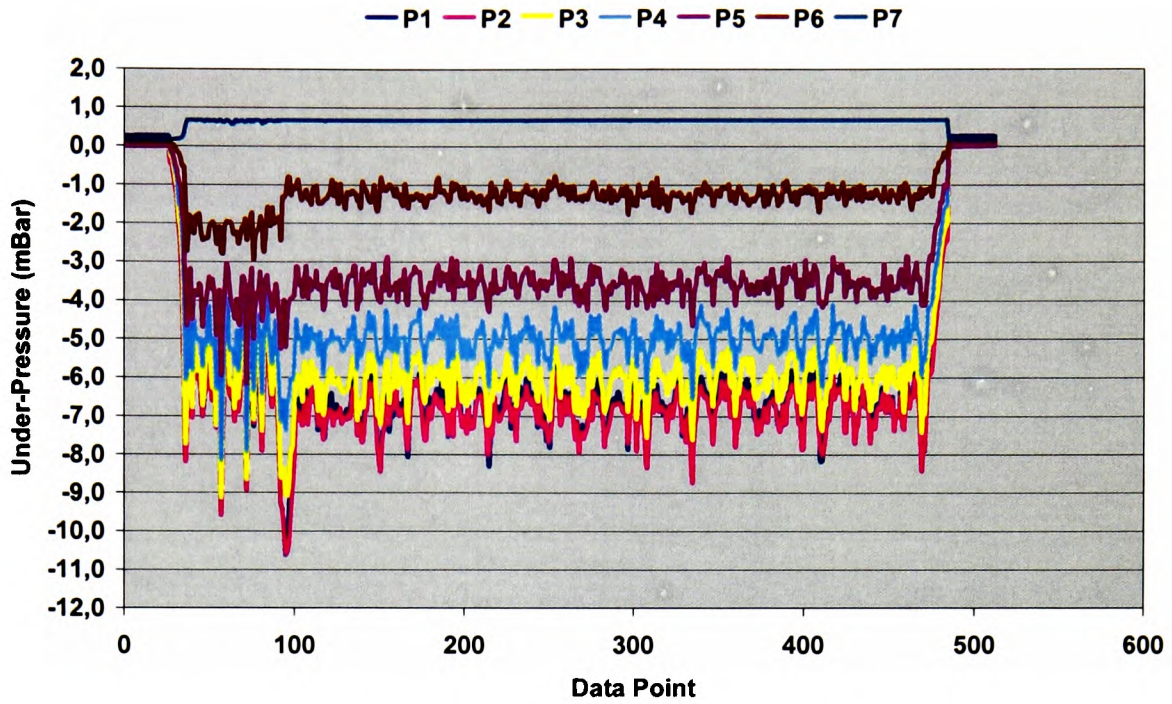


Figure 4-24. Example of pressure values measured for 7 t/h.

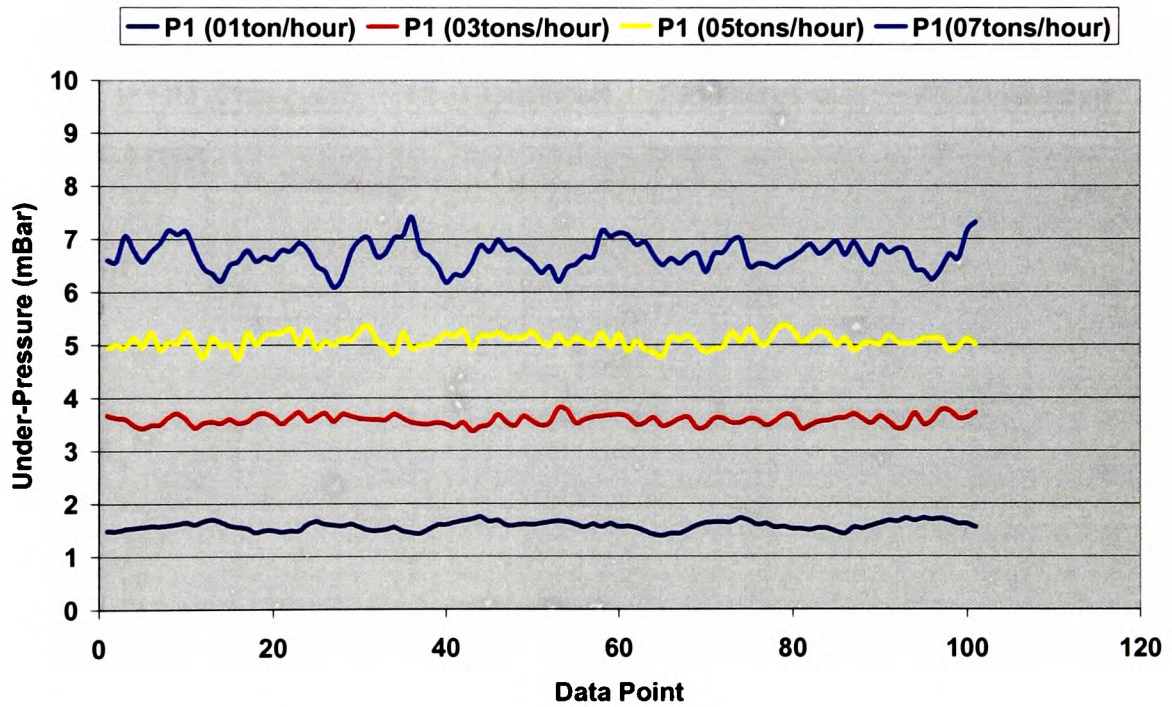


Figure 4-25. Average pressure measurement for all tests for transducer P1 (each line is an average of 5 tests).



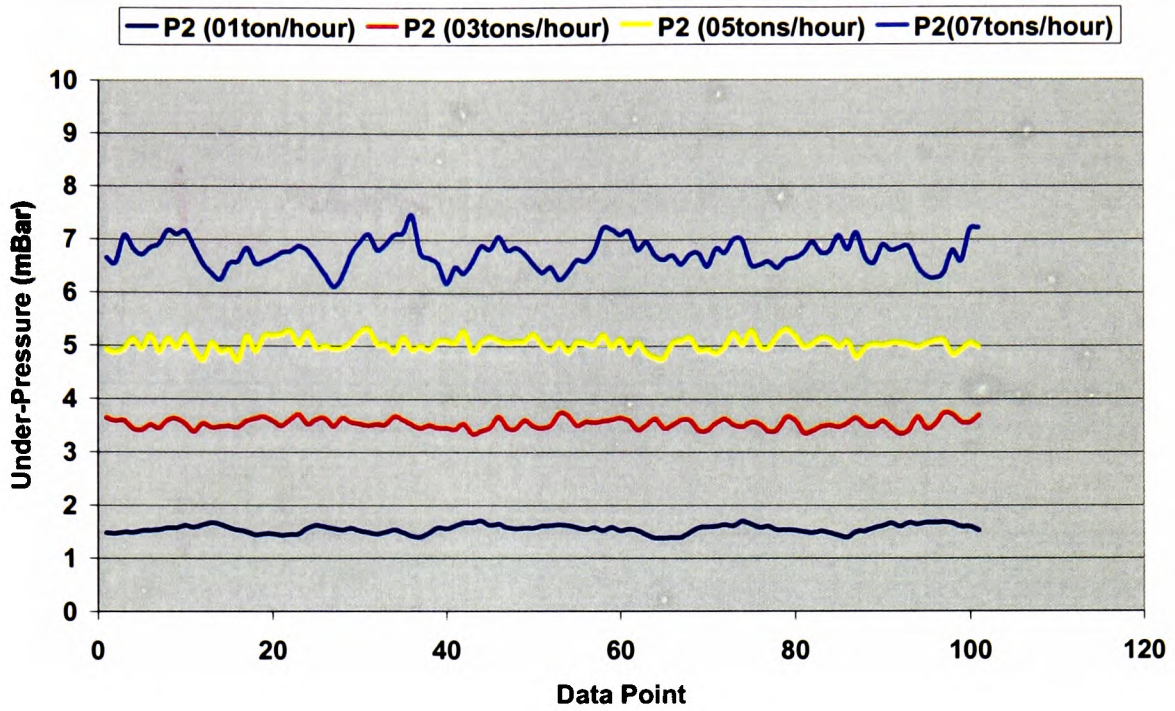


Figure 4-26. Average pressure measurement for all tests for transducer P2 (each line is an average of 5 tests).

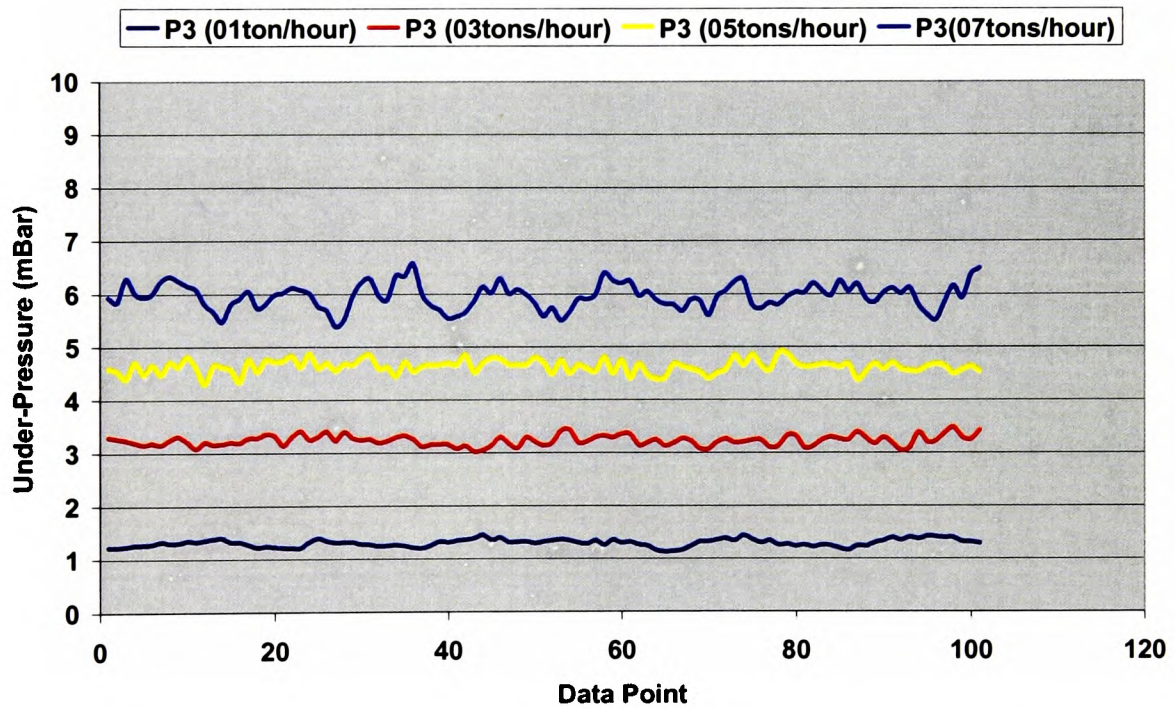


Figure 4-27. Average pressure measurement for all tests for transducer P3 (each line is an average of 5 tests).

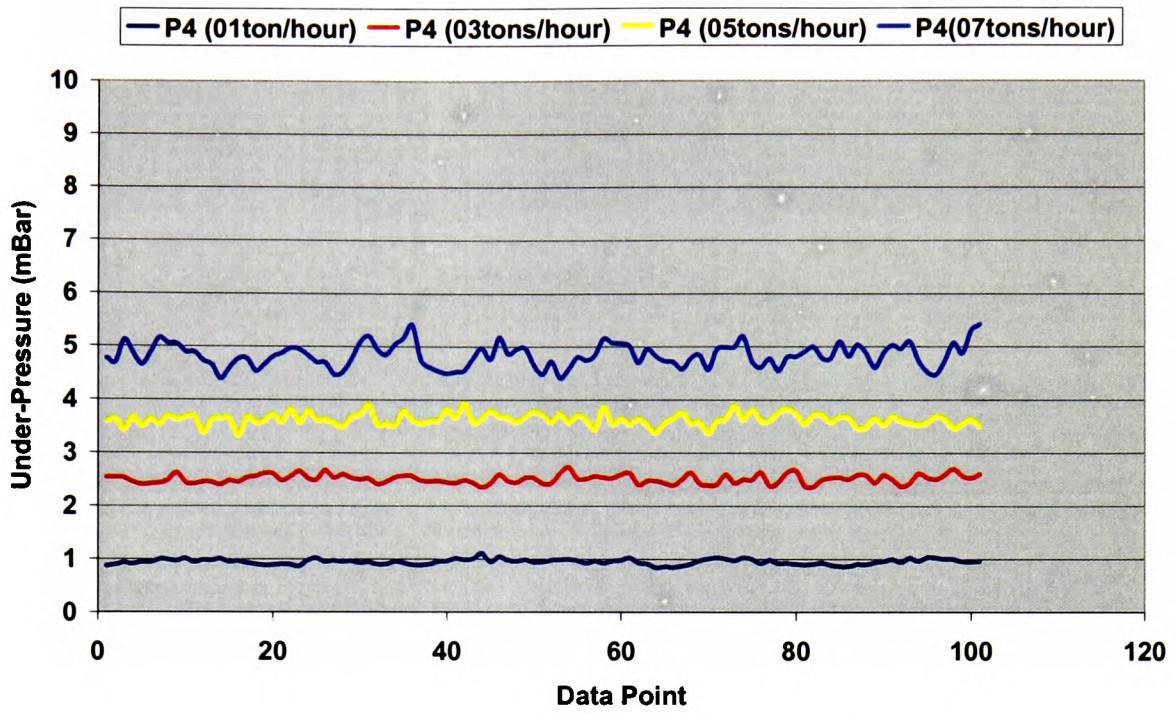


Figure 4-28. Average pressure measurement for all tests for transducer P4 (each line is an average of 5 tests).

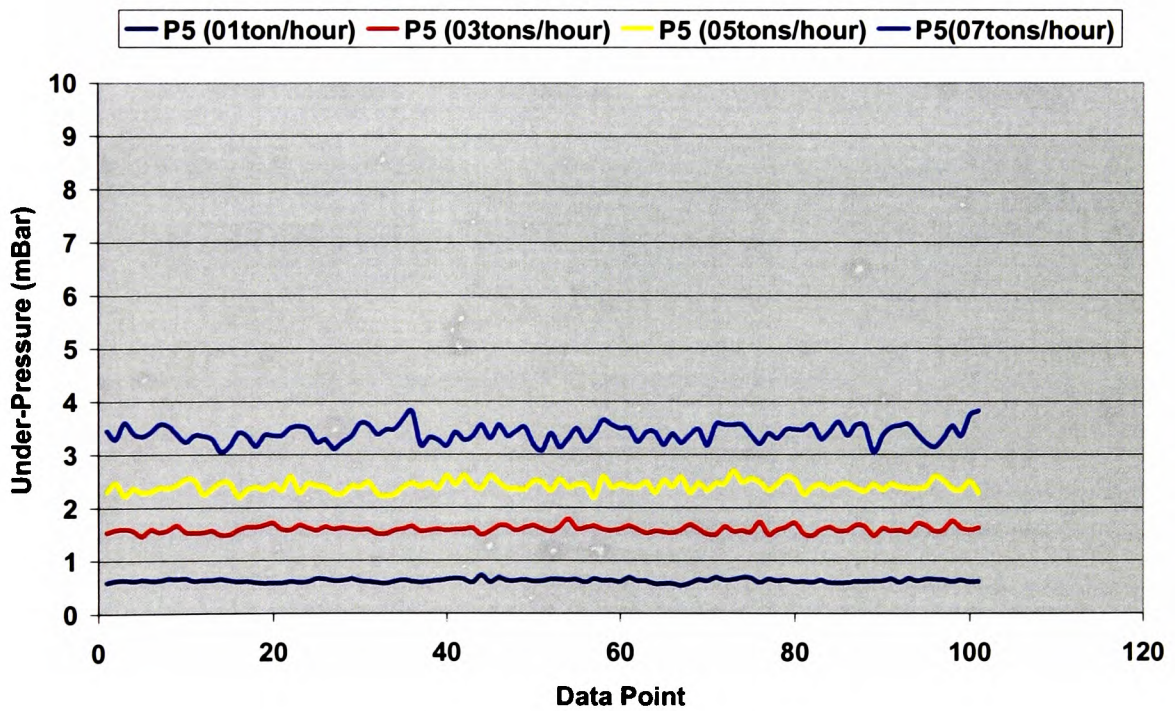


Figure 4-29. Average pressure measurement for all tests for transducer P5 (each line is an average of 5 tests).

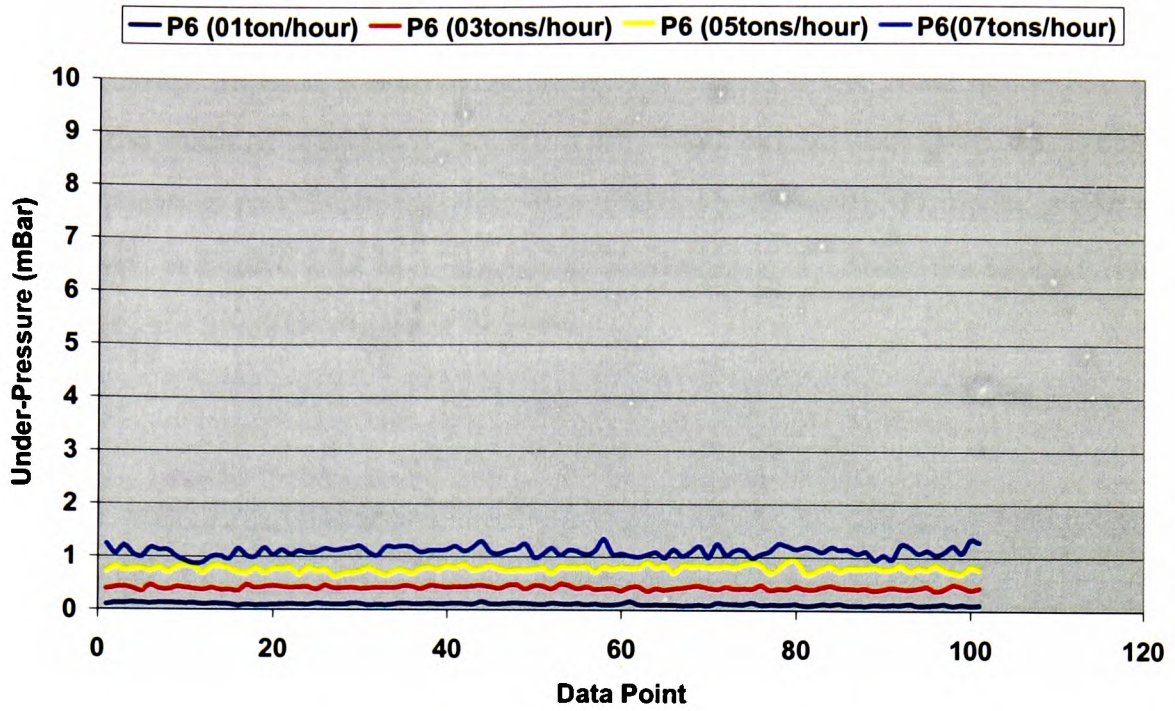


Figure 4-30. Average pressure measurement for all tests for transducer P6 (each line is an average of 5 tests).

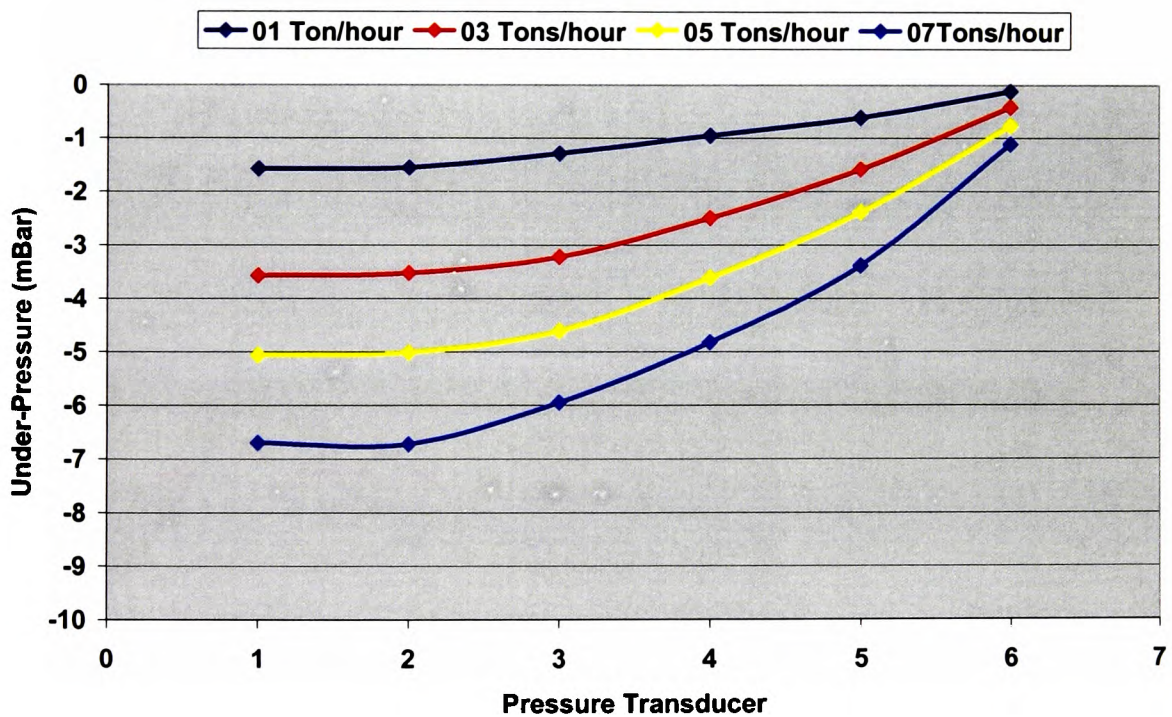


Figure 4-31. Pressure profile along the length (h) of the tube.

Calculating the averages of the values plotted in Figure 4-25 through Figure 4-30 for each

pressure transducer, the pressure profile in the tube as shown in Figure 4-31 are obtained. Here the pressure transducer number seven (P7) is not included, since this would be submerged in the mass of alumina inside the tube. What can be seen from this picture is a non-linear pressure profile as expected. For model verifications, the under pressure profiles are given in Figure 4-32 as a function of the height  $h$ . To make the comparison more easy numbers are given by the basic Si units.

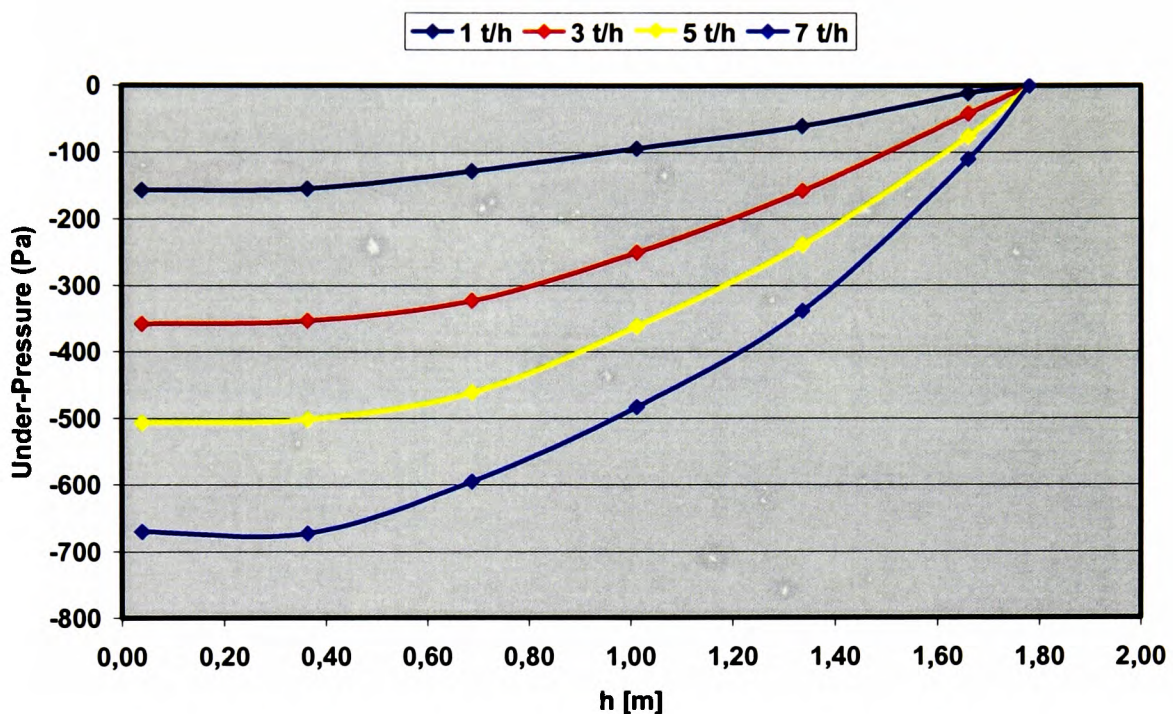


Figure 4-32. Basis plot for comparison with data from mathematical models.

#### 4.7 Lab-scale tests of the effect from anti segregation tubes

After the anti segregation tube had been further developed to become the Anti Segregation System, a lab scale test of the total system was carried out.

Figure 4-33 shows the test set up. Tests were carried out to quantify the difference in variation of the fines content of the alumina discharged from the silo when filling and emptying the silo as indicated in Figure 2-14, first by filling through one central filling point, then through the AS-System.

The test-rig shown in Figure 4-33 consists of the following:

- Distribution unit A, with inner tube A0, and three outlets A1, A2, and A3.
- Inlet box B, one for each of A's outlets, B1, B2 and B3 (hidden in the picture)
- Anti segregation tube C, one for each of A's outlets, where C1 and C2 are hidden in the picture, and C3 is visible
- Silo D.

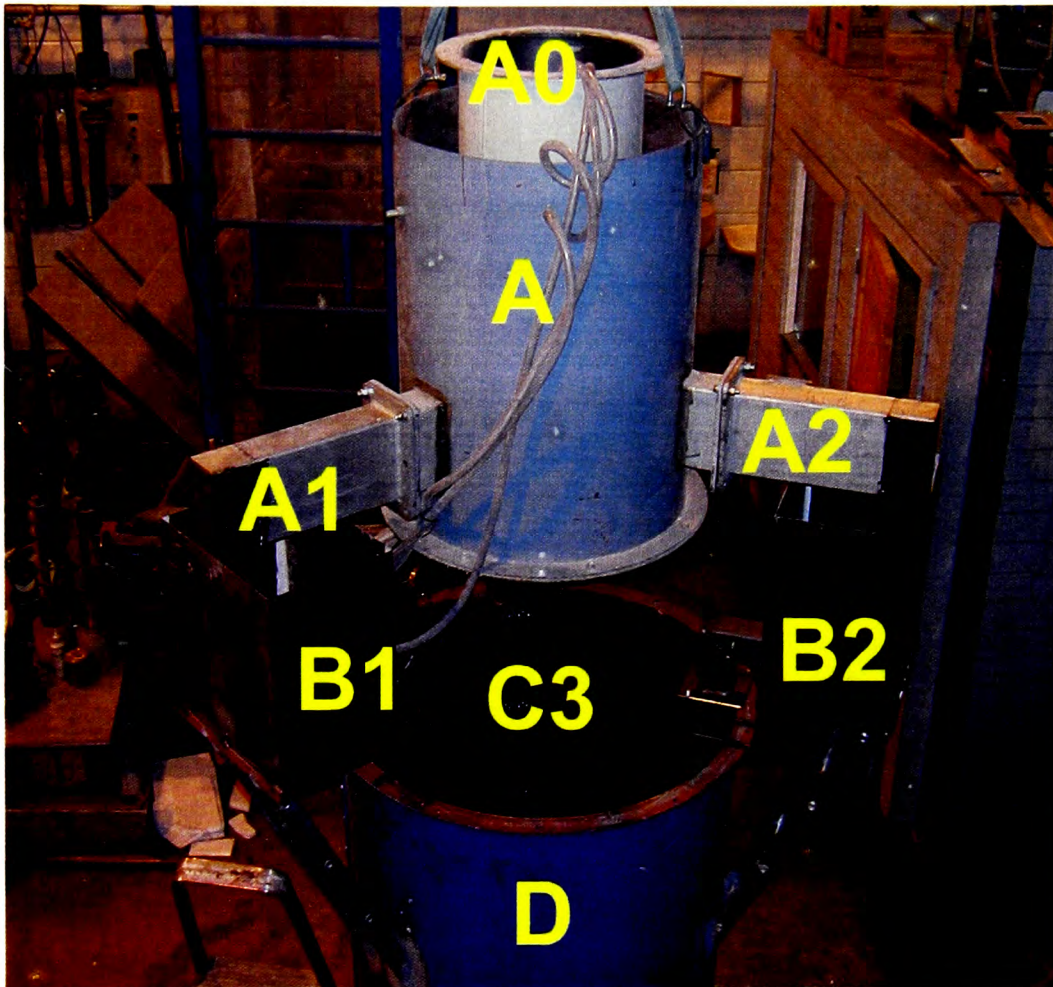


Figure 4-33. Lab scale set up of the AS-System, with 3 AST's and a central distribution unit.

When using the ASS the silo was filled with 600 kg of alumina through the inner tube A0. The alumina in the distribution unit A is fluidised and distributed to each of the tubes C<sub>x</sub> (x= 1-3) through the A<sub>x</sub> and B<sub>x</sub>. After filling the silo, 100 kg was discharged, and one sample was collected for each increment of 100 kg.

When not using the ASS, a bottom discharge valve in A was used to fill the silo.

The samples during the tests were collected from the whole cross section of the flow at the outlet of the air slide as follows:

- One sample when discharging a small amount ( 100 kg) before topping up the silo
- This was repeated 20 times
- After 20 fillings and discharges of 100 kg, the silo was emptied completely (600 kg), and samples were collected at short intervals during the whole discharging sequence.

The results are seen in Figure 4-34, where the sample numbers are given by cycle number before comma and sample number from that cycle after the comma, i.e. 1,03 would be first cycle and sample number three from that emptying cycle.

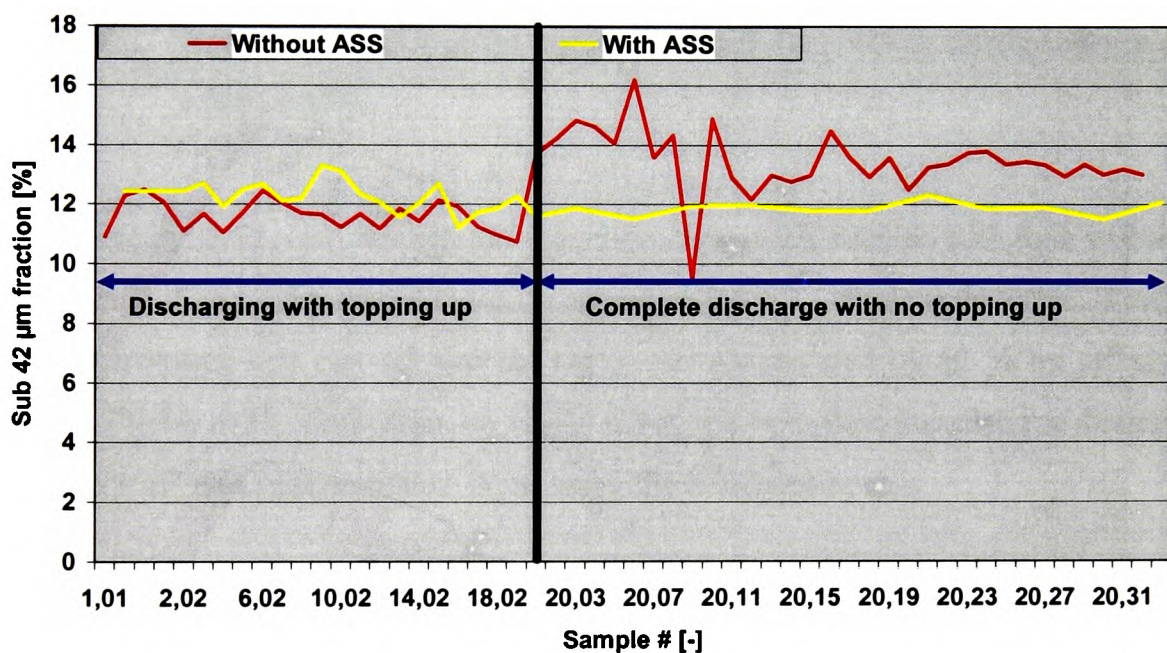


Figure 4-34. Results from lab AS-System test.

From Figure 4-34 it is clearly seen that the variations are much larger when completely emptying the silo. One might also pay attention to the fact that during the small discharges, the average of fines without the ASS are lower than during the complete discharge, clearly indicating that the fines are accumulating in the silo due to segregation during filling.



Figure 4-35. Result from pilot scale comparison between filling of the silo with and without ASS.

When using the ASS, one can see that variations are much smaller with than without the ASS. In fact, if one calculates the coefficient of variations (standard deviation divided by the series average) one can see that the variations are reduced by 62 % by utilising the ASS, see Figure 4-35. Tests done on single tubes and complete installations demonstrate an overall reduction in segregation when using the AS-System.

#### 4.8 Summary and Commentary of AST development

The development of the Anti segregation Tube (AST) and later Anti Segregation System (AS-System), was originated by a need for such a tool in industry. From the literature, one could clearly conclude that air current segregation, when filling large and/or tall silos with alumina, caused much segregation. The initial design originated from a commercial brochure on equipment meant for preventing dusting during filling of particulate material. Dusting can be interpreted as air current segregation, hence the work of developing an anti segregation system suited for the aluminium industry started based on the principles of anti dusting equipment. Several configurations of the AST were tested. In the beginning,

the tube had an inlet utilising an inclined chute, that filled a layer of material across the cross section of the top of the tube and thereby sealing it. Since the negative pressure was a function of the capacity, the idea was that the inlet would be self-regulate since both the thickness of the layer and the negative pressure would increase with capacity. However, the pressure inside the tube is also a function of fall height, hence when the height increased, the inlet seal based on the chute experienced problems in industrial installations. When the material started to flow, the generated negative pressure became so large that it sucked the layer sealing across the top of the tube downwards so much that it punctuated, and after that, the inlet blocked when the negative pressure vanished. From this problem, the need of a new inlet led the development through several stages, ending up with the hydrostatic inlet box with its 90-degree elbow for powder lock. This solution proved itself capable to handle the variations and vibrations occurring in industry, furthermore, it was self-regulating, hence a large operational range capacity wise, all the way from no transport to an upper limit defined by the AST system all together.

The test leading to the initial design was based on the assumption that the pressure was linear, and that the dispersion of the alumina was complete inside the tube. Based on this one point of pressure in the top of the tube was measured. Since the tube have many valves, a test rig measuring pressure in several heights to detect potential leakages in the valves was put up, and the real pressure distribution turned out to be non-linear. To measure this efficiently, a totally new test rig was designed. The new measurements gave such stable a reproduce able results that it could later be used as a basis to develop a mathematical model of the AST and its pressure distribution.

The new test rig also included a complete AS-System consisting of three ASTs. To test the potential effect of this system, in the terms of efficiency countering segregation, tests were carried out copying repeated filling and emptying of a silo, hence accumulating segregated fines at the silo walls. The results clearly revealed that the AS-System prevented segregation, compared to conventional filling.



## 5. MODELLING OF THE AST

### 5.1 Initial simple linear model

Initially only one point of pressure measurement was installed in the top of the tube, since the estimates of under pressure generated inside the tube was based on a linear model as seen already in Equation 4-1. The under pressure  $-P_2$  was calculated for the full height of the tube using Equation 4-2 with the concentration  $\rho_2$  of alumina in the tube as the density. By determining the velocity  $v_2$  of the alumina inside the tube based on free fall as given in Equation 5-1 and Equation 5-2 (basic kinetic and potential energy from general physics), the under pressure  $-P_2$  can be written as below in Equation 5-3.

$$m \cdot g \cdot h_2 = \frac{1}{2} m \cdot v_2^2 \quad \text{Equation 5-1}$$

$$v_2 = \sqrt{2 \cdot g \cdot h_2} \quad \text{Equation 5-2}$$

$$P_2 = \frac{\dot{m}}{A_{\text{cross}} \sqrt{2}} \cdot \sqrt{g \cdot h_2} \quad \text{Equation 5-3}$$

Where:

- $\dot{m}$  The filling capacity [kg/s]
- $P_2$  Pressure inside the tube [Pa]
- $A_{\text{cross}}$  Cross section area of the tube [m<sup>2</sup>]
- $h_2$  Total height of the tube [m]
- $g$  Gravitational acceleration 9,81 [m/s<sup>2</sup>]

As can be seen in Figure 5-1, this way of calculation gives a very rough basis for design, but the information obtained by calculating only this single value is limited.

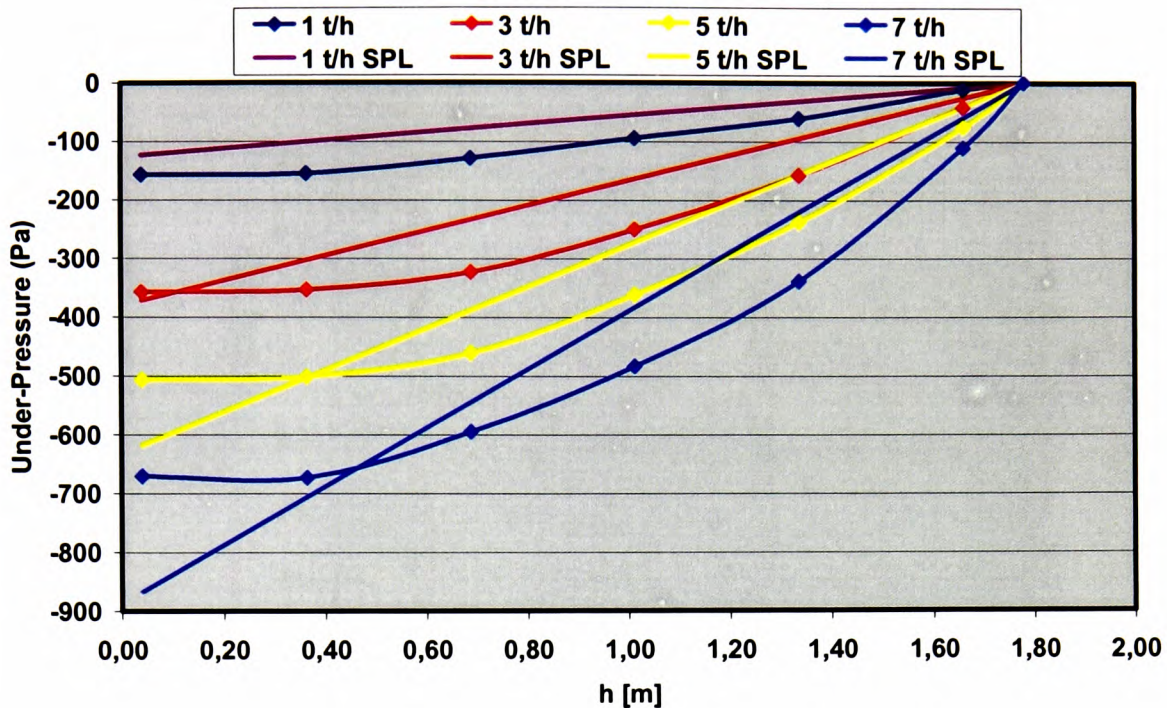


Figure 5-1. Single Point Linear (SPL).

In Figure 5-1 one can see that the initial estimate of the pressure does not end up too far off when compared with the measured data. Furthermore, the estimate gives a conservative result when the capacity increases, so if dimensioning the anti segregation tube using this simple linear model (SPL), one would be on the safe side concerning the sealing of the valves. However, the SPL does not describe correctly how the AST works. The measured data clearly show a rapid non-linear increase in negative pressure when moving upwards from the open valve levelling off in the upper part of the tube. This is very important in order to make sure that powder only is discharged through the active valve. Hence, a more accurate model is needed.

An easier way to compare the data is to plot measured versus predicted, as shown in Figure 5-2. In the plot the linear regression should be with a correlation factor ( $R^2$ ) of 1 and a slope of 1, i.e.  $y=1x$ . However, as clearly seen the SPL predicted values do not agree with the measured ones, and the deviations tend to become larger as the measured pressure increases.

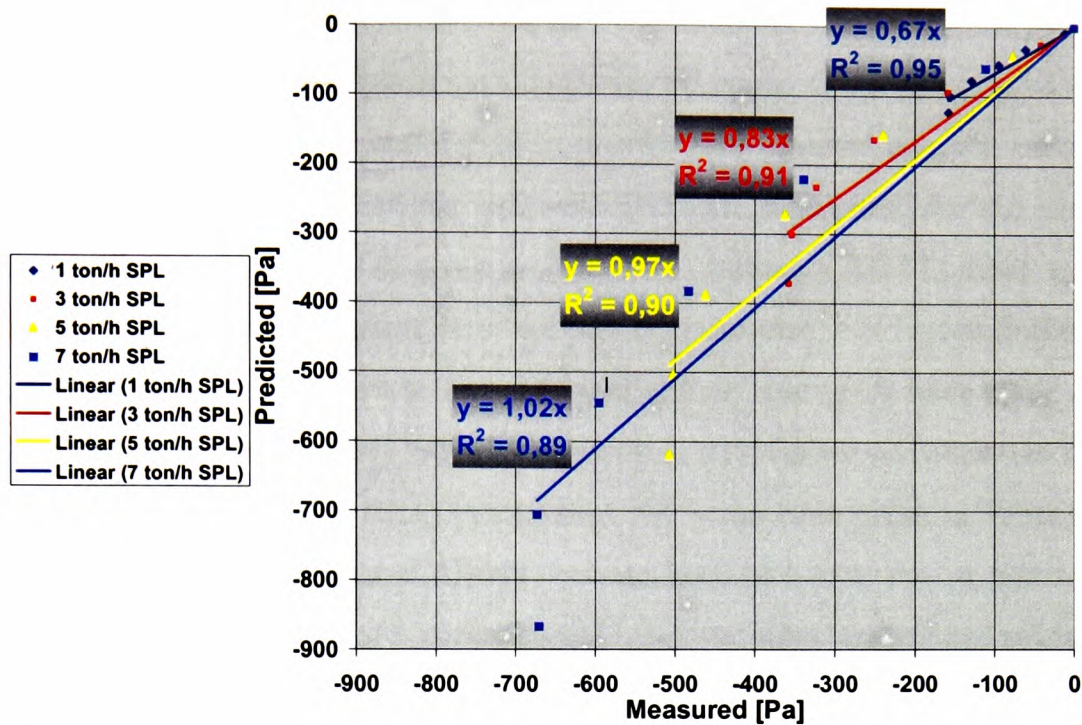


Figure 5-2. Measured versus predicted using SPL.

## 5.2 FLUENT simulations

Stillwell [Stillwell 2003] used the program package FLUENT 6.1. This package is capable of modelling many types of flow regimes including compressible or incompressible, Newtonian or non-Newtonian, steady state or transient and laminar or turbulent flows. One can select from various types of turbulence models, including standard and modified models, which may be more appropriate for different situations. A selection of multi-phase models is also available for use when fluid-fluid or solid-fluid situations are simulated. Before running a simulation, the most suitable turbulence and multi-phase models must be chosen and the correct physical properties of the materials entered. FLUENT is capable of modelling any number of different phases but this will affect the computational resources of the CPU.

For all flow regimes, FLUENT will solve the fundamental equations of mass and momentum conservation. Additional equations are then derived depending upon the specific situation to be modelled. The 2D and 3D grid geometries allow the system to be considered as a large number of individual meshes or control volumes, and solves the governing

equations using the Finite Volume Method. This involves integrating the governing equations for each control volume to give algebraic equations of the discrete variables. These are subsequently linearised and solved to provide new updated discrete variables that describe the flow-field. The settings Stillwell [Stillwell 2003] used for the simulations are many, but some basics are as given in Table 5-1. Although the FLUENT is a highly sophisticated simulation program, it is not just to press start. Several definitions of model choices and parameters have to be calculated and set and grids have to be defined. The calculations and work needed before starting upon simulations are many, as can be understood when looking on the small extract from the parameters given in Table 5-1. This author will not claim to master FLUENT, but has been as a tutor during Stillwell's simulations, guiding calculations of parameters and input variables, and helped evaluations of the results.

Table 5-1. Extract of settings of one of the FLUENT simulations undertaken by Stillwell [Stillwell 2003]

<b>Models</b>	
Define/Models/Solver:	<ul style="list-style-type: none"> <li>• Segregated</li> <li>• 2D</li> <li>• Unsteady</li> <li>• First Order Implicit</li> <li>• Implicit</li> </ul> (Cell based gradient option; absolute velocity formulation; superficial velocity porous formulation)
Define – Models – Multiphase:	<ul style="list-style-type: none"> <li>• Eulerian</li> <li>• 2 Phase</li> </ul>
Define – Models – Viscous:	<ul style="list-style-type: none"> <li>• k-ε (2 eqn)</li> <li>• Standard equation.</li> <li>• Standard wall functions</li> <li>• Per Phase model</li> </ul> Use default equation constants
Define – Operating Conditions:	Turn gravity on; $-9.81\text{m/s}^2$ in the 'y' direction; move the pressure reference location to (0, 0.2); Select an operating density value of $1.225\text{kg/m}^3$ , under variable-density parameters

The pressure profiles in the AST predicted by FLUENT simulations are shown in Figure 5-3. As can be seen the FLUENT simulates a negative pressure profile that decreases from the entrance to a minimum of a certain distance below the entrance. Below the minimum, the pressure gradually increases to zero at the level of the open valve where the alumina is discharged into the silo. The decrease in pressure in the top of the tube could probably be explained as a dynamic pressure generated by the alumina flowing from the inlet box through the 90-degree bend. Nevertheless, this is not seen in the measured data, perhaps with the exception of the curve for 7 t/h, where there is a slight decrease from the top transducer and the one below. If there is such an effect, the FLUENT simulations clearly exaggerate it considerably. The experiments indicate merely no pressure gradient in the top of the tube, and an increasing gradient towards the outlet. However, main problem with the simulations is that the effect of the capacity is very under-estimated. The simulated values over estimated the under pressure for 1 t/h but increases only with a factor of less than two when the capacity increases to 7 t/h. The measured values increase with a factor larger than four for the same capacity range, and except for the 1 t/h, the simulations give far less under pressure than measured in the experiments.

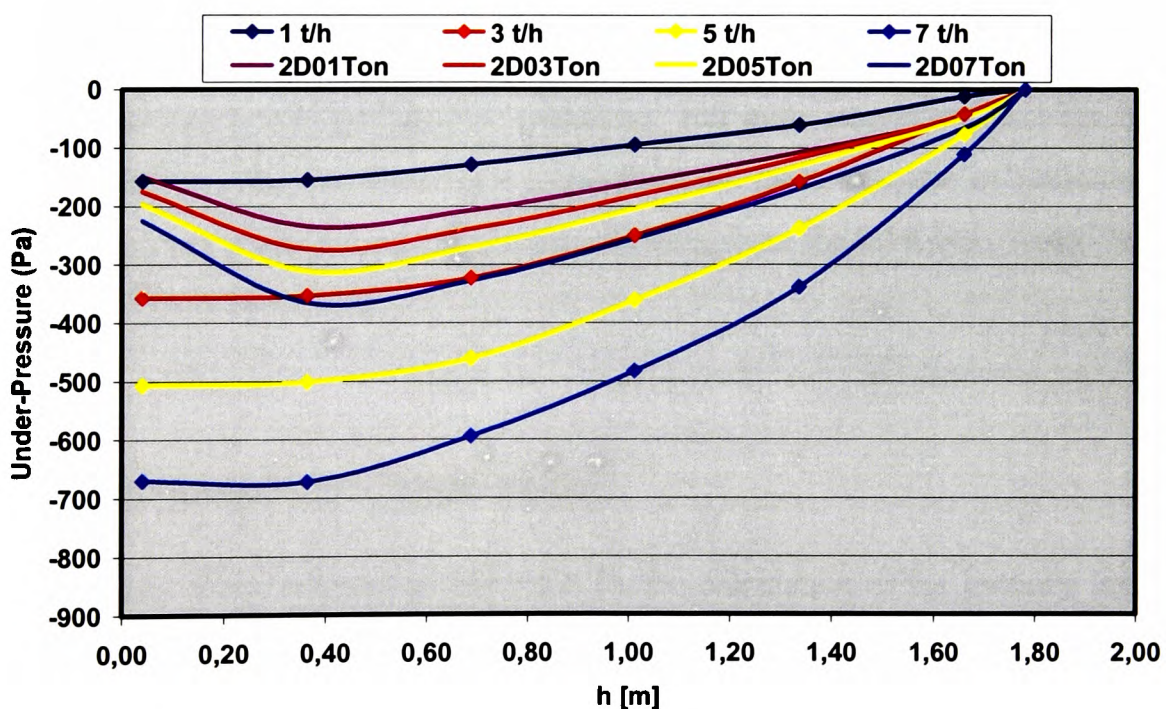


Figure 5-3. FLUENT results compared to measured data.

Using the data from Figure 5-3, and plotting measured versus predicted results the curves

shown in Figure 5-4 are obtained.

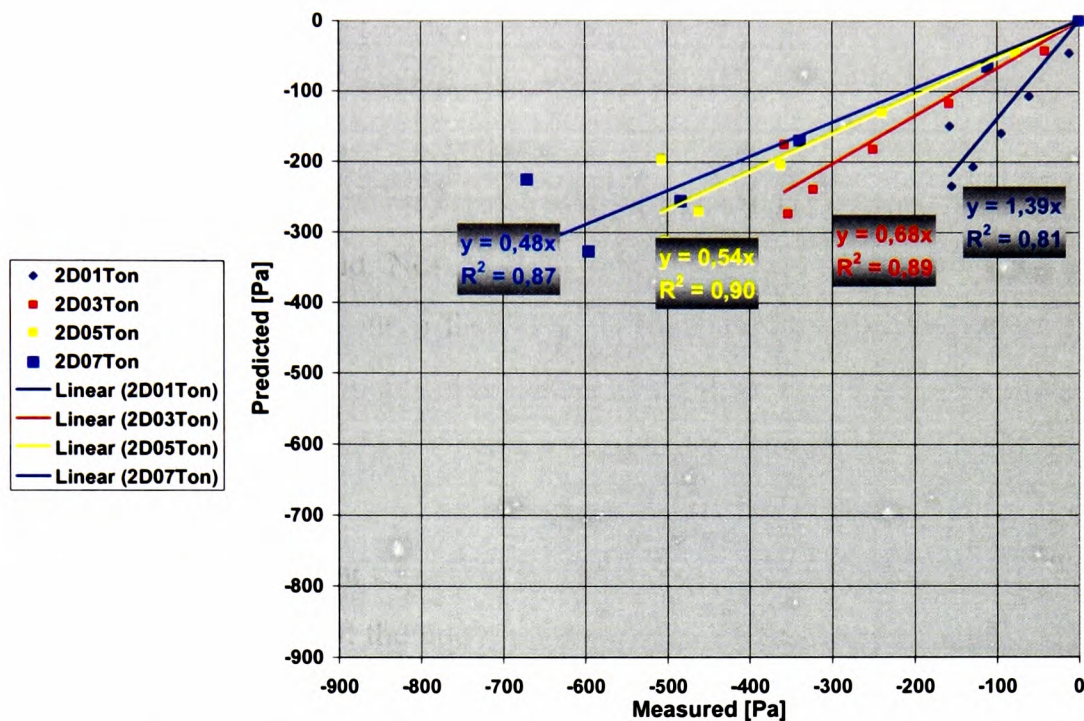


Figure 5-4. Measured versus the FLUENT predicted pressure values when calculated for all heights.

The results from the FLUENT simulations, are not matching the measured data, see Figure 5-4. The trend described by FLUENT results are still quite interesting, and the reduced negative pressure in the top of the tube could point out quite essential information, since the initial pressure generated by the alumina flowing from the inlet box, would limit the capacity of a given tube profile.

### 5.3 Initial simple non linear model

The calculation of the velocity, giving basis for the calculation of the pressure inside the tube, should be a function of the actual and not only the total fall height. In Figure 5-5 the pressure inside the tube is predicted using the fall velocity of alumina based on the gradual transfer of potential into kinetic energy as the particles drop downwards inside the tube. The calculated diagrams shown in Figure 5-5 are based on Equation 5-4, where now the  $h_i$  represents the height in any position.

$$P_2 = \frac{\dot{m}}{A_{cross} \sqrt{2}} \cdot \sqrt{g \cdot h_i}$$

Equation 5-4

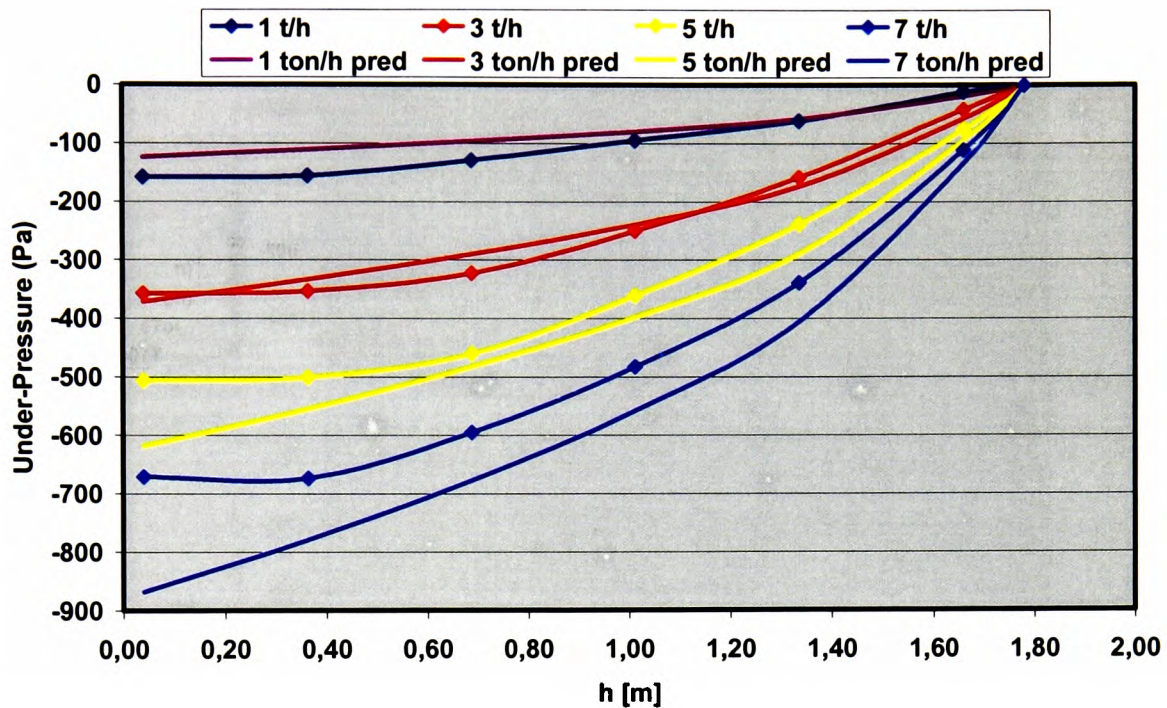


Figure 5-5. Simple model, using transfer of potential to kinetic energy to calculate velocity.

As for the SPL approach, the measured values can be plotted against the predicted, Figure 5-6. Here the predicted values show a much closer relation to the measured, but also in this case the deviations increase with the capacity. At 1 t/h and partly also 2 t/h, the under pressure is under predicted, whereas there is an increasing over prediction with increasing capacities.

Both the SPL and the simple non-linear model could be used for rough design purposes. However, they will not give a correct picture of the pressure distribution and the velocities in the tube, as is clearly seen when the complete data are presented. However, as a tool for developing the AST these simple approaches have been very useful both for the design of the inlet box and the valve configurations. When defining the pressure drop through the 90 degree bend, which is more or less constant for a given capacity (see section 4.3), and is driving force for the flow of alumina into the AST, the basic simple physics of the AST

can be understood by means of these models.

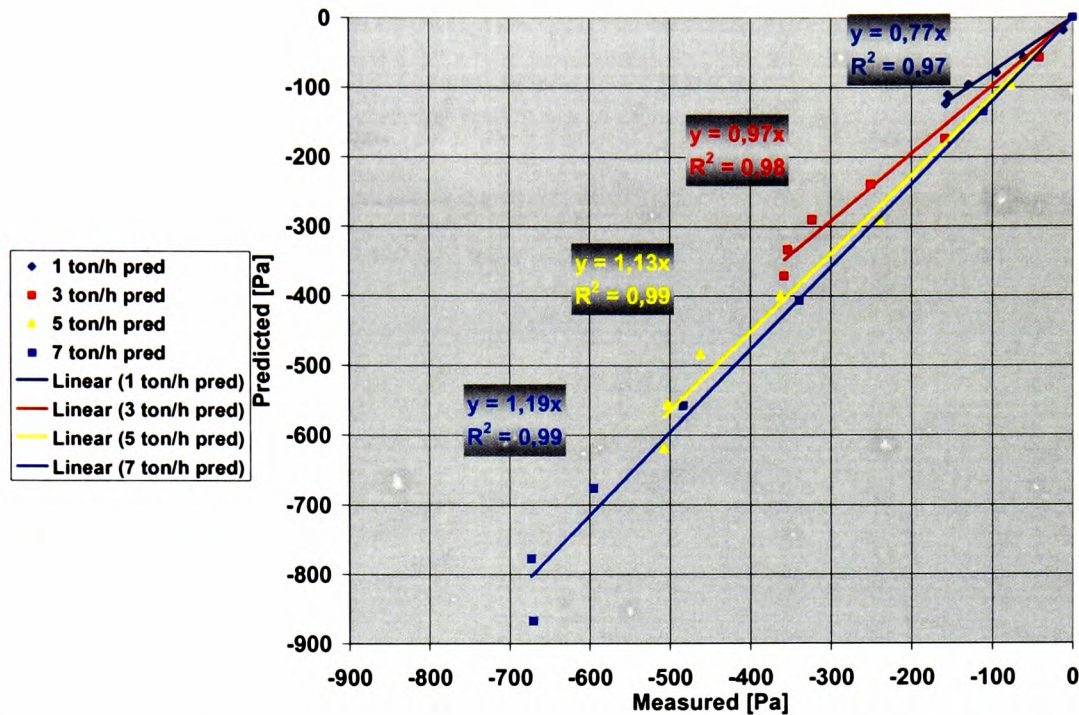


Figure 5-6. Measured versus predicted pressure values when calculated for all heights.

The FLUENT simulations indicated that a positive pressure was generated by the flowing powder from the inlet box, reducing the negative pressure in the top of the tube. By using the simple Bernoulli Equation 5-5, a value of this initial pressure can be calculated.

$$P_0 = \frac{1}{2} \cdot \rho \cdot v^2 \quad \text{Equation 5-5}$$

$$v = \frac{\dot{m}}{\rho \cdot A_{cross}} = \frac{\dot{m}}{\rho \cdot b^2} \quad \text{Equation 5-6}$$

$$P_2 = \frac{\dot{m}}{A_{cross} \sqrt{2}} \cdot \sqrt{g \cdot h_i} - P_0 \quad \text{Equation 5-7}$$

In Equation 5-5 the density  $\rho$  of alumina when fluidised is used, i.e. 90% of the bulk density. Calculating the velocity by means of Equation 5-6 one will get a rough estimate of the positive pressure caused by the entrance of alumina into the top of the tube. Adding that to the simple model given by Equation 5-4, Equation 5-7 is obtained, which gives, the results shown in Figure 5-7. In Figure 5-7 the results of the simple models predictions are



compared with the pressure profiles of the measurements. As can be seen the model is matching both the trend and the values quite closely, but still there are some deviations in the top of the tube. Plotting the measured versus the predicted the results as in Figure 5-8 shows a slight improvement from the previous Figure 5-6.

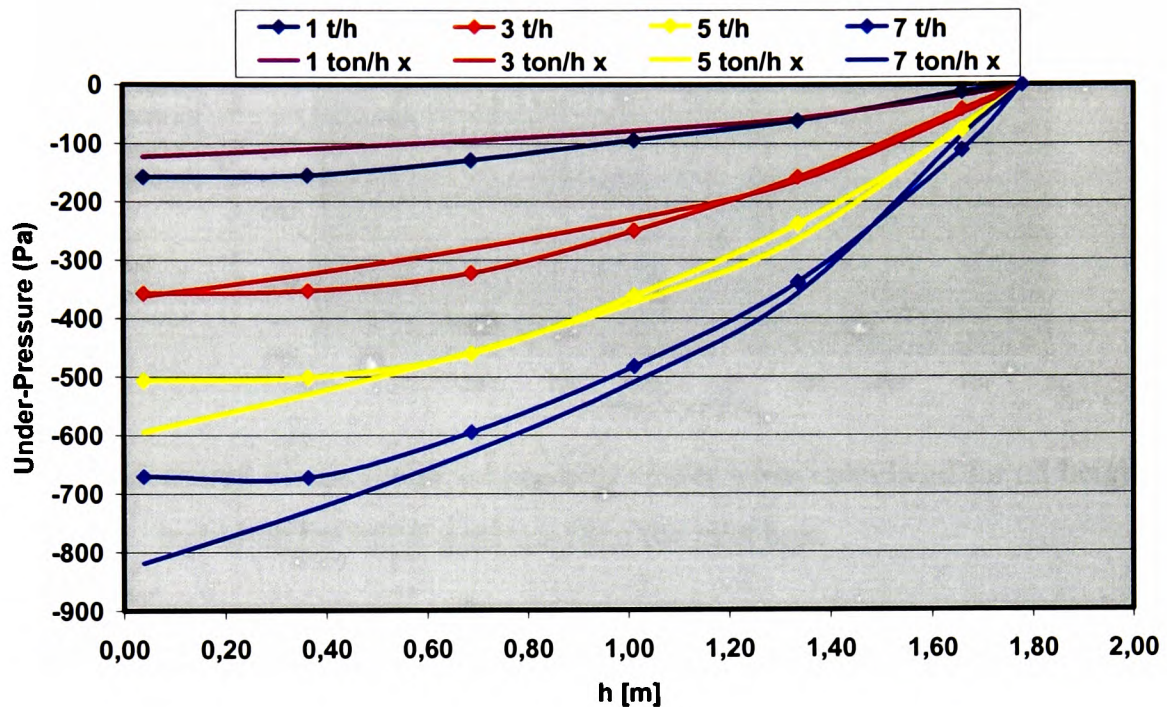


Figure 5-7. Comparing the results of the simple model corrected with initial pressure.

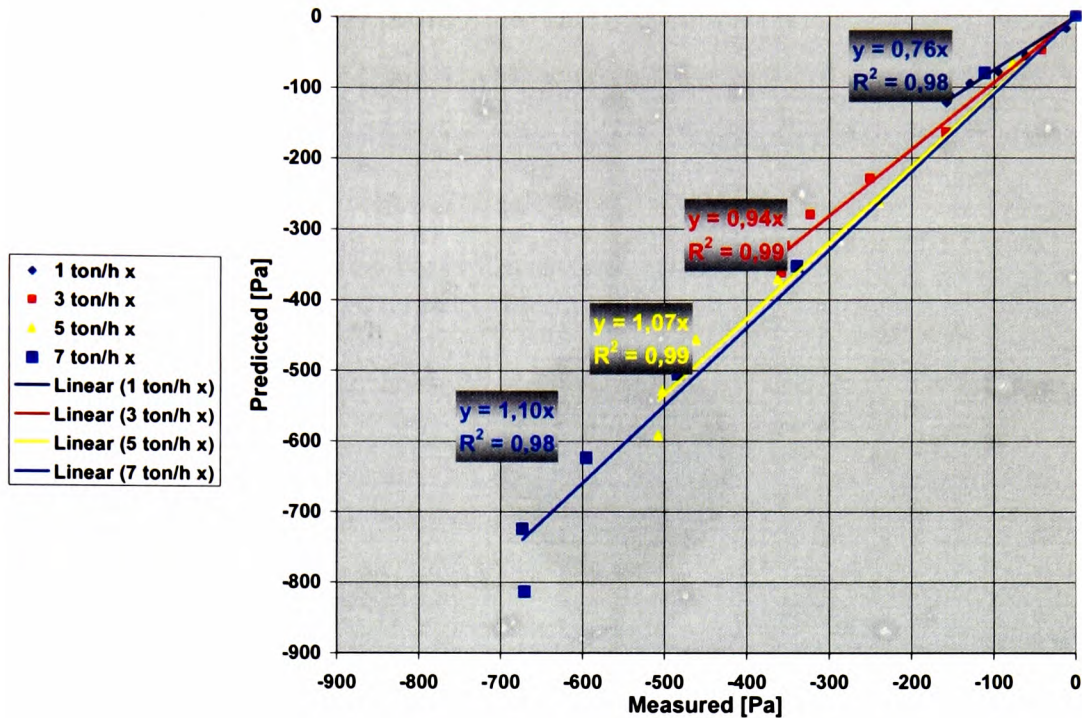


Figure 5-8. Measured versus predicted pressure values when calculated for all heights and including the initial pressure from the inlet box.

Of course, one can say that these initial models are not realistic, since one is assuming free fall without any air drag, which should have been included even in the earliest stage. However, considering the fact that these models provided a conservative design, resulting in successful installations that can be seen in Appendix E, one cannot easily dismiss their importance. In addition, the effects of these early installations are demonstrated in section 3.3.4.2. Furthermore, as will be seen later, the initial models are giving quite good guidelines when more advanced models are developed.

#### 5.4 Single Particle Drag Model (SPDM)

As mentioned before, the initial models were perhaps over simplified, and more realistic models are required. One of the initial assumptions implicit in the early models is full dispersion of the bulk solid flowing downwards inside the AST. A model based on single particle free fall subjected to gravity and air drag should therefore be a natural extension of the initial models. Starting with the usual assumption of spherical particles, the forces are acting on a single particle in free fall are illustrated in Figure 5-9.

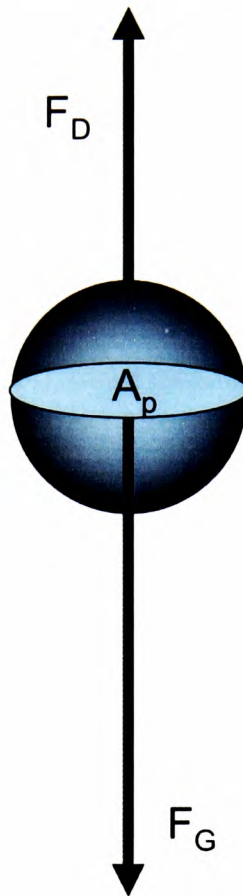


Figure 5-9. Force balance for particle drag ( $F_G$  – gravitational force,  $F_D$  – drag force and  $A_p$  – cross sectional area of the particle perpendicular to the velocity).

A simple force balance can be established of the forces acting on a falling particle, as sketched in Figure 5-9.

$$F_{tot} = F_G - F_D \quad \text{Equation 5-8}$$

$F_{tot}$  is the resulting force,  $F_G$  is gravity force, and  $F_D$  is the air drag. In Equation 5-8, the gravitational force is shown positive downwards. In the following, the direction will be assumed positive downwards, since the tubes extend from the inlet and down and the fixed point of the AST will be the inlet. Geankoplis [Geankoplis 1993], gives the equation for drag force as, shown in Equation 5-9.

$$F_D = \frac{C_D \cdot A_p \cdot \rho_l \cdot v^2}{2} \quad \text{Equation 5-9}$$

Where  $A_p$  is the cross sectional area of the particle,  $\rho_f$  is the density of the fluid, and the coefficient of drag  $C_D$  is expressed in Equation 5-10 [Geankoplis 1993].

$$C_D = \frac{24}{\text{Re}} = \frac{24 \cdot \mu}{\rho_f \cdot v \cdot D_p} \quad \text{Equation 5-10}$$

Re is the Reynolds number of the particle,  $D_p$  is the particle diameter, and  $\mu$  is the viscosity of the fluid. Putting Equation 5-9 and Equation 5-10 into Equation 5-8, the calculation below can be made.

$$\rho_p \cdot V_p \cdot a = \rho_p \cdot V_p \cdot g - \frac{12 \cdot \mu \cdot A_p \cdot v}{D_p}$$

Where  $a$  is the acceleration  $a = \frac{dv}{dt}$ , and  $V_p = \frac{\pi \cdot D_p^3}{6}$  is the volume of the particle, which gives:

$$\rho_p \cdot \frac{\pi}{6} \cdot D_p^3 \cdot a = \rho_p \cdot \frac{\pi}{6} \cdot D_p^3 \cdot g - \frac{12 \cdot \mu \cdot \frac{\pi}{4} \cdot D_p^2 \cdot v}{D_p}$$

Here also  $A_p = \frac{\pi \cdot D_p^2}{4}$  has been introduced. By simplifying one gets:

$$\frac{dv}{dt} = g - \frac{18 \cdot \mu \cdot v}{D_p^2 \cdot \rho_p}$$

This can be written as

1)

$$\frac{dv}{dt} = g - k_1 \cdot v \quad \text{where: } k_1 = \frac{18 \cdot \mu}{D_p^2 \cdot \rho_p}$$

Solving this differential equation with regards to  $v$  is straight forward, resulting in

$$v = \frac{g}{k_1} (1 - e^{-k_1 t}). \quad \text{For } t=0 \text{ it is here assumed } v=0. \text{ When time } t \text{ approaches infinity the ve-}$$

locity  $v$  will approach a constant velocity, which is denoted as given below.

$$v_\infty = \frac{g}{k_1} = \frac{D_p^2 \cdot \rho_p \cdot g}{18 \cdot \mu}$$

$$v_{\infty} = \frac{D_p^2 \cdot \rho_p \cdot g}{18 \cdot \mu}$$

Equation 5-11

Using Equation 5-11, a weighted average terminal velocity is calculated for the typical alumina with its typical particle size distribution as shown, Figure 5-10. The maximum possible capacity can be calculated for a given AST if the alumina is completely dispersed and falls at the average terminal velocity for single particles, with a particle density of 2 800 kg/m<sup>3</sup>.

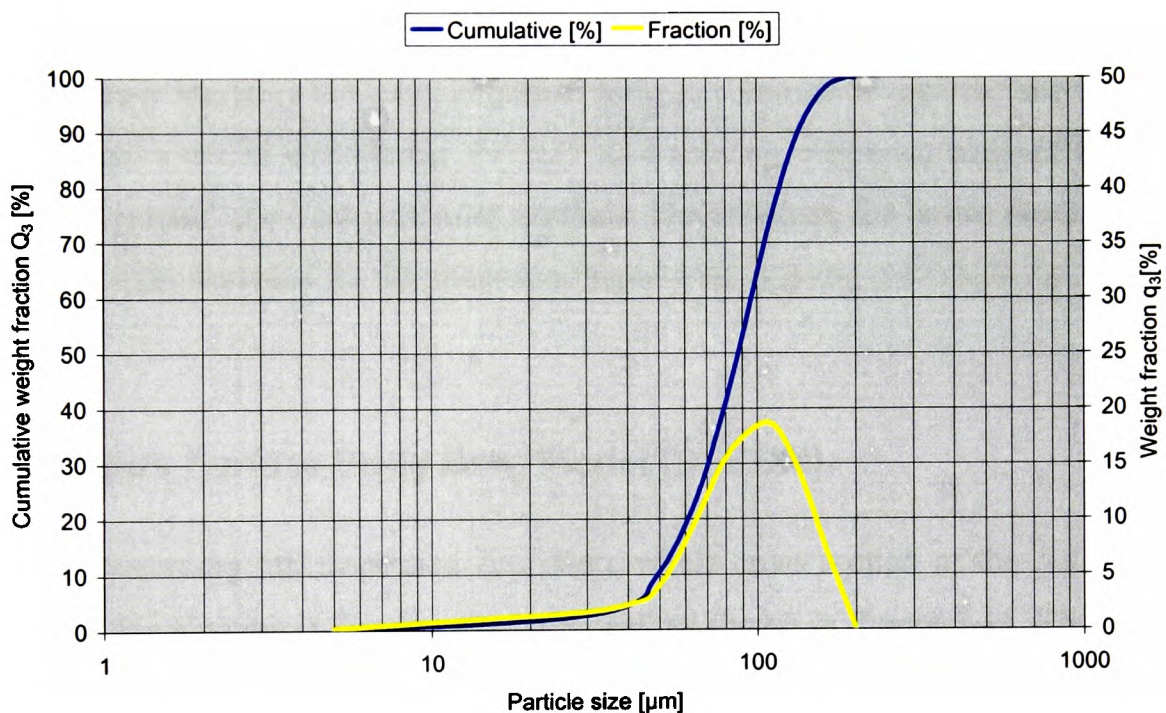


Figure 5-10. “Typical” size distribution for alumina in industry.

Assuming that the density of the bulk flowing in the AST is 90 % of the bulk density for alumina (equivalent to fully fluidised alumina with 10 % expansion), and a filling degree of the tube of 100% of this suspension, the maximum capacities become as given in Table 5-2 below.

As can be seen from the table, the capacities are only slightly more than half the initial design capacity. Furthermore, the initial design capacities are shown to be on the conservative side since the already installed tubes are running at considerably higher capacities. The full dispersion and single particle drag approach is therefore not even close to estimat-

ing the real capacities of the AST, and therefore has to be completely dismissed. Instead more realistic models taking into account that the particles will generate a drag zone behind them during the fall, reducing the amount of drag on each particle.

Table 5-2. Estimated capacities using average terminal velocity for alumina.

Tube Size [b x b]	Cap [kg/s]	Cap [t/h]	Initial design
80	5,08	18	32
90	6,43	23	42
100	7,94	29	50
150	17,86	64	113
200	31,76	114	200

Although some literature are using empirical ways to compensate for this “slip streaming” phenomenon, a model considering the bulk as a moving continuous body of bulk could probably “by-pass” the inter particular relations. Nevertheless, the basics occurring in the SPDM, are quite essential for the understanding of what is going on inside the AST.

## 5.5 Solids Surface Body Drag Model (SSBDM)

Instead of assuming full dispersion across the whole cross section of the AST, it is assumed that the alumina is flowing along the wall as shown in Figure 5-11. The flow pattern sketched in Figure 5-11 is also in agreement with what Stillwell [Stillwell 2003] got using FLUENT. Although the results from FLUENT did not agree with the experimental results, the flow pattern obtained by the simulations were similar to what was observed during tests. If assuming this flow pattern, the alumina falls more or less as a sheet of material along one wall, giving room for circulation of air in the rest of the cross section of the AST. Instead of single particle drag, there will be drag force only on the surface of the falling alumina stream, and the velocities will get considerably larger than for the single particles falling in still air. A small element of the falling body of alumina is shown in Figure 5-12.

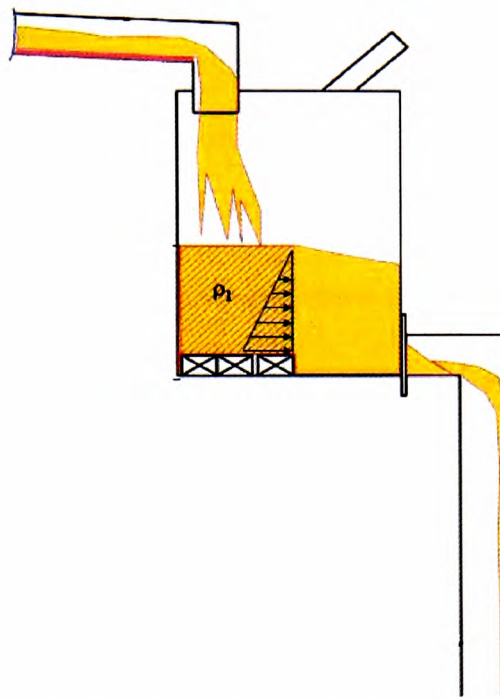


Figure 5-11. Assumed flow inside the AST during filling of silo.

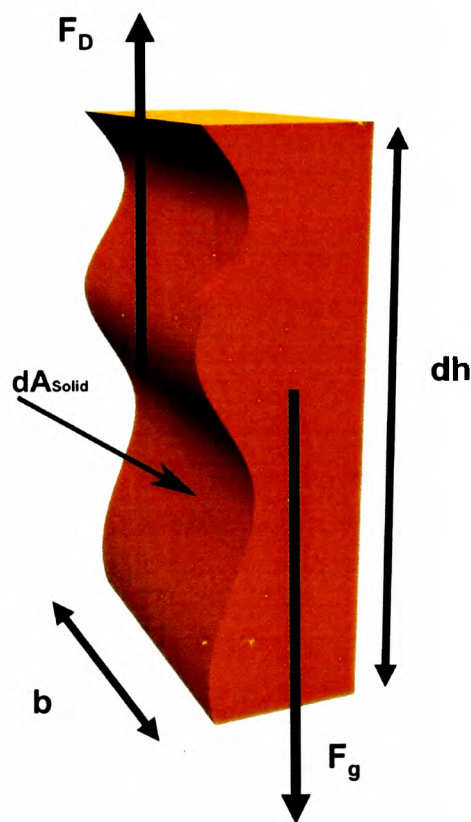


Figure 5-12. Element of the flowing material inside the AST, with the height  $dh$  and width  $b$ , and indicated forces.

As for the single particle, the balance of forces can be written as in Equation 5-8, as indi-

cated in Figure 5-12.

$$F_{tot} = F_G - F_D \quad \text{Equation 5-8}$$

Introducing Equation 5-9 [Geankoplis 1993] for the drag force  $F_D$  in Equation 5-8 the force balance develops as given in Equation 5-12, where the mass of the element is given by  $\dot{m} \cdot dt$ , and total force  $F_{tot}$  results in the acceleration force  $\dot{m} \cdot dt \cdot \frac{dv}{dt}$ . Here the drag is

not based on the cross sectional area of the flowing body of particles, but on the outer surface of the falling solid, assuming only skin drag.

$$\dot{m} \cdot dt \cdot \frac{dv}{dt} = \dot{m} \cdot dt \cdot g - \frac{C_D \cdot \rho_f \cdot dA_{Solid} \cdot v^2}{2} \quad \text{Equation 5-12}$$

Where  $\rho_f$  is the density of the fluid.  $\dot{m}$  is the capacity. The small area  $dA_{Solid}$  (Equation 5-12 and Figure 5-12), can be written as shown in Equation 5-13 below.

$$dA_{Solid} \square b \cdot dh \quad \text{Equation 5-13}$$

$$\dot{m} \cdot dt \cdot \frac{dv}{dt} = \dot{m} \cdot dt \cdot g - \frac{C_D \cdot \rho_f \cdot dh \cdot b \cdot v^2}{2} \quad \text{Equation 5-14}$$

$$\frac{dv}{dt} = g - \frac{1}{2} \cdot \frac{C_D \cdot \rho_f \cdot dh \cdot b \cdot v^2}{\dot{m} \cdot dt} \quad \text{Equation 5-15}$$

Introducing

$$\frac{dh}{dt} = v \quad \text{Equation 5-16}$$

in Equation 5-15, Equation 5-17 is obtained.

$$\frac{dv}{dt} = g - \frac{C_D \cdot \rho_f \cdot b \cdot v^3}{2 \cdot \dot{m}} \quad \text{Equation 5-17}$$

By introducing the Equation 5-18 into, Equation 5-17 one gets Equation 5-19.

$$dt = \frac{dh}{v} \quad \text{Equation 5-18}$$

$$v \cdot \frac{dv}{dh} = g - \frac{C_D \cdot \rho_f \cdot b \cdot v^3}{2 \cdot \dot{m}} \quad \text{Equation 5-19}$$



$$B \equiv \frac{C_D \cdot \rho_f \cdot b}{2 \cdot \dot{m}} \quad \text{Equation 5-20}$$

By introducing the constant B (Equation 5-20) the equation boils down to a handle able differential equation, as shown in Equation 5-21.

$$v \cdot \frac{dv}{dh} = g - B \cdot v^3 \quad \text{Equation 5-21}$$

Before moving on, an interesting result is obtained from the differential equation by letting h (i.e. time) increase towards infinity, as the velocity increases towards a certain value  $v_\infty$  the acceleration approaches zero, as indicated in Equation 5-22.

$$\lim_{h \rightarrow \infty} \left( v \cdot \frac{dv}{dh} \right) = 0 \quad \text{Equation 5-22}$$

Combining the Equation 5-21 and Equation 5-22 the maximum relative velocity between the falling powder and the air can be found by solving Equation 5-23 and the solution is given by Equation 5-24.

$$0 = g - B \cdot v^3 \quad \text{Equation 5-23}$$

$$v_\infty = \left( \frac{g}{B} \right)^{\frac{1}{3}} \quad \text{Equation 5-24}$$

$$\frac{v}{g - B \cdot v^3} dv = dh \quad \text{Equation 5-25}$$

Combining Equation 5-24 and Equation 5-25 which is a rearrangement of Equation 5-21, the expression for dh can be written as in Equation 5-26.

$$\frac{1}{B} \frac{v}{(v_\infty^3 - v^3)} dv = dh \quad \text{Equation 5-26}$$

Integrating Equation 5-26, an expression of the height h as a function of the velocity v, is obtained as shown in Equation 5-27.

$$h = -\frac{\sqrt{3} \cdot \arctan\left(\frac{\sqrt{3} \cdot (v_{\infty} + 2 \cdot v)}{3 \cdot v_{\infty}}\right)}{3 \cdot B \cdot v_{\infty}} - \frac{\ln\left(\frac{(v_{\infty} - v)^2}{v_{\infty}^2 + v_{\infty} \cdot v + v^2}\right)}{6 \cdot B \cdot v_{\infty}} + C_{f1} \quad \text{Equation 5-27}$$

$C_{f1}$  is the integration constant, which is determined by using the boundary conditions  $h_{v=0}=0$ , with the result as shown in Equation 5-28.

$$C_{f1} = \frac{\sqrt{3} \cdot \pi}{18 \cdot B \cdot v_{\infty}} \quad \text{Equation 5-28}$$

Adding the integration constant  $C_{f1}$  to the previous expression of  $h(v)$ , the final equation ends up as shown below in Equation 5-29. As can be seen from this equation, solving it for  $v(h)$  becomes quite difficult, if not impossible. Therefore, a direct solution of  $v(h)$  cannot be found, however, the way to use the result will be addressed later.

$$h = -\frac{\sqrt{3} \cdot \arctan\left(\frac{\sqrt{3} \cdot (v_{\infty} + 2 \cdot v)}{3 \cdot v_{\infty}}\right)}{3 \cdot B \cdot v_{\infty}} - \frac{\ln\left(\frac{(v_{\infty} - v)^2}{v_{\infty}^2 + v_{\infty} \cdot v + v^2}\right)}{6 \cdot B \cdot v_{\infty}} + \frac{\sqrt{3} \cdot \pi}{18 \cdot B \cdot v_{\infty}} \quad \text{Equation 5-29}$$

In order to find a corresponding expression for the pressure drop through the tube as a function of the height  $h$ ,  $p(h)$  in the pneumatic conveying literature should provide a suitable starting point. A suitable equation is given by Bradley [Bradley et al. 2000], as shown below in Equation 5-30.

$$\frac{dp}{dl} = -K_p \rho_{Susp} v^2 = \frac{dp}{dh} \quad \text{Equation 5-30}$$

For the AST  $dl$ , exchanged with  $dh$ , and the equation is re-written to Equation 5-31.

$$dh = -\frac{dp}{K_p \rho_{Susp} v^2} \quad \text{Equation 5-31}$$

Combining Equation 5-31 with found Equation 5-21, Equation 5-32 is obtained.

$$\frac{v}{g - B \cdot v^3} dv = dh \quad \text{Equation 5-21}$$

$$\frac{v}{g - B \cdot v^3} dv = -\frac{dp}{K_p \rho_{Susp} v^2} \quad \text{Equation 5-32}$$

Re-arranging this equation, and introducing the terminal velocity from Equation 5-24, the

differential equation for  $dp$  is given as shown in Equation 5-33.

$$dp = -\frac{K_p \rho_{Susp}}{B} \frac{v^3}{v_\infty^3 - v^3} dv \quad \text{Equation 5-33}$$

To condense the expression a constant  $B_2$  is introduced (Equation 5-34).

$$B_2 \equiv \frac{K_p \rho_{Susp}}{B} \quad \text{Equation 5-34}$$

$$dp = -B_2 \cdot \frac{v^3}{v_\infty^3 - v^3} dv \quad \text{Equation 5-35}$$

After integrating the differential equation for the pressure, the equation for pressure as a function of the velocity becomes as shown in Equation 5-36. Both a computer based programme called Derive 6.0 and mathematical tables have been used for the integration of Equation 5-35.

$$p = \left( \begin{array}{l} \frac{B_2 \cdot v_\infty \sqrt{3} \cdot \arctan\left(\frac{\sqrt{3} \cdot (v_\infty + 2 \cdot v)}{3 \cdot v_\infty}\right)}{3} \\ - \frac{B_2 \cdot v_\infty \cdot \ln\left(\frac{(v_\infty - v)^2}{v_\infty^2 + v_\infty \cdot v + v^2}\right)}{6} + C_{f_2} + B_2 \cdot v \end{array} \right) \quad \text{Equation 5-36}$$

Determining the integration constant  $C_{f_2}$ , by using the conditions at the entrance of the AST,  $p_{v=0} = P_0$ , where  $P_0$  is the pressure generated by the alumina flow from the inlet box (Equation 5-5).

$$C_{f_2} = \frac{\sqrt{3} \cdot \pi \cdot B_2 \cdot v_\infty}{18} + P_0 \quad \text{Equation 5-37}$$

$$p = B_2 \cdot v_\infty \cdot \left( \begin{array}{l} \frac{\arctan\left(\frac{\sqrt{3} \cdot (v_\infty + 2 \cdot v)}{3 \cdot v_\infty}\right)}{\sqrt{3}} - \frac{\ln\left(\frac{(v_\infty - v)^2}{v_\infty^2 + v_\infty \cdot v + v^2}\right)}{6} \\ + \frac{\pi}{6 \cdot \sqrt{3}} + \frac{v}{v_\infty} + \frac{P_0}{B_2 \cdot v_\infty} \end{array} \right) \quad \text{Equation 5-38}$$

Introducing the functions  $f_1$  and  $f_2$  (Equation 5-39 and Equation 5-40, to simplify the writing, and substituting for  $B_2$ , the equation of the pressure as a function of  $v$  ( $p(v)$ ), is trans-

ferred to Equation 5-41.

$$f_1(v, v_\infty) \equiv -\frac{\arctan\left(\frac{\sqrt{3} \cdot (v_\infty + 2 \cdot v)}{3 \cdot v_\infty}\right)}{\sqrt{3}} \quad \text{Equation 5-39}$$

$$f_2(v, v_\infty) \equiv -\frac{\ln\left(\frac{(v_\infty - v)^2}{v_\infty^2 + v_\infty \cdot v + v^2}\right)}{6} \quad \text{Equation 5-40}$$

$$p = \frac{K_p \rho_{Susp}}{B} \cdot v_\infty \cdot \left( f_1(v, v_\infty) + f_2(v, v_\infty) + \frac{\pi}{6 \cdot \sqrt{3}} + \frac{v}{v_\infty} + \frac{P_0}{\frac{K_p \rho_{Susp}}{B} \cdot v_\infty} \right) \quad \text{Equation 5-41}$$

It is quite impossible to use Equation 5-41 and Equation 5-29 to express  $p$  as a function of  $h$  directly, therefore the solution has to be used in its present form and solved parametrically. This since both the height  $h$  and the pressure drop  $p$  are given as functions of the velocity. Height and pressure drop are calculated for small increments of the velocity, as indicated in Table 5-3, then the pressure drop is determined as a function of the height. Note that the calculations stops before reaching exactly the relative terminal velocity, because this velocity gives a singularity of the functions both for height and pressure.

Table 5-3. Solving method for the SSBDM.

$v$ [m/s]	$h(v)$ [m]	$p(v)$ [Pa]
0,001	$h(0,001)$	$p(0,001)$
0,002	$h(0,002)$	$p(0,002)$
....	....	....
....	....	....
$v_\infty - 0,001$	$h(v_\infty - 0,001)$	$p(v_\infty - 0,001)$

After the pressure drop and corresponding height is found, Equation 5-42 is used to calculate the static negative pressure, which the pressure transducer in the test measures. Here

$H=1,78$  m, since this was the distance from the inlet box to the open valve in the AST.

$$P_{stat\ i} = p(v(h_i)) - p(v(H)) \quad \text{Equation 5-42}$$

When plotting Equation 5-41, using  $K_p=1$ , the model give a humongous over prediction of the pressure drop, therefore  $K_p$ , had to be determined on some other basis. Examining Equation 5-41, all sections are either a difference or a ratio with the relative terminal velocity. Furthermore, the equation demands that  $K_p$  is dimensionless, therefore the idea emerged to calculate the actual mass flow rate  $\dot{m}$  relative to the maximum possible mass flow rate. A full tube of fluidised alumina ( $\rho_{Susp}=0,9 \rho_{Bulk}$ ) at a velocity of the terminal velocity constitutes the maximum possible mass flow rate. Based on this idea  $K_p$  ends up as Equation 5-43.

$$K_p \equiv \frac{\dot{m}}{v_{\infty} \cdot \rho_{Susp} \cdot A_{Cross}} \quad \text{Equation 5-43}$$

Using the expression for  $K_p$ , and determine the drag coefficient  $C_D$ , in the expression for  $v_{\infty}$ , giving the best fit for one capacity and then keeping it constant at 0,16 for all calculations, the static pressure distribution can be calculated by Equation 5-41, Equation 5-29 and Equation 5-42 as explained above. The results of the calculations are as shown in Figure 5-13.

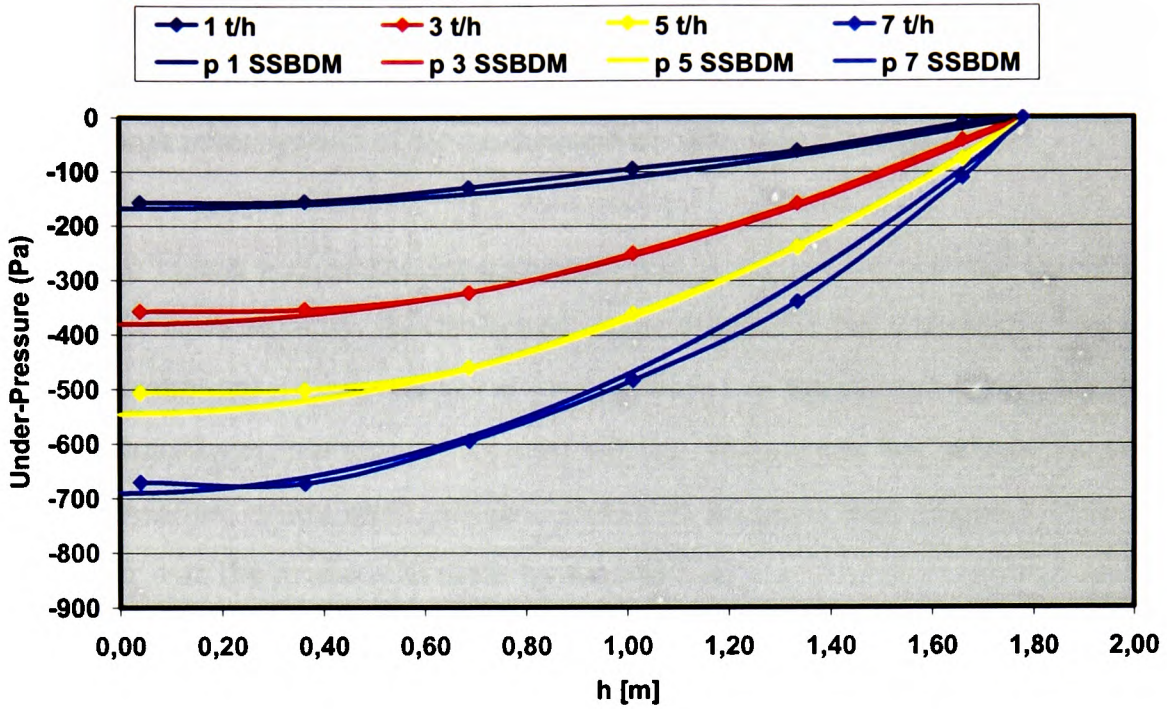


Figure 5-13. SSBDM predictions of pressure distribution compared with respective measured data.

Figure 5-13, clearly shows a good match between data predicted by the model and the measured data. As for the other models, the measured plotted against the predicted shows how good the match is, Figure 5-14.

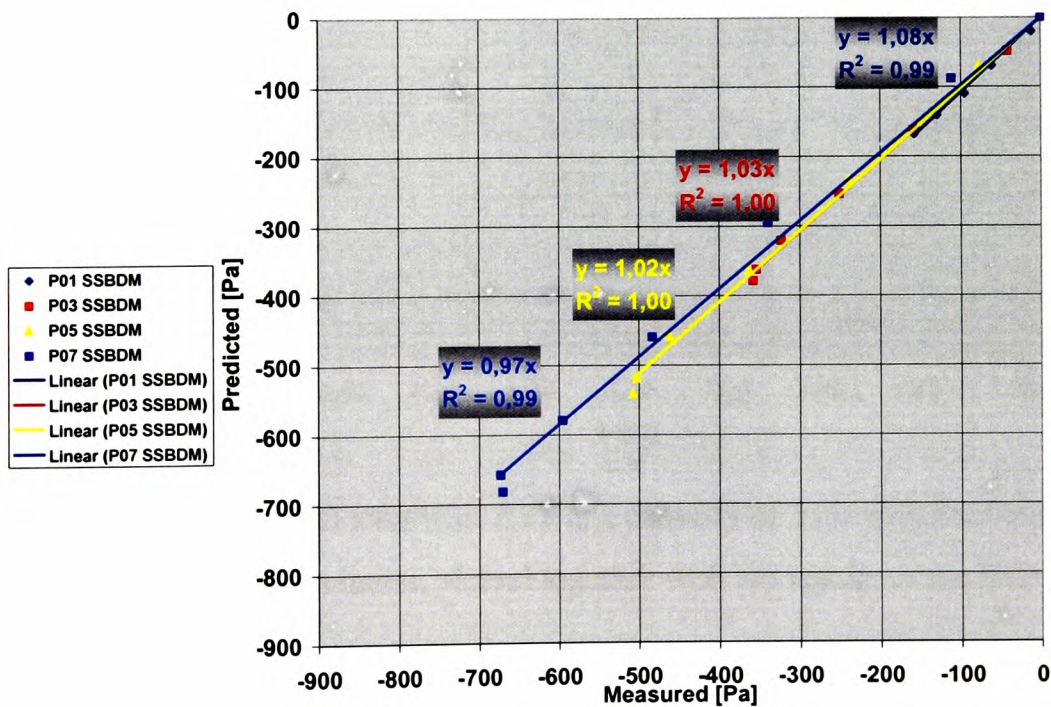


Figure 5-14. Measured versus predicted pressure values when using the SSBDM.

As can be seen from Figure 5-14, both the slopes for the different capacities as well the correlation coefficients  $R^2$  are quite near the magic number 1. Since this match is so close, a more thorough investigation of the predictions are undertaken below.

Figure 4-25 to Figure 4-30 shows the measurements of each of the pressure transducers at steady state for each capacity. As can be seen these curves are not completely flat, and the variations/ fluctuations of these curves are the variations of the measurements, not only for the pressure transducer, but also for the total test rig. That means that each of the tests has a standard deviation, or test error, which is shown on the plots from Figure 5-15 to Figure 5-18, together with the predictions made by the SSBDM.

Compared to the data for 1t/h, the SSBDM results are outside the boundaries for made by the one standard deviation. However, the model follows the trend, and has a slight over-prediction.

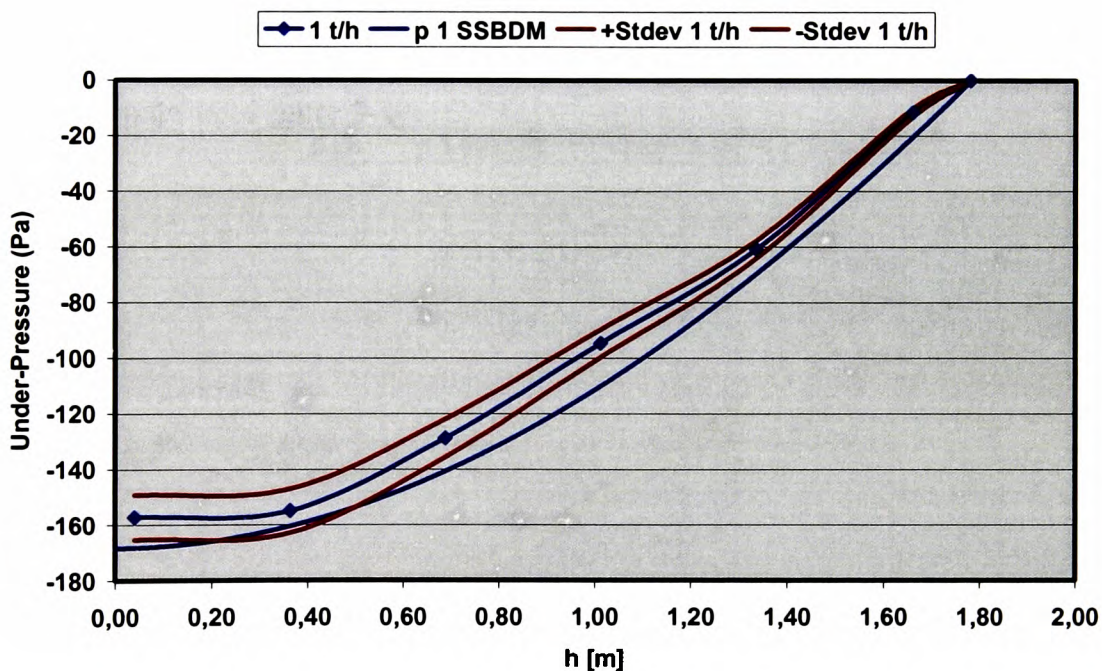


Figure 5-15. Results from tests with AST at a capacity of 1 t/h with the boundaries  $\pm$  one standard deviation, plotted together with the results of the SSBDM.

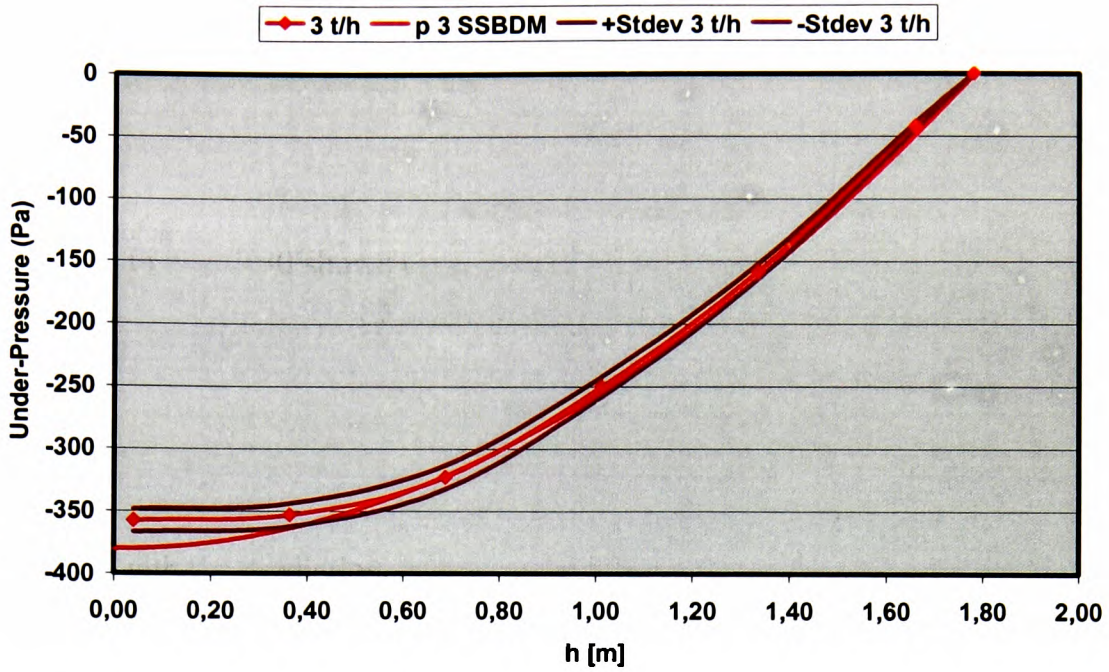


Figure 5-16. Results from tests with AST at a capacity of 3 t/h with the boundaries  $\pm$  one standard deviation, plotted together with the results of the SSBDM.

For the Capacity of 3 t/h the SSBDM results are within the standard deviation all the way except for the top of the tube, and is then on the conservative side.

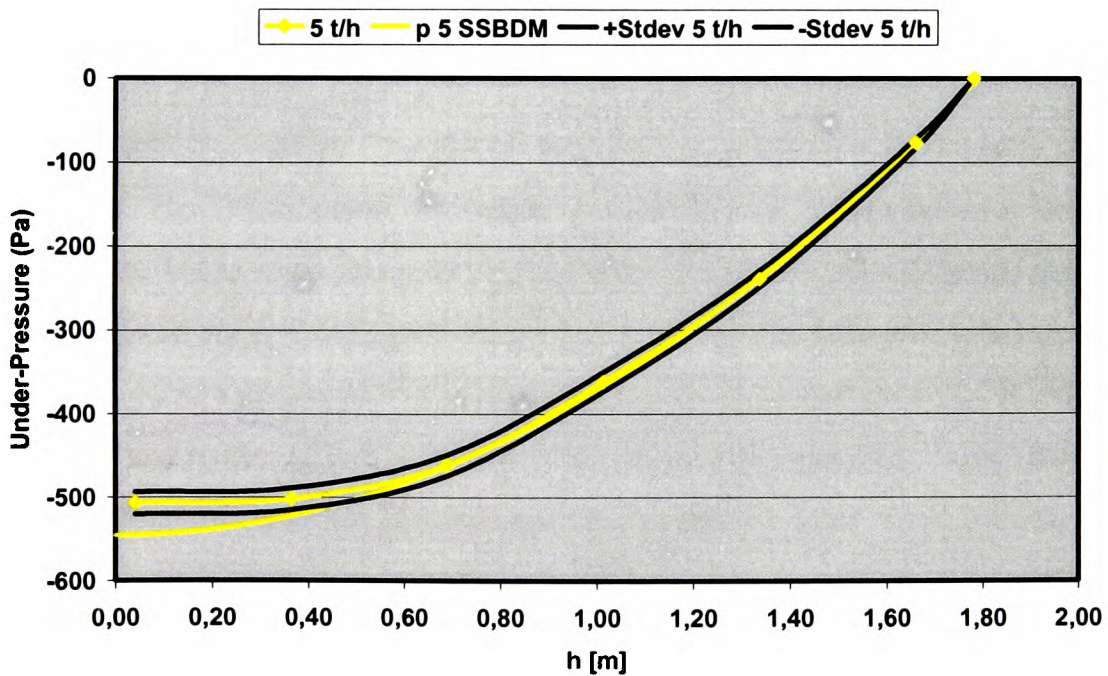


Figure 5-17. Results from tests with AST at a capacity of 5 t/h with the boundaries  $\pm$  one standard deviation, plotted together with the results of the SSBDM.



The capacity 5 t/h, is the same as for the 3 t/h, but it goes outside the boundary slightly earlier than what is the case for the 3 t/h.

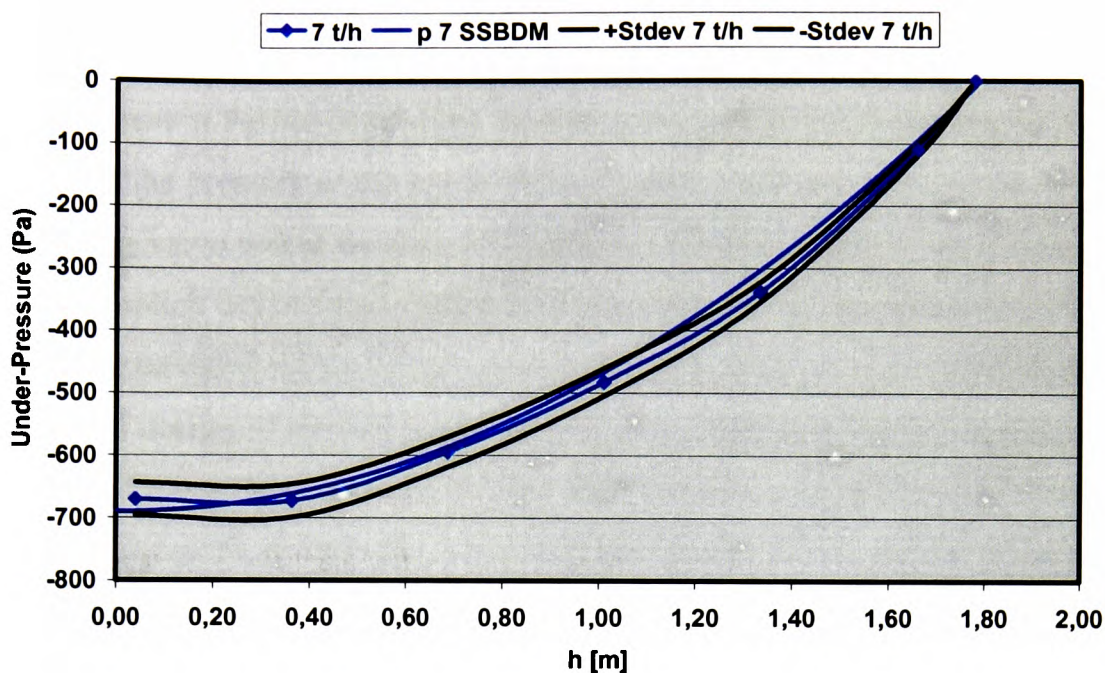


Figure 5-18. Results from tests with AST at a capacity of 7 t/h with the boundaries  $\pm$  one standard deviation, plotted together with the results of the SSBDM.

Looking at last at the result for 7 t/h, the predictions are inside the boundaries all the way.

All in all the SSBDM, with its assumption and settings, is suitable for pressure prediction inside the AST. The SSBDM does not taking into account the friction between the walls of the tube and the falling material, however, considering that the falling alumina is assumed to be in a fluidised state, the friction would be very low. Furthermore, looking at Figure 4-21 to Figure 4-24, a pressure peak is found during the start up before the establishing of a steady state flow in the AST. The SSBDM can explain this since the cross sectional area of the falling material, and not the side surface, during the start up is causing the drag force. This will result in an area perpendicular to the drag force, and therefore have a much higher drag coefficient.

## **5.6 Summary and Commentary of modelling the AST**

Several models are possible to put up for the anti segregation tube. Here the models and methods used historically for the AST have been verified against measured results. The early version of test rigs for AST used only one tube mounted in the centre, with one pressure measurement in the top of the tube. Based on the assumption of a linear pressure distribution, only the pressure at the top of the tube was measured, as the under pressure at the discharging valve would be zero. Furthermore, full dispersion of the falling material was also an implicit assumption. Although in principle wrong, this model has been used calculating conservative values of the negative pressure, more or less for all the initial development and design of the AST, and later the AS-System (Anti Segregation System). After designing a new test rig measuring the pressure at several levels along the height of the tube, initially made in order to detect leakages of the valves, it was noticed that the pressure distribution was not linear, which actually was not a big surprise. The second model was developed, where the velocity was calculated for each height by assuming free fall and ignoring air drag. The second model still was based on the assumption of full dispersion, and although deviating somewhat the agreement with the measured values during tests, was reasonable.

When using computer programs to simulate the AST, the results were quite disappointing. However, the FLUENT program identified one important issue, namely the positive pressure contribution generated by the flow from the inlet box to the tube. After the FLUENT gave this indication, the simple non-linear model was adjusted, and now both the trend and the actual values started to get into a good agreement with the measured values. Moreover, the simple non-linear model clearly is useful for quick pre-estimates of the pressure distribution in an AST.

To get more accurate modelling an attempt based on the drag from single particles was made. However, before fully developing the model, the terminal velocity of an average sized particle in the actual alumina material was calculated, and it was found that the capacities, with that terminal velocity and assuming full dispersion of alumina in the AST, were much lower than what actually had been obtained in existing tubes, hence this attempt had to be abandoned.

Not giving up the drag approach for modelling, an approach based on the material distribution inside the tube, as given by the FLUENT modelling was chosen. Instead of fully dispersed particles filling the whole cross section of the tube, the material flowed along one wall, leaving the rest of the cross section free for air circulation. In this situation, the drag from single particles becomes of less importance. Instead, the dominating drag will be the skin drag on the surface falling solid powder. This surface is defined by the length of the tube, and the width of the chosen AST profile. This approach assumes that the powder is falls a film along the tube wall opposite to the 90-degree bend on the AST. Following the mathematical rules and including theory for pressure drop in pneumatic conveying, the Solid Surface Body Drag Model (SSBDM) was developed. When first tried, this model was not very promising. However, after implementing a factor function (function of set parameters), the model gives very good correspondence with the measured data for the pressure distribution inside the AST. When comparing the model with measured data, and adding the test error (plus minus one standard deviation), the SSBDM was able to predict the pressure distribution within the test error boundaries in most cases. The negative factor about the SSBDM is that it is a complex model, and cannot be solved directly, but has to be solved parametrically. The simple non-linear model will therefore still be used for rough estimates determining the starting point of the design and SSBDM will be used for the final description of a chosen system.

## 6. DESIGNING THE ANTI SEGREGATION TUBE

The anti segregation tube can be designed for any fluidisable powders. However, the powder should preferably have a short de-aeration time, in order to make sure that the inlet box will work optimally. The inlet box described earlier must of course be adjusted according to the powder in question. Hence, the design that follows will not necessary is applicable for other materials than alumina. The characteristics of the alumina used for the development of the AST, and on later investigations, are as follows:

- Fluidisable, for alumina  $v_{\text{fluid min}}$  between 0,8 and 1,2 cm/s
- Expansion during fluidisation approximately 10%
- Angle of repose (upstream of AST), 30°
- Dynamic angle of repose, 28-50(60)°
- Maximum particle size, 3.5 mm
- Loose bulk density, alumina, 900 – 1 100 kg/m<sup>3</sup>

### 6.1 Designing the size of the tube for capacity

To choose a tube for a specific capacity, the old design suggested a 0,5 (t/h)/cm<sup>2</sup>. Moreover, during installations of Anti Segregation Systems consisting of several tubes, large fractions of the total filling capacities meant for distribution to several tubes in parallel have been routed towards one AST, and it has handled it. This suggests that the capacity is more than proportional to the cross sectional area of the tube. Looking back at the equation for the pressure drop, and knowing that the capacity can be calculated from the pressure difference from the inlet box to the AST, the  $K_p$  factor plays a role. In Equation 6-1, the  $K_p$  is shown, with the expression for the relative terminal velocity incorporated.

$$K_p = \frac{\dot{m}}{\rho_{\text{susp}} \left( \frac{2 \cdot \dot{m} \cdot g}{C_D \cdot \rho_f \cdot b} \right)^{\frac{1}{3}} A_{\text{Cross}}} \quad \text{Equation 6-1}$$

Assuming that the cross section of the tube is squared the cross sectional area  $A_{\text{cross}}$  can be expressed as in Equation 6-2.

$$A_{Cross} = b^2$$

⇓

$$b = A_{Cross}^{\frac{1}{2}}$$

Equation 6-2

$$\dot{m} = \left( \frac{K_p^3 \cdot \rho_{susp}^3 \cdot 2 \cdot g \cdot A_{Cross}^{\frac{5}{2}}}{C_D \cdot \rho_{fl}} \right)^{\frac{1}{2}}$$

Equation 6-3

$$Q \equiv \frac{K_p^{\frac{3}{2}} \cdot \rho_{susp}^{\frac{3}{2}} \cdot (2 \cdot g)^{\frac{1}{2}}}{(C_D \cdot \rho_{fl})^{\frac{1}{2}}}$$

Equation 6-4

Using Equation 6-1 and Equation 6-2 the expression of the capacity can be written as Equation 6-3. Condensing the expression by the use of Equation 6-4, the capacity can be given by Equation 6-5.

$$\dot{m} = Q \cdot A_{Cross}^{\frac{5}{4}}$$

Equation 6-5

$$\dot{m} \propto A_{Cross}^{\frac{5}{4}}$$

Equation 6-6

From Equation 6-5 one can then see that the capacity is not only proportional to the cross area as assumed in the old design, but rather proportional to the cross sectional area in the power 1,25 (Equation 6-6). The old design was largely based on a tube with inner cross sectional area of 92 mm by 92 mm, running at a maximum capacity of 42,32 t/h. From Equation 6-1 this will result in a  $K_p$  equal to 0,0681. Using that as a constant value and then calculating a new capacity plot and comparing it with the old design Figure 6-1 is obtained.

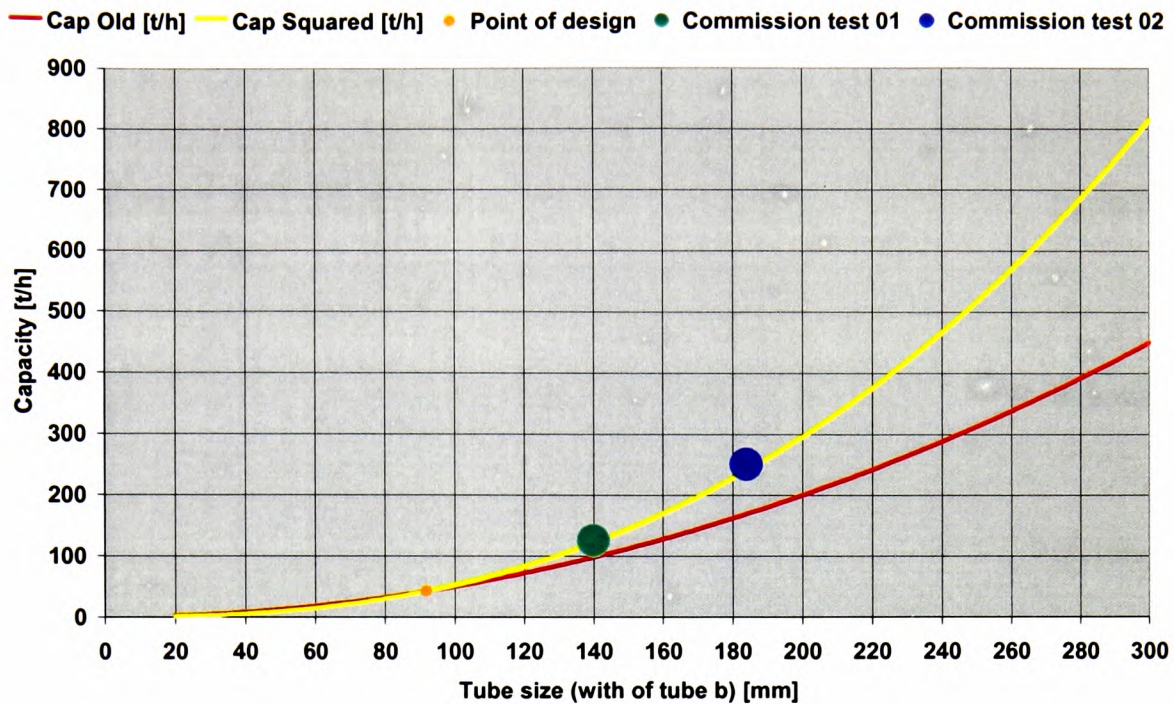


Figure 6-1. Designed capacity vs tube width, comparing old design with new.

From Figure 6-1, one can see that the capacity increases much more with the tube for the new model than what was the case with the old model. However, the old model was always thought to be conservative, and this is true for larger tubes. However, for tubes smaller than the designed 92 mm, the tubes becomes optimistic, while on the upper side of the 92 mm design basis, the old design model gets more and more conservative. As also can be seen from Figure 6-1, experimental data from commissions for installations matches the new model. The points are here plotted large, to illustrate some insecurity of the values.

Starting with Equation 6-1, but now using a rectangular tube, with a cross sectional area given by Equation 6-7, where  $w$  is the longest side in the rectangular profile, and  $b$  is the width as before, the relation between the cross sectional area and the capacity is given by Equation 6-8.

$$K_p = \frac{\dot{m}}{\rho_{susp} \left( \frac{2 \cdot \dot{m} \cdot g}{C_D \cdot \rho_f \cdot b} \right)^{\frac{1}{3}} A_{Cross}}$$

Equation 6-1

$$A_{\text{Cross}} = b \cdot w \quad \text{Equation 6-7}$$

$$\dot{m} = \left( \frac{K_p^3 \cdot \rho_{\text{susp}}^3 \cdot 2 \cdot g \cdot b^2 \cdot w^3}{C_D \cdot \rho_{\text{fl}}} \right)^{\frac{1}{2}} \quad \text{Equation 6-8}$$

$$\dot{m} = Q \cdot b \cdot w^{\frac{3}{2}} \quad \text{Equation 6-9}$$

$$\dot{m} \propto b \cdot w^{\frac{3}{2}} \quad \text{Equation 6-10}$$

What is interesting is that Equation 6-10, shows the capacity is proportional to the width  $b$  of the side which the powder flows along, but is proportional to the perpendicular side  $w$  of the tube to the power of 1,5. From all this the tube will be more effective capacity wise if one chooses to utilise a rectangular tube, making sure the powder flows along the shortest side. From Figure 6-2 where the longest side of the cross sectional area is twice the width of the tube ( $b$ ), one can clearly see a much higher capacity pro unit cross-area sectional.

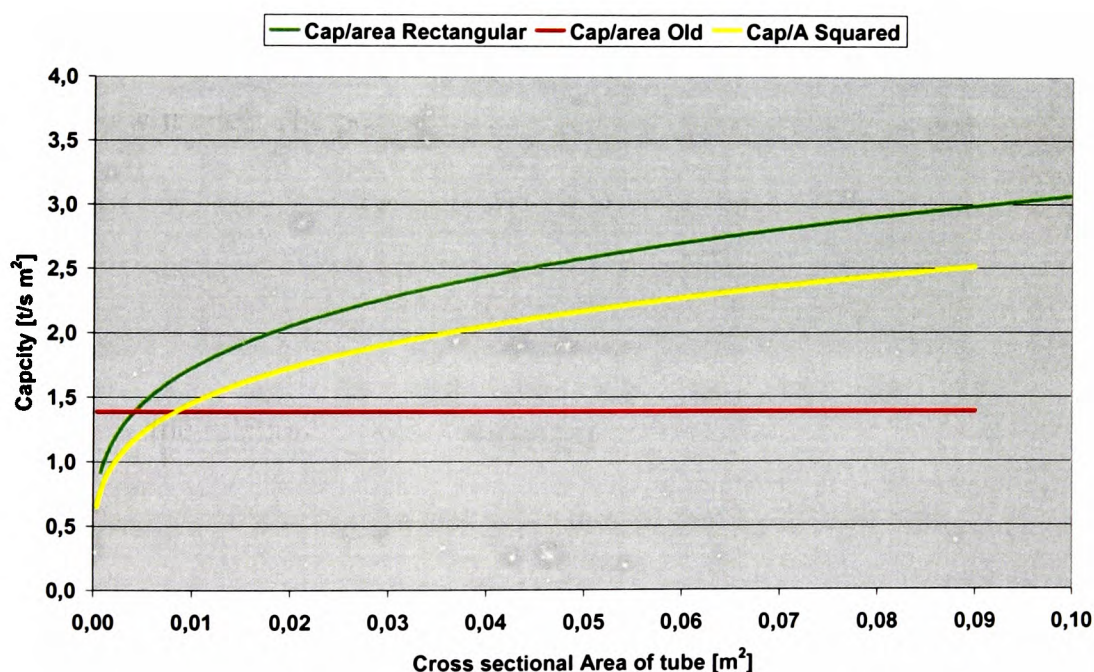


Figure 6-2. Capacity pro cross sectional area of a square and a rectangular tube ( $w=2b$ ), comparing old with new design theory.

However, since this has been derived from the equations and the friction between the wall and powder is not taken into account, one should not use the new design without caution. Nevertheless, the relations between both the cross section and especially the discovery of the potential effect of the rectangular tube are quite promising.

## 6.2 Placing the first valve at the top of the AST

In Equation 5-41 the pressure drop is calculated. However, the initial pressure  $P_0$  is a positive pressure, and when placing the first valve at the top of the AST, the generated negative pressure in the position of the valve must be higher than the initial positive pressure generated by the flow from the inlet box. By putting Equation 5-41 equal to zero, and then plotting the pressure drop as a function of its corresponding height (Equation 5-29) the placement of the first valve can be determined.

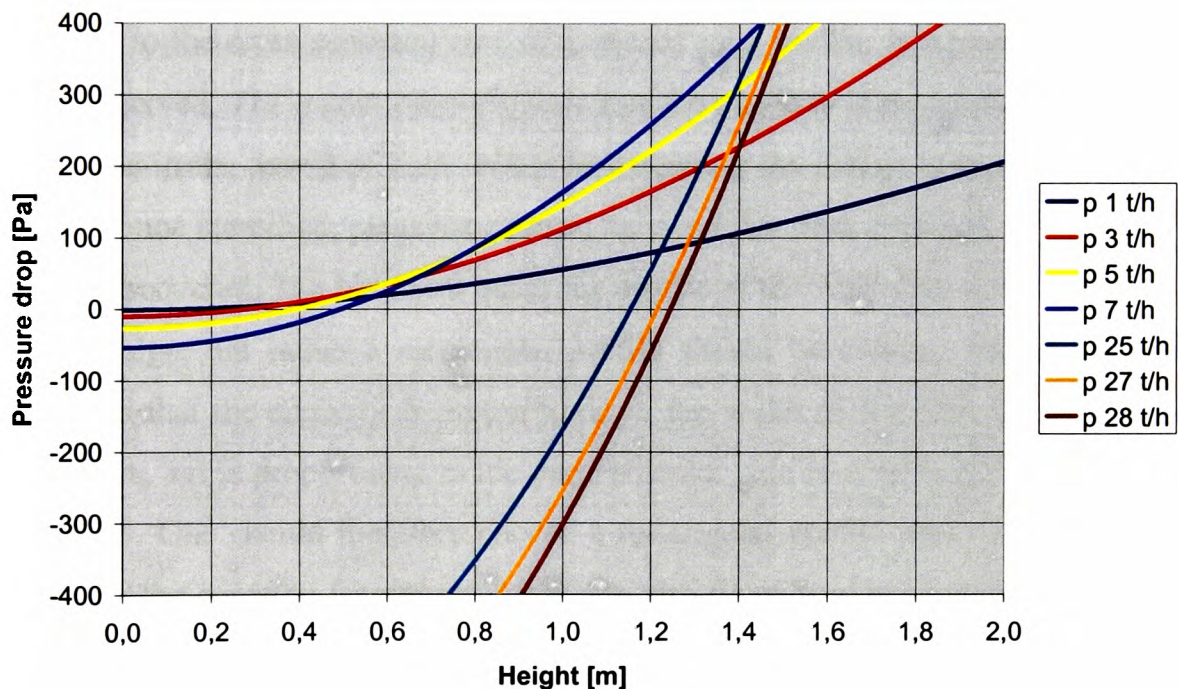


Figure 6-3. Example of placing the first valve in a 80 mm by 80 mm tube.

If by any chance the placement of the first valve gets so far down into the silo that it starts to affect the degree of filling of the silo, the tube size must be increased.



### 6.2.1 Choice of configuration and placement

With large silos, where the diameter is the dominant dimension, the use of an ASS with several AST's is the most suitable solution. With tall silos of smaller diameters, a single centre mounted AST may be used. Moreover using the multi AST version of the AS-System, will give a bonus in terms of better filling degree of the silo.

## 6.3 Summary and commentary of designing the AST

A new method of design of the AST can be derived from the theoretical models. Using the dimensionless parameter function determined for the pressure drop model Equation 6-1, one can derive a relative formula of capacity, Equation 6-5, and by including data from the initial design model for capacity a design for capacity can be undertaken based on empirical data. The models giving the design clearly demonstrate that the capacity is more than proportional to the cross sectional area of a chosen tube profile, in agreement with what has been observed. The model even suggests that the capacity is proportional to the cross sectional area in the power of 1,25. When investigating the design criteria further, a surprising, but once identified, plausible relation between the cross sectional area and the capacities is discovered. The historical quadratic profile of the AST does not seem to be the optimum design, but rather a rectangular profile should be chosen. The design model demonstrates that the capacity is proportional to the width of the tube along which the powder flows, but is proportional to the perpendicular side in a rectangular profile to the power of 1,5. One should therefore choose a rectangular profile when designing ASTs. Furthermore, the equation for pressure drop can also be utilised to position the first valve on the tube, in such a way that squirting does not occur during filling of a silo, no matter how low the filling height is. This can be done by balancing the initial positive pressure from the inlet box, with the pressure of the AST. The height where the pressure drop equals the initial pressure is the critical height for placing the upper valve. If a valve is placed closer to the 90-degree bend, the upper valve will not keep closed during the last stages of the filling of the silo. If the height in which the upper valve has to be placed interferes with the filling degree of the silo, a larger AST profile needs to be chosen.

For height capacities, and large silos, a system consisting of several AST should be chosen. This will not only reduce the capacity needed in one AST, but also increase the degree of filling in the silo. If a surplus capacity in the AST design is large enough, alternate feeding through the different AST can even result in a larger homogenising effect than just the traditionally 1-1,5.

## **7. CONCLUSIONS**

The segregation phenomena have been discussed in many publications, dating back to as early as 1915, and perhaps even earlier. Discussions about mechanisms or processes will not be of focus here, rather the outcome and the countering of the segregation.

- Overall, there has been singled out 12 mechanisms from the literature during this work, and the processes and situations in which they are active.
- The literature on segregation is quite extensive, but it seems that the description of segregation itself is in the focus and not the impact segregation has in a given situation/process.
- The literature shows that when handling alumina, the mechanism called air current segregation is dominant. The air current mechanism can and will accumulate fines at the silo walls, if the material surface there is not renewed frequently.
- The literature suggests that variations in any of the raw material compositions will affect the heat balance, i.e. the energy consumption of production, as well as the occurrence of anode effects, and hence the current efficiency when producing aluminium. And when forcing the process the need for raw material control will increase in importance.
- The quantification of segregation is the most important “Anti Segregation Measure”. Without the information about the situation in the process stream, the information necessary to decide how and where to fight segregation is missing, and one can simply not do anything about the problem.
- Full factory sampling campaigns have been found possible. Although this means sometimes to deviate from what is stated as good sampling practice in literature and standards, implementing sampling as a natural part of a process has a high value.
- Standardised statistical expressions can then be used for analysing the bottlenecks of the logistic loops, and from this information one can implement any suitable anti segregation measures.
- The degree of segregation when handling alumina has proven itself to be quite considerable. The powder technology part of it clearly shows that the transportability and flowability of alumina can become very altered by the handling processes in a logistic loop.

- In industry there are old logistic loops, and are usually designed for their functions, not for their purposes. The transport is usually designed without any consideration of crushing or suitability for the material in hand. Storages are usually designed only for gross volume, not available volume.
- Direct influences on the processes and environment from segregation have been found. Correspondence between variations in fines, due to segregation, and dust concentration in the smelter pot room, and correspondence between variations of fines content and anode effects are examples of such influences. Hence, process influence by segregation has been made plausible including reduced current efficiency of electrolysis cells, especially cells running towards optimum performance.
- An economical evaluation of an investment in an anti segregation system has been made, clearly justifying both the investigations in segregation and the implementation of anti segregation measures.
- The AS-System clearly demonstrated a homogenising effect no matter how low the ingoing variations were.
- Other systems can only be considered as Segregation Effect Damping Systems, since they only seek to reduce the effects of segregation instead of directly attacking the segregation mechanism itself.
- A new inlet for the Anti segregation Tube for real industrial installations has been found. A semi hydrostatic inlet box proved itself capable to handle the variations and vibrations occurring in industry, furthermore, it was self-regulating with a large operational range of capacities, all the way from no transport to an upper limit defined by the AST system all together.
- A new test rig for model verifying has been developed, revealing new information about the pressure inside the anti segregation tube. The new test rig was also designed in the fashion of a complete AS-System consisting of three ASTs, and was also used to test the potential effect of this system in the terms of efficiency in countering segregation.
- Tests copying the repeated emptying and filling of a silo, hence accumulating segregated fines at the silo walls, were tested. The results clearly showed that the AS-System prevented segregation, compared to conventional filling, even in a small scale.
- The models and methods used historically for the AST have been verified against

measured results, using the new test rig.

- The new test rig proved that early models based on full dispersion and simple equations from the conversion from potential to kinetic energy, were valid although in a conservative way.
- When using FLUENT to simulate the AST, the results were quite disappointing, however, the FLUENT program identified an initial positive pressure generated by the flow from the inlet box to the tube. Implemented into the simple non-linear model, both the trend and the actual values corresponded even better with the measured values.
- To get more realistic model an attempt of modelling based on complete dispersion and the drag from single particles was considered. However, when validating this idea, results showed that this approach was insufficient.
- The Solid Surface Body Drag Model (SSBDM) has been developed. After implementing a factor function (function of set parameters), this model gives very good correspondence with the measured data for the pressure distribution inside the AST.
- When comparing the model with measured data, and adding the test error (plus minus one standard deviation), the SSBDM was able to predict the pressure distribution within the test error boundaries in most cases.
- The negative factor of the SSBDM is that it is a complex model, and cannot be solved directly, but has to be solved parametrically.
- A method of new design of the AST can be derived from the model.
- The models giving the design clearly demonstrate a fact that the capacity is more than proportional to the cross sectional area of a chosen tube profile, in agreement with previous observations.
- The model even suggests that the capacity is proportional to the cross sectional area in the power of 1,25.
- Historically quadratic profiles of the AST have been used, but this is not the optimum design. A rectangular profile appears to be a better choice, because the models suggest that the capacity is proportional to the width of the tube along which the layer of alumina flows, but proportional to the perpendicular side in a rectangular profile to the power of 1,5.

## **8. SUGGESTED FURTHER WORK**

Further topics of work in segregation can be many. However, to move this particular work forward the topics could be divided into five points:

- i.) Further, develop the SSBDM, by implementing friction between the wall of the tube and the falling powder stream.
- ii.) Test and quantify the suggested relation between capacity and AST profile choice.
- iii.) Directly identify the flow patterns inside the AST by the use of a tomography method. There are several, and preferably, one could be able to use ultra sound. Nevertheless, using gamma- or x-rays could also be an alternative.
- iv.) Keep up and improve the sampling campaigns in full-scale factories, by moving towards a more and more ideal and correct sampling.
- v.) Study and quantify directly the influence the variations of alumina quality have on the electrolysis process, with the aim to be able to put the effect directly into cost numbers.

The above six points would probably give basis for many years of study, and the results would not only be interesting, but also of great economical importance for the aluminium industry.

## 9. REFERENCES

- Alonso, M., Satoh, M., Miyanami, K. (1991): "Optimum Combination of Size Ratio, Density Ratio and Concentration of Minimise Free Surface Segregation". *Powder Technology* 68, 145-152
- Artega, P. and Tuzün, U. (1990): "Flow of Binary Mixtures of Equal Density Gradients in Hoppers – Size Segregation, Flowing Density and Discharge Rates". *Chem. Eng. Sci.* 45/1, 205-223.
- Bagster, D.F. (1983): "The Influence of Cohesion on the Segregation Pattern in Bins". *Proc. Int. Conf. on Bulk Materials Storage, Handling and Transportation, Newcastle, Australia*, 203-206.
- Bagster, D.F. (1985): "The Effect of Coarse Particle Concentration and of Water Content on the Segregation of Particulate Solids in Bins". *Proc. RELPOWFLO I, Bergen, Norway*, 289-302.
- Bagster, D.F. (1996): "Studies of the Effect of Moisture Content and Coarse and Fine Particle Concentration on Segregation in Bins". *KONA* 14, 138-143.
- Bates, L. (1997): *User Guide to Segregation*. British Materials Handling Board.
- Bicking, C.A. (1967): *The Sampling and Bulk Materials*. Materials Research & Standards.
- Borho, K., Polke, R., Wintermantel, K., Schubert, H., Sommer, K. (1993): *Product Properties and Process Engineering*. Video and Handbook produced by BASF, Ludwigshafen, Germany.
- Bradely M.S.A, Fransih R.J & Hyder L.M.: "A novel analytical model for the acceleration of particles following bends in pneumatic conveying system". The 3<sup>rd</sup> Israel Conference and Handling of Particulate Solids, Dead Sea, May 2000.
- Bridgwater, J., Foo, W.S., Stephens, D.J.: *Particle Mixing and Segregation in Failure Zones: Theory and Experiment*. *Powder Technology*, 41, p.147-158.
- Bridgwater, J., Ingram, N.D.: *Rate of Spontaneous Interparticle Percolation*. *Transactions of the Institution of Chemical Engineers*, 49, p.163-169.
- Brown, R.L. (1939): *The Fundamental Principles of Segregation*. I. *Inst. Fuel*, 13.
- Bruff, W. (1974): *Industrisiloer*. Ingeniørforlaget, Oslo, Norway.
- Carruthers, A.N. (1987): *Segregation in Flat Bottomed Alumina Silos*. *Light Metals*, 151-156
- Carson, J.W., Royal, T.A., Goodwill, D.A. (1986): *Understanding and Eliminating Segregation Problems*. *Bulk Solids Handling* 6, 1, p.139-144.
- Cooke, M.H., J. Bridgwater, et al. (1978): *Interparticle percolation: lateral and axial diffusion coefficients*. *Powder Technology*, 21, p.183-193.

- de Silva, S.R. (1997): Mixing and Segregation in Industrial Processes: A Review. IFPRI Report. Tel-Tek Report 410037-1.
- de Silva, S.R., Enstad, G.G. (1991): Bulk Solids Handling in Scandinavia: A Case Study. *Bulk Solids Handling* 11, 1, p.65-68.
- Dolgunin, V.N., Ukolov, A.A. (1995): "Segregation Modelling of Particle Rapid Gravity Flow". *Powder Technology* 83, 95-103.
- Drahn, J.A., Bridgwater, J. (1983): The Mechanisms of Free Surface Segregation. *Powder Technology*, 36, p.39-53.
- Dyrøy, A, Berdal, A.(1999): Effekt av segregering på luftrenners transport kapasitet, Tel-Tek report 410089-2, Norwegian, Classification; open for reference.
- Dyrøy, A., Enstad, G.G. (1996): Motvirkning av segregering i eglisatorceller. Tel-Tek Report 410046-1.
- Dyrøy, A., Karlsen, M., Enstad, G.G., de Silva, S.R. (2000): Air Current Segregation: Quantification of Effects and Avoidance. 3<sup>rd</sup> Israeli Conference for Conveying and Handling Particulate Solids. The Dead Sea.
- Dyrøy, A.: Effekt av segregering fra kai til celle i aluminiumsproduksjon. Tel-Tek-report no. 410088-1, Porsgrunn, 1998 December 31. P.61. K1. H.A.Å. ATA
- Dyrøy, A.: Segregering og nedknusing fra hovedlager i Øvre Årdal, til elektrolysecelle i ÅIIC og ÅIII. Tel-Tek-report no. 410089-3, Porsgrunn, 2000 March 13. P.43. K1. H.A.T. Årdal
- Dyrøy, A.: Analyser av prøver fra flatelager ved Årdal Metall-verk, ved resttømming. Tel-Tek-report no. 410080-2, Porsgrunn, 2000 May 24. P.16. K1. H.A.Å. (ATA)
- Dyrøy, A.: Effekt av AS-System i sammenligning med vanlig fylling av silo - Tester i liten skala. Tel-Tek-report no. 410059-3, Porsgrunn, 2001 May. P.9. A. H.A.Å.T. (ATA)
- Dyrøy, A., Berdal, A.: Prøvekampanje AAM'00 - Effektmåling av installasjon av AS-System. Tel-Tek-report no. 410080-8, Porsgrunn, 2002 January 23. P.32. K1. H.Å.T. (ATA)
- Dyrøy, A., Berdal, A.,: Prøvekampanje AHO'01. Tel-Tek-report no. 410081-4, Porsgrunn, 2002 December 19. P.35. K1. H.Å.T. (TO&S)
- Dyrøy, A., Berdal, A.: Praktisk pulverhåndtering - Prøvekampanje KAPP 2002. Tel-Tek-report no. 410082-5, Porsgrunn, 2003 December 12. P.47. K1. H.Å.T. (TO&S)
- Dyrøy, A., Berdal, A.: Effekt verifisering AS-System installasjon AHO-Hovedlager. Tel-Tek-report no. 410083-3, Porsgrunn, 2003 October 22. P.14. K1. H.Å.T. (TO&S)
- Engrav, S., Halvorsen, K., Holberg, J.K., Wndelborg, K. (1989): Segregering av partikulære materialer ved strømning gjennom skrånstilte rør og påfølgende fylling i haug. Studentprosjekt, Telemark University College.



- Enstad, G.G. Knutsen, G.F., Mosby, J., Leaper, M. and Bergland, W. Motvirking av luftindusert segregering ved fylling av siloer. POSTEC-report no. 921301-5.
- Enstad, G.G., Knutsen, G.F. (1997): Utvikling av en passiv homogenisator for pulvere. Tel-Tek report 41066-1.
- Enstad, G.G., Stoltenberg-Hansson, E. (1993): Blending and Dosage of Relinker - Resulting Effect of Segregation and Ways to Counteract it. VDZ-Kongress. Düsseldorf, Germany.
- Foo, W.S., Bridgwater, J. (1983): Particle Migration (short communication). Powder Technology, **36**, p.217-273.
- Garve, T.W. (1925): I. Amer. Ceram. Coc., **8**, 668.
- Geankoplis C.J.; "Transport processes and unit operations". Prentice -Hall International Editions. Third Editions. ISBN 0-13-045253-x. USA 1993.
- Geldart, D. "Types of Gas Fluidisation" Powder Technology no. 7, 1973. pp. 285.
- Holmes (1934): Colliery Engineering, **11**.
- Hubrich M. : "Further Development And Testing Of The Anti Segregation Tube", Studienarbeit Martin Hybrich, Tel-Tek student report. December 1998.
- Johanson, J.R. (1978): Particle Segregation, and What to do About it. Chemical Engineering.
- Johanson, J.R. (1987): Solids Segregation - Case Histories and Solutions. Bulk Solids Handling, **7**, 2, p.205-208.
- Johanson, J.R. (1988): Solids Segregation - Causes and Solutions. Powder and Bulk Engng., p.13-19.
- Johanson, J.R. (1991): Solids Segregation: Causes and Solutions. Powder & Bulk Solids Conf., Rosemont, Illinois, USA.
- Karlsen, M., Dyrøy, A., Kvande, H. (1999): Anti-segregation Tubes - An Efficient Way of Filling Alumina Silos. TMS Annual Meeting. San Diego, USA.
- Kaye, B. (1997): Powder Mixing, Chapman and Hall.
- Leenders, F. (1993): Investigation of Segregation in Silos with Special Emphasis on Percolation. Diploma thesis. Thelemark University College/University of Twente.
- Mathee, H. (1967/78): Segregation Phenomena Related to Bunkering of Bulk Materials: Theoretical Considerations and Experimental Investigations. Powder Technology, **1**, p.265-271.
- Meckin, P. and Jullien, R. (1992): "Simple Models for Two- and Three Dimensional Particle Size Segregation". Physica A **180**, 1-18.
- Medema, J.G. (1991): An Experimental Study of the Effect of Air Induced Segregation of Alumina during the Filling of Silos. M.Eng. thesis Tel-Tek/University of Twente..

- Mitchell, D.R. (1998): Segregation in the Handling of Coal. Trans. A.I. Min. Metall and Pet. Engrs.
- Mosby, J, Enstad, G.G. (1996): Segregation of Particulate Solids Mapret Lecture. CHISA '96. Prague.
- Mosby, J. (1996): Investigation of the Segregation Particulate Solids with Emphasis on the Use of Segregation Testers. Dr.Ing. Thesis. Norwegian University of Science and Technolgy/Telemark University College.
- Mosby, J., Enstad G.G. (1994): Innledende studier av blanding og segregering av kobberkonsentrat og sand ved fylling i haug. Tel-Tek Report 41006-1.
- Peacock, H.M. (1938): The Design or Adaptation of Storage Bunkers to Prevent Size Segregation of Solids. J. Inst. Fuel, 11, p.230-239.
- Penne, H. (1991): Undersøkelse av problemet med finstøv i oksider. Når, hvordan og hvorfor. Hovedoppgave NTNU i samarbeid med Elkem Aluminium, Lista.
- Popplewell, L.M., Campanella, O.H., Sapru and Peleg, M. (1989): "Theoretical Comparison of Two Segregation Indices for Binary Powder Mixtures". Powder Technology 58, 55-61
- Savage, S.B. (1984): Particle Size Segregation in Inclined Chute Flow: McGill University, Montreal, Canada H3A 2K6 (September 3.-7.), p.1-16.
- Savage, S.B. (1984): Particle Size Segregation in Inclined Chute Flow: Theory and Experiments. 8<sup>th</sup> CHISA: 9.
- Savage, S.B. and Lun, C.K.K. (1988): Particle Size Segregation in Inclined Chute Flow of Dry Cohesionless Granular Solids. J. Fluid Mech., 189, p.311-335.
- Scott, A.M. and J. Bridgwater (1976): Self-Diffusion of Spherical Particles in a Simple Shear Apparatus. Powder Technology, 14, p.177-183.
- Scott, A.M., Bridgewater, J. (1975): Interparticle Percolation: A Fundamental Solids Mixing Mechanism. Ind. & Eng. Chemistry, 14, 1, p.22-27.
- Sherman, R.A., Kaiser, E.R (1937): Segregation of Coal in an Industrial Steam Plant Bunker. Combustion. December, 25-28.
- Shinohara, K. (1979): Mechanism of Segregation of Differently Shaped Particles in Filling Containers. Ind. Eng. Chem. Process Design and Development, 18, 2.
- Shinohara, K. (1985): Some models on particle-segregation in filling hoppers. Aufbereitung-Technik, 3, p.116-122.
- Shinohara, K. (1987): General Mechanism of Particle Segregation during Filling of Hoppers. Proceedings of 9<sup>th</sup> CHISA Congress, section H: Particulate Solids, H.3.5, Prague, Czech.
- Shinohara, K. (1990): General Segregation Mechanism of Binary Solids Mixtures Filling Two-Dimensional Hoppers. Aufbereitungs-Technik, 31, 9, p.482-488.

- Shinohara, K., Enstad, G.G. (1990): Segregation Mechanism of Binary Solids in Filling Axi-Symmetric Hoppers. Proceedings of 2<sup>nd</sup> World Congress Particle Technology, Kyoto, Japan.
- Shinohara, K., Enstad, G.G. (1993): Some Segregation Mechanisms and their Prevention. Reliable Flow of Particulate Solids II, Oslo, Norway.
- Shinohara, K., Idemitsu, Y., Gotah, k., Tanaka, T. (1968): Mechanism of Gravity Flow of Particles from a Hopper. Ind. Eng. Chem. Process Design and Development, 9, 2.
- Shinohara, K., Miyata, S. (1984): Mechanism of Density Segregation of Particles in Filling Vessels. Ind. Eng. Chem. Process Design and Development, 23, 3, p.423-428.
- Shinohara, K., Saitoh, J. (1993): Mechanism of Solids Segregation over a Two-Dimensional Dead Man in Blast Furnace. The Iron and Steel Institute of Japan, 33, 6, p.672-680.
- Shinohara, K., Shaitoh, J. (1992): Segregation by Multi-Point Feeding of Binary Solids Mixture onto Two-dimensional Heap. Intnt. Conf. Bulk Mat. Hand. and Transp.; Symposium on Freight Pipelines, Wollongong, Australia.
- Shinohara, K., Shoji, K., Tanaka, T. (1970): Mechanism of Segregation and Blending of Particles Flowing out of Mass-Flow Hoppers. Ind. Eng. Chem. Process Design and Development, 9, 2, p.369-376.
- Shinohara, K., Shoji, K., Tanaka, T. (1972): Mechanism of Size Segregation in Filling a Hopper. Ind. Eng. Chem. Process Design and Development, 11, 3, p.369-376.
- Spain, R.W. (1965): Segregation in Batch Handling and Storage Systems. Ceramic Industry, 65.
- Standish, N. (1985): "Studies of Size Segregation in Filling and Emptying a Hopper". Powder Technology 45, 43-56
- Stephens, D.J., Bridgwater, J. (1978): The Mixing and Percolation of Cohesionless Particulate Materials, Part I: Failure Zone Formation. Powder Technology, 21, p.17-28.
- Stephens, D.J., Bridgwater, J. (1978): The Mixing and Percolation of Cohesionless Particulate Materials, Part II: Microscopic Mechanisms of Particles Differing in Size. Powder Technology, 21, p.17-28.
- Stillwell, M. (2003): Development Work on the Anti-Segregation Tube, Tel-tek Report no. 410033-01
- Stock, A.J. (1944): Coal Segregation in Boiler Plant. Mech. Engng., 66.
- Sydsæter, K., Strøm A. and Berck P. (1998): "Matematiske Formler for økonomer 3. utgave", Universitetsforlaget ISBN 82-00-12797-4.
- Syskov, K.I., Lyan, T. (1960): Investigation of the Process of Segregation in Ore-Coal Mixtures. Coke and Chemistry, 2.
- Taggart (1927): Handbook of Ore Dressing. McGraw Hill. 1087.

Tanaka, T. (1971): Segregation Models of Solid Mixtures Composed of Different Densities and Particle Sizes. *Ind. Eng. Chem. Process Design and Development*, **10**, 3, p.332-340.

Wettich (1915): *Tonindustrie Zeitung*, Juli.

Williams, J.C. (1963): *The Segregation of Powders and Granular Materials*. Fuel Society, Sheffield, Journal, **14**.

Williams, J.C. (1976): *The Segregation of Particulate Materials. A Review*. *Powder Technology*, **15**, p.245-251.

Williams, J.C., Kahn, M.I. (1973): *The Mixing and Segregation of Particulate Solids of different Particle Size*. *Chemical Engineering*, **19**, p.169.

**APPENDIX A  
NOMECLATURE AND ABBREVIATIONS**

**Abbreviations used:**

MNOK	Million Norwegian Korner
AS-System	Anti segregation system
AST	Anti Segregation Tube
USD	United States of America Dollars
SPDM	Single Particle Drag Model
SPL	Single Point Linear
SSBDM	Solid Surface Body Drag Model

**Variable(s) used for statistics and normalisation**

$C_{var}$	The coefficient of variation for a sample series
$H_{fact \frac{i}{j}}$	The homogenisation factor between the series i and j
$S$	The standard deviation, based on n-1, for a series of samples
$\bar{X}$	The average value of a sample series of n samples
$X_i$	measured value
$Y_i$	normalized and centred value

**Variable(s) used for Electrolysis cell calculation**

I	Current used in electrolysis cell [kA]
CE	Current Efficiency [-]

**Variable(s) used for Economical calculations**

$A_t$	Net present value after t periods
r	Interest rate [-]
R	The periodic return, if constant [NOK, £ or US\$]
$R_i$	Periodic return for the periode i [NOK, £ or US\$]
t	Period number [#]

T Definite number of periods (f.ex. number of years)

### **Variables And Constants For the Inlet Box**

DL Distance between the outlet and the fluidizing element

L Length of the horizontal part of the 90° tube bend

H<sub>0</sub> Height of the outlet opening

H Total height of the inlet seal

## Variables And Constants Used For Modeling

$\rho_1$	Density of materil in the inlet box, for the first initial model [ $\text{kg/m}^3$ ]
$\rho_2$	Calculated density for material in the tube for the initial model [ $\text{kg/m}^3$ ]
$\rho_{\text{Bulk}}$	Bulk density for the material, here Alumina 960 [ $\text{kg/m}^3$ ]
$\rho_{\text{fl}}$	Density for the fluid, here air 1,189 [ $\text{kg/m}^3$ ]
$\rho_{\text{Susp}}$	Density of the flowing flidised material inside the tube, here 90% of $\rho_{\text{Bulk}}$ , i.e. 864 [ $\text{kg/m}^3$ ]
$\mu$	Dynamic viscosity [ $\text{Pa s}$ ]
$a$	Netto acceleration [ $\text{m/s}^2$ ]
$A_1$	
$A_2$	Cross sectional area of the Anti segregation Tube [ $\text{m}^2$ ], used for the first initial model
$A_{\text{Cross}}$	Cross sectional area of the Anti segregation Tube [ $\text{m}^2$ ]
$A_{\text{p}}$	Perpendicular projected area for a falling object [ $\text{m}^2$ ]
$A_{\text{Solid}}$	Area of interface between the falling powder and air, inside the tube [ $\text{m}^2$ ]
$b$	Widht of the AST [ $\text{m}$ ]
$B$	Simplification constant used for SSBDM, def Equation 5-20
$B_2$	Simplification constant used for SSBDM, def Equation 5-34
$C_{j1}$	Integration constant used for development of Equation 5-27, def Equation 5-28
$C_{j2}$	Integration constant used for development of Equation 5-36, def Equation 5-37
$C_D$	Drag coefficient, here used as 0,16 [-]
$f_1(v, v_{\infty})$	Simplification function, defined in Equation 5-39
$f_2(v, v_{\infty})$	Simplification function, defined in Equation 5-40
$F_D$	Drag force [ $\text{N}$ ]
$F_G$	Force from the gravitational acceleration [ $\text{N}$ ]
$F_{\text{tot}}$	Total or resulting force from the netto acceleration $a$ [ $\text{N}$ ]
$g$	Gravitational acceleration 9,81 [ $\text{m/s}^2$ ]
$h$	Height distance along the direction of the AST. Positive downwards and zero on the top [ $\text{m}$ ]



---

$h_2$	Total height of the tube [m]
$H_{tot}$	Maximum height for a given AST configuration, or the height down to the first open valve [m]
$k_1$	Simplification konstant for single particle drag model
$K_p$	Dimensionless function of set parameters used for pressure drop calculations [-]
$\dot{m}$	Massflowrate through the AST [kg/s]
$DP$	Delta pressure between the pressure at the outlet of the inletbox and static negative pressure inside the AST [Pa]
$P_0$	Initial dynamic pressur from the flow out of the inlet box, def Equation 5-5
$p_1$	Hydrostatic pressure in the inlet box [Pa]
$p_2$	Pressure inside the AST, when calculating it hydrostatically, initial model. [Pa]
$p_i$	Pressure drop in point I, inside the AST [Pa]
$P_{stat i}$	Static pressure generated by the pressure drop in position i, def Equation 5-42
$Q$	Simplification constant, def Equation 6-4
$Re$	Renolds Number
$v$	Velocity of powder [m/s]
$v_\infty$	Terminal velocity, calculated maximum relative velocity between air and powder/ particle [m/s]
$w$	Length of the AST profile, perpendicular to b [m]

**APPENDIX B  
LIST OF FIGURES  
AND  
TABLES**

## Figures

FIGURE 2-1	MECHANISMS OF SEGREGATION AND WHERE THEY OCCUR, E.G. DURING FILLING OF A SILO, ON A TRANSPORT BELT, OR IN A MIXER. ....	17
FIGURE 2-2.	TRAJECTORY (OR INERTIA) SEGREGATION. ....	18
FIGURE 2-3.	AIR-CURRENT SEGREGATION. ....	19
FIGURE 2-4.	ROLLING OF COARSE PARTICLE ON SURFACE MADE BY FINER PARTICLES. ....	19
FIGURE 2-5.	SIFTING OF FINER PARTICLES BETWEEN COARSER PARTICLES WHEN LAYERS SLIDE DOWN A HEAP SURFACE. ....	20
FIGURE 2-6.	IMPACT EFFECTS WHEN FILLING A HEAP. ....	21
FIGURE 2-7.	PUSH-AWAY OR EMBEDDING EFFECT. ....	21
FIGURE 2-8.	ANGLE OF REPOSE EFFECTS (HERE ILLUSTRATED BY SAND AND COPPER CONCENTRATE). ..	22
FIGURE 2-9.	DISPLACEMENT SEGREGATION IN A VERTICAL VIBRATING REGIME. ....	22
FIGURE 2-10.	PERCOLATION IN A HORIZONTAL SHEAR REGIME. ....	23
FIGURE 2-11.	FLUIDIZATION SEGREGATION WHEN FILLING A SILO. ....	23
FIGURE 2-12.	CONCENTRATION DRIVEN DISPLACEMENT (DIFFUSION) ....	24
FIGURE 2-13.	AGGLOMERATION OF FINES CREATING COARSER PARTICLES, WITH DIFFERENT MOBILITY. ..	25
FIGURE 2-14.	AIR CURRENT SEGREGATION WHEN FILLING A SILO CAUSES ACCUMULATION OF FINES WHEN KEEPING A CONSTANT LEVEL, WHICH IS INTRODUCED TO THE PROCESS WHEN THE SILO IS DISCHARGED MORE THAN NORMALLY [CARRUTHERS, 1987]. ....	28
FIGURE 2-15.	BAUXITE, ALUMINA AND ALUMINIUM. ....	29
FIGURE 3-1.	PHILOSOPHIES BEHIND THE ANTI SEGREGATION WORK IN INDUSTRY. ....	39
FIGURE 3-2.	SIMPLIFIED LAYOUT OF ALUMINIUM PLANT. ....	41
FIGURE 3-3.	GENERATED DATA FOR DIFFERENT SAMPLING POINTS GIVEN IN FIGURE 3-2. ....	47
FIGURE 3-4.	SAMPLES GIVEN IN FIGURE 3-3 COMBINED IN ONE PLOT. PLUS AND MINUS ONE STANDARD DEVIATION FOR EACH SAMPLING POINT ARE INDICATED BY THE RED LINES. ....	47
FIGURE 3-5.	AVERAGES FOR THE SAMPLES SHOWN IN FIGURE 3-3. ....	48
FIGURE 3-6.	STANDARD DEVIATIONS OF THE DATA GIVEN IN FIGURE 3-3. ....	49
FIGURE 3-7.	COEFFICIENT OF VARIATION FOR THE DATA GIVEN IN FIGURE 3-3. ....	49
FIGURE 3-8.	HOMOGENISING FACTORS BETWEEN THE SAMPLING POINTS FOR THE SAMPLES GIVEN IN FIGURE 3-3. 50	
FIGURE 3-9.	HOMOGENISING FACTORS FOR SAMPLES GIVEN IN FIGURE 3-3, RELATIVE TO SAMPLING POINT A (THE INPUT). ....	51
FIGURE 3-10	VARIATION OF FINES CONTENT OF ALUMINA DISCHARGED FROM A SILO, AND THE FILLING LEVEL IN THE SILO. ....	52
FIGURE 3-11.	DIAGRAM FOR CLASSIFYING POWDERS ACCORDING TO THEIR FLUIDISATION BEHAVIOUR, FROM GELDART. ....	55
FIGURE 3-12.	TEST SET UP FOR AIR SLIDE CAPACITY FOR DIFFERENT FINES FRACTIONS. ....	55
FIGURE 3-13.	AIR SLIDE CAPACITY FOR ALUMINA WHEN FINES CONTENT INCREASES. ....	56

FIGURE 3-14.	A-FRAME STORAGE SAMPLED. ....	57
FIGURE 3-15.	A-FRAME SAMPLING RESULTS, SHOWING THE SUB 42 $\mu\text{M}$ FRACTIONS IN DIFFERENT AREAS IN THE A-FRAME.....	58
FIGURE 3-16.	AVERAGES OF SUB 42 $\mu\text{M}$ FRACTION FOR A GIVEN LOGISTIC LOOP IN CAMPAIGN IN 1999, DYRØY [1999].....	59
FIGURE 3-17.	AVERAGES OF SUB 42 $\mu\text{M}$ FRACTION FOR A GIVEN LOGISTIC LOOP IN CAMPAIGN IN 2000, SAME LOOP AS GIVEN IN FIGURE 3-16, DYRØY [2000].....	60
FIGURE 3-18.	AVERAGES RELATIVE TO THE FINES CONTENT OF MATERIAL PUT INTO THE PROCESS AT POINT A FOR THE LOGISTIC LOOP BEFORE AND AFTER ADJUSTMENTS (1999 AND 2000) DYRØY [1999,2000].	60
FIGURE 3-19.	RECYCLING OF FINES THROUGH RAW GAS LOOP.....	61
FIGURE 3-20.	CENTRED AND NORMALIZED SUB 42 $\mu\text{M}$ CONTENT AND NUMBER OF ANODE EFFECTS (AE) PER DAY.	63
FIGURE 3-21.	CELL VOLTAGE VERSUS ALUMINA CONCENTRATION [GRJOTHEIM & WELSH 1998].....	64
FIGURE 3-22.	CENTRED AND NORMALIZED DATA FOR SUB 42 $\mu\text{M}$ CONTENT AND DUST CONCENTRATION IN POT ROOM. ....	65
FIGURE 3-23.	SEGREGATION EFFECT DAMPING SYSTEM, MEASURED EFFECT IN FOUR CASES. ....	67
FIGURE 3-24.	SUB 42 $\mu\text{M}$ FRACTION FOR DIFFERENT CELLS, DISTRIBUTION BY OVERHEAD CRANE, I.E. LARGE AMOUNT AT LOW FREQUENCY.....	69
FIGURE 3-25.	SUB 42 $\mu\text{M}$ FRACTION FOR DIFFERENT CELLS, DISTRIBUTION BY AERATED DISTRIBUTION SYSTEM (ADS©), I.E. SMALL AMOUNT AT A HIGH FREQUENCY.....	69
FIGURE 3-26.	COEFFICIENT OF VARIATION FOR STORAGE BEFORE AND AFTER IMPLEMENTATION OF AS- SYSTEM.	70
FIGURE 3-27.	HOMOGENISING FACTOR FOR 3 CASES BEFORE AND AFTER IMPLEMENTATION OF AS- SYSTEM	71
FIGURE 3-28	NET PRESENT VALUES (NPV) FOR DIFFERENT GAINED CURRENT EFFICIENCY (CE) WITH 10% INTEREST RATE, 46 MNOK INVEST, 800\$US SELF COST, LME 1700\$US AND EXCHANGE RATE 6,5 NOK/ \$US.	75
FIGURE 3-29.	PERIODS FOR BREAK EVEN ON INVESTMENT, FOR DIFFERENT GAINING CURRENT EFFICIENCY (CE) WITH 10% INTEREST, 46 MNOK INVESTMENT, 1200\$US SELF COST, LME 1800\$US AND EXCHANGE RATE 6,5 NOK/ \$US.....	76
FIGURE 4-1.	AST WITH VALVES. THE DIAGRAM SHOWS THE UNDER PRESSURE IN THE TUBE DUE TO FALLING POWDER. ....	80
FIGURE 4-2.	TOTAL SYSTEM OF THE AST, INLET BOX AND TUBE WITH MOUNTED VALVES.....	81
FIGURE 4-3.	INLET SLIDE TO THE AST, USING A POWDER BED AS SEALING MECHANISM.....	81
FIGURE 4-4.	INLET SEAL DESIGNED BY DYRØY AND KNUTSEN AT POSTEC, [DYRØY, AND ENSTAD, 1997].	82
FIGURE 4-5.	DIFFERENT VALVE CONFIGURATIONS. ....	84
FIGURE 4-6.	AST PARAMETERS AND VARIABLES. ....	86

FIGURE 4-7.	TEST SET-UP DURING INITIAL DEVELOPMENT, FROM HUBRICH [1998].	87
FIGURE 4-8.	DEVELOPMENT TESTS, 1 T/H, FILLING HEIGHT AND NEGATIVE PRESSURE IN TUBE.	88
FIGURE 4-9.	DEVELOPMENT TESTS, 3 T/H, FILLING HEIGHT, AND NEGATIVE PRESSURE IN TUBE.	89
FIGURE 4-10.	DEVELOPMENT TESTS, 5 T/H, FILLING HEIGHT, AND NEGATIVE PRESSURE IN TUBE.	89
FIGURE 4-11.	DEVELOPMENT TESTS, 7 T/H, FILLING HEIGHT, AND NEGATIVE PRESSURE IN TUBE.	90
FIGURE 4-12.	HIGH CAPACITY TESTS DURING INITIAL DEVELOPMENT, FROM HUBRICH [1998].	91
FIGURE 4-13.	CALIBRATION OF CAPACITY AS A FUNCTION OF THE INITIAL PRESSURE FOR PNEUMATIC CONVEYING OF ALUMINA.	92
FIGURE 4-14.	HIGH CAPACITY TEST EXAMPLE, HERE 30 T/H.	93
FIGURE 4-15.	DRIVING FORCE PLOT FOR A 5 T/H TEST.	93
FIGURE 4-16.	HIGH CAPACITY TESTS, MAX NEGATIVE PRESSURE, AND FILLING HEIGHT OF INLET BOX.	94
FIGURE 4-17.	CALCULATED DRIVING FORCE BASED ON THE MEASUREMENTS SHOWN IN FIGURE 4-16.	94
FIGURE 4-18.	ANTI SEGREGATION SYSTEM DEVELOPED AND TEST RIG.	96
FIGURE 4-19.	THE ASSEMBLED TEST EQUIPMENT.	97
FIGURE 4-20.	(A) TRANSDUCERS P2 TO P7 LOCATED ON THE TUBE CROSS-SECTION (B) P1 LOCATED ABOVE THE FLANGE (C) TUBE-SECTION INSTALLED INTO THE SILO (D) HETHON SCREW-FEEDER LOCATED ABOVE THE AST BOX-SECTION.	98
FIGURE 4-21.	EXAMPLE OF PRESSURE VALUES MEASURED FOR 1 T/H.	102
FIGURE 4-22.	EXAMPLE OF PRESSURE VALUES MEASURED FOR 3 T/H.	103
FIGURE 4-23.	EXAMPLE OF PRESSURE VALUES MEASURED FOR 5 T/H.	103
FIGURE 4-24.	EXAMPLE OF PRESSURE VALUES MEASURED FOR 7 T/H.	104
FIGURE 4-25.	AVERAGE PRESSURE MEASUREMENT FOR ALL TESTS FOR TRANSDUCER P1 (EACH LINE IS AN AVERAGE OF 5 TESTS).	104
FIGURE 4-26.	AVERAGE PRESSURE MEASUREMENT FOR ALL TESTS FOR TRANSDUCER P2 (EACH LINE IS AN AVERAGE OF 5 TESTS).	105
FIGURE 4-27.	AVERAGE PRESSURE MEASUREMENT FOR ALL TESTS FOR TRANSDUCER P3 (EACH LINE IS AN AVERAGE OF 5 TESTS).	105
FIGURE 4-28.	AVERAGE PRESSURE MEASUREMENT FOR ALL TESTS FOR TRANSDUCER P4 (EACH LINE IS AN AVERAGE OF 5 TESTS).	106
FIGURE 4-29.	AVERAGE PRESSURE MEASUREMENT FOR ALL TESTS FOR TRANSDUCER P5 (EACH LINE IS AN AVERAGE OF 5 TESTS).	106
FIGURE 4-30.	AVERAGE PRESSURE MEASUREMENT FOR ALL TESTS FOR TRANSDUCER P6 (EACH LINE IS AN AVERAGE OF 5 TESTS).	107
FIGURE 4-31.	PRESSURE PROFILE ALONG THE LENGTH (H) OF THE TUBE.	107
FIGURE 4-32.	BASIS PLOT FOR COMPARISON WITH DATA FROM MATHEMATICAL MODELS.	108
FIGURE 4-33.	LAB SCALE SET UP OF THE AS-SYSTEM, WITH 3 AST'S AND A CENTRAL DISTRIBUTION UNIT.	109
FIGURE 4-34.	RESULTS FROM LAB AS-SYSTEM TEST.	110
FIGURE 4-35.	RESULT FROM PILOT SCALE COMPARISON BETWEEN FILLING OF THE SILO WITH AND	

WITHOUT ASS.....	111
FIGURE 5-1. SINGLE POINT LINEAR (SPL).....	114
FIGURE 5-2. MEASURED VERSUS PREDICTED USING SPL. ....	115
FIGURE 5-3. FLUENT RESULTS COMPARED TO MEASURED DATA. ....	117
FIGURE 5-4. MEASURED VERSUS THE FLUENT PREDICTED PRESSURE VALUES WHEN CALCULATED FOR ALL HEIGHTS. ....	118
FIGURE 5-5. SIMPLE MODEL, USING TRANSFER OF POTENTIAL TO KINETIC ENERGY TO CALCULATE VELOCITY. ....	119
FIGURE 5-6. MEASURED VERSUS PREDICTED PRESSURE VALUES WHEN CALCULATED FOR ALL HEIGHTS. ....	120
FIGURE 5-7. COMPARING THE RESULTS OF THE SIMPLE MODEL CORRECTED WITH INITIAL PRESSURE. ....	121
FIGURE 5-8. MEASURED VERSUS PREDICTED PRESSURE VALUES WHEN CALCULATED FOR ALL HEIGHTS AND INCLUDING THE INITIAL PRESSURE FORM THE INLET BOX.....	122
FIGURE 5-9. FORCE BALANCE FOR PARTICLE DRAG ( $F_G$ –GRVITIONAL FORCE, $F_D$ – DRAG FORCE AND $A_p$ –CROSS SECTIONAL AREA OF THE PARTICLE PERPENDICULAR TO THE VELOCITY).....	123
FIGURE 5-10. “TYPICAL” SIZE DISTRIBUTION FOR ALUMINA IN INDUSTRY. ....	125
FIGURE 5-11. ASSUMED FLOW INSIDE THE AST DURING FILLING OF SILO. ....	127
FIGURE 5-12. ELEMENT OF THE FLOWING MATERIAL INSIDE THE AST, WITH THE HEIGHT $D_H$ AND WIDTH $B$ , AND INDICATED FORCES.....	127
FIGURE 5-13. SSBDM PREDICTIONS OF PRESSURE DISTRIBUTION COMPARED WITH RESPECTIVE MEASURED DATA.....	134
FIGURE 5-14. MEASURED VERSUS PREDICTED PRESSURE VALUES WHEN USING THE SSBDM. ....	134
FIGURE 5-15. RESULTS FROM TESTS WITH AST AT A CAPACITY OF 1 T/H WITH THE BOUNDARIES $\pm$ ONE STANDARD DEVIATION, PLOTTED TOGETHER WITH THE RESULTS OF THE SSBDM. ....	135
FIGURE 5-16. RESULTS FROM TESTS WITH AST AT A CAPACITY OF 3 T/H WITH THE BOUNDARIES $\pm$ ONE STANDARD DEVIATION, PLOTTED TOGETHER WITH THE RESULTS OF THE SSBDM. ....	136
FIGURE 5-17. RESULTS FROM TESTS WITH AST AT A CAPACITY OF 5 T/H WITH THE BOUNDARIES $\pm$ ONE STANDARD DEVIATION, PLOTTED TOGETHER WITH THE RESULTS OF THE SSBDM. ....	136
FIGURE 5-18. RESULTS FROM TESTS WITH AST AT A CAPACITY OF 7 T/H WITH THE BOUNDARIES $\pm$ ONE STANDARD DEVIATION, PLOTTED TOGETHER WITH THE RESULTS OF THE SSBDM. ....	137
FIGURE 6-1. DESIGNED CAPACITY VS TUBE WIDTH, COMPARING OLD DESIGN WITH NEW. ....	142
FIGURE 6-2. CAPACITY PRO CROSS SECTIONAL AREA OF A SQUARE AND A RECTANGULAR TUBE ( $w=2B$ ), COMPARING OLD WITH NEW DESIGN THEORY. ....	143
FIGURE 6-3. EXAMPLE OF PLACING THE FIRST VALVE IN A 80 MM BY 80 MM TUBE. ....	144

**Tables**

TABLE 3-1.	AVERAGES AND STANDARD DEVIATIONS FOR THE CASES IN FIGURE 3-23.....	68
TABLE 3-2.	NPV CALCULATION FOR DIFFERENT CE INCREASES. ....	75
TABLE 4-1.	SCREW-FEEDER SPEED SETTINGS FOR ALUMINA (HETHON 500). ....	101
TABLE 5-1.	EXTRACT OF SETTINGS OF ONE OF THE FLUENT SIMULATIONS UNDERTAKEN BY STILLWELL [STILLWELL 2003] .....	116
TABLE 5-2.	ESTIMATED CAPACITIES USING AVERAGE TERMINAL VELOCITY FOR ALUMINA.....	126
TABLE 5-3.	SOLVING METHOD FOR THE SSBDM. ....	132

**APPENDIX C**  
**CALIBRATION CERTIFICATES AND RE CALIBRATIONS**  
**OF PRESSURE TRANSDUCERS**



SD 062F/00/a3/03 99  
P4MYYY

Endress+Hauser GmbH+Co  
Postfach / P.O. Box 1261  
D-79690 Maulburg

**Calibration Report**  
**Kalibrationsprotokoll**  
**Procès verbal de contrôle de calibration**

Endress+Hauser confirms that all measuring equipment used to assure the quality of our products has been calibrated and is traceable to national and international standards

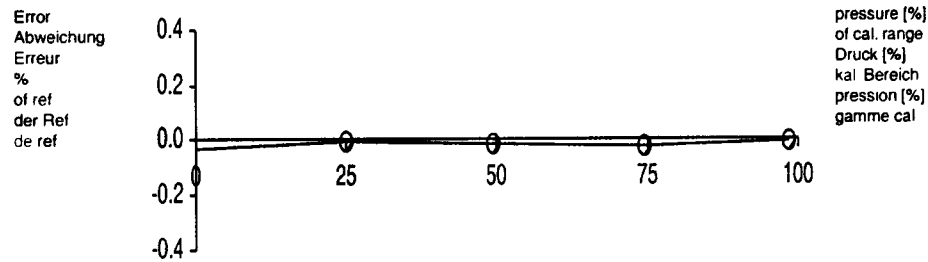
Endress+Hauser bestätigt, daß die zu Qualitätsprüfungen des Erzeugnisses eingesetzten Meßmittel gültig kalibriert waren und auf nationale bzw. internationale Standards und Normen rückführbar sind.

Endress+Hauser certifie que la calibration des appareils a été effectuée avec des instruments de mesure étalonnés selon les normes nationales et internationales.



Cerabar M			
TAG-No. Commission / pos.	Meßstelle Kommission / Pos	point de mesure commission / pos.	45708653/0010
Instrument type	Geräte Typ	type de l'appareil	PMC41-RE25CBJ11R1
Serial number	Seriennummer	numéro de série	53027001020
Sensor limits	Sensor-Meßgrenzen	gamme de mesure cellule	-100 - 100 mbar <b>P1</b>
Adjusted measuring range	Eingestellter Meßbereich	gamme de mesure ajustée	0 - -50 mbar
Electronic type	Elektronik-Typ	type d'électron.	4-20 mA

Measurement at ambient temperature 23 °C ± 5 °C  
Messung bei Umgebungstemperatur 23 °C ± 5 °C  
Mesure à température ambiante 23 °C ± 5 °C



%	ref pressure Ref. Druck pression de réf. (mbar )	actual pressure Istdruck pression réelle (mbar )	target output Sollausgang sortie théor. ( mA)	actual output Istausgang sortie réelle ( mA)	error Abweichg. erreur (%) span
99	-49.2775	-49.2753	19.769	19.768	-0.00
75	-37.2743	-37.2653	15.928	15.925	-0.02
50	-24.7936	-24.7869	11.934	11.932	-0.01
25	-12.4560	-12.4539	7.986	7.985	-0.00
-0	0.0072	0.0241	3.998	3.992	-0.03

Date Print tested by	Datum Ausdruck geprüft von	Date Impression testé par	20.03.2003 6829
-------------------------	-------------------------------	------------------------------	--------------------

Quality made by  
Endress+Hauser



ISO 9001

Überwacht vom  
E+H-Kalibrationslabor  
DKD-K-13001

Endress + Hauser



SD 062F/00/a3/03.99  
P4MYYY

Endress+Hauser GmbH+Co  
Postfach / P.O. Box 1261  
D-79690 Maulburg

**Calibration Report**  
**Kalibrationsprotokoll**  
**Procès verbal de contrôle de calibration**

Endress+Hauser confirms that all measuring equipment used to assure the quality of our products has been calibrated and is traceable to national and international standards.

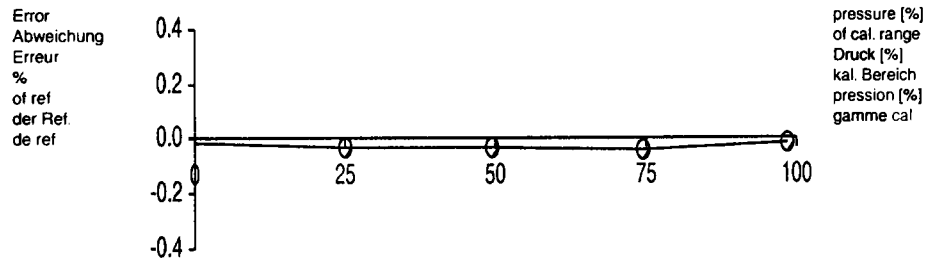
Endress+Hauser bestätigt, daß die zu Qualitätsprüfungen des Erzeugnisses eingesetzten Meßmittel gültig kalibriert waren und auf nationale bzw. internationale Standards und Normen rückführbar sind.

Endress+Hauser certifie que la calibration des appareils a été effectuée avec des instruments de mesure étalonnés selon les normes nationales et internationales



Cerabar M			
TAG-No. Commission / pos.	Meßstelle Kommission / Pos	point de mesure commission / pos.	45708653/0010
Instrument type	Geräte Typ	type de l'appareil	PMC41-RE25CBJ11R1
Serial number	Seriennummer	numéro de série	53027101020
Sensor limits	Sensor-Meßgrenzen	gamme de mesure cellule	-100 - 100 mbar <b>P2</b>
Adjusted measuring range	Eingestellter Meßbereich	gamme de mesure ajustée	0 - -50 mbar
Electronic type	Elektronik-Typ	type d'électron.	4-20 mA

Measurement at ambient temperature 23 °C ± 5 °C  
Messung bei Umgebungstemperatur 23 °C ± 5 °C  
Mesure à température ambiante 23 °C ± 5 °C



%	ref. pressure Ref. Druck pression de réf. (mbar )	actual pressure Istdruck pression réelle (mbar )	target output Sollausgang sortie théor. ( mA)	actual output Istaussgang sortie réelle ( mA)	error Abweichg. erreur (%) span
99	-49.2775	-49.2706	19.769	19.767	-0.01
75	-37.2743	-37.2545	15.928	15.921	-0.04
50	-24.7936	-24.7786	11.934	11.929	-0.03
25	-12.4560	-12.4387	7.986	7.980	-0.03
-0	0.0072	0.0151	3.998	3.995	-0.02

Date Print tested by	Datum Ausdruck geprüft von	Date Impression testé par	20.03.2003 6829
-------------------------	-------------------------------	------------------------------	--------------------

Quality made by  
Endress+Hauser



ISO 9001

Überwacht vom  
E+H-Kalibrationslabor  
DKD-K-13001

Endress + Hauser



SD 062F/00/a3/03.99  
P4MYYY

Endress+Hauser GmbH+Co  
Postfach / P.O. Box 1261  
D-79690 Maulburg

**Calibration Report**  
**Kalibrationsprotokoll**  
**Procès verbal de contrôle de calibration**

Endress+Hauser confirms that all measuring equipment used to assure the quality of our products has been calibrated and is traceable to national and international standards.

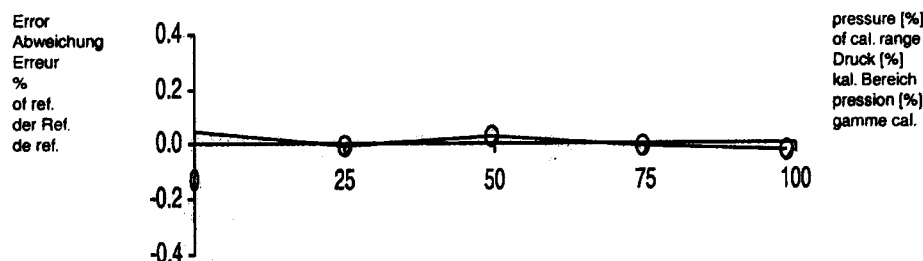
Endress+Hauser bestätigt, daß die zu Qualitätsprüfungen des Erzeugnisses eingesetzten Meßmittel gültig kalibriert waren und auf nationale bzw. internationale Standards und Normen rückführbar sind.

Endress+Hauser certifie que la calibration des appareils a été effectuée avec des instruments de mesure étalonnés selon les normes nationales et internationales.



Cerabar M			
TAG-No. Commission / pos.	Meßstelle Kommission / Pos	point de mesure commission / pos.	45708653/0010
Instrument type	Geräte Typ	type de l'appareil	PMC41-RE25CBJ11R1
Serial number	Seriennummer	numéro de série	53027201020
Sensor limits	Sensor-Meßgrenzen	gamme de mesure cellule	-100 - 100 mbar <b>P3</b>
Adjusted measuring range	Eingestellter Meßbereich	gamme de mesure ajustée	0 - -50 mbar
Electronic type	Elektronik-Typ	type d'électron.	4-20 mA

Measurement at ambient temperature 23 °C ± 5 °C  
Messung bei Umgebungstemperatur 23 °C ± 5 °C  
Mesure à température ambiante 23 °C ± 5 °C



%	ref. pressure Ref. Druck pression de réf. (mbar )	actual pressure Istdruck pression réelle (mbar )	target output Sollausgang sortie théor. ( mA)	actual output Istausgang sortie réelle ( mA)	error Abweichg. erreur (%) span
99	-49.2775	-49.2687	19.769	19.766	-0.02
75	-37.2743	-37.2730	15.928	15.927	-0.00
50	-24.7936	-24.8071	11.934	11.938	0.03
25	-12.4560	-12.4548	7.986	7.986	-0.00
-0	0.0072	-0.0179	3.998	4.006	0.05

Date Print tested by	Datum Ausdruck geprüft von	Date Impression testé par	20.03.2003 6829
-------------------------	-------------------------------	------------------------------	--------------------

Quality made by Endress+Hauser



ISO 9001  
Überwacht vom  
E+H-Kalibrationslabor  
DKD-K-13001

Endress + Hauser



SD 062F/00/a3/03 99  
P4MYYY

Endress+Hauser GmbH+Co  
Postfach / P.O. Box 1261  
D-79690 Maulburg

**Calibration Report**  
**Kalibrationsprotokoll**  
**Procès verbal de contrôle de calibration**

Endress+Hauser confirms that all measuring equipment used to assure the quality of our products has been calibrated and is traceable to national and international standards.

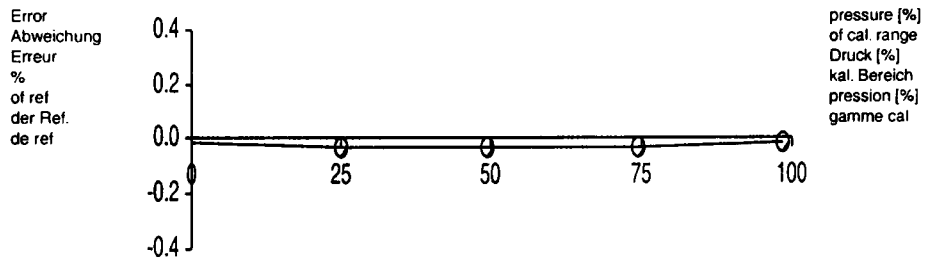
Endress+Hauser bestätigt, daß die zu Qualitätsprüfungen des Erzeugnisses eingesetzten Meßmittel gültig kalibriert waren und auf nationale bzw internationale Standards und Normen rückführbar sind

Endress+Hauser certifie que la calibration des appareils a été effectuée avec des instruments de mesure étalonnés selon les normes nationales et internationales.



Cerabar M			
TAG-No	Meßstelle	point de mesure	45708653/0010 PMC41-RE25CBJ11R1 53027301020 -100 - 100 mbar <b>P4</b> 0 - -50 mbar 4-20 mA
Commission / pos.	Kommission / Pos	commission / pos.	
Instrument type	Geräte Typ	type de l'appareil	
Serial number	Seriennummer	numéro de série	
Sensor limits	Sensor-Meßgrenzen	gamme de mesure cellule	
Adjusted measuring range	Eingestellter Meßbereich	gamme de mesure ajustée	
Electronic type	Elektronik-Typ	type d'électron.	

Measurement at ambient temperature 23 °C ± 5 °C  
Messung bei Umgebungstemperatur 23 °C ± 5 °C  
Mesure à température ambiante 23 °C ± 5 °C



	ref. pressure Ref. Druck pression de réf. %	actual pressure Istdruck pression réelle (mbar )	target output Sollausgang sortie théor. ( mA)	actual output Istausgang sortie réelle ( mA)	error Abweichg. erreur (%) span
99	-49.2775	-49.2699	19.769	19.766	-0.02
75	-37.2743	-37.2569	15.928	15.922	-0.03
50	-24.7936	-24.7774	11.934	11.929	-0.03
25	-12.4560	-12.4420	7.986	7.981	-0.03
-0	0.0072	0.0152	3.998	3.995	-0.02

Date Print tested by	Datum Ausdruck geprüft von	Date Impression testé par	20.03.2003 6829
-------------------------	-------------------------------	------------------------------	--------------------

Quality made by  
Endress+Hauser



ISO 9001

Überwacht vom  
E+H-Kalibrationslabor  
DKD-K-13001

Endress + Hauser



SD 062F/00/a3/03 99  
P4MYYY

Endress+Hauser GmbH+Co  
Postfach / P.O. Box 1261  
D-79690 Maulburg

**Calibration Report**  
**Kalibrationsprotokoll**  
**Procès verbal de contrôle de calibration**

Endress+Hauser confirms that all measuring equipment used to assure the quality of our products has been calibrated and is traceable to national and international standards.

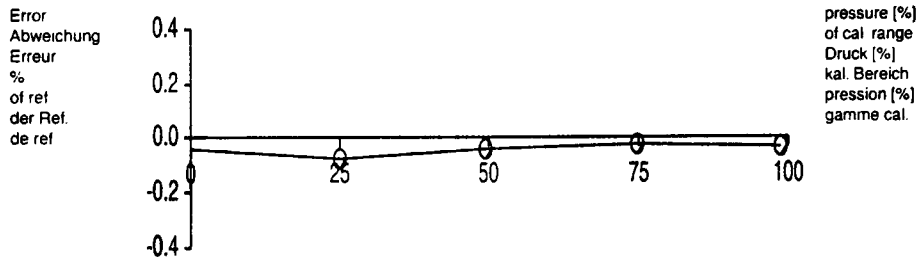
Endress+Hauser bestätigt, daß die zu Qualitätsprüfungen des Erzeugnisses eingesetzten Meßmittel gültig kalibriert waren und auf nationale bzw internationale Standards und Normen rückführbar sind

Endress+Hauser certifie que la calibration des appareils a été effectuée avec des instruments de mesure étalonnés selon les normes nationales et internationales.



Cerabar M			
TAG-No. Commission / pos.	Meßstelle Kommission / Pos	point de mesure commission / pos.	45708653/0010
Instrument type	Geräte Typ	type de l'appareil	PMC41-RE25CBJ11R1
Serial number	Seriennummer	numéro de série	53027401020
Sensor limits	Sensor-Meßgrenzen	gamme de mesure cellule	-100 - 100 mbar <b>P5</b>
Adjusted measuring range	Eingestellter Meßbereich	gamme de mesure ajustée	0 - -50 mbar
Electronic type	Elektronik-Typ	type d'électron.	4-20 mA

Measurement at ambient temperature 23 °C ± 5 °C  
Messung bei Umgebungstemperatur 23 °C ± 5 °C  
Mesure à température ambiante 23 °C ± 5 °C



%	ref pressure Ref Druck pression de réf (mbar )	actual pressure Istdruck pression réelle (mbar )	target output Sollausgang sortie théor. ( mA)	actual output Istausgang sortie réelle ( mA)	error Abweichg. erreur (%) span
99	-49.2942	-49.2803	19.774	19.770	-0.03
75	-37.3471	-37.3381	15.951	15.948	-0.02
49	-24.7094	-24.6905	11.907	11.901	-0.04
25	-12.4709	-12.4341	7.991	7.979	-0.07
-0	0.0076	0.0265	3.998	3.992	-0.04

Date Print tested by	Datum Ausdruck geprüft von	Date Impression testé par	20.03.2003 6829
-------------------------	-------------------------------	------------------------------	--------------------

Quality made by  
Endress+Hauser



ISO 9001  
Überwacht vom  
E+H-Kalibrationslabor  
DKD-K-13001

Endress + Hauser



SD 062F/00/a3/03.99  
P4MYYY

Endress+Hauser GmbH+Co  
Postfach / P.O. Box 1261  
D-79690 Maulburg

**Calibration Report**  
**Kalibrationsprotokoll**  
**Procès verbal de contrôle de calibration**

Endress+Hauser confirms that all measuring equipment used to assure the quality of our products has been calibrated and is traceable to national and international standards.

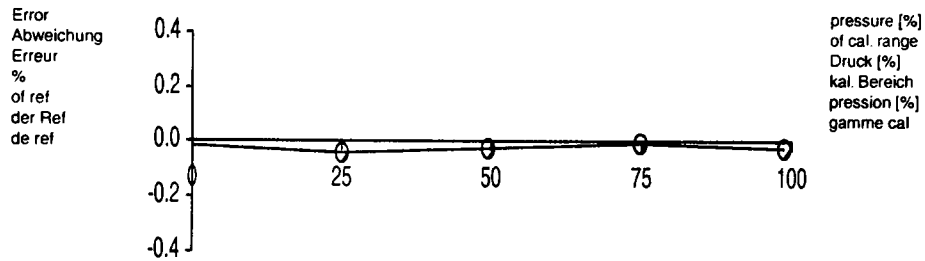
Endress+Hauser bestätigt, daß die zu Qualitätsprüfungen des Erzeugnisses eingesetzten Meßmittel gültig kalibriert waren und auf nationale bzw internationale Standards und Normen rückführbar sind.

Endress+Hauser certifie que la calibration des appareils a été effectuée avec des instruments de mesure étalonnés selon les normes nationales et internationales.



Cerabar M			
TAG-No.	Meßstelle	point de mesure	45708653/0010 PMC41-RE25CBJ11R1 53027501020 -100 - 100 mbar <b>P6</b> 0 - -50 mbar 4-20 mA
Commission / pos.	Kommission / Pos	commission / pos.	
Instrument type	Geräte Typ	type de l'appareil	
Serial number	Seriennummer	numéro de série	
Sensor limits	Sensor-Meßgrenzen	gamme de mesure cellule	
Adjusted measuring range	Eingestellter Meßbereich	gamme de mesure ajustée	
Electronic type	Elektronik-Typ	type d'électron	

Measurement at ambient temperature 23 °C ± 5 °C  
Messung bei Umgebungstemperatur 23 °C ± 5 °C  
Mesure à température ambiante 23 °C ± 5 °C



%	ref. pressure Ref. Druck pression de réf. (mbar )	actual pressure Istdruck pression réelle (mbar )	target output Sollausgang sortie théor. ( mA)	actual output Istausgang sortie réelle ( mA)	error Abweichg erreur (%) span
99	-49.2942	-49.2812	19.774	19.770	-0.03
75	-37.3471	-37.3464	15.951	15.951	-0.00
49	-24.7094	-24.6985	11.907	11.904	-0.02
25	-12.4709	-12.4513	7.991	7.984	-0.04
-0	0.0076	0.0148	3.998	3.995	-0.01

Date Print tested by	Datum Ausdruck geprüft von	Date Impression testé par	20.03.2003 6829
-------------------------	-------------------------------	------------------------------	--------------------

Quality made by  
Endress+Hauser



ISO 9001  
Überwacht vom  
E+H-Kalibrationslabor  
DKD-K-13001

Endress + Hauser



SD 062F/00/a3/03.99  
P4MYYY

Endress+Hauser GmbH+Co  
Postfach / P.O. Box 1261  
D-79690 Maulburg

**Calibration Report**  
**Kalibrationsprotokoll**  
**Procès verbal de contrôle de calibration**

Endress+Hauser confirms that all measuring equipment used to assure the quality of our products has been calibrated and is traceable to national and international standards.

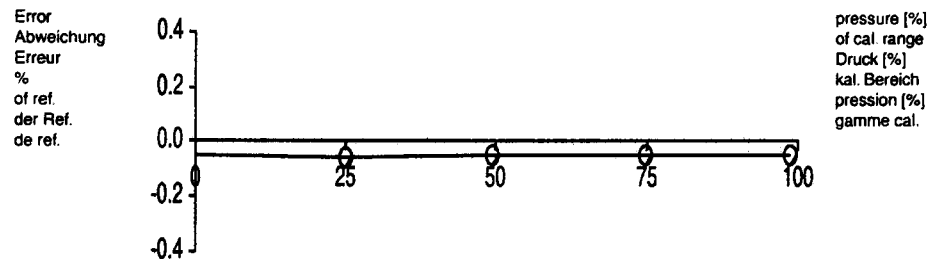
Endress+Hauser bestätigt, daß die zu Qualitätsprüfungen des Erzeugnisses eingesetzten Meßmittel gültig kalibriert waren und auf nationale bzw. internationale Standards und Normen rückführbar sind.

Endress+Hauser certifie que la calibration des appareils a été effectuée avec des instruments de mesure étalonnés selon les normes nationales et internationales.



Cerabar M			
TAG-No. Commission / pos.	Meßstelle Kommission / Pos	point de mesure commission / pos.	45708653/0010
Instrument type	Geräte Typ	type de l'appareil	PMC41-RE25CBJ11R1
Serial number	Seriennummer	numéro de série	53027601020
Sensor limits	Sensor-Meßgrenzen	gamme de mesure cellule	-100 - 100 mbar <b>P7</b>
Adjusted measuring range	Eingestellter Meßbereich	gamme de mesure ajustée	0 - -50 mbar
Electronic type	Elektronik-Typ	type d'électron.	4-20 mA

Measurement at ambient temperature 23 °C ± 5 °C  
Messung bei Umgebungstemperatur 23 °C ± 5 °C  
Mesure à température ambiante 23 °C ± 5 °C



%	ref. pressure Ref. Druck pression de réf. (mbar )	actual pressure Istdruck pression réelle (mbar )	target output Sollausgang sortie théor. ( mA)	actual output Istausgang sortie réelle ( mA)	error Abweichg. erreur (%) span
99	-49.2942	-49.2685	19.774	19.766	-0.05
75	-37.3471	-37.3225	15.951	15.943	-0.05
49	-24.7094	-24.6834	11.907	11.899	-0.05
25	-12.4709	-12.4441	7.991	7.982	-0.05
-0	0.0076	0.0304	3.998	3.990	-0.05

Date Print tested by	Datum Ausdruck geprüft von	Date Impression testé par	20.03.2003 6829
-------------------------	-------------------------------	------------------------------	--------------------

Quality made by  
Endress+Hauser



ISO 9001  
Überwacht vom  
E+H-Kalibrationslabor  
DKD-K-13001

Endress + Hauser



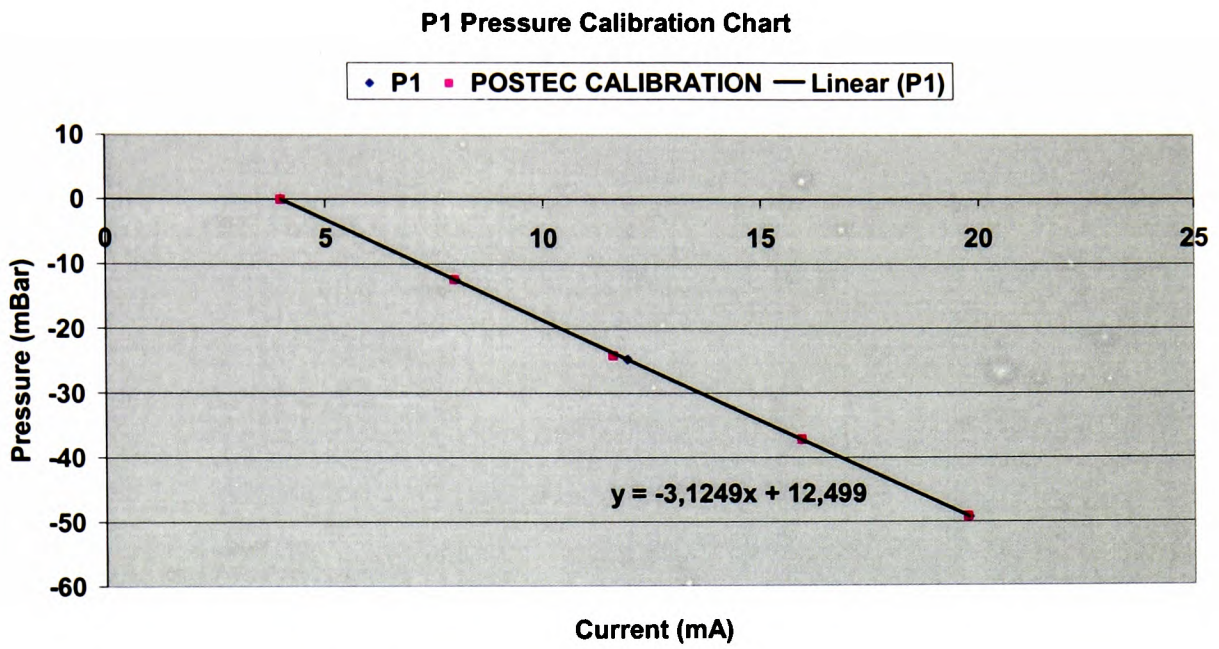


Figure C 1. E&H and POSTEC calibration chart for pressure transducer P1

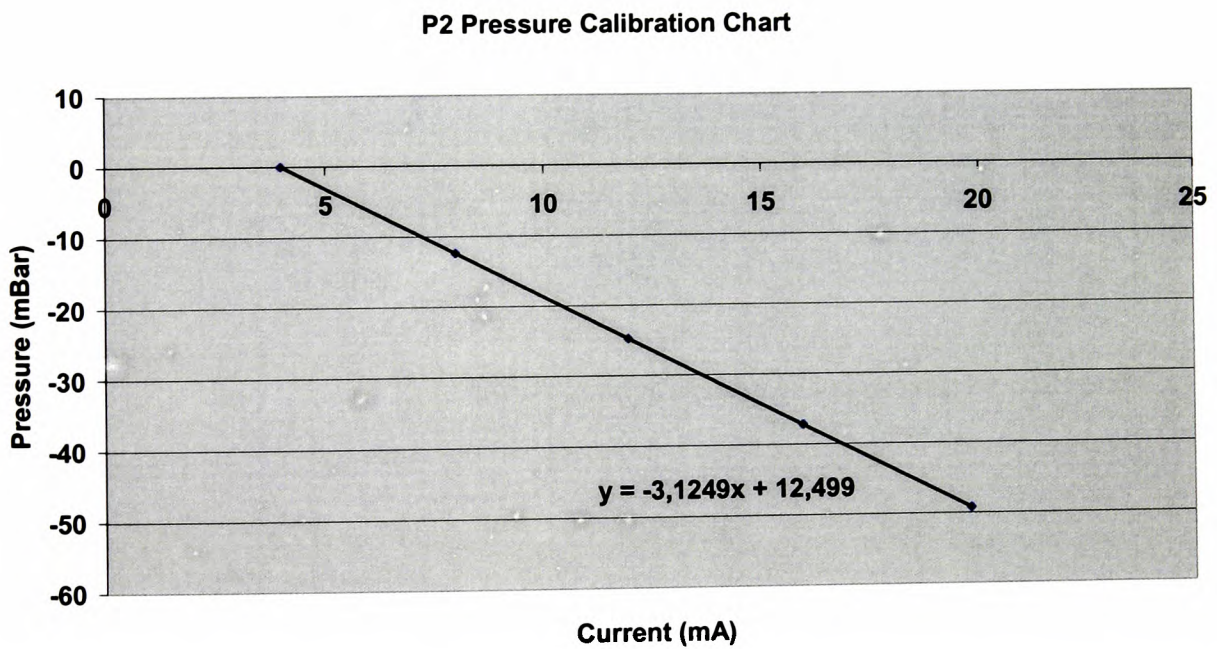


Figure C 2. E&H calibration chart for pressure transducer P2



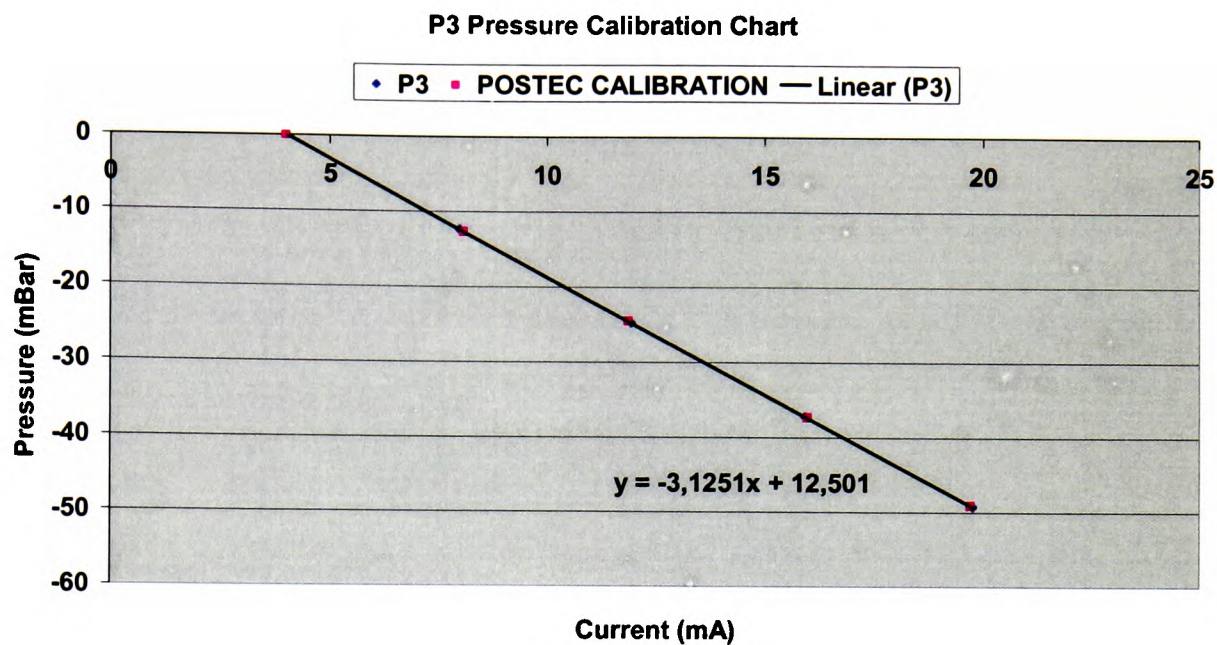


Figure C 3. E&amp;H and POSTEC calibration chart for pressure transducer P3

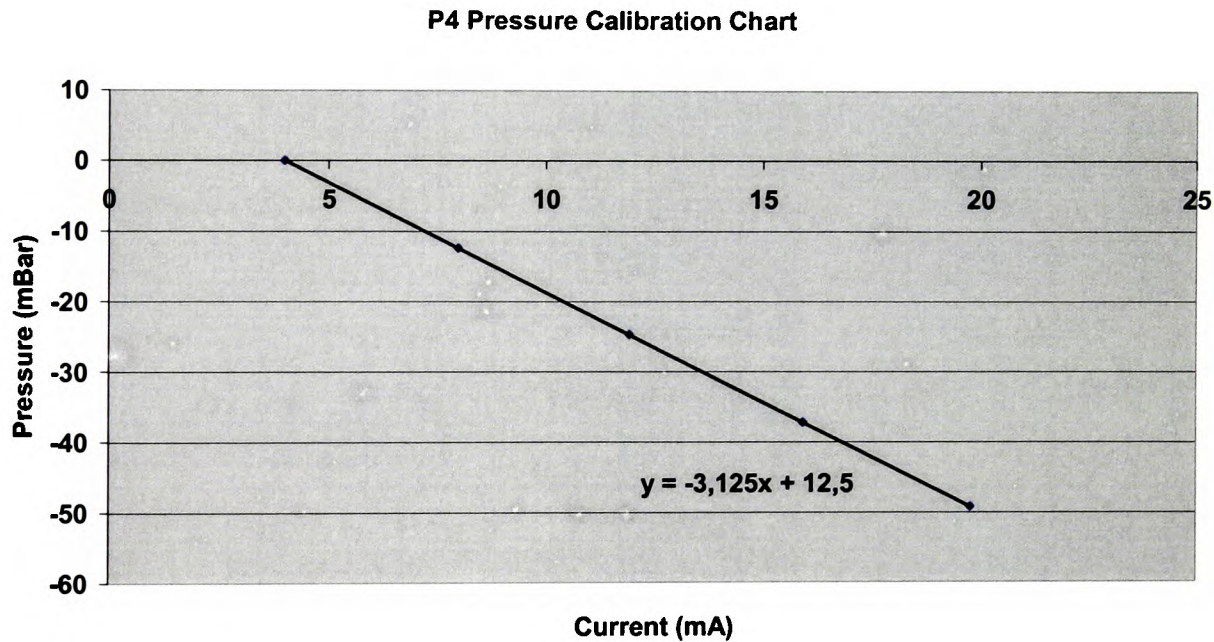


Figure C 4. E&amp;H calibration chart for pressure transducer P4

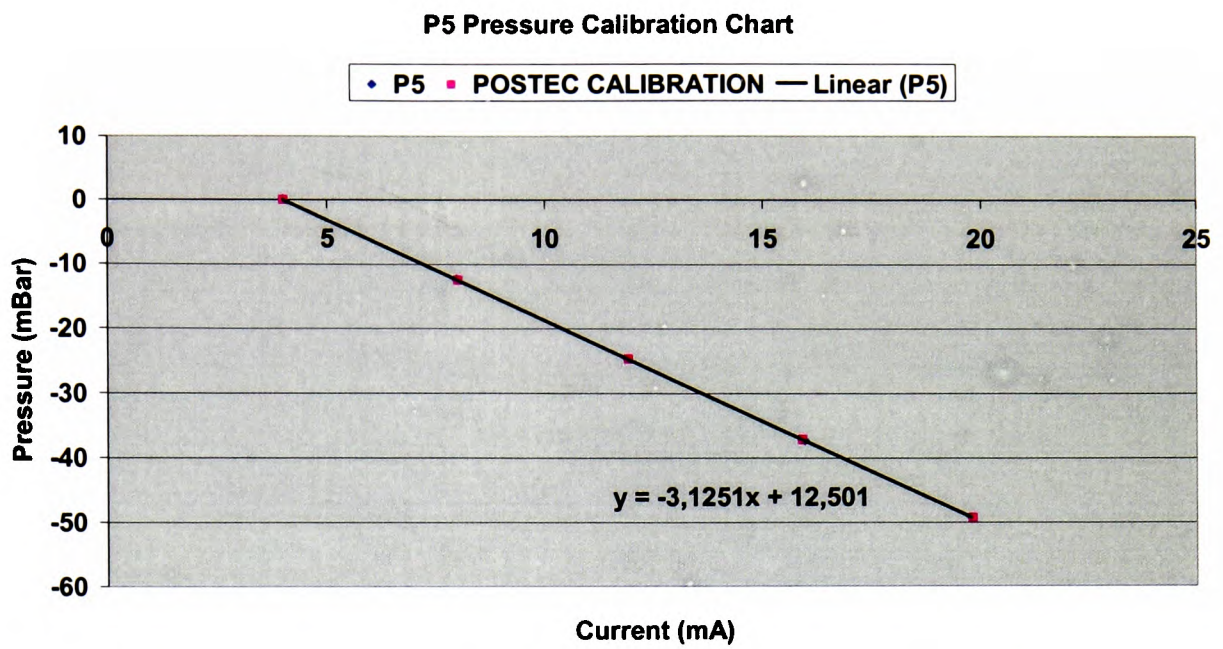


Figure C 5. E&H and POSTEC calibration chart for pressure transducer P5

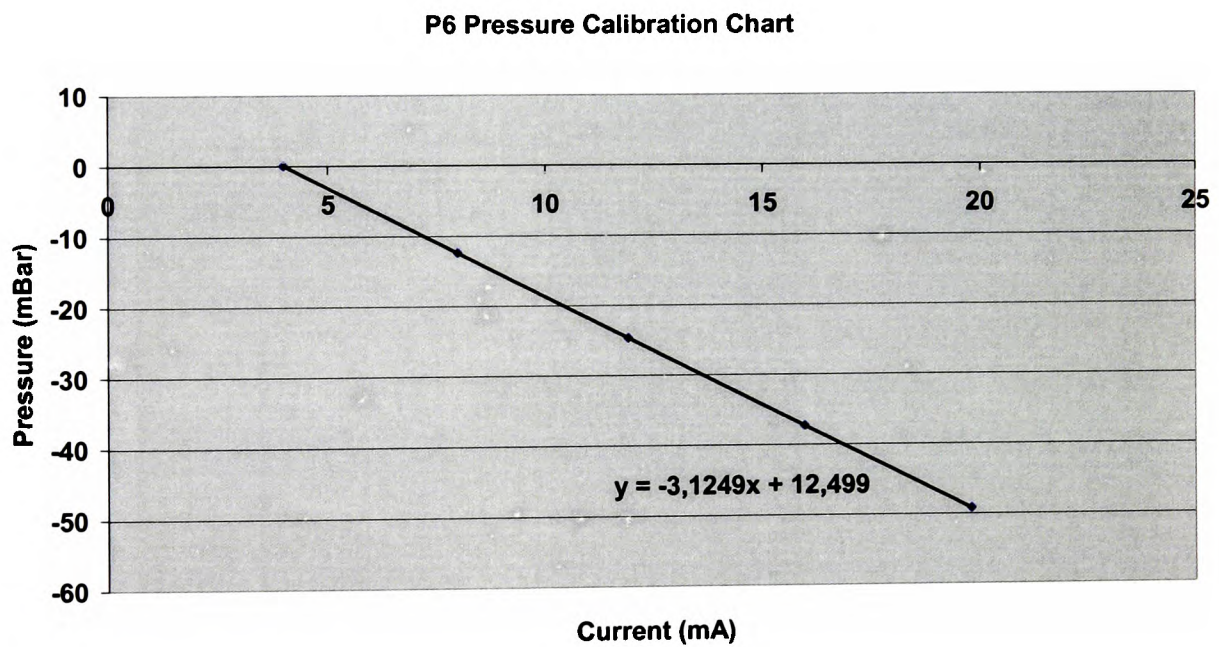


Figure C 6. E&H calibration chart for pressure transducer P6

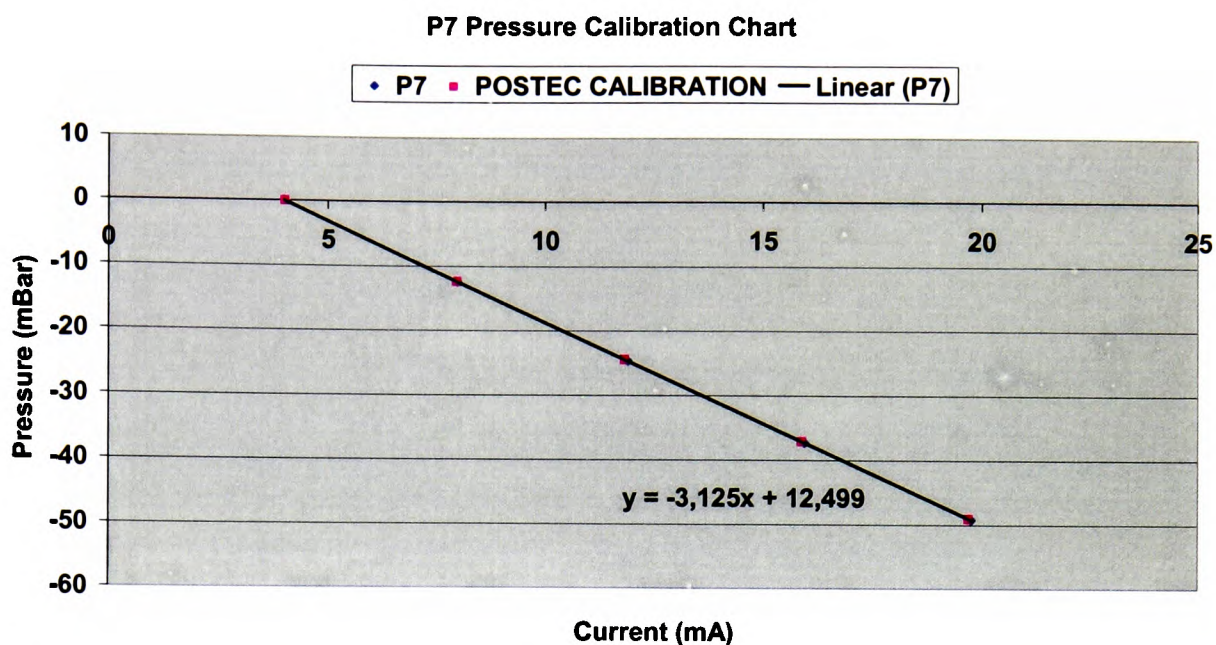


Figure C 7. E&H and POSTEC calibration chart for pressure transducer P7

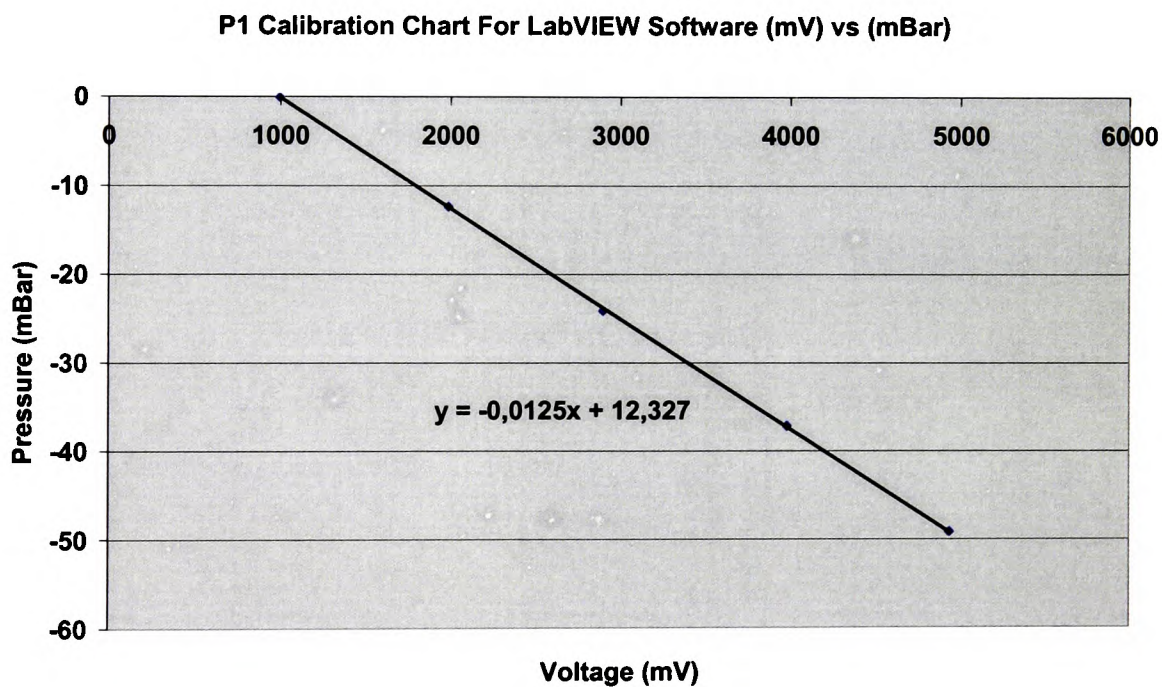


Figure C 8. P1 calibration chart and linear equation for the conversion from mV to mbar for the LabVIEW computer programme.

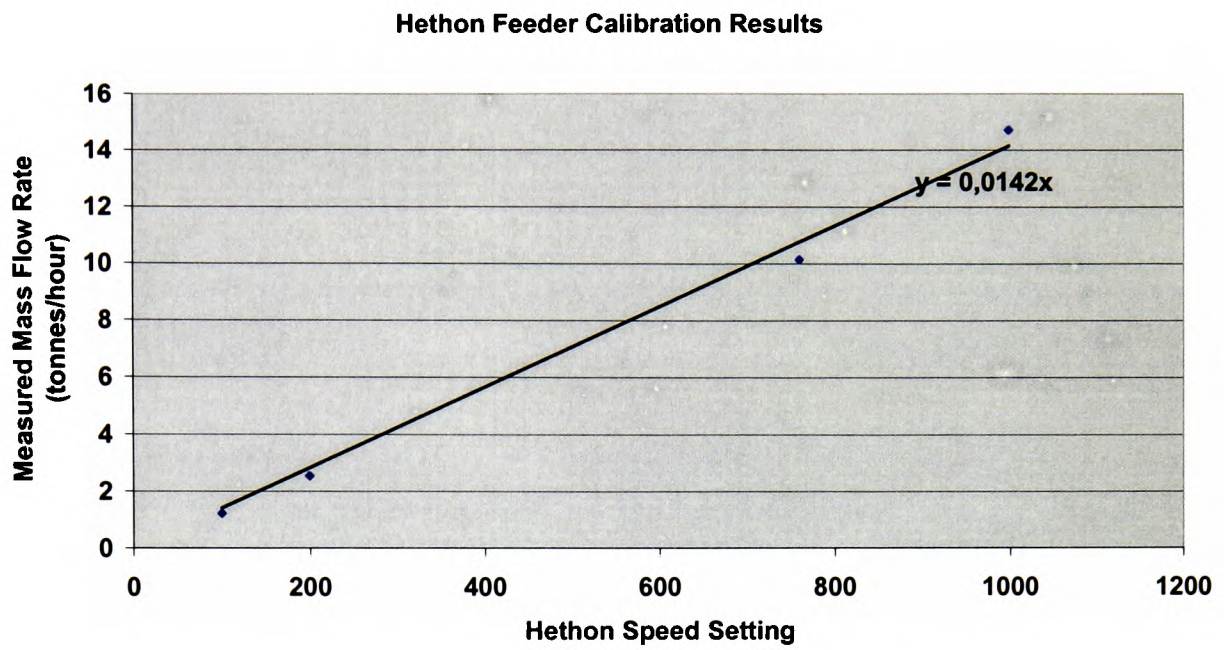


Figure C 9. Hethon 500 screw-feeder speed setting calibration chart for alumina powder

**APPENDIX D**  
**PCT PATENT OF THE AS-SYSTEM**

AU 200029503



PCT

WORLD INTELLECTUAL PROPERTY ORGANIZATION  
International Bureau

## INTERNATIONAL APPLICATION PUBLISHED UNDER THE PATENT COOPERATION TREATY (PCT)

<p>(51) International Patent Classification 7 : B65G 65/32, 69/04 // (B65D 88/72, B65G 53:52)</p>	A1	<p>(11) International Publication Number: WO 00/51924 (43) International Publication Date: 8 September 2000 (08.09.00)</p>
<p>(21) International Application Number: PCT/NO00/00066 (22) International Filing Date: 25 February 2000 (25.02.00) (30) Priority Data: 19990998 1 March 1999 (01.03.99) NO (71) Applicant (for all designated States except US): NORSK HYDRO ASA [NO/NO]; N-0240 Oslo (NO). (72) Inventors; and (75) Inventors/Applicants (for US only): KARLSEN, Morten [NO/NO]; Årdalsvegen 19, N-6884 Øvre Årdal (NO). DYRØY, Are [NO/NO]; Langgaten 53, N-3920 Porsgrunn (NO). (74) Agent: BERG, André; Norsk Hydro ASA, N-0240 Oslo (NO).</p>		<p>(81) Designated States: AE, AL, AM, AT, AU, AZ, BA, BB, BG, BR, BY, CA, CH, CN, CR, CU, CZ, DE, DK, DM, EE, ES, FI, GB, GD, GE, GH, GM, HR, HU, ID, IL, IN, IS, JP, KE, KG, KP, KR, KZ, LC, LK, LR, LS, LT, LU, LV, MA, MD, MG, MK, MN, MW, MX, NO, NZ, PL, PT, RO, RU, SD, SE, SG, SI, SK, SL, TJ, TM, TR, TT, TZ, UA, UG, US, UZ, VN, YU, ZA, ZW, ARIPO patent (GH, GM, KE, LS, MW, SD, SL, SZ, TZ, UG, ZW), Eurasian patent (AM, AZ, BY, KG, KZ, MD, RU, TJ, TM), European patent (AT, BE, CH, CY, DE, DK, ES, FI, FR, GB, GR, IE, IT, LU, MC, NL, PT, SE), OAPI patent (BF, BJ, CF, CG, CI, CM, GA, GN, GW, ML, MR, NE, SN, TD, TG).</p> <p>Published With international search report. Before the expiration of the time limit for amending the claims and to be republished in the event of the receipt of amendments.</p>
<p>(54) Title: METHOD AND AN ARRANGEMENT FOR FILLING A SILO</p>		
<p>(57) Abstract</p> <p>The present invention concerns a method and an arrangement for filling a silo (1) with a fluidisable material. The arrangement comprises means (5, 9) for supplying material to an upper area of the silo and also comprises a central material distributor (10). The material distributor comprises a tank (29) which has an inlet (28) and one or more distributor pipes (26, 26') for distributing material to one or more feed units (11, 11') which convey the material down towards the surface of the material in the silo.</p>		

## **APPENDIX E**

### **INSTALLATIONS OF THE AS-SYSTEM**

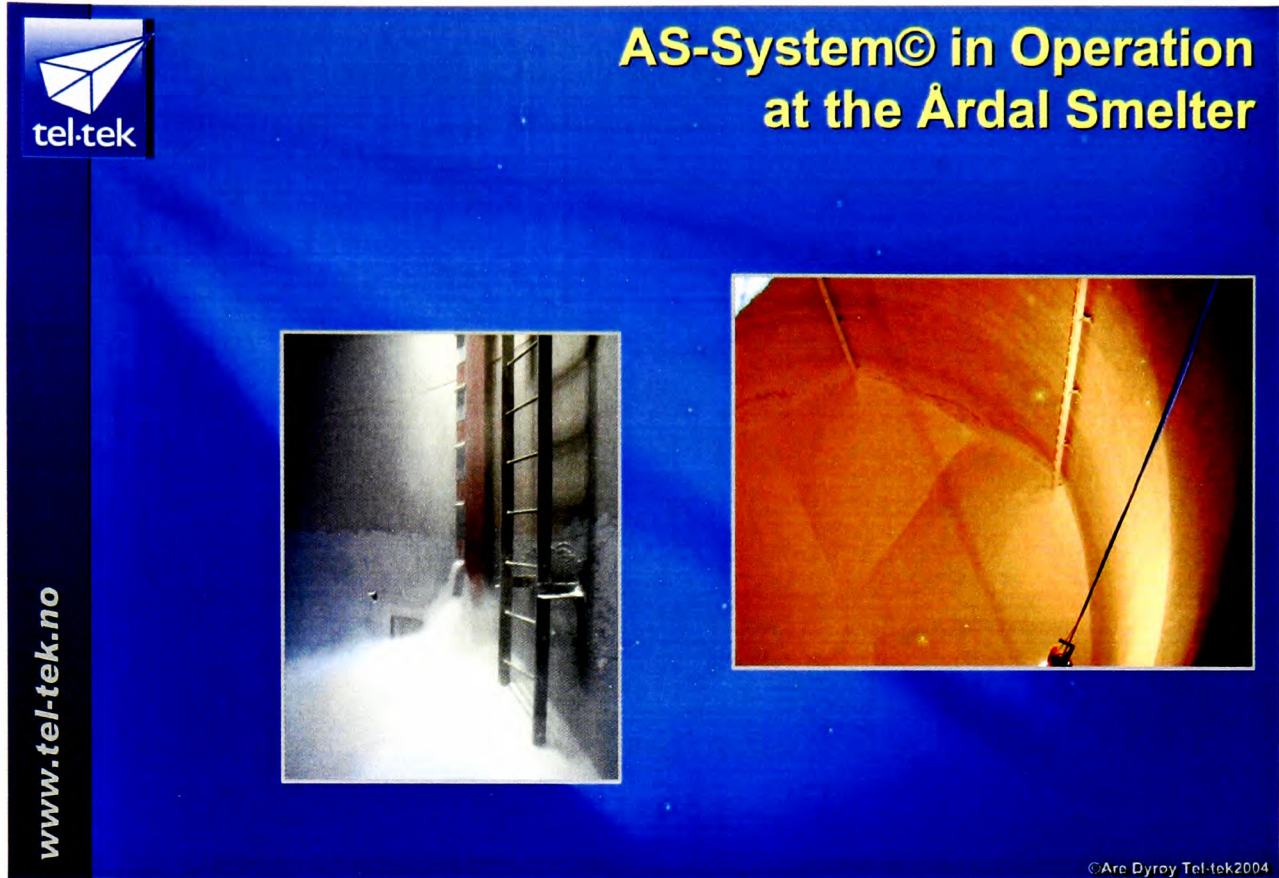


Figure E 1 Inside silos with AS-System Hydro Aluminium Årdal Smelter.

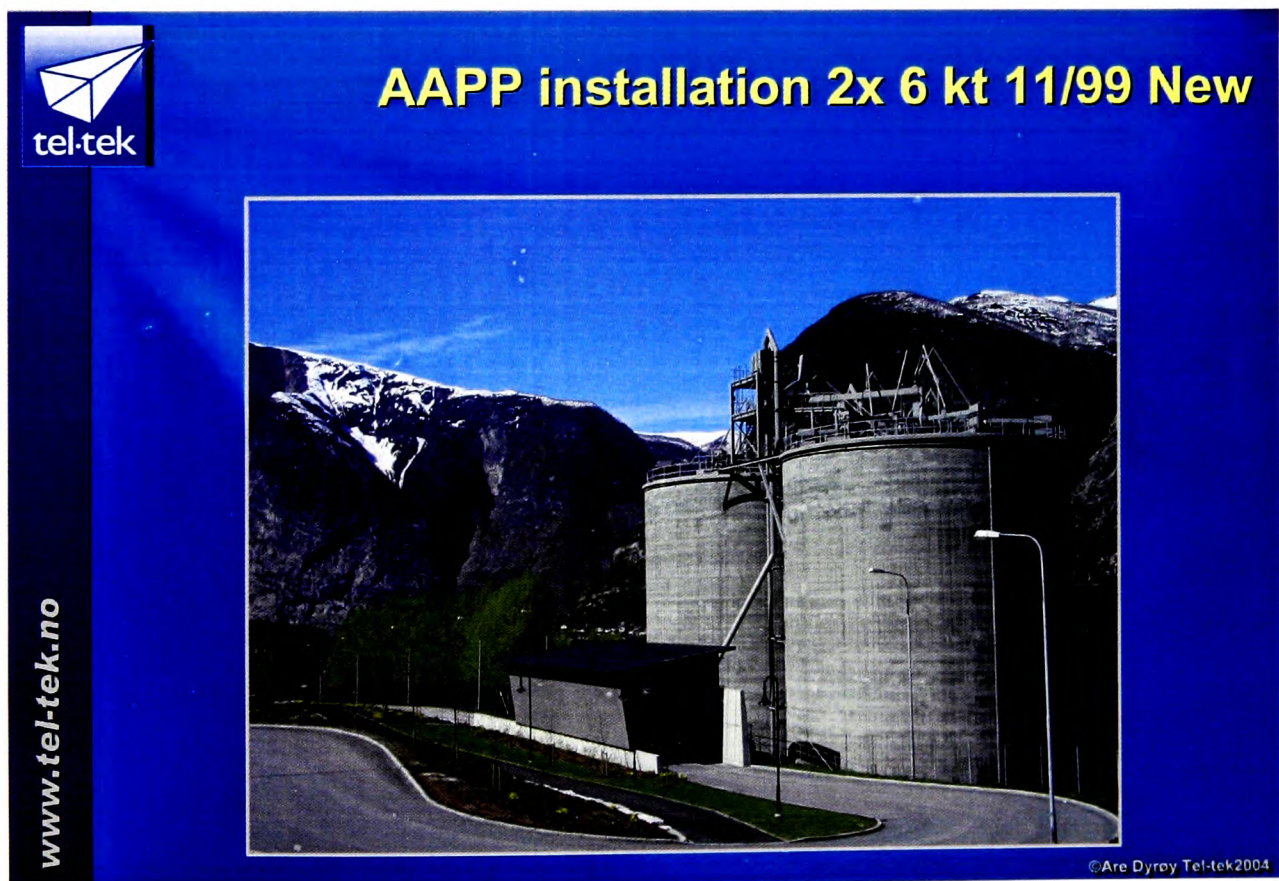


Figure E 2. AS-System implemented at Hydro Aluminium Årdal Smelter main storage.



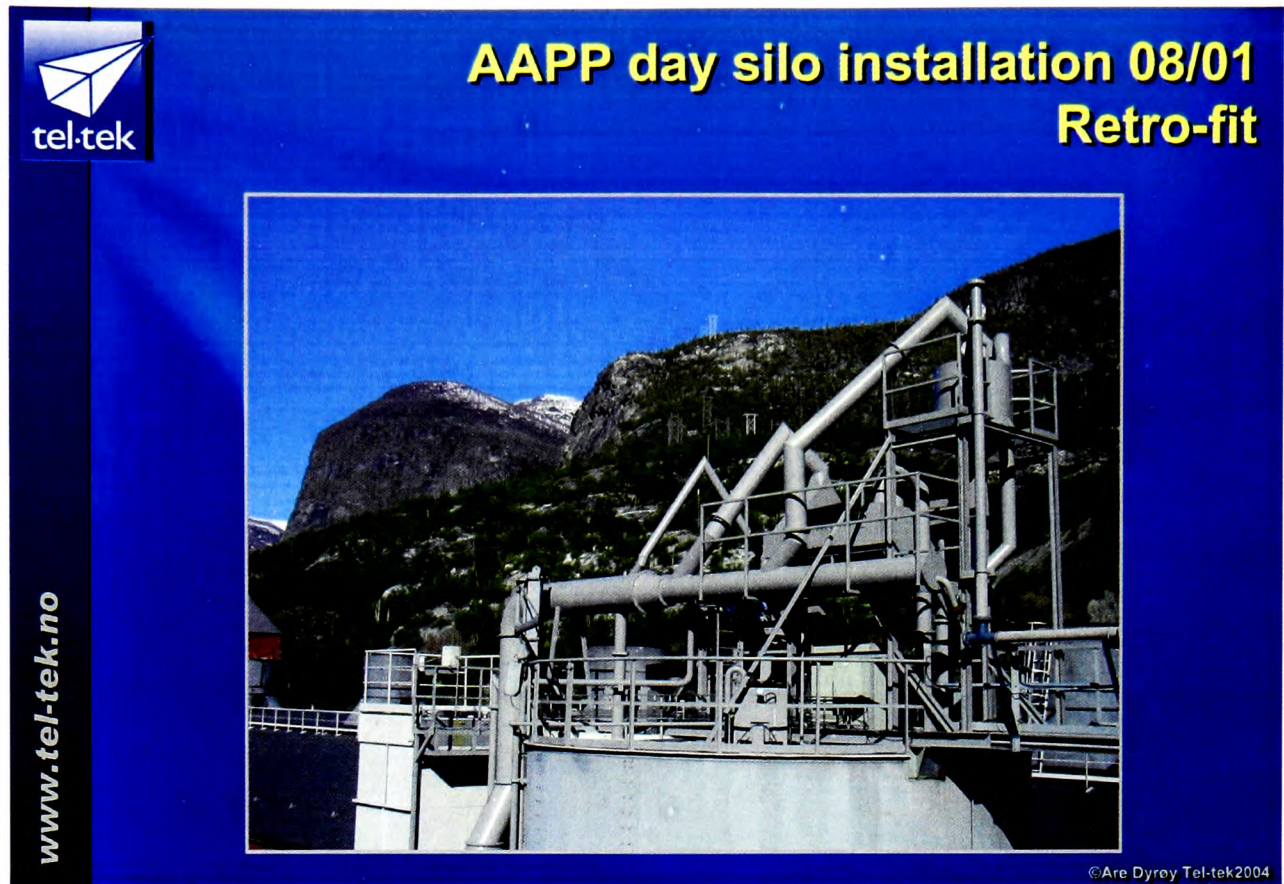


Figure E 3. AS-System in buffer silo at Hydro Aluminium Årdal Smelter.

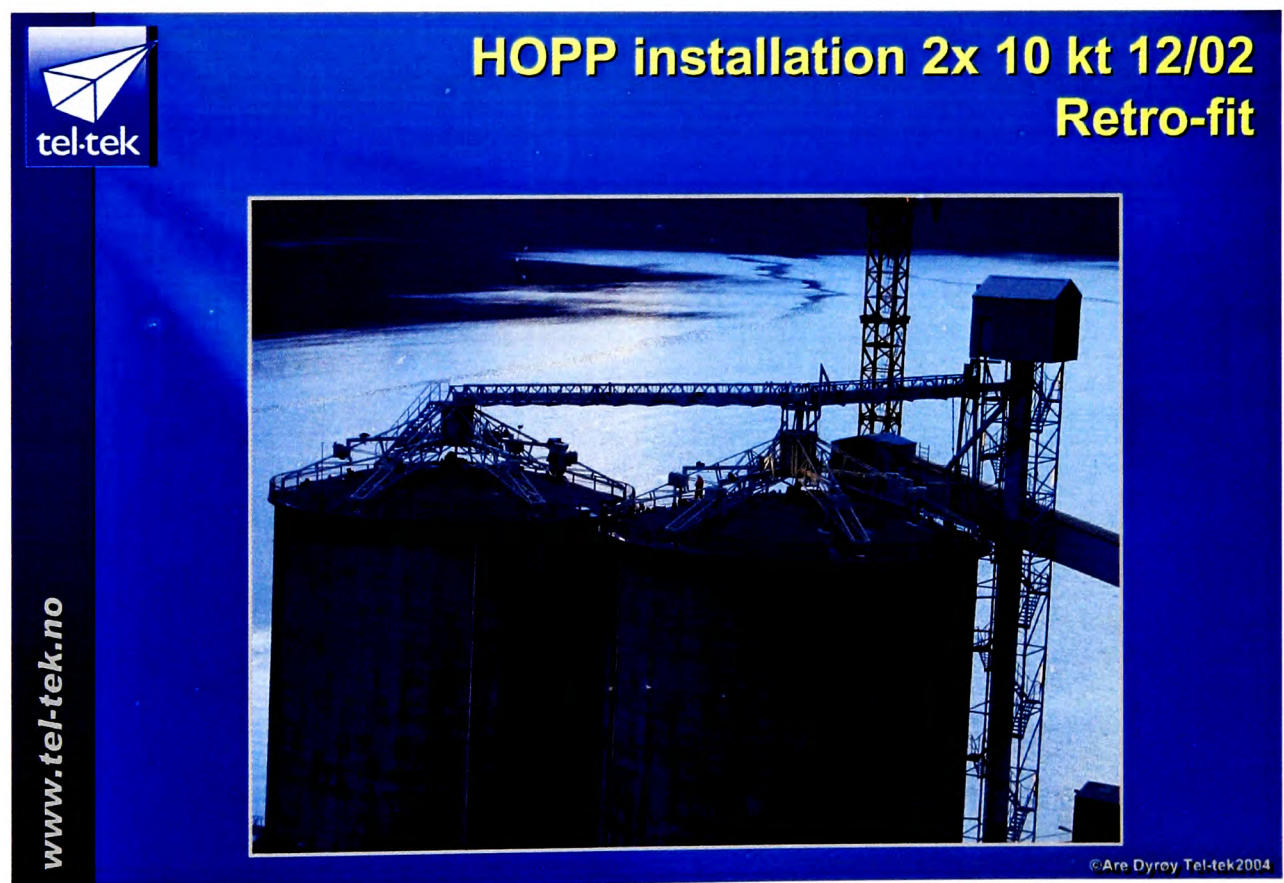


Figure E 4. AS-System retro-fit at Hydro Aluminium Høyanger Smelter.

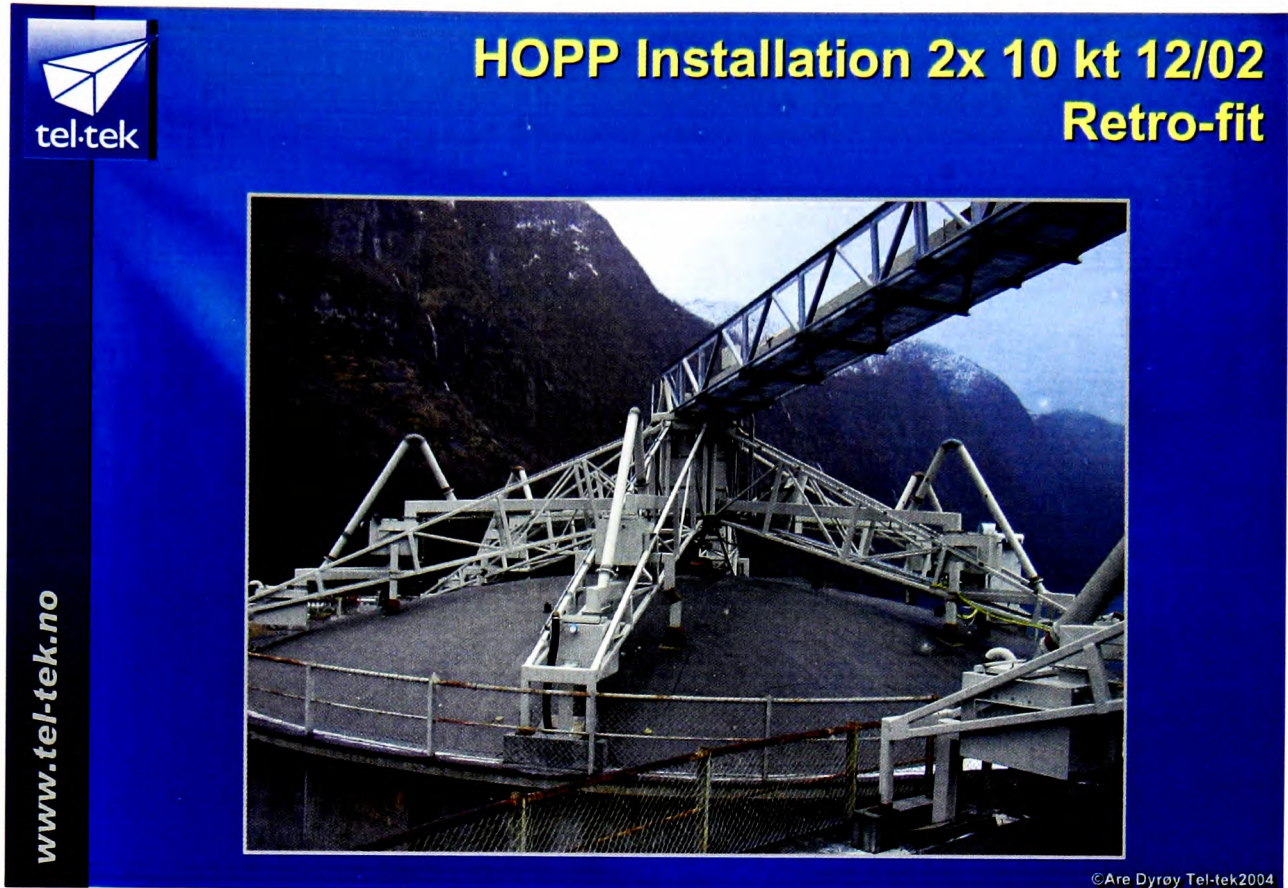


Figure E 5. AS-System retro-fit at Hydro Aluminium Høyanger Smelter, top of silo.

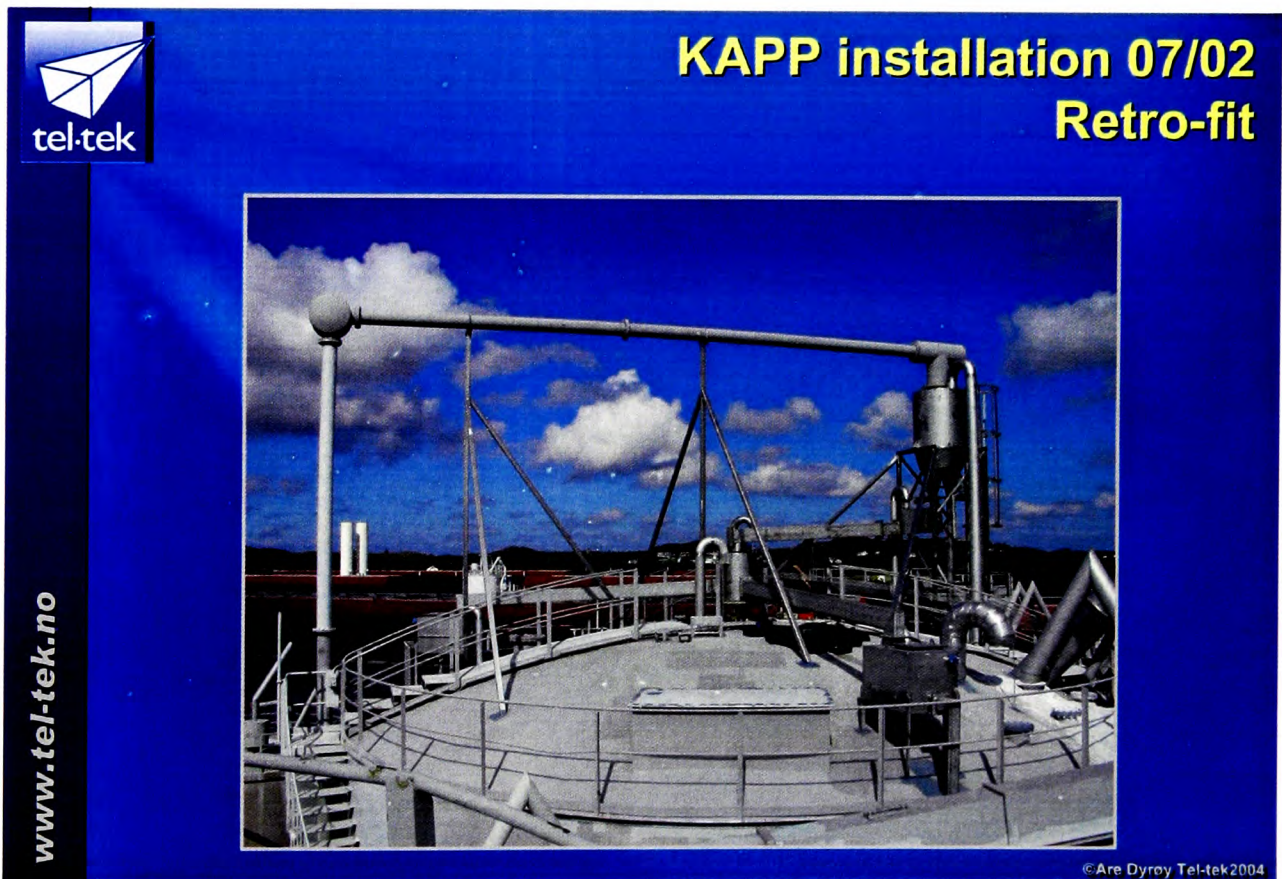


Figure E 6. AS-System retro fit on buffer silo at Hydro Aluminium Karmøy smelter.



Figure E 7. First sold commercially AS-System at Alpart refinery Jamaica.



Figure E 8. Second commercially sold AS-System, Alunorte refinery Brasil.

## **APPENDIX F**

### **TEST SET UP FOR AS-SYSTEM**

